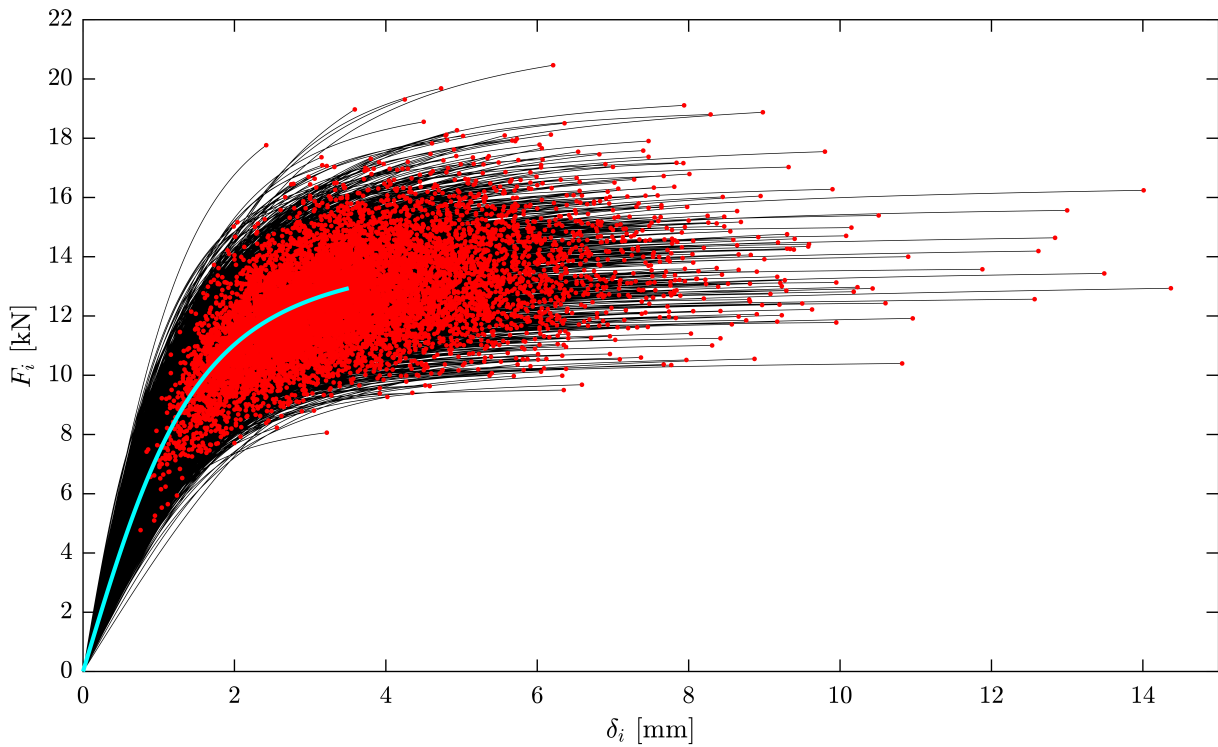
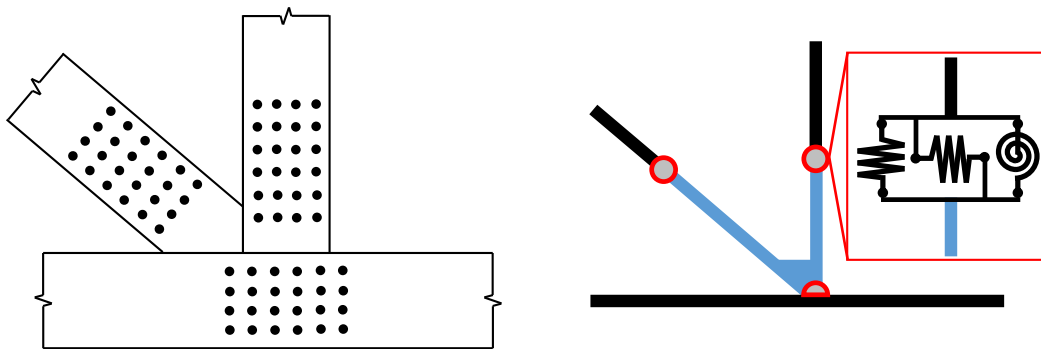


Structural behaviour and reliability of timber trusses with dowelled steel-to-timber connections



Stephan Georg Schilling

DISS. ETH NO. 28128

**STRUCTURAL BEHAVIOUR AND RELIABILITY OF
TIMBER TRUSSES WITH DOWELLED STEEL-TO-TIMBER
CONNECTIONS**

A thesis submitted to attain the degree of
DOCTOR OF SCIENCES of ETH ZURICH
(Dr. sc. ETH Zurich)

presented by

STEPHAN GEORG SCHILLING

MSc ETH Civil Eng, ETH Zurich

born on 09.06.1989

citizen of Hornussen AG

accepted on the recommendation of

Prof. Dr. Andrea Frangi (ETH Zurich, examiner)

Dr. René Steiger (Empa, co-examiner)

Prof. Dr. Bruno Sudret (ETH Zurich, co-examiner)

Prof. Dr. Thomas K. Bader (Linnæus University, co-examiner)

Acknowledgements

This doctoral thesis concludes my four year long activity as research and teaching assistant at the Chair of Timber Structures of the Institute of Structural Engineering (IBK) at ETH Zurich. It is part of the project *Structural behaviour and reliability of connections in timber structures* (200021_175821 / 1) funded by the Swiss National Science Foundation (SNSF), which is gratefully acknowledged.

To Prof. Dr. Andrea Frangi I would like to express my sincere gratitude for offering, supporting and advising this thesis but also for his trust regarding various activities during these years. His mentoring can truly be described in the words of a civil engineer: balanced.

For the support, guidance and constructive criticism of Dr. René Steiger and Dr. Pedro Palma on many occasions such as milestone and timber meetings and in the course of preparing publications and other documents I am deeply grateful and I am looking forward to future collaborations. To all three and to Prof. Dr. Robert Jockwer, who offered his support and expertise especially in the beginning of this project, I would like to thank for the initiation and application of the project.

Prof. Dr. Thomas K Bader and Prof. Dr. Bruno Sudret I want to thank for taking the time and to share their expertise in their functions as co-examiners of this thesis.

Concerning aspects of reliability and statistics I got supported on several occasions by Dr. Stefano Marelli and Xujia Zhu and regarding the development of the finite element code by Prof. Dr. Giuseppe Abbiati and Dr. Konstantinos Agathos. To all four (former) members of our institute I want to express my gratitude.

Only little information could be found with respect to the design and manufacturing of timber hall structures in Switzerland. To fill this gap, Peter Makiol (management board member of Makiol Wiederkehr engineering) and Lukas Rüegeegger (management board member of Timbatec) provided valuable insights based on their experience and expertise, for which both are gratefully acknowledged.

For providing numerous data sets, a warm thank you goes to PD Dr.-Ing. Matthias Frese. These data sets build a solid basis for the probabilistic models developed in this thesis.

It has been a pleasure to work alongside Jonas Wydler in this project, who is writing his dissertation with a focus on connections. The lengthy white board sessions and phone calls have been fruitful to both of our theses and to our friendship.

A special thanks goes to Dr. Reto Fahrni and my long-term office mates Dr. Claude Leyder and Dr. Benjamin Kreis with whom I had many interesting discussions on their, mine or other topics. Dominik Bissig and Alex Cao I want to thank for always picking up my calls when I was in trouble at a later stage of this project. For the background support and warm-heartedness a special thanks goes to Johanna Saladin-Michel. Not less I want to express my gratitude to all of the other group members who accompanied me on this journey with inputs on timber meetings, travelling to conferences, enjoying Feierabendbier, in-person and virtual coffee breaks and on many more occasions: Miriam Kleinhenz, Dr. Thomas Ehrhart, Dr. Marcel Muster, Dr.

Joachim Schmid, Dr. Katharina Müller, Dr. Michael Klippel, Tsuyoshi Aoyama, Konstantinos Voulpiotis, Julian Brogli, Dr. Philippe Grönquist, Charles Binck, Chamith Karannagodage, Dr. Peter Kobel, Dr. Jelena Ogrizovic, Dr. Ljupko Peric, Dr. Lukas Blank, Dr. Flavio Wanninger. Robert Kroyer and Andreas Müller from the steel group I also want to thank for valuable discussions and support. Last but not least a big thank you goes to Roberto Pascolo who took care of many IT-related issues. I am looking forward to seeing you all again on a regular basis, after a long time of home-office.

For proofreading parts of the thesis a special thanks goes to: Charles Binck, Jonas Wydler, Alex Cao, Miriam Kleinhenz and Dominik Bissig.

The master students who wrote their master theses or master-project theses under my supervision I want to thank for the good collaboration and valuable exchange of ideas: Nadja Manser, Nicolas Vollenweider, Julian Merkel, Hannes Zimmermann, Lucas Schnell, David Signer, Dominique Karlen and Niels Hellrigl.

My deepest gratitude goes to my family from whom I always got unconditional support and understanding. My biggest supporter in general, but also with respect to this thesis, my wife Martina, I can't thank enough. On various occasions she lent an ear and helped reordering my thoughts when I got stuck, asked the right questions, gave inputs, proofread various documents and even got me support with IT issues – and all this during challenging times like shared home-office with wedding preparations during the corona-lock-down, pregnancy, moving and raising our son Marlo.

Zurich, October 2021

Stephan Schilling

Abstract

Timber trusses with dowelled steel-to-timber connections have been used since decades and still present a competitive high performance structure for large-span applications. Nevertheless, for the design of such structures, simplified design approaches need to be applied, mostly due to the lack of a holistic connection model and high efforts of modelling truss joints. Such simplified approaches, as well as the general approaches from state-of-the-art design codes, strictly separate the design with respect to the ultimate capacity of the individual elements and their respective load-deformation behaviour, that is only applied to verify serviceability limit states. Such element-by-element design approaches are subsequently incapable of considering system effects and neglect the interactions of deformations and the force distribution within a structure. Therefore, a system-based design approach is explored by combining enhanced mechanical and probabilistic models allowing for both the application of the current design codes and reliability assessments that are capable of considering system effects.

First, a comprehensive state-of-the-art report is provided to present the backgrounds of the different aspects relevant to this thesis. It addresses timber trusses in general and the development of corresponding design rules, considerations of the connections, aspects of structural reliability, system effects and structural robustness. A multi-scale modelling approach builds the basis of the intended system-based design, considering the underlying material, single-dowel connection behaviour, full connections and members, and finally the reliability. On its basis, a modelling framework was developed, which consists of a beam-based finite element model, where the pre-processing is parametrised and automated to allow for an efficient modelling of all parts such as the connections and steel plates. A connection subroutine was implemented to account for the coupled degrees of freedom in-plane of dowelled steel-to-timber connections and all resistance models are evaluated automatically in the post-processing. The resulting maximum utilisation of the trusses, subsequently, serves as limit-state function for reliability analyses. Due to a lack of provisions of probabilistic models for glued laminated timber, such models were derived by means of further evaluation of existing test and simulation data and respective size-effect models were developed. For the implemented connection behaviour, the necessary model uncertainties were derived and for further aspects such as the steel products or the actions, the probabilistic models are presented.

Finally, investigations with respect to the structural behaviour and reliability of timber trusses are presented. Various modelling approaches considering different levels of complexity of truss joints were assessed. Subsequently, the best model was applied to evaluate the simplified design approach from the Swiss codes and a show-case structure was designed to demonstrate the potential of the developed framework. For the reliability assessments, the subset simulation technique was applied and evaluated with respect to its capability of considering the numerous limit-state functions and other aspects. For the show-case structure, it was demonstrated that system effects can be considered, although the precision of the method has to be improved.

Kurzfassung

Holzfachwerke mit Stahl-Holz Stabdübelverbindungen werden seit Jahrzehnten eingesetzt und stellen nach wie vor leistungsfähige und konkurrenzfähige Tragwerke für grosse Spannweiten dar. Dennoch werden für die Bemessung solcher Fachwerke vereinfachte Bemessungsansätze verwendet, da ganzheitliche Verbindungsmodelle fehlen und der Aufwand für die Modellierung der Verbindungsbereiche zu aufwändig ist. Diese vereinfachten Ansätze, aber auch die allgemeinen Bemessungsverfahren nach Stand der Technik, vernachlässigen bei der Nachweisführung zur Tragfähigkeit der einzelnen Elemente das zugehörige Last-Verformungs-Verhalten, welches nur zum Nachweis der Gebrauchstauglichkeit herangezogen wird. Solche elementweisen Bemessungsansätze sind daher nicht in der Lage Systemeffekte zu berücksichtigen und vernachlässigen die Wechselwirkungen von Verformungen und der Kraftverteilung innerhalb eines Tragwerks. In dieser Arbeit wird daher ein systembasierter Bemessungsansatz mittels Kombination von erweiterten mechanischen und probabilistischen Modellen untersucht. Dieser ermöglicht sowohl die Anwendung der aktuellen Bemessungsregeln als auch Zuverlässigkeitsanalysen, welche in der Lage sind Systemeffekte zu berücksichtigen.

Zuerst wurde ein umfassender Bericht zum Stand der Technik erarbeitet, um die Hintergründe der verschiedenen Aspekte der Arbeit zu erläutern. Dieser befasst sich mit Holzfachwerken im Allgemeinen und der Entwicklung entsprechender Bemessungsregeln, Betrachtungen der Verbindungen, Aspekten der Zuverlässigkeit, Systemeffekten und schliesslich der Robustheit. Ein mehrskaliger Modellierungsansatz bildet die Grundlage für den angestrebten systembasierten Entwurf, der das zugrundeliegende Material, das Verhalten von Einzeldübelverbindungen, ganzen Verbindungen und Stäben und schliesslich deren Zuverlässigkeit berücksichtigt. Darauf aufbauend wurde ein Modell entwickelt, welches aus einem 1D Finite-Elemente-Modell besteht, bei dem der Modellaufbau parametrisiert und automatisiert wurde, um eine effiziente Modellierung aller Teile wie Verbindungen und Stahlplatten zu ermöglichen. Eine Verbindungs-Subroutine wurde implementiert, um die gekoppelten Freiheitsgrade in der Ebene von Stahl-Holz Stabdübelverbindungen zu berücksichtigen. Alle Widerstandsmodelle werden automatisch ausgewertet. Die daraus resultierende maximale Ausnutzung des Fachwerks dient anschliessend als Grenzwertfunktion für Zuverlässigkeitsanalysen. Aufgrund fehlender Vorgaben für probabilistische Modelle von Brettschichtholz wurden solche Modelle durch weitere Auswertung vorhandener Versuchs- und Simulationsdaten abgeleitet und entsprechende Grösseneffekt Modelle entwickelt. Für das implementierte Verbindungsverhalten wurden die zu berücksichtigenden Modellunsicherheiten abgeleitet und für weitere Aspekte wie Stahlprodukte und Einwirkungen werden die probabilistischen Modelle aufgezeigt.

Schliesslich werden Untersuchungen zum Tragverhalten und zur Zuverlässigkeit von Holzfachwerken vorgestellt. Es wurden verschiedene Modellierungsansätze unter unterschiedlich genauer Berücksichtigung der Verbindungsbereiche ausgewertet. Anschliessend wurde das beste Modell angewandt, um den vereinfachten Bemessungsansatz aus den Schweizer Normen zu evaluieren. Das Potenzial des Modells wurde anhand eines Mustertragwerks demonstriert. Für die Zuver-

lässigkeitsanalysen wurden Subset Simulationen angewendet. Diese wurden hinsichtlich ihrer Eignung bewertet, die zahlreichen Grenzwertfunktionen und andere Aspekte zu berücksichtigen. Für das Mustertragwerk konnte gezeigt werden, dass Systemeffekte berücksichtigt werden können, obwohl die Genauigkeit der Methode noch gesteigert werden muss.

Contents

1	Introduction	1
1.1	Background and motivation	1
1.2	Objectives	1
1.3	Limitations	2
1.4	Outline	3
2	State of the art	5
2.1	Introduction	5
2.2	Timber trusses	5
2.2.1	Overview of timber structures	5
2.2.2	Timber hall structures in Switzerland	6
2.2.3	Different girder types for beam structures	6
2.2.4	Typical layouts and dimensions of timber trusses used as beams	9
2.2.5	Terminology of timber trusses	10
2.2.6	Connection typology of timber trusses	12
2.3	Design of timber trusses	14
2.3.1	Introduction	14
2.3.2	Development of timber trusses and corresponding design strategies	15
2.3.3	Design of timber trusses according to SIA 265	25
2.3.4	Design of timber trusses according to Eurocode 5	26
2.4	Load-carrying capacity and load-deformation behaviour of dowelled steel-to-timber connections	26
2.4.1	Introduction	26
2.4.2	Load-carrying capacity of dowelled steel-to-timber connections	27
2.4.3	Load-deformation behaviour of dowelled connections	30
2.5	Structural reliability	33
2.5.1	Introduction	33
2.5.2	Problem statement	34
2.5.3	Methods of structural reliability	36
2.5.4	Target reliabilities	39
2.6	System effects	43
2.6.1	Introduction	43
2.6.2	System modelling	43

2.6.3	Statistical system effects of within member variability	45
2.6.4	System factors for light-frame wood truss assemblies	45
2.6.5	Influence of ductility in timber structures on the system reliability	46
2.6.6	Weibull's weakest link theory	47
2.7	Structural robustness	50
2.7.1	Introduction	50
2.7.2	Aspects of structural robustness in codes	51
2.7.3	Aspects of structural robustness in literature	53
2.7.4	Structural robustness of large-span timber hall structures	57
2.8	Conclusions	59
3	Mechanical modelling	61
3.1	Introduction	61
3.2	Modelling of timber trusses	61
3.2.1	Introduction	61
3.2.2	Modelling of timber beams	62
3.2.3	Modelling of truss joints	62
3.2.4	Modelling of connections	63
3.2.5	Multi-scale modelling approach	64
3.3	Framework	65
3.3.1	Introduction	65
3.3.2	Beam-based finite element model	65
3.3.3	Load-deformation behaviour of dowelled steel-to-timber connections	82
3.4	Truss design tool	90
3.4.1	Introduction	90
3.4.2	Input	90
3.4.3	Ultimate limit state	91
3.4.4	Connection and beam dimensions	91
3.4.5	Serviceability limit state	92
3.4.6	Output	93
3.5	Conclusions	93
4	Probabilistic modelling	95
4.1	Introduction	95
4.2	Timber products	96
4.2.1	Overview of timber products	96
4.2.2	Glued laminated timber	97
4.3	Resistance models for truss members	119
4.3.1	Introduction	119
4.3.2	Applied model uncertainties for truss members	119
4.4	Dowelled connections	121

4.4.1	Introduction	121
4.4.2	Load-carrying capacity	121
4.4.3	Load-deformation behaviour	126
4.5	Steel products	128
4.5.1	Introduction	128
4.5.2	Steel S355	128
4.6	Actions	129
4.6.1	Introduction	129
4.6.2	Snow loads	130
4.6.3	Self-weight of timber trusses	130
4.6.4	Self-weight of roof structures	131
4.7	Conclusions	133
5	Structural behaviour of timber trusses	135
5.1	Introduction	135
5.2	Modelling of timber trusses	135
5.2.1	Introduction	135
5.2.2	Investigated trusses	135
5.2.3	Modelling details	139
5.2.4	Results	139
5.2.5	Discussion	151
5.3	Evaluation of the simplified design approach according to SIA 265:2021	152
5.3.1	Introduction	152
5.3.2	Investigated trusses	152
5.3.3	Results	153
5.3.4	Discussion	158
5.4	Potential of the modelling framework	159
5.4.1	Introduction	159
5.4.2	Example truss structure: beam grid	159
5.5	Conclusions	164
6	Reliability of timber trusses	167
6.1	Introduction	167
6.2	Applied models and limit states	167
6.3	Evaluation of the method of structural reliability	169
6.3.1	Introduction	169
6.3.2	Preliminary investigations	169
6.3.3	Influence of the model uncertainties	171
6.3.4	Combination of the single limit states	174
6.3.5	Scatter of the results	176
6.4	Target reliability	177

6.4.1	Introduction	177
6.4.2	Results	177
6.4.3	Discussion	177
6.5	Potential of system-based design approaches	179
6.5.1	Introduction	179
6.5.2	Reliability of beam grid sub-systems	179
6.6	Conclusions	180
7	Conclusions and outlook	185
7.1	Conclusions	185
7.2	Outlook	187
	Nomenclature	191
	Bibliography	199

Chapter 1

Introduction

1.1 Background and motivation

Timber trusses with dowelled steel-to-timber connections are common structures that have been built since decades. Usually, they are used in large-span timber structures, i.e. in halls and roofs. These trusses mostly are built with (partially) continuous chords and web members with different arrangements. It is common knowledge that the connections play a crucial role and often dominate the design of such trusses. However, in practice the actual design of such structures depends on simplified design approaches, which are only valid for limited geometric configurations. They make use of a simple determination of the normal forces in the timber members that are calculated based on the assumption that the connections are friction free hinges and use global reduction factors to account for the negligence of the true connection behaviour and the continuity of the chords. The entire process follows an element-by-element approach and the interactions between different structural components are neglected. Although today user-friendly and powerful software is available to facilitate the design process, it is still not possible to design timber trusses based on their true connection behaviour. The truss joints are often modelled inaccurately due to missing automation and no established models of the strongly non-linear load-deformation behaviour and the load-carrying capacity under complex loading of dowelled steel-to-timber connections are available. With respect to the probabilistic modelling, needed to conduct reliability analyses, fundamental information on the timber and connection properties is missing. Therefore, a two-theses-project (SNSF project 200021_175821 / 1) was initiated to investigate different aspects of such timber trusses. Jonas Wydler focuses on the connection behaviour and in this thesis, the focus is on the behaviour of the entire trusses.

1.2 Objectives

The objectives of this study, on the one hand, are to investigate the structural behaviour and on the other hand, to assess the reliability of timber trusses with dowelled steel-to-timber connections. To pursue these goals the following aspects will be considered:

- Provide a profound state-of-the-art report with insights into the background and development of such timber trusses with respective design approaches and fundamentals of mechanical and probabilistic aspects.

- Develop an enhanced modelling framework to investigate the structural behaviour of timber trusses.
- Embed the mechanical model into a probabilistic environment to enable reliability assessments.
- Gather probabilistic input for reliability assessments and adapt the mechanical models where necessary.
- Evaluate and compare the developed modelling framework with established design approaches.
- Conduct reliability assessments of timber trusses.

Next to the provision of specific details concerning timber trusses, this study intends to be a show-case for the transformation of the commonly applied element-by-element design approach following today's design codes into a system-based design.

1.3 Limitations

The first limitation is already stated in the title of this thesis: only trusses with dowelled steel-to-timber connections are investigated. Other connection typologies are briefly discussed in Chapter 2. Since this thesis was finalised before the one from Jonas Wydler, his experimental investigations of dowelled steel-to-timber connections could not be included. To fill this gap, in the master thesis of Manser (2021) [91] models for the load-deformation behaviour and load-carrying capacity of connections under eccentric loading were derived from available data in literature. In these investigations regular dowelled steel-to-timber connections with dowel diameters between 6-12 mm without reinforcements against splitting were considered.

As outlined in Chapter 4, for the timber beams only glued laminated timber is considered herein. Other timber products are briefly discussed. The derived probabilistic models for the different mechanical properties are based on an extensive literature study – still, for certain properties there might be more data available which could not be found within the limited scope of this thesis.

The loading situation of hall and roof structures usually depend on snow and wind loads next to the self-weight of the construction and the superstructure. Within the scope of this thesis wind loads are generally neglected. On the one hand, snow loads are typically dominating and on the other hand, the complexity of the probabilistic modelling would have increased disproportionately due to time-dependent considerations and influences of the stiffening systems of the entire structural systems.

The joint model from Schweigler et al. (2018) [115], which is used within the developed framework, could theoretically consider contact between the timber members in the truss joints. However, this feature is not applied in the present study due to an immensely increased complexity in the modelling process, which is and has to be parametrised.

Effects from duration of load and moisture are only included in the load case of serviceability limit states, i.e. no specific investigations in that field were conducted. Generally, such effects are non-negligible and lead to reductions of strength and stiffness properties.

1.4 Outline

For this thesis, a classic structure was chosen which takes the reader on a journey starting with an extensive state-of-the-art report (Chapter 2) with methodical but also historical background information on timber trusses in general, respective design strategies, aspects of the connection behaviour, structural reliability, system behaviour and finally structural robustness.

The methodical part is separated into two chapters. In Chapter 3, the mechanical modelling is addressed with a focus on multi-scale modelling and on the developed framework consisting of a non-linear finite element model, the connection subroutine and the relevant aspects of the pre- and the post-processing such as parametric approaches for an automated modelling and applied limit state functions. Further, details like the used load-deformation behaviour of the connections or the model for buckling out-of-plane are provided. In Chapter 4, the probabilistic modelling is addressed. On the one hand, pure probabilistic aspects are presented such as the applied distribution functions to describe the timber elements, steel parts and the actions. On the other hand, necessary adaptations of the deterministic part are introduced like the removal of hidden safety factors from the connection resistance model or the expansion of the limit state equations by respective model uncertainties.

Following the same logic, also the results and their discussions and conclusions are separated into two chapters. The structural behaviour is addressed in Chapter 5. On the example of four trusses, different modelling approaches that were presented in Chapter 2 & 3 are compared and discussed. Then the simplified design approach according to SIA 265:2021 [121] is evaluated by means of checking the limits of the design rules with the developed modelling framework. Finally, a show-case is presented that illustrates the potential of the developed modelling framework in contrast to the simplified design rules. Chapter 6 addresses the reliability. First, an evaluation of the applied method of structural reliability is conducted on the example of different trusses. Second, the method is applied on trusses that represent the state-of-the-art provisions in order to assess the target reliability. Third, the reliability of the show-case structures from Chapter 5 are assessed in order to discuss the full potential of a system-based design approach.

Finally, in Chapter 7, the entire thesis is concluded and an outlook is provided, which intends to present research gaps concisely.

Chapter 2

State of the art

2.1 Introduction

This chapter introduces and summarises state-of-the-art knowledge, literature and methods for six different topics:

- timber trusses in general with a focus on the situation in Switzerland, the terminology and the detailing
- design of timber trusses with a historical background report, insights into design methodologies and standardised design rules
- load-carrying capacity and load-deformation behaviour of dowelled steel-to-timber connections as a brief introduction to the most relevant issues that are considered within the scope of this thesis
- structural reliability in general with detailed explanations of some fundamentals, an overview of existing methods and an insight into target reliabilities
- system effects with an overview of fundamentals, a literature review and Weibull's weakest link theory
- structural robustness with an overview of definitions and appropriate terminology, presentation of design principles and conclusive literature for the structural robustness of large-span timber hall structures

Finally, the most relevant conclusions are drawn to emphasise important considerations and to layout some aspects which are followed up in the course of the thesis.

2.2 Timber trusses

2.2.1 Overview of timber structures

A huge variety of engineered timber structures exists. Natterer et al. [99] and Herzog et al. [61] present a good overview of most types which were built before 2004. Since then, most of the development took place with respect to residential and office buildings, including mid- and high-rise buildings. Nevertheless, within the scope of this thesis the structural types are addressed,

which find their application in hall and roof structures, bridges and space structures. Therefore, in Tab. 2.1 and 2.2 these structures are summarised according to the systematic composition of Natterer et al. (1996). For the hall and roof *structures* a classification with respect to the *dimensionality* of the span is introduced by the author of this thesis. E.g. a simply supported truss girder is categorised in 1D-span, where the structure itself is related to two dimensions. On the next level within the hierarchical representation of both tables the *structural systems* are addressed. On the lowest level possible *structural elements* are listed. The huge share of trusses and truss-related structural elements within this level is emphasised and has to be kept in mind, although the state-of-the-art design approaches and most of the considerations within this thesis deal with rather standardised applications.

2.2.2 Timber hall structures in Switzerland

Developments in the field of fire safety during the last two decades together with an increasing interest in ecological building materials lead to a boom of multi-story timber buildings. This is why nowadays, the structural timber market in Switzerland is dominated by residential and office buildings. Especially for design offices, building projects take the biggest share. [66, 89]

Nevertheless, timber hall projects did not disappear and still are one of the main pillars in timber industry. The Saldomes from Häring or the latest manufacturing halls of Pilatus Aircraft Ltd are very good examples for up-to-date innovative timber hall structures [59, 103]. However, standard fabrication halls take the biggest share of timber halls, for which low costs and functionality are of high importance. Those structures typically show a square floor plan, simple geometries and often use big doors on the short sides. The structural system usually consists of beams with 1D-spans. These structures are ideal for industrial processes from the delivery to the pickup. Such industrial halls often are not designed within design offices. The manufacturers rather build standardised solutions or use replicates from similar structures with slight adaptations. The steel industry represents the biggest concurrence for this type of timber halls. The actual selection of a timber or steel solution is often based on ideology and not on variant studies. [66]

Facade and roof systems are of utmost importance for hall structures. These elements are standardised and very economic. In other words, they are ideal for halls with simple geometries. Vice versa, for complex, eye-catching structures these elements are cost driving. [66]

The best selling halls in timber industry are the simple ones with wooden girders and dependent on the requirements combined with timber or steel columns. The huge variety presented in Tab. 2.1 nowadays rather represents a niche product. [66]

2.2.3 Different girder types for beam structures

The latest developments in the manufacturing of glued laminated timber (GLT) allows for beams of huge dimensions regarding height and length. GLT girders are very economic, since the production process is not work intensive. Nowadays, even haunched or curved girders are easy

Tab. 2.1: Timber structures - Hall & roof structures (own table with values from [61, 99]).

1D-span							
Linear members	Beams (single-/multi-span)	Cantilevers	Articulated linear members	Frames (with pins)	Arches (compr./susp.)		
Propped beams	Solid-web	Solid-web	Solid-web	Solid-web	Solid-web		
Kneebraces	Trusses	Trusses	Trusses	Trusses	Trusses		
Trussed beams	Trussed beams		Trussed beams				
Strut frames							
2D-span							
Linear members	Beams (single-span)	Articulated linear members	Frames (with pins)	Arches (compr./susp./ mesh.)	Beam grids	Space frames	Folded plate systems
Propped beams	Solid-web	Solid-web	Solid-web	Solid-web	Solid-web	Trusses	Shells
Kneebraces	Trusses	Trusses	Trusses	Trusses	Trusses	Trusses	Trusses
Trussed beams	Trussed beams	Trussed beams					
Strut frames							
Curved plane and beam structures							
Barrel vaults	Domes	Saddle shells					
(Ribbed) Shells	(Rib.) lattice shells	(Rib.) lattice shells					
	Arches						
	Frames						
	Trusses						
	Meshes						
	Grids						

Tab. 2.2: Timber structures - Bridges and space structures (own table with values from [61, 99]).

Bridges				
Linear members	Beams (single- / multi-span)	Articulated linear members	Arches (compr. / susp.)	Cable-stayed bridges
Propped beams	Solid-web	Solid-web	Solid-web	Solid-web
Kneebraces	Trusses	Trusses	Trusses	Trusses
Trussed beams	Trussed beams	Trussed beams		Trussed beams
Strut frames	Guyed beams			
Space structures				
Towers				
Solid-web				
Trusses				

to realise. With proper reinforcement, openings for technical installation can be realised. Such reinforcements are uneconomic though. [66]

Trusses represent next to GLT beams the other big share of timber girders. They often cost a bit more but come with a variety of advantages [66]:

- Light, filigree and thereby translucent structures are possible. Therefore, they can be used for sawtooth and similar roof structures, which allow for a natural lighting. Combined with steel cables as diagonals this effect can be maximised. One can even use trusses as room-high structural elements through which e.g. personnel in an office can pass.
- The basic material consists of easy-to-handle straight beams and less material is used.
- Technical installations like exhaust systems are common for industrial halls and can be placed easily through the trusses.
- The inherent low weight of trusses leads to an easy handling at the construction site and allows for lighter cranes.
- Although GLT girders can reach huge dimensions, trusses are applicable to even longer spans.
- Huge dimensions are often of concern considering transportation. Truss joints are easy to realise with steel connector elements and allow for a simple fragmented transport.




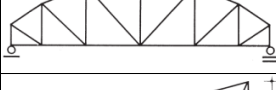

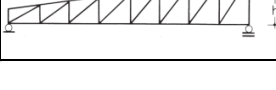
When used for bridges or in ice arenas there is a certain disadvantage of trusses: Dripping water, which can cause rotting in the joint areas, can be of concern if not addressed properly [49, 66].

2.2.4 Typical layouts and dimensions of timber trusses used as beams

Several different layouts of timber trusses are possible when used as beams, e.g. triangular, parallel chord, duopitch, bowstring and monopitch trusses. In Tab. 2.3 typical dimensions of these different static systems are listed according to [61]. In contrast to the suggestions of the terms *symmetrical* and *arch* truss, herein the respective terms *triangular* and *bowstring* truss are preferred and the definitions provided for the height were adapted (maximum height h vs. medium height h_m). Additionally, [61, 84, 99] provide typical distances between the girders of 4-10 m and distances between the purlins of 1.0-2.5 m. Evidently, for all static systems a huge variety of the absolute dimensions but also a certain variety of the slenderness ratio exists depending on the boundary conditions such as span width, distance between the girders or the loading situation.

Each truss layout can be realised with a variety of arrangements of the web members such as combinations of posts and diagonals or crossed layouts. A non-exhaustive overview based on [61, 99] is given in Fig. 2.1.

Tab. 2.3: Typical dimensions of timber trusses (own table with values and pictures from [61, 99]).

Static system	Sketch	Span-width [m]	Height [m]	Roof inclination [°]
Triangular truss (Symmetrical truss)		7.5 - 30	$h_m = \frac{l}{10}$	12 - 30
Parallel chord truss		20 - 80	$h = \frac{l}{10} - \frac{l}{15}$	0 - 4
Duopitch roof truss with raised eaves		7.5 - 35	$h_m \geq \frac{l}{12}$	3 - 8
Bowstring truss (Arch truss)		20 - 50	$h = \frac{l}{6} - \frac{l}{8}$	-
Monopitch roof truss		7.5 - 20	$h_m \geq \frac{l}{10}$	12 - 30
Monopitch roof truss with raised eave		7.5 - 35	$h_m \geq \frac{l}{12}$	3 - 8

2.2.5 Terminology of timber trusses

In English the terminology of the different truss types and their specific arrangement of the web members are based on patents, i.e. on the inventors names, or on the type of structural system [53, 61]. An extensive investigation of literature and the world wide web revealed many attempts of systematic descriptions. Most of them are lacking references, are unsystematic after all or even partly contradicting. Further, for the single elements of truss assemblies different vocabulary is used.

Therefore, it is proposed to separate the terminology of the overall static system and the web member layout. A non-exhaustive overview of names for static systems was already presented in Tab. 2.3. There it can be seen that only the layout of the top and bottom chords is indicative for the names. For vertical beams, the term *post* and for non-vertical beams the term *diagonals* is proposed. For the web member layouts, it is proposed to use descriptive vocabulary, i.e. for the specification of the diagonal beams terms like *rising* and *falling* or *crossed* can be used. In the following list this concept is applied on the layouts shown in Fig. 2.1.

- Fig. 2.1a: Triangular trusses with 1) falling and rising diagonals, 2) falling and rising diagonals with mid-post, 3) crossed diagonals with mid-post, 4) diagonals falling towards the centre with posts, 5) diagonals rising towards the centre with posts, 6) crossed diagonals with posts.
- Fig. 2.1b: Parallel chord trusses with 1) rising and falling diagonals, 2) falling and rising diagonals, 3) diagonals rising towards the centre with posts, 4) diagonals falling towards the centre with posts, 5) crossed diagonals, 6) crossed diagonals with posts.

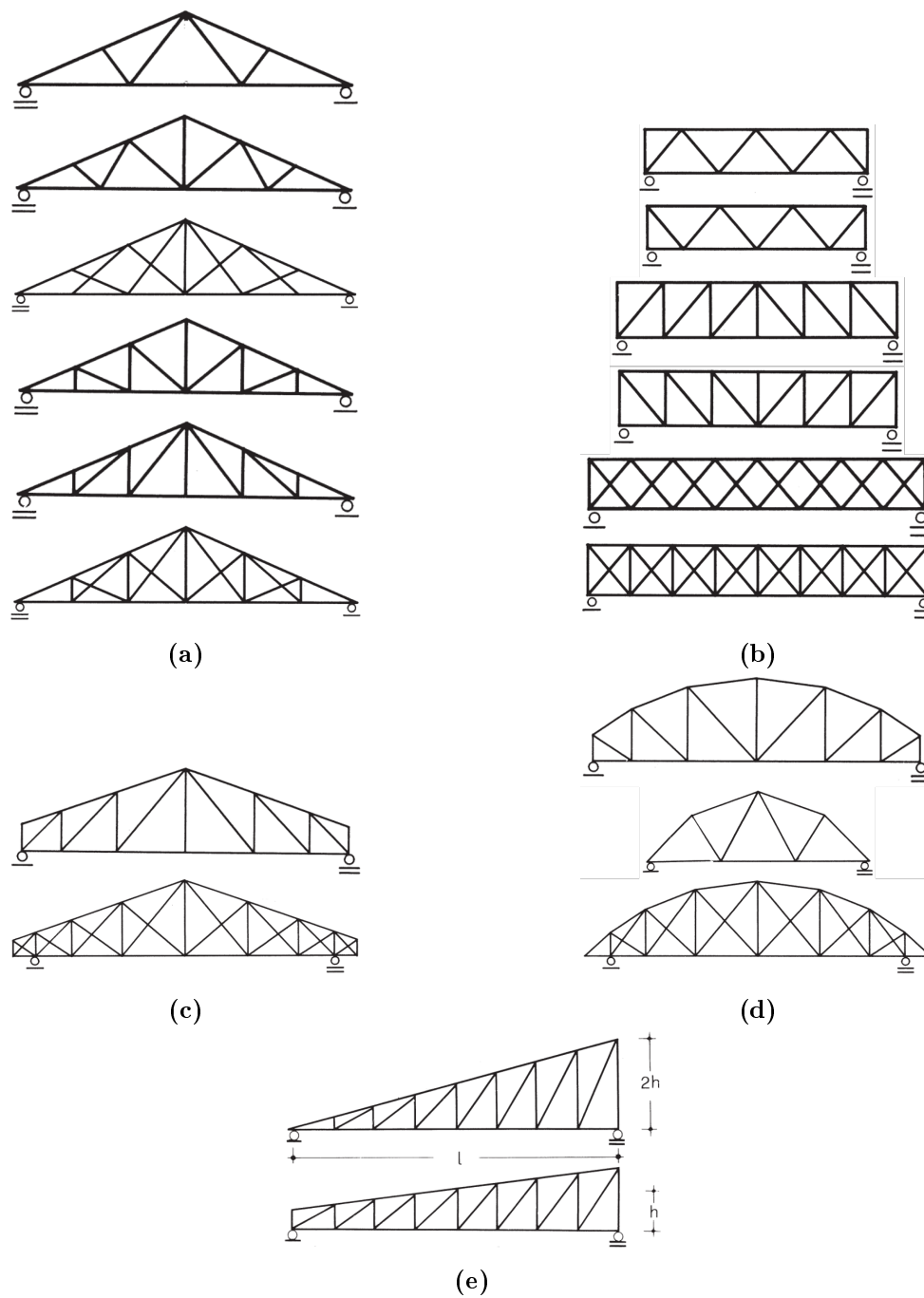


Fig. 2.1: Typical layouts of the web members of timber trusses [61, 99]; (a) triangular trusses; (b) parallel chord trusses; (c) dupitch roof trusses; (d) arched roof trusses; (e) monopitch roof trusses.

- Fig. 2.1c: Dupitch roof trusses with raised eaves and 1) diagonals rising towards the centre with posts, 2) crossed diagonals with posts.
- Fig. 2.1d: Bowstring trusses with 1) raised eaves and diagonals falling towards the centre with posts, 2) falling and rising diagonals 3) crossed diagonals with posts.

- Fig. 2.1e: 1) Monopitch roof truss with diagonals rising towards the higher end with posts and 2) monopitch roof truss with raised eave and diagonals rising towards the higher end with posts.

2.2.6 Connection typology of timber trusses

Nowadays, typically three different connection typologies are used for truss joints: *nail plates*, *glued-in rods*, and *steel dowels*. All three types have a common concern: The quantity of joints and their design is strongly cost-relevant, since steel parts and work are disproportionately expensive. By adjusting the truss geometry, the forces in the beams and joints can be manipulated directly. However, in practice the optimisation potential is often limited due to necessary load introduction points, where the loads should act in truss joints directly. [66]

Although in many cases roof structures do not underlie requirements concerning fire safety, it is briefly discussed for all three systems in the following paragraphs.

2.2.6.1 Nail plates

Nail plates in Switzerland are nowadays considered obsolete and are mainly used for reinforcement and conservation measures [66]. In other countries, e.g. Germany, they are still widely used for industrial constructions [10], where optics are of little importance (Fig. 2.2). They come with the advantage of small reductions of the cross-section, the load-carrying capacity is rather limited though [10]. Originally, they were foreseen to be used with boards rather than GLT and were used as multi-shear connectors. To reduce the work, they were sometimes installed with presses. Many different systems with one- or two-sided nail plates are known, which were used widely some decades ago. [49, 52]

With respect to fire safety external nail plates are of concern, since they are directly exposed to fire. Without requirements they are applicable though. [10, 66]



Fig. 2.2: Nail plate [60].

2.2.6.2 Glued-in rods

Glued-in rods (GIR) offer nice optics since no connectors can be seen (Fig. 2.3). They reach the highest utilisation factor of the residual wood cross-section with almost 100%. For such high percentages, often reinforcements with hardwood are necessary though, which considerably increases the work. The glueing is a critical process, which is in need of a proper quality management. Air and grease residuals in the boreholes are non-negligible dangers. This is why the production of such connections is only possible for manufacturers, who specialise in this field. Another concern for non-experienced manufacturers is the lack of codification of GIR. A very promising development for GIR is the necking of the rods, which supports ductile failure modes. [66]

GIR show a certain fire protection by construction. For higher requirements the steel rods just need more covering wood. [66]

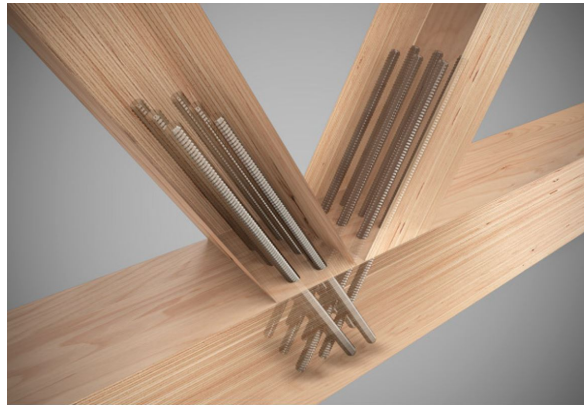


Fig. 2.3: Glued-in rods in truss joint with BauBuche LVL [77].

2.2.6.3 Steel dowels

Steel dowel connections are nowadays almost exclusively used with steel plates (dowelled steel-to-timber connections), which allows for the force flow being in plane. The biggest concern is the reduction of the cross-section in the truss joints, but still high utilisation factors of wood with up to 85% are possible. Practitioners appreciate this connection type due to its simple mechanics and carpenter-like handling. Execution control is visually possible and therefore appreciated. Thanks to advancements in prefabrication the boreholes can be drilled very precise. [66] Standard configurations, which are viable in most cases are tabulated [63].

Several different product types are available on the market. System solutions with regular steel dowels (Fig. 2.4) [1, 49] can be found as well as self-tapping dowels, which can penetrate unpunched steel plates [13, 93]. The usage of self-tapping dowels results in negligible slip. They are also used in different structural systems, where they e.g. are used to handle construction tolerances. [10, 66]

Steel dowels are normally as long as the beam width and the gaps for the steel plates are generally left open. This is why both are exposed to fire at their ends, which can result in higher

temperatures in the connections [101]. However, 30 min fire resistance is given in most cases without special measures and reaching 60 min is feasible with edge-spacings or simple protection measures [36, 66].

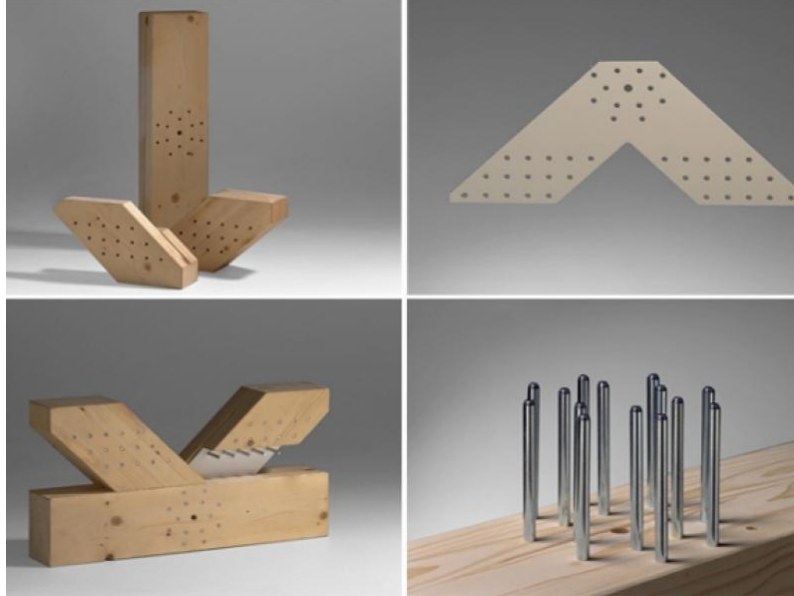


Fig. 2.4: BSB system [1].

2.2.6.4 Other connections

Similar to GIR also fully threaded screws can be used for timber trusses. The application is rather for smaller trusses though. Therefore, performance-wise they are in concurrence for light trusses made with nail plates. [50]

Another interesting truss joint layout was presented in Blaß & Enders-Comberg (2012) [10] (Fig. 2.5). There, enhanced step joints in the hardwood lamellas of the hybrid GLT chords are used for diagonals under compression and screwed in rods for diagonals under tension. The main goal of this joint layout is an efficient construction process by compliance with good aesthetics.

2.3 Design of timber trusses

2.3.1 Introduction

Through the assembly of single elements to trusses, timber members can be used in an efficient way. The members are mainly loaded along their axis, which is the optimal loading situation for timber. In section 2.2.3 many advantages considering the application of such structures were shown. Dimensioning of trusses mainly depends on geometrical aspects as system height, web member layout and position of loads as well as on the connection type [26].

To prevent the reader from a confusion concerning terminology of dowelled steel-to-timber connections in the following section 2.3.2, here a brief explanation of the terms is presented

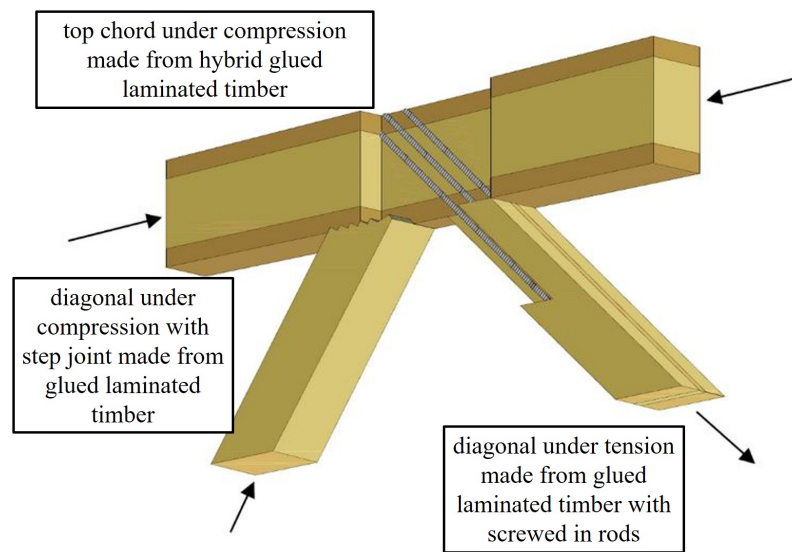


Fig. 2.5: Screwed in rods & step joint combined with hybrid GLT, translated from [10].

in English and in German [26, 48]. Bolts (in German "Bolzen") can denote screws from steel structures or pin-shaped connectors. If pin-shaped, the pre-drilled holes need to be tight-fitted. This is why in German the term "Passbolzen" can be used and was used in early times. Nowadays, such tight-fitted bolts are called steel dowels or just dowels (in German "Stabdübel"). The issue is aggravated by the differentiation between dowels as tight-fitted bolts and dowels as split ring dowels and alike. The latter are from the category embedded connectors (in German "Einlassdübel"). Similar to these embedded connectors, there also exist driven connectors (in German "Einpressdübel").

The confusion gets worse, when comparing the terminology from steel structures and timber structures [119, 121]: A bolt (in German "Bolzen" or "Bauschraube") in timber structures is defined as a screw from steel structures and is applied with head, nuts and washers and is not tight-fitted in the pre-drilled hole. In steel structures there exist screws (in German "Schraube") which are used with nuts and washers and bolts (in German "Bolzen") which refer to thick pin-shaped elements.

Nowadays, a bolt in the sense of timber structures refers to screws from steel structures. Thin pin-shaped connectors in timber structures are called dowels. In German, the term "Stabdübel", can refer to both thin pin-shaped connections without or with two-sided nuts and washers (then also called "Passschraube"). [63]

2.3.2 Development of timber trusses and corresponding design strategies

In the early 19th century trusses with parallel chords were built from squared timber connected by step joints or dowels such as split ring dowels (Fig. 2.6 & Fig. 2.7) and were used for timber bridges and falseworks [52, 97]. A special principle with crossed timber diagonals, which are under compression only – thanks to prestressed vertical tension bars – was used in the USA since

1840 and is called HOWE's principle [52]. In Fig. 2.8 one can see that for the connections simple hardwood elements were used.

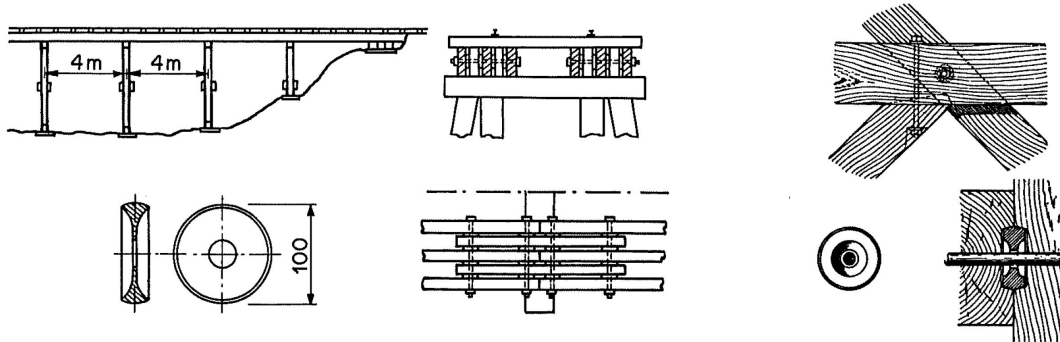


Fig. 2.6: Split ring connections from the early 19th century as used in the USA [52].

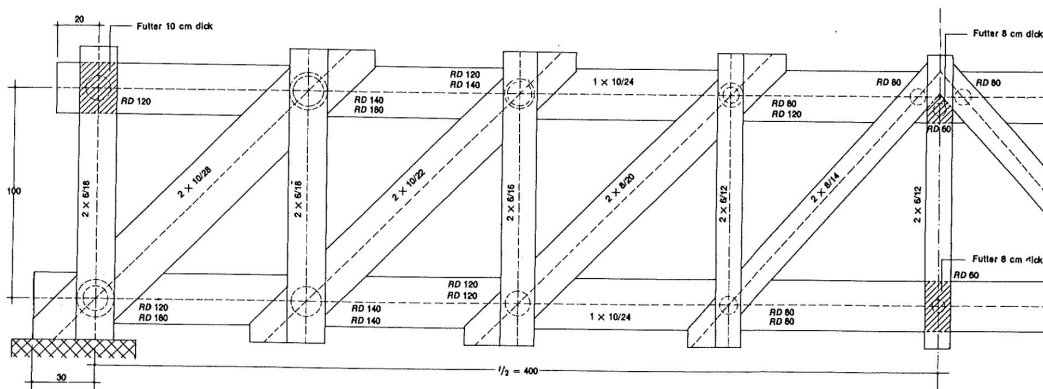


Fig. 2.7: Timber truss with split ring connections [52].

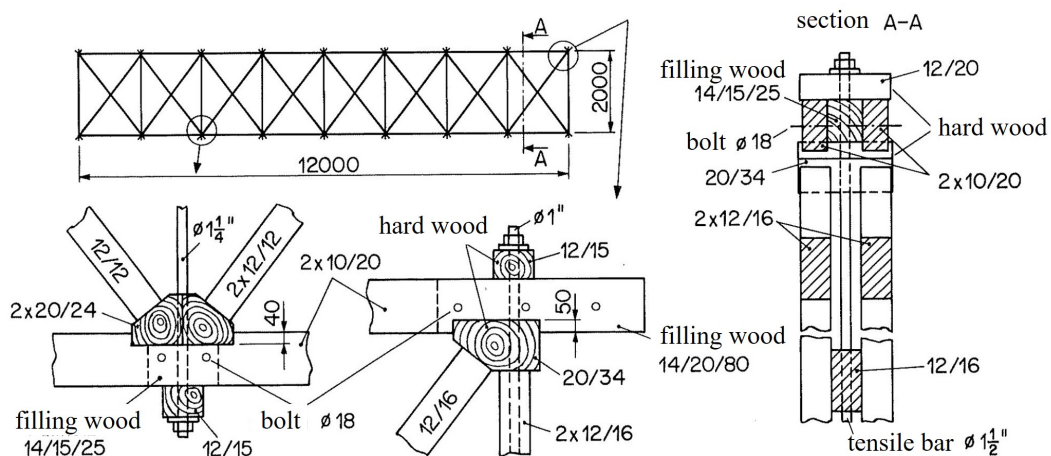


Fig. 2.8: HOWE's truss with vertical prestressed steel bars, translated from [52].

Since 1850 steel bolts have been used [48]. Later timber nails, mostly from oak, were used as pin-shaped connectors in tight-fitted predrilled holes. A logical derivation followed in the

usage of nails and pin-shaped connectors made of steel. [52] In the beginning of the 19th century several patents ("Meltzer-" and "Ambistifte") for a more economic application of pin-shaped bolts with tight-fitted predrilled holes were developed in the range of 8 to 12 mm diameter and tensile strengths of 800-900 MPa (Fig. 2.9) [48]. With the emergence of nails and the arrival of the dowel connections such as split ring dowels in Europe in the 1930s bolted connections were suppressed. This process was not due to supremacy of nailed connections but a different treatment of the two connection types in the codes. Nail connections were overestimated due to too favourable testing conditions, whereas the bolted connections were underestimated. [48, 52] In the 1940s nailed timber trusses were especially pushed in Germany for heavily loaded and wide-spanned timber bridges for road, rail and construction bridges. Their single elements were made from boards or planks and were jointed with double shear nail connections. Furthermore, the chord joints were made from nailed butt strap joints. Such structures usually were built with heights $h \geq l/10$ and global safety factors $v_B \geq 2.0$ for adequate stiffness and structural safety. Therefore, the belief was that no further analysis of the flexibility of the connections and its consequences for the load-deformation behaviour was necessary. The bigger deflections due to the connection deformations were compensated by cambering. [52, 97]

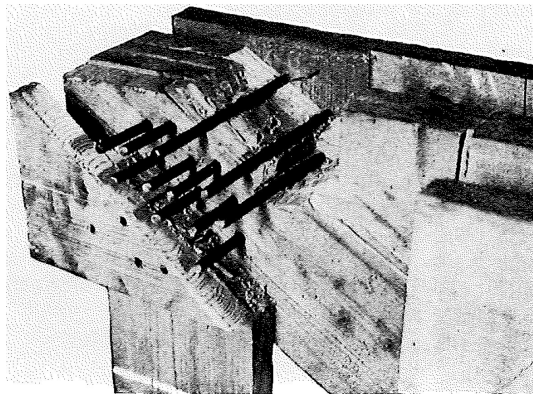


Fig. 2.9: Bolted connection with "Meltzer-Stifte" $d = 8$ mm [52].

Due to the development and usage of nails and glue in timber construction in the 1950s and 1960s, trusses with parallel chords were used more and more in simple building constructions. Within these applications the slenderness ratios (height-to-length ratio) of such trusses started to vary in a wide range. For trusses with small slenderness ratios, it was realised that the influence of the load-deformation behaviour of the beams and the connections could no longer be neglected. Furthermore, it was realised that the bending moments in continuous chords could not be neglected. In the German design code of that time different structures were already subjected to rules that demanded the consideration of the real connection behaviour. Therefore, investigations were conducted by Möhler (1966) [97], to derive similar rules for timber trusses.

Scheer & Golze (1981) [110] investigated the design of timber trusses under consideration of the continuous chords. For the calculation of the section forces finite element models were used with combinations of freely rotational nodes, rigid nodes, small beams representing eccentricities and linear elastic normal force springs representing the connections. The first model represents

the ideal truss with beams which carry only normal forces (Fig. 2.10). The calculations with continuous chords showed only 1-2% less normal forces and deflections but self-evidently there were considerable bending moments within the chords (Fig. 2.11). In combination with eccentrically jointed diagonals these bending moments increased further. The diagonals themselves were generally oversized due to large necessary connection areas. That is why their eccentric connections were not considered as problematic.

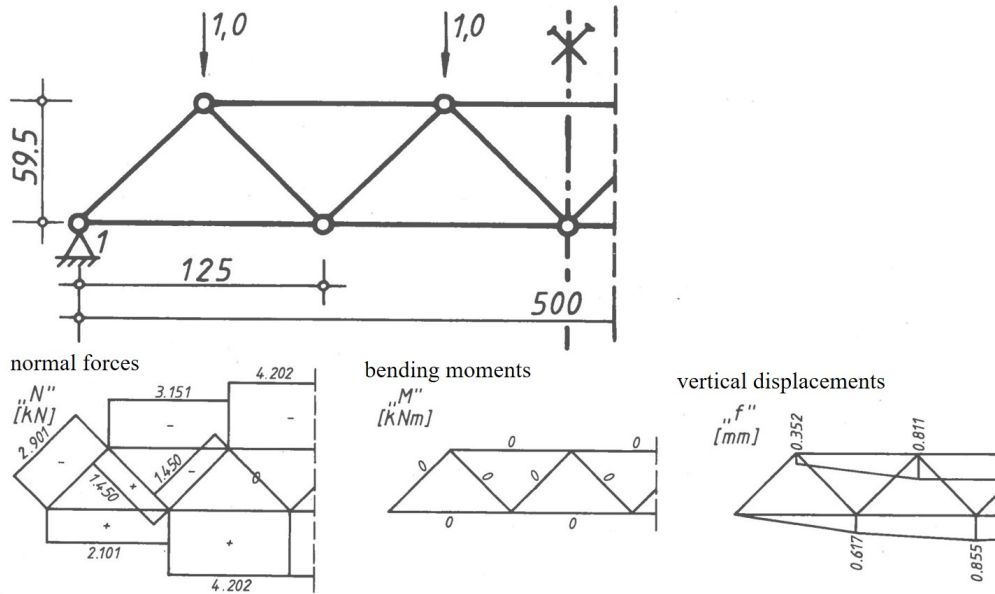


Fig. 2.10: Section forces and deflection of the ideal truss model, translated from [26, 110].

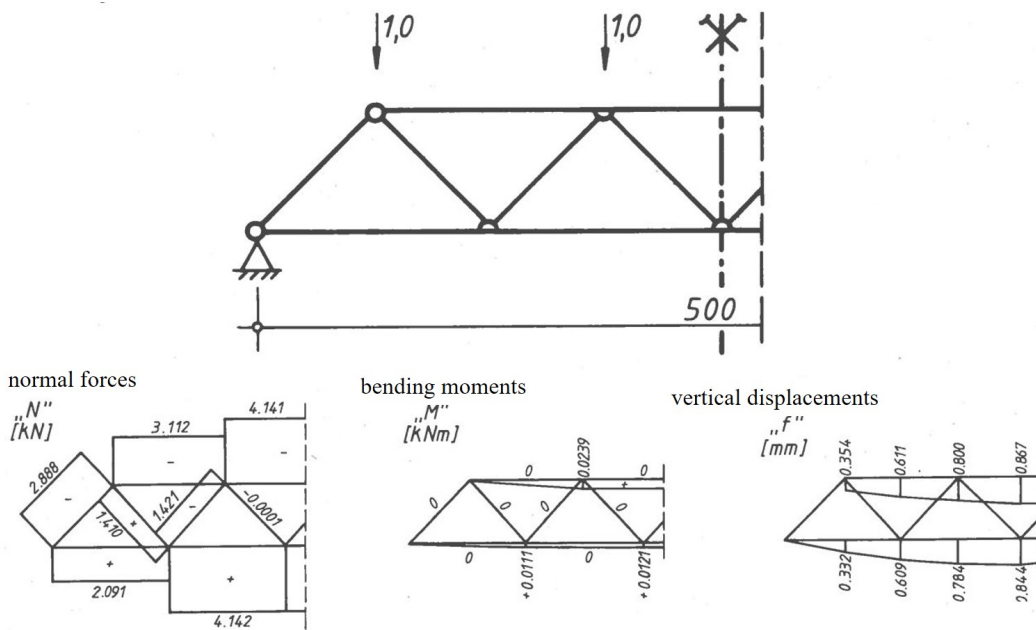


Fig. 2.11: Section forces and deflection of the truss model with ideal hinges but continuous chords, translated from [26, 110].

In Dubas et al. (1981) [26] it was stated that in practice only normal forces were considered, which were calculated under the assumptions postulated by Culmann (1866) [22]: For the calculation, the connections are replaced by friction-free hinges. Such a strong assumption can only be justified if the connections allow for a certain free rotation or if a local overstress from bending moments leads to a plastification without loss of resistance. There was an understanding that these prerequisites are not fulfilled for most timber trusses. In grain direction the slip behaviour and the initial stiffness of connectors were known but no systematic investigations about the bending behaviour of connections were conducted. This is why pinned and rigid moment-connections were assumed as lower and upper limits for further investigations.

Some single-dowel connections as bolts or split ring dowels obviously exhibit a low degree of clamping, which results only from friction along the connector and therefore the assumptions by Culmann are justified. For multi-connector connections the degree of clamping depends on the geometric layout as well as on the embedment behaviour (different load-to-grain directions). Therefore, for small connection areas and connectors with small diameters, a moderate bending stiffness can be assumed. As another extreme case glued butt strap joints are extremely stiff and therefore the assumption of rigid nodes is plausible. For laterally loaded dowel-type fasteners it was common knowledge that with slender dowels and larger spacings a certain plasticity within the connectors can be reached, however, such applications were not standard in practise. Another concern were constraint stresses within the connections, which lead to tension perpendicular to the grain. Tests were carried out (Fig. 2.12), which showed a decreasing load-carrying capacity in tension with increasing eccentricity, which induced additional bending moments, representing the constraint moments. It was estimated that representative bending moments for timber trusses lead to a reduction of the connection resistance of 10-15%. [26, 48]

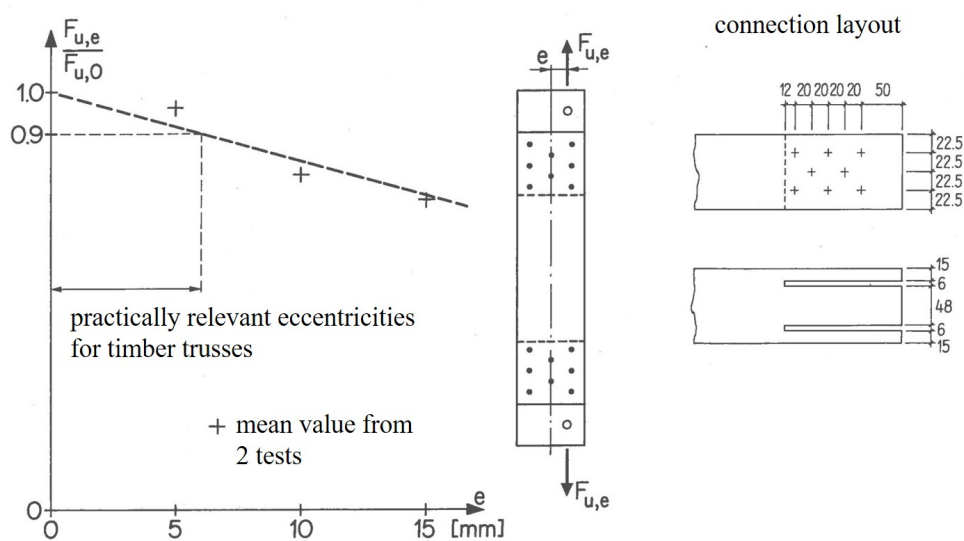


Fig. 2.12: Influence of the beam-end-moments on the connection resistance $F_{u,e}$ compared to the resistance without bending moments $F_{u,0}$, translated from [26, 48].

In Dubas et al. (1981) [26] a further evaluation of Möhler (1966) [97] revealed that for the given truss layout there are considerable differences in the overall stiffness due to different connection types (Fig. 2.13). The glued connection resulted on average (non-linear behaviour) in a 15% lower and the nail connection in a 25% lower stiffness in comparison to the rigid model. These lower stiffnesses come with higher deflections, which lead to bigger bending moments in the continuous chords. In Fig. 2.14 the corresponding model with continuous chords and normal force springs is shown.

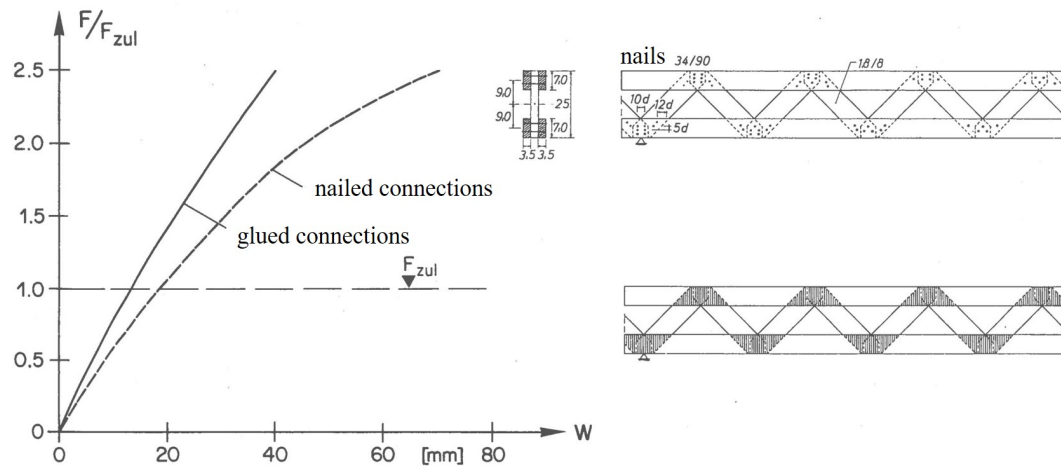


Fig. 2.13: Load-deformation-diagram from tests on Trigonit-trusses with nailed and glued connections, translated from [26].

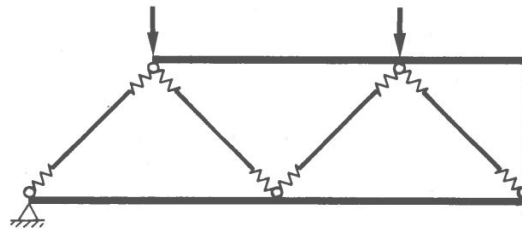


Fig. 2.14: Model with continuous chords and normal force springs [26].

The best possible model was recognised to be one that additionally includes springs, representing the bending stiffness of the connections (Fig. 2.15). In contrast, the actual spring stiffness was unknown. Experiments with slotted-in steel plates and steel dowels as connectors were conducted by [26, 51], which revealed that on the load level of the serviceability limit state (SLS) rigid behaviour was a good assumption. Furthermore, a general understanding was gained that the influence of the connection stiffness is highly relevant for trusses with parallel chords but less relevant for triangular trusses. For triangular ones, the web members are of secondary importance and mainly support load introduction points. For trusses with parallel chords, they have a primary function and therefore the connection stiffness with resulting bending moments are of high importance. System slenderness and beam dimensions are important concerning the deflections and section forces: the smaller the slenderness of the system, the more deflections and

hence, larger bending moments; the bigger the cross-sections of the chords, the more bending stiffness and therefore larger bending moments. [26]

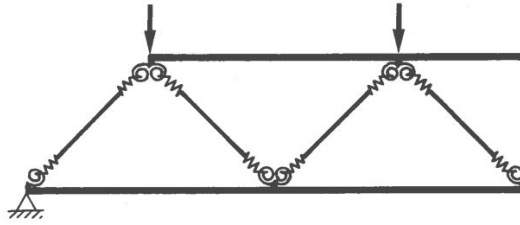


Fig. 2.15: Model with continuous chords and normal force and moment springs [26].

From all these considerations design rules were derived. Basically, the real behaviour of all elements needed to be accounted for. Continuous chords should be modelled as such and the flexibility of the connections should be considered according to slip moduli from the code. Due to lack of knowledge of the bending stiffness of connections this should be simplified to either pinned or rigid nodes. [26]

Alternatively, a simplified calculation according to Culmann or Ritter with pinned, indeformable nodes was presented in [26] for trusses with chord heights smaller than $1/7$ of the system height. To compensate the missing bending moments induced from the chord deformation, the capacity of the chords had to be reduced by $1/3$. The capacity of the diagonals and their connections did not have to be reduced. This rule could only be applied to trusses with connections with rather flexible or pin-like connections and therefore not for dowelled steel-to-timber connections. The overall truss deflection had to be limited to $2/3$ of the allowable deformation to account for the negligence of the connection flexibility. As a basis for the derivation of the reduction factors the model from Fig. 2.14 was used. [26]

In Gehri et al. (1982) [51] tests with trusses from European beech (*Fagus sylvatica* L.) and Norway spruce (*Picea abies* L.) with connections with pin-shaped bolts and slotted-in steel plates were evaluated. From this investigation it was concluded that for the simplified design approach the connection itself and the connection area in the diagonals should be designed with reduced resistances. In accordance with [48] (Fig. 2.12) for trusses with stiff connections like dowelled steel-to-timber connections, a reduction of the connection resistance of 15-20% should be selected. As in previous investigations, the connections showed a non-linear load-deformation behaviour. It was stated that these non-linearities can reduce for example the induced bending moments in the diagonals but then lead to increased bending moments in the chords. This is why the above-mentioned reduction of the resistance of the chords to $2/3$ was acknowledged, although a more favourable value of 0.75 was found from the experiments. The above-mentioned reduction of the deformation on the level of service loads could be confirmed in the tests.

Regarding the wood species European beech GLT clearly shows higher load-carrying capacity, which allows for more slender chords and web-members in comparison to an equally loaded truss of the same layout from Norway spruce. This higher slenderness brings the advantage of less bending moments due to the truss deformation, which allows for a better section utilisation. [51]

The stability of trusses and their elements were addressed in Dubas et. al (1981) [26] holistically. In-plane, generally the buckling length is chosen equivalent to the length between the truss nodes. Due to certain clamping effects of the connections this length theoretically could be reduced. However, this reduction is not relevant since the buckling out-of-plane is decisive in the vast majority of the cases. Out-of-plane the buckling lengths depend on the arrangement as well as on the stiffness of the lateral support system. If all nodes of the beams under compression are supported rigidly enough, the buckling length can be chosen to the length between the nodes, similar as in-plane.

Cross-section reductions from holes for connectors under compression forces usually are not critical concerning the load bearing capacity, since they are filled with stiffer material. The issue of stability is much more pronounced though. Slots for steel plates lead to a massive reduction of the bending stiffness out-of-plane. Chords as well as web members can be affected. The longer the slots are, the more relevant this reduction of the bending stiffness is. The second influencing factor is the distance between the slots, which should be chosen as large as possible. A simplified modelling approach is to determine an equivalent cross-section in the connection area according to Fig. 2.16 and to consider this weakening appropriately in the buckling resistance. Further, the steel plates need to be thick enough for transferring the loads without buckling. [26]

The weakening of the joint areas of beams with respect to out-of-plane stability can be considered as a necking. According to Tölke (1929) [128] this necking can be treated as a reduction of the critical buckling resistance according to Euler. For a given layout of the connection the ratio of the moments of inertia as well as the ratio of the joint-length to the beam-length can be calculated and the reduction factor φ can be selected according to Fig. 2.17. As a conservative simplification this factor φ could be used on the buckling-load according to the codes directly [26].

Considering continuous chords with partial connection to the lateral stiffening system, different cases need to be investigated. The first case is the symmetric buckling over the full length between the lateral supports, which is illustrated in Fig. 2.18. The mid connection is exactly in the midpoint of the buckling beam, where the shear force is zero. This is why the beam can be assumed to have a continuous full bending stiffness over its length (the so-called Steiner portion of the moment of inertia can be taken into account). Only at its ends the reduction due to the slots is important. The second case is the antisymmetric buckling, with a buckling length corresponding to the length between two truss nodes. In this case, the reduction of the bending stiffness out-of-plane due to the slots needs to be considered at both beam ends. Further, in Fig. 2.18 the buckling length of a diagonal is illustrated, which corresponds to the length between the truss nodes.

In Gehri (1983) [49] findings of [51] are discussed further and summarised. Only parallel chord trusses were used in the tests, since the joints were of interest. For triangular shaped trusses the web members and therefore the connections represent merely a support system for the load introduction points. Nevertheless, the results should be applicable to triangular trusses as well. All possible failure modes of timber trusses with dowelled steel-to-timber connections

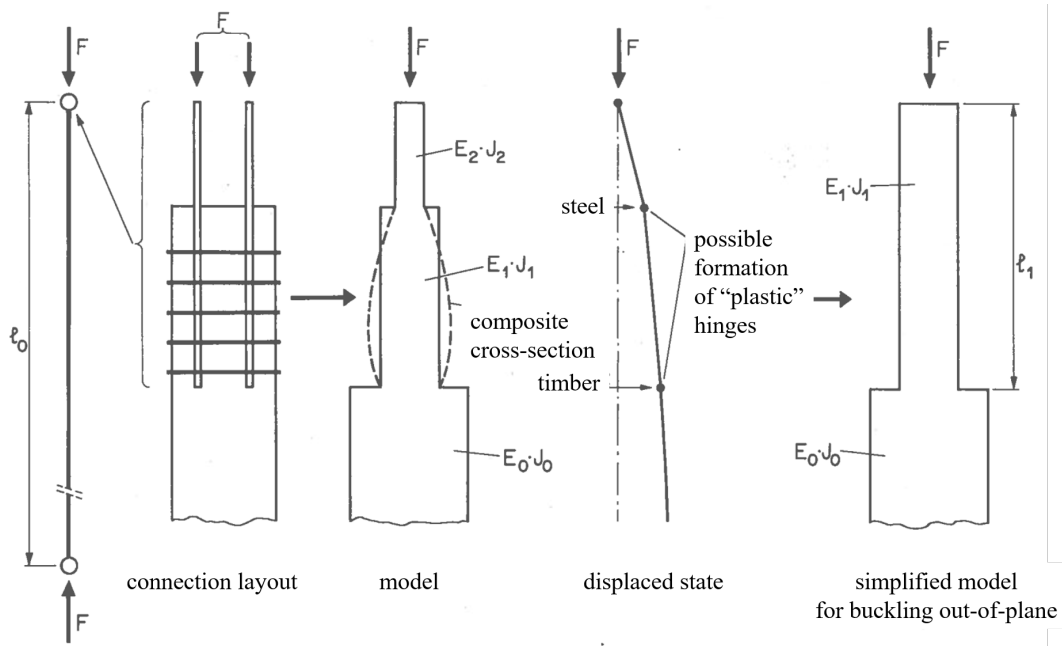


Fig. 2.16: Simplified model for beams under compression with reduced bending stiffness out-of-plane in the connection area, translated from [26].

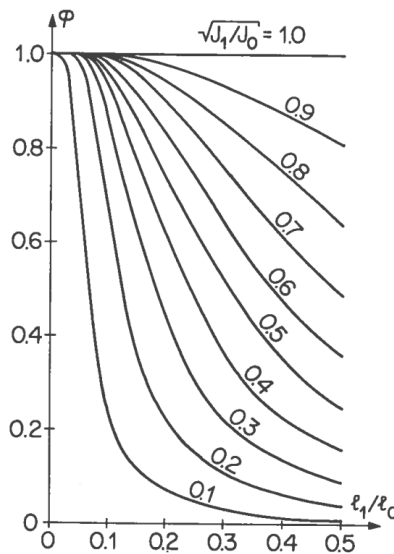


Fig. 2.17: Reduction factor of buckling resistance due to slots in connection area [26].

observed in a test series conducted by [49] are presented in Fig. 2.19 and are summarised in the following list:

- Chords under compression: global stability out-of-plane and local buckling due to slots for steel plates.
- Chords under tension: net-cross-section failure due to slots for steel plates and holes for connectors.

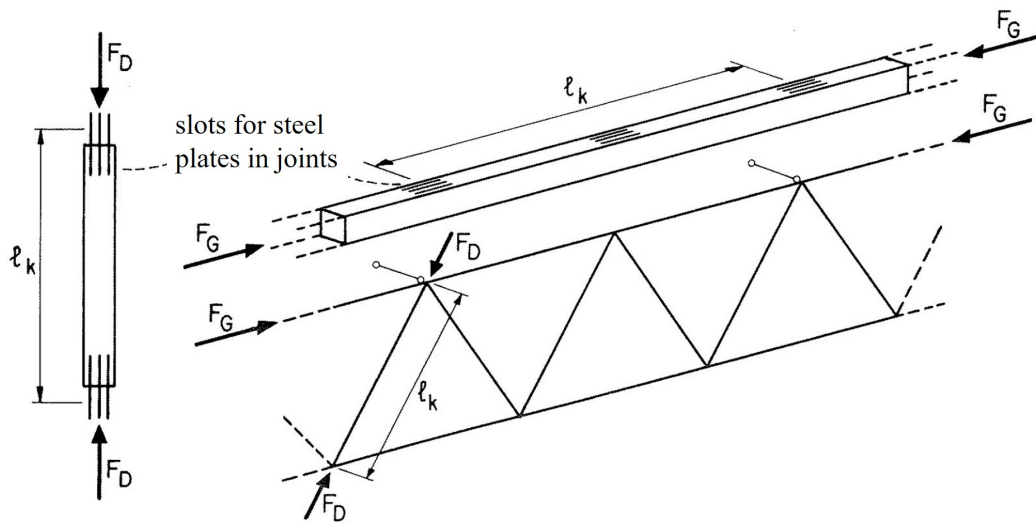


Fig. 2.18: Buckling length for symmetric buckling of the chord with lateral support at every second node and buckling length of a diagonal, translated from [26, 51].

- Diagonals under compression: failure in net-cross-section and local buckling due to slots for steel plates.
- Diagonals under tension: net-cross-section failure due to slots for steel plates and holes for connectors.
- Connectors: embedment failure or other failure modes within the timber, rarely failure in the connector.
- Node plates from steel: buckling (tension, shear and embedment failure can be dealt with easily).
- Node plates from cross-laminated veneer lumber: tension-shear failure.

Concerning the truss joint system, the following was pointed out: (1) thin connection plates are of immense concern because of buckling issues; (2) the usage of thick plates may weaken the timber part in such a way that the overall load bearing capacity may not be enhanced; (3) the distance between the plates should be large enough; and (4) long connections compromise the buckling behaviour. [49]

The above-mentioned considerations only take into account forces acting in the truss nodes. If load introduction points exist between truss nodes, these forces should be taken into account additionally. [26, 49] propose to calculate the section forces from these loads with the model of a multi-span beam on fixed supports. Finally, the utilisation of the stresses from bending and the utilisation due to the simplified calculation from the normal forces with the reduction of the resistance can be superimposed.

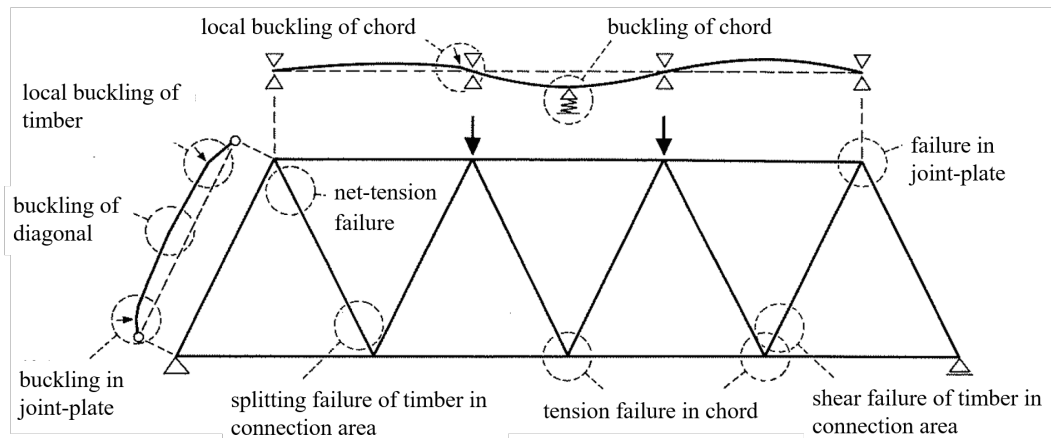


Fig. 2.19: Observed failure modes in tests on timber trusses with dowelled steel-to-timber connections conducted by [49] (translated).

2.3.3 Design of timber trusses according to SIA 265

2.3.3.1 Calculation of section forces and displacements

According to the Swiss Standard for the design of timber structures SIA 265:2021 [121], timber trusses generally have to be considered as frames with connections with an inherent stiffness. The influence of eccentricities in the joints and in the support areas as well as loads which do not act in truss nodes have to be considered.

Under certain prerequisites, the calculation of the member forces can rely on a simplified approach with the assumptions from Culmann: The connections in the truss joints are replaced by friction-free hinges. Therefore, only normal forces need to be considered. [26, 121]

According to SIA 265:2021 [121] these prerequisites are the following:

- continuous chords (possible joints rigidly connected)
- centred beams (trusses from triangles)
- loads act in truss nodes (otherwise this additional loading has to be account for)
- the chord height has to be smaller than $1/7$ of the medium truss height.

2.3.3.2 Dimensioning of the truss components

According to SIA 265:2021 [121] for the dimensioning of the components the normal forces, shear forces and bending moments have to be considered. If the analysis is done with the above-mentioned simplified approach with only normal forces, the load-carrying capacities need to be reduced accordingly. The following requirements are listed in SIA 265:2021 [121]:

- The load-carrying capacity of the chords under in-plane actions has to be reduced to $2/3$.

- The load-carrying capacities of all connections and the wood in the connection areas of the web members have to be reduced; for connections with high bending stiffness the reduction factor is specified to 0.75.
- The calculated deflections have to be limited to $2/3$ of the allowable deflections.

2.3.4 Design of timber trusses according to Eurocode 5

2.3.4.1 Calculation of section forces and displacements

According to the European Standard for the design of timber structures EN 1995:2004 [31], the calculation of the section forces should be done with models for frame structures. For frame structures, the deformations of the beams and connections, as well as eccentricities and the stiffness of the substructure have to be considered.

Alternatively, for trusses with connections from nail plates a simplified design approach is applicable. It can be applied if some geometric prerequisites are fulfilled. Concerning the truss height two rules exist: The height of the truss has to be larger than 15% of the span width, and it has to be higher than 10 times the chord height. Under those assumptions the calculation of the normal forces can be conducted with friction-free hinges in the truss nodes.

2.3.4.2 Dimensioning of the truss components

According to EN 1995:2004 [31] for trusses in which the forces act mainly in the nodes the combined ratios of the stresses from bending and normal forces have to be smaller than 0.9.

If trusses with nail plate connections are designed with the simplified approach, there are certain requirements: several rules concerning buckling length exist; and if the loads act only in the truss nodes, the utilisation level of the normal force resistance has to be reduced to 70%.

2.4 Load-carrying capacity and load-deformation behaviour of dowelled steel-to-timber connections

2.4.1 Introduction

Nowadays, the design of connections is mostly based on the load-carrying capacity only. The actual load-deformation behaviour is not considered explicitly and an implicit consideration mostly concerns aspects of ductility. The Eurocode 5 and other standards provide equations for the initial stiffness relevant for the serviceability limit states (SLS) or simplified approaches to estimate the deformations in the ultimate limit state (ULS). As shown below, these provisions are vague though.

Therefore, and since the focus within the scope of this thesis is on the overall structural behaviour and not on the connection behaviour, only a limited overview is provided here. For a deeper insight into the development of today's design concept, the interested reader is referred

to [72] and [80]. Later in this thesis the actually implemented connection behaviour will be explained.

2.4.2 Load-carrying capacity of dowelled steel-to-timber connections

2.4.2.1 Load-carrying capacity of single-dowel connections

The load-carrying capacity of single-dowel connections can be calculated according to the design framework presented in EN 1995-1-1:2004 [31], the so-called European Yield Model (EYM) [72], which is based on the findings presented by Johansen (1949) [74]. It considers different failure modes, which are based on the type of failure within the single elements of the connections, i.e. the timber members and the steel dowels. Basically, a series system consisting of the capacity of each part is considered and the weakest link reveals the load-carrying capacity of a specific connection layout of a single fastener.

The capacity within the timber members is limited by the embedment strength. The capacity within the steel dowels is limited by its plastic bending capacity. Blaß et al. (2001) [8] stated that in actual connections a full plastification cannot be reached, which would require a bending angle in the plastic hinges of 45° . They proposed an equation which takes into account the tensile strength of the fastener instead and corresponds to a dowel-deformation of 15 mm. This equation is the one used in the design approach applied in EN 1995-1-1:2004 [31] and SIA 265:2021 [121]. In [121] the characteristic plastic bending capacity in [Nmm] of a dowel is specified to:

$$M_{u,k} = 0.3 f_{u,k} d^{2.6}, \quad (2.1)$$

where $f_{u,k}$ is the characteristic ultimate tensile strength of steel and d the dowel diameter.

In SIA 265:2021 [121] a simplified approach based on the same mechanics is used. This approach provides equations to determine the minimum thickness of the different timber members in order to reach a specified failure mode. These minimum thicknesses are determined by the embedment strength and the fastener bending capacity, as explained above. The side members can show three different failure modes, i.e. mode I: timber failure, mode II: mixed failure and mode III: failure in the steel dowel (Fig. 2.20). The middle members show only mode I or III failure (Fig. 2.21).

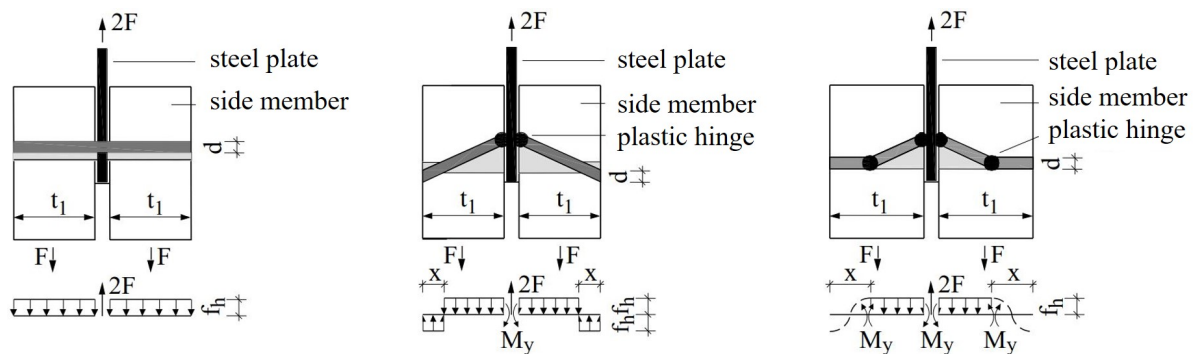


Fig. 2.20: Failure modes I (left), II (middle) and III (right) in side members, translated from [32].

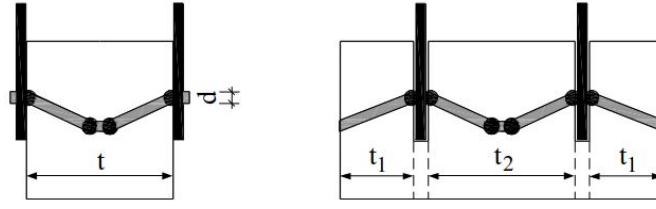


Fig. 2.21: Failure mode III in middle members [32].

The embedment strength depends on the wood density and the dowel diameter only. The dowel capacity depends as well on the dowel diameter and as explained above on the tensile strength. Therefore, it can be summarised that the load-carrying capacity and the corresponding failure modes I-III of a single-dowel connection only depend on the density of the timber, the tensile strength of the dowel, the dowel diameter and the timber member thicknesses. In SIA 265:2021 [121] for solid timber and GLT made from softwood the following equation is provided to calculate the embedment strength parallel to the grain for connections with pre-drilled holes in N/mm^2 :

$$f_{h,0,k} = 0.082 (1 - 0.01 d) \rho_k, \quad (2.2)$$

where d is the dowel diameter and ρ_k is the characteristic density of the timber product. The embedment strength perpendicular to the grain of pre-drilled holes in softwood is also provided in [121] in relation to the embedment strength parallel to the grain:

$$f_{h,90,k} = \frac{f_{h,0,k}}{1.35 + 0.015 d}. \quad (2.3)$$

For load-to-grain angles between 0 and 90° , a linear interpolation between the respective values parallel and perpendicular to the grain is specified.

The design approach provided in SIA 265:2021 [121] emphasises the compatibility between the failure modes of the side and middle members by prescribing that middle members need to be at least twice as thick as side members and that side members have to be at least 35% as thick as middle members. Further, in the practical guidelines [63], it is explicitly recommended not to use connections that fail in mode I.

For side members mode II can be reached with a member thickness of:

$$t_{1,1} = 0.89 \sqrt{\frac{f_{u,k}}{f_{h,k}}} d^{0.8}, \quad (2.4)$$

where $f_{u,k}$ is the characteristic ultimate tensile strength of the steel dowel, $f_{h,k}$ the characteristic embedment strength of the wood and d the dowel diameter. This leads to the factor:

$$k_{\beta 1,1} = 1.2. \quad (2.5)$$

Side members reach mode III with a member thickness of:

$$t_{1,2} = 2.52 \sqrt{\frac{f_{u,k}}{f_{h,k}}} d^{0.8}, \quad (2.6)$$

which leads to:

$$k_{\beta 1,2} = 2. \quad (2.7)$$

As explained above, middle members show only mode I and III failure. To reach mode III they need a member thickness of:

$$t_{2,2} = 2.52 \sqrt{\frac{f_{u,k}}{f_{h,k}}} d^{0.8}, \quad (2.8)$$

which leads to:

$$k_{\beta 2,2} = 2. \quad (2.9)$$

2.4.2.2 Load-carrying capacity of multi-dowel connections

When using multiple dowels in a connection, for both design approaches according to EN 1995-1-1:2004 [31] and SIA 265:2021 [121] minimal spacings and edge distances are provided to implicitly guarantee the formation of the intended failure modes. Still, in dependence of the spacings between the dowels, a connection cannot reach the pure multiple of the number of dowels times the load-carrying capacity of a single dowel. Therefore, a reduction factor in dependence of the spacing between the dowels on one axis is applied:

$$k_{red} = n^{-0.1} \sqrt[4]{\frac{a_1}{10d} \frac{90^\circ - \alpha}{90^\circ} + \frac{\alpha}{90^\circ}}, \quad (2.10)$$

where $k_{red} \leq 1.0$. n is the number of fasteners in a row along the grain, a_1 is the distance between the dowels parallel to the grain, d is the dowel diameter and α is the load-to-grain angle. The resistance of a full connection can then be calculated with:

$$R_{d,con} = k_\alpha k_{red} n_{tot} p k_\beta \sqrt{M_{u,k} f_{h,k} d}, \quad (2.11)$$

where the safety factor $k_\alpha = 0.73$, k_{red} is the reduction factor for the dowels in a row, n_{tot} is the total amount of dowels in the connection, $p k_\beta$ corresponds to the sum of the products of the factors k_β per shear plane with the respective number of shear planes, $M_{u,k}$ is the characteristic value of the plastic bending capacity of a dowel, $f_{h,k}$ the characteristic embedment strength and d is the dowel diameter.

2.4.2.3 Limitation of the approach

The limitation of this approach comes with its validity being restricted to uni-axial loading situations. Complex loading situations cannot be taken into account. This is why in both simplified design approaches for timber trusses presented in Sec. 2.3.3 and 2.3.4 global reduction factors are applied due to additional bending moments and shear forces in the connections.

Furthermore, the latest approaches for an enhanced estimation of the brittle failure modes, which will most likely find their way into the new generation of Eurocodes, only consider uni-axial loading [19, 20].

So-far no well-established model to determine the load-carrying capacity of dowelled steel-to-timber connections under complex loading exists. Hochreiner et al. (2016) [62] presented a step in this direction by discussing the failure of the timber matrix around the dowels by means of stress analysis with finite element models. The above-presented global reduction approach in dependence of the eccentricity presented by Gehri (1980) [48] (Fig. 2.12) is based on one connection layout only. Still, it seems to be the only available analytical approach to take into account the effect of bending moments in a loading situation dominated by normal forces how they occur in trusses.

2.4.3 Load-deformation behaviour of dowelled connections

2.4.3.1 Load-deformation behaviour of single-dowel connections

According to EN 1995-1-1:2004 [31] the slip modulus K_{ser} per shear plane and per fastener under service load can be calculated with Eq. 2.12:

$$K_{ser} = \rho_m^{1.5} d / 23. \quad (2.12)$$

For steel-to-timber connections the value may be multiplied by 2.0.

SIA 265:2021 [121] specifies the slip modulus K_{ser} for steel-to-timber connections per shear plane and per fastener under service load in dependence of the load-to-grain angle according to Eq. 2.13 and 2.14:

$$K_{ser,0} = 6\rho_k^{0.5} d^{1.7} \quad (2.13)$$

$$K_{ser,90} = 3\rho_k^{0.5} d^{1.7}. \quad (2.14)$$

For angles between 0° and 90° a linear interpolation is proposed.

The main difference in both approaches are the coefficients and exponents on the density ρ and the dowel diameter d . Further, in Eq. 2.12 for the density the mean value ρ_m is applied, where in Eq. 2.13 and 2.14 for the density the characteristic value ρ_k is specified.

2.4.3.2 Load-deformation behaviour of multi-dowel connections under lateral loading

Jockwer & Jorissen (2018) [73] discussed the load-deformation behaviour and stiffness of lateral connections with multiple dowel-type fasteners. It was concluded, that the approach to determine the stiffness provided in EN 1995-1-1:2004 [31] is vague and inaccurate when comparing to test data and that different standards suggest different equations. The following recommendations with regard to design were made [73]:

- "The fastener diameter shows a larger impact on the stiffness of a connection compared to the value currently given in EC5.
- A linear impact of the number of fasteners in a row can be assumed if sufficient member thickness, spacing and distances is satisfied.

- For connections without or with low ductility (embedment failure modes and brittle failure modes) the 5 and 95 percentile fractiles of K_{ser} , respectively, should be used.
- For connections with high ductility either K_u (slip modulus per shear plane and per fastener under ultimate loading conditions) can be used or the ductility is considered directly (linear elastic - ideal plastic behaviour with ultimate deformation).
- The failure mode with plastic hinges in the fastener should serve as the reference when specifying stiffness values."

Jockwer & Jorissen (2018) [73] conducted investigations of the stiffness of dowelled timber-to-timber connections and proposed to apply regression functions in the form of power functions with more parameters than only the timber density and the dowel diameter. They additionally used the number of fasteners in a row, the number of rows of fasteners and the relative thickness of the timber members (i.e. the ratio of the timber member thickness and the dowel diameter).

2.4.3.3 Load-deformation behaviour of multi-dowel connections under complex loading

Schweigler et al. (2018) [115] presented a semi-analytical approach to describe the load-deformation behaviour of multiple dowel connections under complex loading, i.e. normal force, shear force and moment in-plane, based on the load-deformation behaviour of single dowels. It relies on vector addition and can be implemented in any beam-based finite element software as a subroutine. A simplification of the real behaviour is implemented in the form of a linearisation of the circular displacement path. A further necessary simplified assumption is, that the steel plates and the timber members are considered as perfectly rigid. In the publication all necessary equations for the implementation are presented nicely. Hence, here only the flow chart of the work-flow is presented (Fig. 2.22). Basically, the model needs the connection geometry, the loading of the connection in the form of displacements per degree of freedom and the load-deformation behaviour of the single dowels as input. Then, through vector addition the dowel displacements for all single dowels are calculated and hence, the corresponding load can be read from the load-deformation plane, which might include the anisotropic behaviour. From this load distribution the internal forces of the full connection can be determined. Finally, the procedure allows to compute the tangential stiffness matrix, which is needed for the implementation as a subroutine. This approach even allows modelling contact by means of discretised contact lines in the form of additional dowels with a coherent load-deformation behaviour.

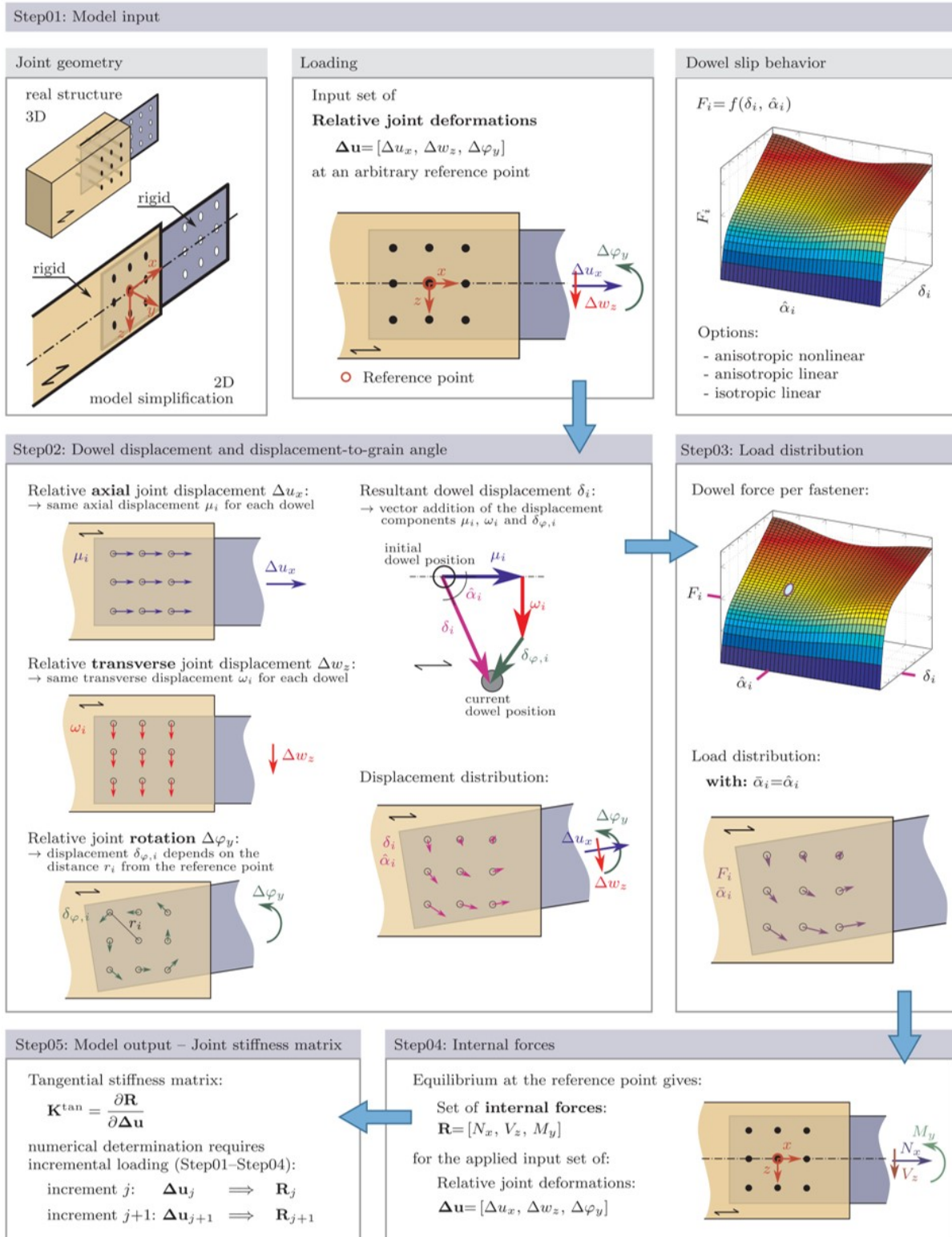


Fig. 2.22: Flow chart of the calculation procedure for the joint model according to [115].

2.5 Structural reliability

2.5.1 Introduction

2.5.1.1 Principle of structural reliability

Structural systems need to provide specific functionality under well-defined safety constraints. During the design phase of the system, such constraints need to be taken into account in view of the expected loads. The physical properties of a system as well as the respective loads are subjected to uncertainties and when a system encounters unexpected conditions a failure will occur. Structural reliability analysis aims at quantifying the probability of occurrence of such failures. [82, 92]

2.5.1.2 Evolution of safety checking

Historically, structural design codes were based on professional experience, judgement and intuition. In the 19th century formal structural calculations came up and with it the use of factors of safety. These factors aimed at ensuring safe and serviceable performance. [28]

These early design methods were based on the elastic behaviour and took the form of the so-called allowable stress design (ASD). It was based on a conservative selection of the load magnitudes based on which stresses were calculated. These stresses then were compared to a fraction of the limiting stress at which failure occurs in yielding, fracture, buckling, etc. The following equation represents this ASD format:

$$\sigma \leq F_k/FS, \quad (2.15)$$

where σ represents the stress due to the applied forces, F_k represents the limit stress and FS is the factor of safety. Uncertainties on both load and resistance are taken into account by this factor FS. [28]

For codification purposes and facility in design, it was desirable to uncouple loads and resistances though [28]. Indeed, in the 1970s-1980s a reliability-based code calibration was formulated and the so-called load and resistance factor design format (LRFD) replaced the ASD [82]. In the LRFD the limit state can be expressed as follows:

$$\frac{z_d r_k}{\gamma_M} = \gamma_G s_{G,k} + \gamma_Q s_{Q,k} + \dots, \quad (2.16)$$

where r_k is the characteristic member resistance, γ_M is the partial factor on r_k and $s_{G,k}$ and $s_{Q,k}$ are the characteristic dead and live load effects. γ_G and γ_Q are the respectively associated partial factors to the loads and z_d is the design variable, e.g. the cross-sectional area. The corresponding characteristic values represent a certain fractile value of the underlying distributions of the variables and are given in the design codes. [82]

The transition between these code formats was done with a so-called *soft-calibration* of the new codes. This means, that the reliability level for the new codes was partly chosen in a way that only minor differences in the design variables occurred. It was recognised, that the experience of

the years revealed an acceptable level of safety and therefore this smooth transition was possible. [41]

The LRFD approach is also called semi-probabilistic design format. For more information about this approach and how to calibrate partial safety factors, the interested reader is referred to [82]. For practitioners it is a very useful approach, since the designer can treat a structure in a deterministic way, which only needs one set of input parameters. However, it comes with a certain degree of conservatism and for more complex analyses the codes should provide more than only characteristic values. The actual probability of failure of the structural system is unknown, but assumed not to be smaller than the reliability of its components. Further, system effects on the levels of assemblies and structures are generally neglected.

In contrast to those generalised approaches, a direct estimation of the probability of failure of structural systems is also possible. For the evaluation the same abstract representations of the structural systems can be used, e.g. analytical or finite element models. The input variables are described statistically. However, it is not possible to evaluate statistical data within such models. This is why methods of structural reliability are applied directly, which propagate the probabilistic input through the model and evaluate the reliability of the modelled structure. [125]

Until recently, the usage of such probabilistic methods for the evaluation of complex structures was not feasible due to time constraints. The recent development of enhanced reliability assessment methods along with performance improvements of computers allows the evaluation of more complex models. For research and codification purposes these methods have huge potential. It seems even possible, that they will allow a direct usage in common design in the near future.

2.5.2 Problem statement

2.5.2.1 Limit-state function

The performance of a system can be satisfactory or not. A limit state describes the ultimate satisfactory performance of the system regarding a certain criterion. In a two-dimensional case one can think of two domains, a safe domain and a failure domain. The two are separated by a discrete line which describes the limit state. [92]

The state of a system can be represented by a random vector of variables $\mathbf{X} \in D_{\mathbf{X}} \subset \mathbb{R}^M$, where $D_{\mathbf{X}}$ is the state space and \mathbb{R}^M are the real numbers in each dimension. Then, the safe and the failure domains are defined as $D_s, D_f \subset D_{\mathbf{X}}$. This means that if the current state $\mathbf{x} \in D_s$ the system is operating safely and otherwise unsafely if $\mathbf{x} \in D_f$. [92]

Limit states are generally associated with a *demand* parameter S (e.g. a load effect or Stress) and a *capacity* (or Resistance) R [125]. In terms of realisations \mathbf{x} of the random vector of variables \mathbf{X} the limit state function then reads [37]:

$$g(\mathbf{x}) = r - s. \tag{2.17}$$

The limit-state function $g(\mathbf{X})$ assumes positive values in the safe domain and negative values in the failure domain [92]:

$$\begin{aligned} \mathbf{x} \in D_s &\iff g(\mathbf{x}) > 0 \\ \mathbf{x} \in D_f &\iff g(\mathbf{x}) \leq 0. \end{aligned} \tag{2.18}$$

As described above, between the two domains in a two-dimensional case there is a line representing the boundary or the limit state. In M dimensions the hypersurface defined by $g(\mathbf{X}) = 0$ is called limit-state surface. Fig. 2.23 shows a graphical representation of these explanations with respect to two dimensions. [92]

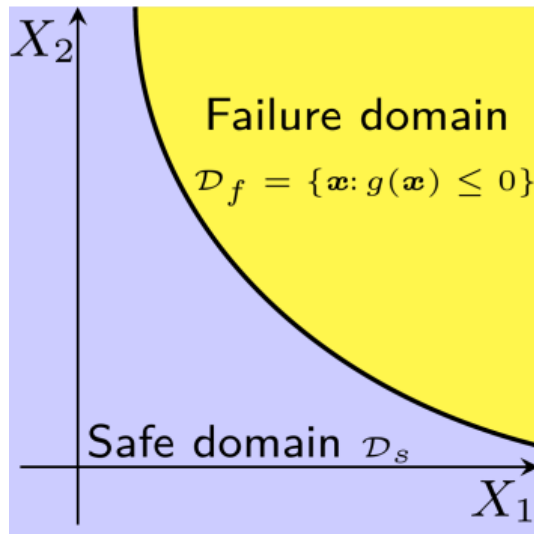


Fig. 2.23: Safe and failure domains D_s and D_f with the corresponding limit-state surface $g(\mathbf{x}) = 0$ in the case of a schematic two dimensional representation [92].

In civil engineering typically two different limit states are considered. One is the so-called serviceability limit state (SLS), which e.g. deals with deformation or vibration problems. The other one is the so-called ultimate limit state (ULS), which typically deals with stability and rupture issues. [37]

2.5.2.2 Probability of failure

The *probability of failure* is defined by the probability that the random vector of state variables \mathbf{X} belongs to the failure domain. Usually the following notation is used [125]:

$$P_f = \mathbb{P}(g(\mathbf{X}), M(\mathbf{X})) \leq 0), \tag{2.19}$$

where \mathbb{P} characterises a probability and $M(\mathbf{X})$ the model of interest.

Under the assumption of independent and uniformly distributed input variables the following ratio together with Fig. 2.23 explains the probability of failure in a very intuitive way [125], i.e. the area of the failure domain D_f is divided by the entire domain $D_{\mathbf{X}}$:

$$P_f = \frac{\text{Area}(D_f)}{\text{Area}(D_{\mathbf{X}})}. \tag{2.20}$$

The random vector of the state variables \mathbf{X} is described by a joint probability density function (PDF) $\mathbf{X} \sim f_{\mathbf{X}}(\mathbf{x})$. Therefore, P_f can be calculated as follows:

$$P_f = \int_{D_f = \{\mathbf{x}: g(\mathbf{X}, M(\mathbf{X})) \leq 0\}} f_{\mathbf{X}}(\mathbf{x}) d\mathbf{x}. \quad (2.21)$$

The dimension of this integral is equal to the number of basic input variables $M = \dim \mathbf{X}$. The domain of integration is not known explicitly: It is defined by a condition related to the sign of the limit state function, which depends itself on the basic variables through a (potentially complex) computational model. [125] This limitation can be circumvented by introducing an *indicator function of the failure domain*:

$$\mathbf{1}_{D_f}(\mathbf{x}) = \begin{cases} 1 & \text{if } g(\mathbf{x}, M(\mathbf{x})) \leq 0 \\ 0 & \text{if } g(\mathbf{x}, M(\mathbf{x})) > 0 \end{cases}, \quad \mathbf{x} \in D_{\mathbf{X}}. \quad (2.22)$$

This allows one to cast Eq. 2.21 as follows:

$$P_f = \int_{D_{\mathbf{X}}} \mathbf{1}_{D_f}(\mathbf{x}) f_{\mathbf{X}}(\mathbf{x}) d\mathbf{x} = \mathbb{E}[\mathbf{1}_{D_f}(\mathbf{X})], \quad (2.23)$$

where $\mathbb{E}[\cdot]$ is the expectation operator with respect to the PDF $f_{\mathbf{X}}(\mathbf{x})$. Therefore, the calculation of P_f reduces to the estimation of the expectation value of $\mathbf{1}_{D_f}(\mathbf{X})$. [92]

The reliability of the structure is defined by $1 - P_f$. It can also be expressed with the reliability index $\beta = -\Phi(P_f)$. [39, 125]

2.5.3 Methods of structural reliability

2.5.3.1 General remarks

Some of the following methods are general approaches, which can be applied in various fields and for different purposes. In structural reliability they are used to solve the integral in Eq. 2.21. Uncertainties in the input variables are propagated through a model and from the model responses the probability of failure is calculated. Mathematically closed form solutions are only possible in special cases, e.g. when both the demand and the resistance variables are Gaussian distributed. [125, 126]

In the general case the different input variables follow different distribution types and the models in use are not analytical but e.g. finite element models. These models can be evaluated for one set of parameters at once. Therefore, the methods of structural reliability consider the models as black boxes. Different sets of parameters are prepared and processed sequentially through the model and the different model responses are statistically evaluated afterwards. [125, 126]

The different methods, which will be presented in the following, have different advantages and disadvantages. Typically, the number of necessary model evaluations and the accuracy of the results vary considerably. The procedure how the different sets of input parameters are chosen is different amongst some methods and is of high importance. [125, 126]

Here a brief overview of some methods of structural reliability is provided to display the fundamentals. These methods are widely used and comprehensive literature can be found easily. For a better overview the interested reader is referred to [92], which presents an ongoing state-of-the-art report thanks to the continuous development of UQLab [92] (the software that is used for all reliability calculations within this thesis). More advanced methods based on adaptive algorithms and surrogate modelling are available in this software. However, for the model used in this thesis, these algorithms could not be applied successfully – most likely due to the huge numbers of input parameters and partly non-continuous limit-state functions.

2.5.3.2 Sampling for simulation methods

As mentioned above, for simulation methods different sample sets are needed as model input variables. The scattering of the input variables can be described with probability density functions. The cumulative distribution function (CDF) defines the probability that a random variable \mathbf{X} is smaller than or equal to \mathbf{x} . A CDF by construction delivers values between 0 and 1. Therefore, given the CDF of a specific input variable, realisations \mathbf{x} can be calculated with the inverse CDF of specific numbers between 0 and 1. [125, 126]

To get a random variables \mathbf{X} of size N , the inverse CDF is applied on N different randomly distributed numbers between 0 and 1. Random number generators fulfil this requirement up to a certain quality. The most robust algorithm known is the so-called Mersenne twister with very good properties of uniformity in large dimensions and a very high period of $2^{19937} - 1$. [125, 126]

Since the CDFs of some distribution functions show a standard normal distribution (by definition between 0 and 1), instead of a uniform distribution an additional procedure is necessary for those cases. With the Box and Muller theorem two independent, uniformly distributed random variables can be transformed into two independent standard normal variables. [125, 126]

The described sampling approach is used for crude simulations. For more advanced simulation methods, it is combined with or replaced by different selection principles. Nevertheless, this overall principle builds a fundamental principle. [125, 126]

2.5.3.3 First Order Reliability Method (FORM)

The First Order Reliability Method (FORM) is an approximation method for the solution of the integral in Eq. 2.21. This method was developed before the upcoming of fast CPU and is very efficient concerning necessary model runs but finds its limitation to almost linear limit state functions. [92]

2.5.3.4 Second Order Reliability Method (SORM)

The Second Order Reliability Method (SORM) is a second-order refinement of the solution of FORM. There is a rapid increase in computational costs with the number of input random variables M and the solution is still an approximation. [92]

2.5.3.5 Monte Carlo Simulation (MCS)

Monte Carlo simulation (MCS) is a generic tool and builds the basis for all following methods. For structural reliability MCS is based on the direct sample-based estimation of the expectation value in Eq. 2.23. Generally, MCS for reliability analyses is computationally very expensive, since the probabilities of failure are usually very low. It has a well-characterised convergence behaviour from which confidence bounds on the resulting P_f can be estimated. Vice-versa this convergence behaviour allows to estimate the number of model evaluations needed for a specific P_f . [92, 125]

In the following the derivation of the confidence intervals is presented and it is shown how to estimate the necessary amount of model runs with crude MCS. All equations and conclusions are based on [92, 125].

Given a sample of size N of the input random vector \mathbf{X} , the unbiased MCS estimator of the expectation value in Eq. 2.23 is given by:

$$P_{f,MC} = \hat{P}_f = \frac{1}{N} \sum_{i=1}^N \mathbf{1}_{D_f}(\mathbf{X}_i) = \frac{N_f}{N}, \quad (2.24)$$

where N_f describes the number of samples such that $g(\mathbf{x}, M(\mathbf{x})) \leq 0$. The indicator function follows by construction a Bernoulli distribution with mean $\mu_{\mathbf{1}_{D_f}} = P_f$ and variance $\sigma_{\mathbf{1}_{D_f}}^2 = P_f(1 - P_f)$. If N is sufficiently large, it can be approximated by the Normal distribution:

$$\hat{P}_f \sim \mathcal{N}\left(P_f, \sigma_f = \sqrt{\frac{P_f(1 - P_f)}{N}}\right). \quad (2.25)$$

From the Normal distribution, the $(1 - \alpha)$ symmetric confidence interval is, using $u_{\alpha/2} = -\Phi(\alpha/2) = \Phi(1 - \alpha/2)$:

$$\mathbb{P}\left(P_f - u_{\alpha/2} \sigma_f \leq \hat{P}_f \leq P_f + u_{\alpha/2} \sigma_f\right) = 1 - \alpha, \quad (2.26)$$

with:

$$\sigma_f = \sqrt{\frac{P_f(1 - P_f)}{N}}. \quad (2.27)$$

By applying \hat{P}_f in σ_f and introducing the coefficient of variation:

$$\widehat{CoV}_{P_f} = \frac{\hat{\sigma}_f}{\hat{P}_f} = \sqrt{\frac{1 - \hat{P}_f}{N \hat{P}_f}}, \quad (2.28)$$

one gets:

$$\hat{P}_f [1 - u_{\alpha/2} \widehat{CoV}_{P_f}] \leq P_f \leq \hat{P}_f [1 + u_{\alpha/2} \widehat{CoV}_{P_f}], \quad (2.29)$$

with confidence level $1 - \alpha$. These confidence bounds allow the determination of the minimal size of the sample set. The coefficient of variation can be calculated:

$$CoV_{P_f} = \sqrt{\frac{1 - P_f}{N P_f}} \approx \frac{1}{\sqrt{N P_f}}. \quad (2.30)$$

When the considered probability of failure is of magnitude $P_f = 10^{-k}$, one can convert Eq. 2.30 to:

$$N = \frac{10^k}{\widehat{CoV}_{P_f}^2}. \quad (2.31)$$

From Eq. 2.29 one can read the accuracy $\pm u_{\alpha/2} \widehat{CoV}_{P_f}$ on P_f . For example, a $\pm 10\%$ accuracy is targeted. Subsequently, with a 95% confidence interval $u_{\alpha/2} = 1.96 \approx 2$ the $\widehat{CoV}_{P_f} \approx 5\%$. With Eq. 2.31 this example leads to $N \geq 4 \cdot 10^{k+2}$.

From this it follows that for small probabilities of failure the necessary number of model evaluations is very high. For applications with e.g. finite element models this method is not efficient or even not feasible. [92, 125]

2.5.3.6 Importance Sampling (IS)

Importance Sampling (IS) is a combination of FORM and MCS. First the design point by FORM is computed. Then, a shifted multinormal PDF is used, which is centred around the design point. Thanks to this shift far less model runs are necessary than with a crude MCS. [125]

2.5.3.7 Subset Simulation or Markov Chain Monte Carlo simulation (MCMC)

Subset simulation (SS) expresses the failure probability as a product of larger conditional failure probabilities by introducing intermediate failure events. When these conditional events are properly chosen, the conditional failure probability of the subsets can be sufficiently large (roughly 10%) and hence, the number of simulations can be kept small. The procedure depends on a Markov chain Monte Carlo simulation technique based on the Metropolis algorithm. This method is reported to be robust to the number of uncertain parameters and efficient in the computation of small probabilities. [6, 92, 125]

More information about the method and its confidence bounds can be found in [92]. [125] provides an estimation of the necessary number of model runs for evaluating $P_f \approx 10^{-k}$:

$$N = k 10^{3-4}. \quad (2.32)$$

2.5.4 Target reliabilities

In a reliability-based design approach a correspondent minimum reliability has to be met. In a rational analysis the design parameters can be optimised to reach this minimum value. Therefore, the term target reliability is more appropriate. [68]

2.5.4.1 Ultimate limit states (ULS) according to JCSS PMC (2001)

The target reliabilities provided by the probabilistic model code of the joint committee of structural safety JCSS PMC (2001) [68] are based on optimisation procedures and on the assumption that for almost all engineering facilities the only reasonable reconstruction policy is systematic rebuilding or repair.

Tab. 2.4 shows target reliability indices β for the ultimate limit states (ULS). The values are based on cost benefit analysis for the public. Characteristic and representative but simple example structures were used that are compatible with calibration studies and statistical observations [68].

Tab. 2.4: Tentative target reliability indices β (and associated target failure rates) related to one year reference period and ultimate limit states according to [68]. The cell with grey shading represents the most common design situation.

Relative cost of safety measure	Consequences of failure		
	Minor $\rho < 2$	Moderate $2 < \rho < 5$	Large $5 < \rho < 10$
Large (A)	$\beta = 3.1 (P_f \approx 10^{-3})$	$\beta = 3.3 (P_f \approx 5 \cdot 10^{-4})$	$\beta = 3.7 (P_f \approx 10^{-4})$
Normal (B)	$\beta = 3.7 (P_f \approx 10^{-4})$	$\beta = 4.2 (P_f \approx 10^{-5})$	$\beta = 4.4 (P_f \approx 5 \cdot 10^{-6})$
Small (C)	$\beta = 4.2 (P_f \approx 10^{-5})$	$\beta = 4.4 (P_f \approx 5 \cdot 10^{-6})$	$\beta = 4.7 (P_f \approx 10^{-6})$

In Tab. 2.4 the cell with grey shading represents the most common design situation. A brief summary of the classification guidelines from JCSS PMC (2001) [68] is given in the following two paragraphs.

Consequence classes

Consequence classes can be defined based on ρ , which is defined as the ratio between total costs (i.e. construction costs plus direct failure costs) and construction costs. Three classes are defined based on the risk to life and economic consequences. Class 1 is defined for minor consequences with $\rho < 2$, class 2 for moderate consequences with $2 < \rho < 5$ and class 3 for large consequences with $5 < \rho < 10$. If ρ is larger than 10 and the absolute values are large, the consequences should be regarded as extreme and a full cost benefit analysis is recommended. A possible conclusion can be that the structure should not be built.

Furthermore, one should consider different failure modes with different levels of reliability. If a collapse is expected to be sudden without warning, the reliability level should be chosen higher than for a structure with failure modes which are preceded by some kind of warning.

The provided values relate to a dominant failure mode of a system. If a structure has multiple equally important failure modes, the level of target reliability should be chosen higher. [68]

Relative cost of safety measures classification

The normal class (B) should be associated with medium variabilities ($0.1 < CoV < 0.3$) of the total loads and resistances, normal design life and normal obsolesce rate composed to construction costs of the order of 3%. The values of Tab. 2.4 are valid for structures or structural elements as designed, not as built. Failures due to human error or ignorance and due to non-structural causes are not covered.

The relative costs of safety measures are influenced by different objectives such as the degree of uncertainty, the quality assurance and inspections, the design service life and if the structures are being planned or if they already exist.

For design situations with large uncertainties in either loading or resistance (e.g. accidental and seismic situations), a lower reliability class should be applied, since the additional costs to achieve a higher reliability are prohibitive. In design situations with small variabilities (e.g. dead loads or small resistance variabilities), a higher reliability can be achieved by very little additional investments. For existing structures, costs for achieving higher reliability usually are higher than compared to structures under design. Therefore, the target level may be selected lower. Evidently, for a short service life, lower reliability levels can be chosen. [68]

2.5.4.2 Ultimate limit states (ULS) according to Eurocode 0

In EN 1990:2002 *basis of structural design* [30] in chapter 2.2 *Reliability management* general statements are provided how to achieve adequate reliability levels and also specific factors are listed:

"The choice of the levels of reliability for a particular structure should take account of the relevant factors, including:

- the possible cause and /or mode of attaining a limit state;
- the possible consequences of failure in terms of risk to life, injury, potential economical losses;
- public aversion to failure;
- the expense and procedures necessary to reduce the risk of failure."

Further, it is stated that for this purpose structures as a whole or components of it should be classified accordingly.

In appendix B3 "Reliability differentiation" of [30] a framework is presented how to allow different reliability levels. It considers consequence classes and different β values.

Consequence classes

Consequence classes (CC) are provided for the purpose of reliability differentiation by considering the consequences of failure of the structure as given in Tab. 2.5. [30]

Differentiation by reliability indices β

Reliability classes (RC) are defined by means of the reliability index β which are provided in Tab. 2.6 for one year as well as for 50 years reference period. The three reliability classes may be associated with the three consequence classes. [30]

Tab. 2.5: Definition of consequence classes according to [30].

Consequence class	Description	Examples of buildings and civil engineering works
CC3	High consequences for loss of human life, <i>or</i> economic, social or environmental consequences very great	Grandstands, public buildings where consequences of failure are high (e.g. a concert hall)
CC2	Medium consequences for loss of human life, economic, social or environmental consequences considerable	Residential and office buildings, public buildings where consequences of failure are medium (e.g. an office building)
CC1	Low consequences for loss of human life, <i>and</i> economic, social or environmental consequences small or negligible	Agricultural buildings where people do not normally enter (e.g. storage buildings, greenhouses)

Tab. 2.6: Recommended minimum values for reliability index β (ULS) according to [30].

Reliability class	Minimum values for β	
	1 year reference period	50 years reference period
RC3	5.2	4.3
RC2	4.7	3.8
RC1	4.2	3.3

2.5.4.3 Serviceability limit states (SLS) according to JCSS PMC (2001)

According to JCSS PMC (2001) [68] for serviceability limit states (SLS) irreversible and reversible limit states need to be differentiated. While for reversible limit states no general values are provided, for the irreversible cases in Tab. 2.7 tentative target values are given. It is stated that a variation from the target values of the order of 0.3 can be considered.

Tab. 2.7: Tentative target reliability indices β (and associated target failure rates) related to a one-year reference period and irreversible serviceability limit states according to [68]. The cell with grey shading represents the most common design situation.

Relative cost of safety measure	Target index (irreversible SLS)
High	$\beta = 1.3 (P_f \approx 10^{-1})$
Normal	$\beta = 1.7 (P_f \approx 5 \cdot 10^{-2})$
Low	$\beta = 2.3 (P_f \approx 10^{-2})$

2.5.4.4 Serviceability limit states (SLS) according to Eurocode 0

In Eurocode EN 1990:2002 [30] in appendix C, for RC2 target reliability indices are provided for irreversible serviceability limit states. For a reference period of one year, the index β is 2.9 and for a period of 50 years, it is 1.5.

2.6 System effects

2.6.1 Introduction

When constructing assemblies or even systems, several single components are joined together. Depending on how they are joined, different system effects can arise. Contemporary design codes mainly focus on component behaviour which means that most of the limit-state equations are related to single failure modes of single components. Most structural systems are assemblies of several components though and even single components can be susceptible to a number of possible failure modes. [38, 68]

2.6.2 System modelling

In Sudret and Marelli (2018) [125] the following definition is given: "A system is defined as a set of components whose joint functioning is required to ensure the performance of the system." In order to decompose a complex system into interconnected components, the understanding of the scenarios that make the link between component failures and system failure is necessary. To visualise the systems, different tools have been proposed: reliability block diagrams, and fault trees. Basically, only two different system typologies need to be considered: series systems, and parallel systems. Any system can be represented by combinations of these two. [78, 125]

2.6.2.1 Series system

In a series system the failure of any single component implies the failure of the system. By definition the failure of a series system F_{series} is the *union* of the component failure events [125]:

$$F_{series} = \bigcup_{i=1}^n F_i. \quad (2.33)$$

The block diagram for a series system is represented by a chain:



Fig. 2.24: Block diagram representation of a series system [125].

To compute the probability of failure a transformation with the De Morgan's law can be applied [125]:

$$P_{f,series} = \mathbb{P} \left(\bigcup_{i=1}^n F_i \right) = 1 - \mathbb{P} \left(\overline{\bigcup_{i=1}^n F_i} \right) = 1 - \mathbb{P} \left(\bigcap_{i=1}^n \overline{F_i} \right) \quad (2.34)$$

When considering *independent* failure events, the following simplification is valid [125]:

$$P_{f,series} = 1 - \mathbb{P}\left(\bigcap_{i=1}^n \overline{F}_i\right) = 1 - \prod_{i=1}^n (1 - p_i). \quad (2.35)$$

In case of small component probabilities ($p_i \ll 1$) the equation reduces to:

$$P_{f,series} \approx \sum_{i=1}^n p_i, \quad (2.36)$$

and the probability of failure for a series system is approximately the *sum* of the probabilities of failure of the single components [125].

2.6.2.2 Parallel system

In a parallel system a failure of the full system only occurs if all components fail. By definition the failure of a parallel system $F_{parallel}$ is the *intersection* of the component failure events [125]:

$$F_{parallel} = \bigcap_{i=1}^n F_i. \quad (2.37)$$

The block diagram for a parallel system is represented as follows:

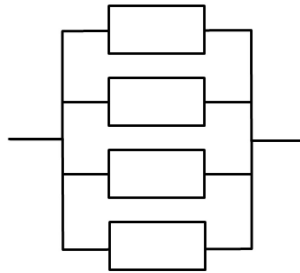


Fig. 2.25: Block diagram representation of a parallel system [125].

Parallel systems are used to introduce *redundancy*. If the failures of the single components are *independent*, the probability of failure of a parallel system can be obtained by:

$$P_{f,parallel} = \mathbb{P}\left(\bigcap_{i=1}^n F_i\right) = \prod_{i=1}^n \mathbb{P}(F_i), \quad (2.38)$$

and the probability of failure for a parallel system is the *product* of the probabilities of failure of the single components [125].

2.6.2.3 Civil engineering systems

Large civil engineering structures are usually one-of-a-kind. Further, a statistical approach is not possible, since failures are rare. Often, unexpectedly large exposure, such as extreme environmental loads, lead to failure of such systems. In contradiction to the above-assumed independent component failures, they are often *correlated* in these systems. This is why a simple representation with combinations of series and parallel interconnected components in general is

insufficient. Nevertheless, for the basic understanding of system effects, they are still useful. The above-described methods of structural reliability can take these system effects with inherit correlations into account, if the system is properly modelled. [125]

2.6.3 Statistical system effects of within member variability

In Fink et al. (2016) [38] it was stated that structural members, such as beams made of solid timber, glued laminated timber or laminated veneer lumber, have three main characteristics with respect to structural reliability: the inherit variability of the material; the homogenisation effect; and the dimensions, i.e. size effects.

In Hansson and Thelandersson (2002 & 2003) [57, 58] the first of these characteristics was addressed for structural timber used as beams for roof trusses. The system effect stems from the reduced probability that the most stressed sections coincide with weak sections of the timber beams. In their model the strength variation of the timber was addressed for both the between and the within beam variability. These effects are not considered in the codes, where it is assumed that all members are homogeneous and therefore all members have the same, low strength value along their length.

In their finite element analysis, the structural system had predefined deterministic stiffness properties. For the strength variability within the structural timber members the model from Isaksson (1998) [67] was used and also the between member variability of the strength was taken into account. The span of the reviewed W-type roof truss (triangular truss with falling and rising diagonals) was 7.8 m. The eccentricities within the joints were considered and for the transversal and rotational springs semi-rigid linear elastic behaviour was assumed. For the load caption area an axis distance between the trusses of 1.2 m was assumed. For the limit-state function they used the combined stress index (CSI) which took into account normal force and moment actions and also second order effects under compression. Out-of-plane action was neglected under the assumption of a bracing system. For all timber failure modes linear elastic behaviour up to failure was reported to be a reasonable assumption. Finally, they compared the CSI from deterministic engineering analysis vs. the CSI found from a MCS with 1'000 model runs. The consideration of this within member variability revealed a reduction in CSI of 12% for Scandinavian spruce and 24% for Radiata pine, which is less homogeneous. In terms of reliability they found in a FORM analysis that thanks to the consideration of this within member variability the loads could be enlarged by +17% and +37% respectively to reach the same reliability index. [57, 58]

2.6.4 System factors for light-frame wood truss assemblies

In Mtenga et al. (1991) [98] light-frame wood truss assemblies were studied with respect to a system effect which stems from load-sharing of neighbouring trusses and reducing variability through the assembly. In the simulations they used a sophisticated finite element framework which even took into account the non-linear steel plate connection behaviour. The span of the trusses was chosen between 6.0 and 10.8 m and the spacing from axis to axis to 0.61 m. To simulate the partial composite action of the top-chords with the plywood sheathing, the beams

were simulated as two-layer components. In cross direction the sheathing was represented by beams at every 1.2 m. The trusses were loaded stepwise and after every step a failure checking was conducted. Three main mechanisms were checked: capacity utilisation of all components, excessive deformations due to loss of stiffness of components, and unstable structure due to component failures. The loads and strengths were modelled probabilistically and as reliability method the so-called first order second moment (FOSM) approach was used.

One of the main conclusions of the study was that the weakest-link-system failure approach is an inappropriate assumption. The 5% quantile value of the strength of the system is 25% higher than the one of a single truss. Further, the variability of the system strength was reported to be half of the variability of the strength of one truss, which in turn is lower than the variability of strength of one component. This leads directly to a higher reliability of the system. [98]

2.6.5 Influence of ductility in timber structures on the system reliability

In Kirkegaard et al. (2011) [78] the influence of ductility was investigated on the example of a Daniels system (Fig. 2.26), i.e. a perfectly parallel system (compare Fig. 2.25). The input variables were modelled probabilistically and different ductility levels were applied.

For a system with elements with low ductility, a higher reliability was observed compared to a system with brittle elements. The increase in ductility had only a minor effect though. With regard to the number of elements it could be observed that even for brittle elements a small positive system effect arises for a high number of elements, at least for low variability. A major effect stems from the variability of the loads. For a high variability the reliability decreases significantly for systems with elements with low ductility but also for systems with highly ductile elements a decrease can be observed. [78]

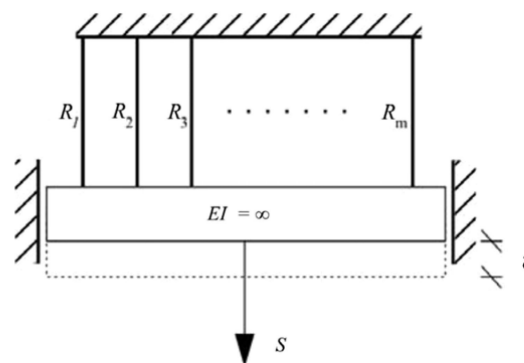


Fig. 2.26: Daniels system [78].

The investigations from [57, 58] (Sec. 2.6.3) were repeated in a similar way in Hansson and Ellegaard (2006) [56]. The decisive difference was that for the load-deformation behaviour of the steel plates a non-linear relationship was implemented. Against their expectation no significant effect could be observed. It was pointed out that the system effects decrease with increasing CoV or when changing the distribution type of the snow load from Normal to Gumbel.

2.6.6 Weibull's weakest link theory

2.6.6.1 Introduction

The two parameter (2-p) Weibull distribution function is defined on the interval $[0, +\infty)$ and its cumulative distribution function (CDF) reads [125]:

$$F_X(x) = 1 - \exp \left[- \left(\frac{x}{a} \right)^b \right], \quad (2.39)$$

where a and b are the parameters that define a certain property of an element. The scale parameter a is the 63.2% fractile value and the shape parameter b has a one-to-one relationship to the CoV and the normalised fractile values of a [54].

When applying the 2-p Weibull distribution on the strength S of the single link from Fig. 2.27a, the probability of failure before the force F is reached reads [54]:

$$S(F) = 1 - \exp \left[- \left(\frac{F}{a} \right)^b \right]. \quad (2.40)$$

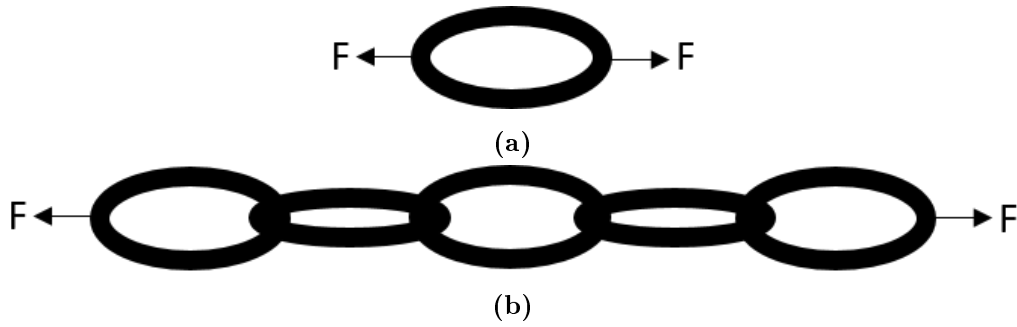


Fig. 2.27: Weibull-weakest-link model with constant loading; (a) single link; (b) chain.

The probability that the chain from Fig. 2.27b with all n single links fails before the links reach their forces F_i can be calculated by Eq. 2.35 leading to:

$$\begin{aligned} S(F) &= 1 - \exp \left[- \left(\frac{F_1}{a} \right)^b \right] \exp \left[- \left(\frac{F_2}{a} \right)^b \right] \dots \exp \left[- \left(\frac{F_n}{a} \right)^b \right] \\ &= 1 - \exp \left[- \sum_{i=1}^n \left(\frac{F_i}{a} \right)^b \right]. \end{aligned} \quad (2.41)$$

2.6.6.2 Weakest link model

For the case of applying equal forces on all n links, i.e. $F_i = F$, the probability of failure then reads [54]:

$$\begin{aligned}
 S(F) &= 1 - \exp \left[- \sum_{i=1}^n \left(\frac{F_i}{a} \right)^b \right] \\
 &= 1 - \exp \left[-n \left(\frac{F}{a} \right)^b \right] \\
 &= 1 - \exp \left[- \left(\frac{F}{a} n^{\frac{1}{b}} \right)^b \right] \\
 &= 1 - \exp \left[- \left(\frac{F}{an^{\frac{1}{b}}} \right)^b \right].
 \end{aligned} \tag{2.42}$$

From Eq. 2.42 the following force scaling factor is found: $n^{\frac{1}{b}}$.

For the case of applying different but proportional forces on the n links, i.e. $F_i = \lambda_i F_{max}$, the probability of failure then reads [54]:

$$\begin{aligned}
 S(F) &= 1 - \exp \left[- \sum_{i=1}^n \left(\frac{F_i}{a} \right)^b \right] \\
 &= 1 - \exp \left[- \sum_{i=1}^n \left(\frac{F_{max} \lambda_i}{a} \right)^b \right] \\
 &= 1 - \exp \left[- \left(\frac{F_{max}}{a} \right)^b \sum_{i=1}^n \lambda_i^b \right] \\
 &= 1 - \exp \left[- \left(\frac{F_{max}}{a} \left(\sum_{i=1}^n \lambda_i^b \right)^{\frac{1}{b}} \right)^b \right] \\
 &= 1 - \exp \left[- \left(\frac{F_{max}}{a \left(\sum_{i=1}^n \lambda_i^b \right)^{\frac{1}{b}}} \right)^b \right].
 \end{aligned} \tag{2.43}$$

From Eq. 2.43 the following force scaling factor is found: $\left(\sum_{i=1}^n \lambda_i^b \right)^{\frac{1}{b}}$.

It is interesting and very convenient that between the extreme value distribution 2-p Weibull of the strength of a link and the strength of a chain the only difference is the above-mentioned scaling factor. This convenient feature also states that both have an equal CoV. [54]

2.6.6.3 Weakest link model for the volume effect

For the weakest link volume effect the beam with volume V made up of small volumes ΔV and arbitrary loading from Fig. 2.28 is analysed. The basic assumption is, that the entire volume fails as soon as any of the small volumes fails, i.e. a brittle failure takes place. [54]

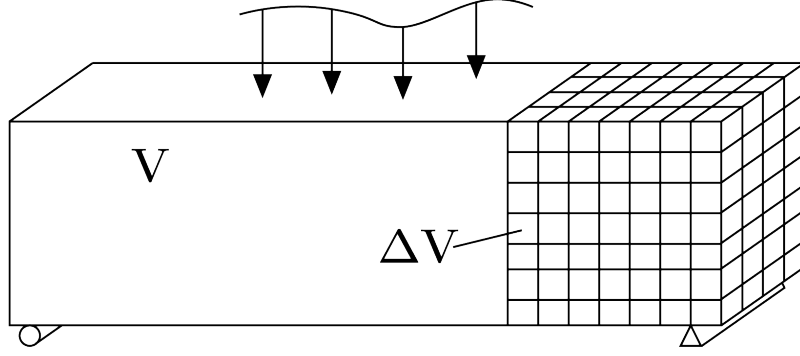


Fig. 2.28: Beam of volume V made up of small volumes ΔV and an arbitrary load.

When every volume ΔV_i is loaded by stress σ_i and the strength properties of the volumes ΔV are defined by a and b the probability that V fails is [54]:

$$S(\sigma) = 1 - \exp \left[- \sum_{i=1}^n \left(\frac{\sigma_i}{a} \right)^b \right], \quad (2.44)$$

where $n = \frac{V}{\Delta V}$. For $\Delta V \rightarrow dV$ it follows [54]:

$$\begin{aligned} S(\sigma) &= 1 - \exp \left[- \sum_{i=1}^{V/dV} \left(\frac{\sigma_i}{a} \right)^b \right] \\ &= 1 - \exp \left[- \text{mean} \left(\left(\frac{\sigma_i}{a} \right)^b \right) \frac{V}{dV} \right] \\ &= 1 - \exp \left[- \frac{\int_V (\sigma(x)/a)^b dV}{V} \frac{V}{dV} \right] \\ &= 1 - \exp \left[- \frac{\int_V (\sigma(x)/a)^b dV}{V} \frac{V}{dV} \right] \\ &= 1 - \exp \left[\frac{-1}{dV} \int_V (\sigma(x)/a)^b dV \right]. \end{aligned} \quad (2.45)$$

For the case with a reference volume V_{ref} and $\sigma(x) = \text{constant}$ the strength distribution reads [54]:

$$S = 1 - \exp \left[- \left(\frac{\sigma}{a} \right)^b \frac{V_{ref}}{dV} \right]. \quad (2.46)$$

For the general case with $\sigma(x) = \lambda(x) \sigma_{max}$ the strength distribution reads [54]:

$$S = 1 - \exp \left[- \left(\frac{\sigma_{max}}{a} \right)^b \frac{V_{ref}}{dV} \frac{1}{V_{ref}} \int_V \lambda(x)^b dV \right]. \quad (2.47)$$

Following the procedure from Sec. 2.6.6.2 the only difference between Eq. 2.46 and 2.47 is the scaling factor: $\left(\frac{1}{V_{ref}} \int_V \lambda(x)^b dV \right)^{\frac{-1}{b}}$. This expression can further be separated into a volume ratio which indicates a size effect and the λ -integral which indicates a stress distribution effect [54]:

$$\left(\frac{V}{V_{ref}} \right)^{\frac{-1}{b}} \left(\frac{1}{V} \int_V \lambda(x)^b dV \right)^{\frac{-1}{b}}. \quad (2.48)$$

In the case of a constantly stressed volume, i.e. $\lambda(x) = 1$ for all incremental volumes, Eq. 2.48 reduces to the volume ratio. When the ratio is inverted, the form of the volume effect is reached which is implemented e.g. in EN 1995 [31]:

$$\left(\frac{V}{V_{ref}}\right)^{-\frac{1}{b}} = \left(\frac{V_{ref}}{V}\right)^{\frac{1}{b}}. \quad (2.49)$$

When the scaling factor or Eq. 2.48 is discretised, i.e. $dV \rightarrow \Delta V$, the following form can be used:

$$\left[\frac{\sum_{i=1}^n \lambda_i^b V_i}{V_{ref}}\right]^{-\frac{1}{b}}. \quad (2.50)$$

2.6.6.4 Length effect on the tensile strength of truss chord members

Lam (2000) [86] adjusted the above-derived Weibull-weakest-link theory for the length effect on the tensile strength of truss chord members. Since truss chords usually have a constant cross-section, Eq. 2.50 can be simplified from a volume to a pure length effect:

$$\xi = \left[\frac{\sum_{i=1}^n \lambda_i^b L_i}{L_{ref}}\right]^{-\frac{1}{b}}, \quad (2.51)$$

where ξ is the tensile length adjustment factor, L_i is the length of the individual chord members, L_{ref} is the reference length of the member under uniform stress and λ_i is the ratio of each normal force N_i acting on L_i to the maximum normal force N_{max} . It was stated, that this approach ignores the within member correlation of strength properties, which could further reduce the value of ξ .

When ξ is applied on the code format it can be used as a direct reduction factor on the tensile strength provided in the code. If used in a probabilistic framework it is applied on the minimum strength S , that is adjusted for the non-uniform stresses of the individual truss chord members [86]:

$$S = \min\left(\frac{S_i}{\lambda_i}\right), (i = 1, \dots, n). \quad (2.52)$$

2.7 Structural robustness

2.7.1 Introduction

Robustness is a very general term used in different fields. The word itself stems from the Latin term *rōbustus* and translates according to different dictionaries to e.g. strength, hardness, oak. Many different definitions of the meaning can be found in literature and the world wide web.

Structural robustness specifically treats structural systems and is often called by the single general term robustness. When thinking of structural robustness, one needs to take into account entire structures, not only single elements. The overall aim of strategies for more robust structures is to reduce the consequences of a failure.

Different structures are in need of different strategies. For enhancing robustness two main principles exist: One is to allow segmentation of certain parts of a structural system. The other is to allow load redistributions within a system. The latter can only be achieved by allowing sufficient ductility. [25] Typically, in timber construction only connections can be designed as ductile elements. That is why they are reported to be a prerequisite for robust timber design [18, 76, 85].

Within this chapter first the definitions from the codes are presented. Then, some relevant literature in the context of this thesis is presented with a focus on definitions and basic methods. Finally, the literature concerning large-span timber hall structures is presented. For a more thorough overview of structural robustness the interested reader is referred to Huber et. al (2018) [65].

2.7.2 Aspects of structural robustness in codes

2.7.2.1 SIA 260:2013

Figure 1 of SIA 260 [117] shows that considerations of robustness have to be part of the conceptual design process. It is underlined again in chapter 2.3 *requirements*.

The technical term robustness is defined as follows:

"Ability of a structure and its members to keep the amount of deterioration or failure within reasonable limits in relation to the cause."

Chapter 4.6 especially mentions that reliability theory can be a mean to secure an adequate level of robustness.

2.7.2.2 SIA 265:2021

In the timber engineering code SIA 265:2021 [121] robustness is addressed in chapter 2.4. It demands conceptual thoughts with respect to suitable stiffening systems as well as immunity against partial failure and to obtain a low wood moisture content. It is mentioned that by means of ductile connections less vulnerable constructions against overloading can be realised. Parallel systems are to be preferred, since certain contributions from all elements can be reached before collapse. This also reduces the impact of spikes in the variability of the timber properties. The last two points are about not putting timber in state of high stresses perpendicular to the grain and using rather compact cross sections for fire safety.

2.7.2.3 EN 1990:2002

In Eurocode EN 1990:2002 [30] in chapter 2.1 *basic requirements* the following requirements are listed, addressing robustness and possible damage:

"A structure shall be designed and executed in such a way that it will not be damaged by events such as:

- explosion,
- impact, and
- the consequences of human errors,

to an extent disproportionate to the original cause.

Potential damage shall be avoided or limited by appropriate choice of one or more of the following:

- avoiding, eliminating or reducing the hazards to which the structure can be subjected;
- selecting a structural form which has low sensitivity to the hazards considered;
- selecting a structural form and design that can survive adequately the accidental removal of an individual member or a limited part of the structure, or the occurrence of acceptable localised damage;
- avoiding as far as possible structural systems that can collapse without warning;
- tying the structural members together."

The term robustness is only mentioned in chapter 2.2 *reliability management*. It is listed as one part of a combination for achieving the levels of reliability. "Degree of robustness" is specified by the term structural integrity.

2.7.2.4 JCSS PMC (2001)

In part 1 - *basis of design* of JCSS PMC (2001) [68] the following robustness requirement was formulated:

"A structure shall not be damaged by events like fire, explosions or consequences of human error, deteriorating effects, etc. to an extent disproportionate to the severeness of the triggering event."

Further, a list of strategies is provided to attain adequate safety in relation with accidental loads:

1. "reduction of the probability that the action occurs or reduction of the action intensity (prevention)
2. reduction of the effect of the action on the structure (protection)
3. making the structure strong enough to withstand the loads
4. limiting the amount of structural damage
5. mitigation of the consequences of failure"

Strategies 1, 2 and 5 are so-called non-structural measures and are considered being very effective with respect to specific accidental actions. Strategies 3 and 4 are so-called structural measures. Strategy 3 is in general extremely expensive, where strategy 4 accepts some members to fail and only requires that the total damage is limited.

2.7.3 Aspects of structural robustness in literature

2.7.3.1 COST Action TU0601 - Robustness of structures: A summary

In Faber & Narasimhan (2011) [34] robustness is mentioned to be broadly recognised as:

"[...] not only associated with the structure itself but needs to be considered as a product of several indicators; risk, redundancy, ductility, consequences of structural component and system failures, variability of loads and resistances, dependency of failure modes, performance of structural joints, occurrence probabilities of extraordinary loads and environmental exposures, strategies for structural monitoring and maintenance, emergency preparedness and evacuation plans and general structural coherence."

It is also mentioned that the most promising contributions are linked to the field of structural reliability. Considerations of risk should build the basis of an establishment of acceptance criteria for the quantification of structural robustness. The term "structural robustness" itself is defined as:

"[...] the ability of the structure to sustain the damages implied by the exposures without partial or fully developing collapse."

2.7.3.2 Starossek and Haberland (2012)

In Starossek and Haberland (2012) [123] the terminology and the interrelations of the most important aspects of structural robustness are summarised concisely:

Exposure

"The exposure is the set of threats that possibly affect a structure during construction and lifetime. In the context of disproportionate collapse, only the threats not considered in the conventional design of a structure are of interest. When they occur they are called abnormal events [...], the threats to a structure can be classified into physical threats and logical threats. The first group is named faults and encompasses all physical threats that may cause a structural damage or failure. They can be again divided into external faults - like extreme environmental actions as well as accidental or intentional explosions or impacts - and immanent faults that are undetected defects of the structure. The second group is named errors and encompasses all logical threats, that is, for instance, human errors in the design and usage of the structure. [...] The exposure of a structure is related to the probability $P[E]$ and can be reduced by event control."

Vulnerability

"Vulnerability is defined here as the susceptibility of a structure to suffer initial damage when affected by abnormal events [...] Vulnerability is a property that depends

on the strength and stiffness of individual structural components, that is, it is related to local conditions. It is associated with the conditional probability $P[D | E]$, and thus the design strategy 'prevent failure initiation'. The vulnerability of a structure can be reduced by protecting the structure or by increasing its local resistance."

Robustness

"Robustness is defined here as the insensitivity of a structure to initial damage [...] Robustness is a property that depends on the structure and the amount of initial damage, that is, it is related to the global system behaviour. Robustness is associated with the conditional probability $P[C | D]$, and thus the design strategy 'prevent disproportionate failure spreading'. Robustness can be enhanced by the design methods alternative load paths and segmentation."

Collapse resistance

"Collapse resistance is defined here as the insensitivity of a structure to abnormal events [...] Collapse resistance is a property that depends on both local and global structural features as well as abnormal events. It is associated with the probability-product $P[D | E] \cdot P[C | D]$ [...] and can be enhanced by reducing the structure's vulnerability or by enhancing its robustness, [...]."

Disproportionate collapse

"A disproportionate collapse is characterised by a pronounced disproportion between a relatively minor abnormal event and the ensuing collapse of a major part or even the whole of a structure. A disproportionate collapse often but not always occurs in a progressive manner. [...] A disproportionate collapse typically develops in three stages. First, an abnormal event, E, acts on a structure. The term abnormal event refers to an event that is unforeseeable or occurs with very low probability and is not considered in the conventional design of a structure. Second, this abnormal event, E, causes an initial damage, D. The initial damage is the damage that can be ascribed directly to the abnormal event without resorting to the response of the structure as a whole. It manifests itself as a reduction in the load-carrying capacity (sectional weakening) or as a complete loss of the load-carrying capacity (component failure) of a part of the structure and is usually locally limited. Damage is understood as deviation from the design state, possibly with partial loss of functionality, whereas failure is understood as total loss of functionality. Third, the initial damage, D, causes disproportionate failure spreading, resulting in a disproportionate collapse, C. The manner in which the structure reacts to the damage D is an inherent structural characteristic, which can be examined by scenario analyses of assumed cases of initial damage D independently of specific abnormal events E (notional damage)."

The probability of disproportionate collapse $P[C]$ can be expressed with the following equation:

$$P[C] = P[C | D] \cdot P[D | E] \cdot P[E]. \quad (2.53)$$

In Fig. 2.29 a concise representation of the above-mentioned terms and equation is provided.

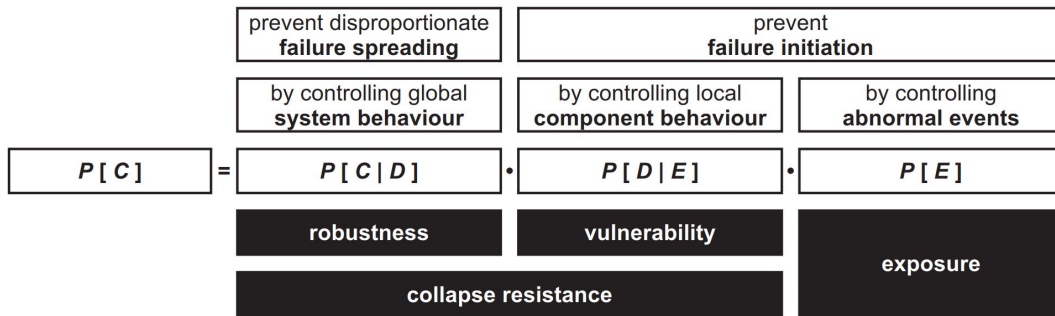


Fig. 2.29: Disproportionate collapse prevention strategies [123].

Five design methods have been identified within the design framework for preventing disproportionate collapse: event control, protection, local resistance, alternative load paths, and segmentation. For more details concerning these design methods, the interested reader is referred to the original publication [123].

An interesting discussion in [123] of 'reducing vulnerability versus enhancing robustness' is summarised in the following:

- **Reducing vulnerability** aims at reducing the probability of failure initiation and thus, preventing initial damage of key elements. *Key elements* are structural components whose failure entail further damage that violates the performance objectives (e.g. building columns, a pier of a continuous bridge, or a cable in a cable-supported structure). One way of ensuring high safety is using higher design loads (local resistance). Another way is protection. Protection measures can be regular inspection, protection against fire or corrosion, etc. Hence, this design strategy is in need of better knowledge of the abnormal events affecting a structure and the actions caused by them, than when using the other strategy of 'enhancing robustness'. Further it was stated, that the abnormal events are unpredictable, which questions the entire approach. This approach should therefore only be used for structures of low significance, for structures with only few, clearly identifiable key elements and in case of inapplicability of 'enhancing robustness'. Another field of application is retrofitting.
- **Enhancing robustness** aims at preventing disproportionate failure spreading. This means initial damage is acceptable when the resulting damage is limited to an acceptable extent. For this strategy reasonable scenarios of initial damage need to be assumed. On this basis the structure is designed in such way that the spread of local initial damage remains limited to an acceptable extent. In contrast to the first strategy, enhancing robustness has no dependency of the failure probability of key elements, which is hard to predict. Triggering abnormal events and their associated uncertainties are irrelevant.

- The first strategy requires changes at key elements, i.e. discrete structural components. The second strategy produces distributed changes in the structural system, and therefore, the improvement of the structure is conducted by modifying its system behaviour.

The design methods for enhancing robustness were already mentioned above: alternative load paths, and segmentation. In the following the discussion of both approaches in [123] is summarised:

- **Alternative load paths** aim at providing alternatives for load transfer between a point of application to a point of resistance. Forces which were acting on failed components can be redistributed towards intact components and therefore further spreading of the failure is prevented. Usually such measures are accompanied by an increase in continuity, strength and ductility. The approach can be designed for directly. Either it can be used in a threat-specific or a threat-unspecific manner. Finally, for both an initial damage has to be taken into account. Also, indirect design can be applied when following prescriptive design rules from codes.
- **Segmentation** prevents spreading of a failure following an initial damage by isolating the failing part from the remaining structure. The so-called segment borders have to be selected by the design engineer meeting the design objectives. Three possibilities exist for the design of segment borders: strong components that can arrest failure spreading; weak components, also called structural fuses, which lead to a safe disconnection of the failing part of the structure; and highly ductile elements with large energy dissipation capacity. Similar to the alternative load paths method also segmentation can be dealt with in a threat-specific or an -unspecific manner for direct design. Indirect design is also possible when following prescriptive design rules.
- Both approaches basically follow the same assumption of initial damage. The actual design follows converse rules though: redundancy vs. isolation. Alternative load paths are widely used where segmentation is rather used scarcely. The authors point out the weakness of the alternative load paths: failure can spread to unacceptable extent if the alternative load paths become overloaded from enhanced continuity. If alternative load paths are not implementable or overly expensive to provide sufficient strengths, segmentation should be selected. On the contrary, segmentation is usually not applicable when the fall of components must be prevented. This is the case when the impact of the falling components could overload key elements below. Therefore, structures that are aligned along vertical axes and are susceptible to pancake-type collapse, i.e. high-rise buildings, alternative load paths should be selected. If a structure is horizontally aligned, i.e. bridges or low-rise buildings, segmentation should be preferred. Other important aspects in the selection process is the assumed size of the initial damage as well as the fixed extent of damage due to segmentation. Both methods can also be combined, e.g. within a segment alternative load paths can be provided.

2.7.4 Structural robustness of large-span timber hall structures

Dietsch (2011) [25] listed certain structural systems, which can be used to build large-span timber roof structures. Usually they consist of a primary structure which carries a secondary structure in the form of purlins. Some possible primary structures, which often are single spanned, are pitched cambered GLT beams, trusses or three hinged frames. The purlins can be built single spanned or as continuous beams. Gerber beams and lap-jointed purlins are also possible. Due to material savings and construction processes, usually some kind of continuous purlin systems are used today. [25]

For the evaluation of typical purlin systems in [25] the "removal of a limited part of the structure" method was applied. These limited parts were purlins between two main girders or one of the girders itself. The study points out that depending on the detailing of the purlin connection single spanned purlins may be better in the sense of no tearing down effect of neighbouring elements. In a more general phrase: Primary systems should be designed more redundant and secondary systems statically determined with appropriate detailing which does not allow large additional loads on the primary system. This compartmentalisation/segmentation seems to be the only feasible approach for the described systems. Specific examples of appropriate connection details are provided in Fig. 2.30. These examples allow for a transfer of lateral loads in different manners. Frame systems or internally indeterminate systems, such as trusses with diagonal cross members or beams which are trussed with sag rods, are mentioned as redundant primary systems. [25]

In the failure scenarios there is a certain redistribution of loads from the failing part on the intact structure. Since global overloading and local damages do not correlate, the remaining structure is typically not loaded to its limit (accidental load case [117]). Therefore, within an overall intact structure generally additional loads due to a local damage can be taken up. In the case of higher correlation of damages, load redistribution is problematic. If e.g. all members suffer from a damage due to global effects such as moisture penetration, a structure will not withstand a large load increase due to load redistribution from one failing member. [25]

This is why in the context of structural robustness it is necessary to differentiate between local and global effects. In [25] different studies on failed timber structures were briefly discussed. They revealed that about 70% of the errors result in global effects. The other 30% can either result in global or local damages. Further, it was concluded that the prevalent cause of failure of large-span timber structures is human error, what was supported by a later study by Dietsch & Winter (2018) [24].

Typical local effects are e.g. local deterioration or weakening of elements, or local overloading. Possible global effects are global weakening of structural elements due to systematic mistakes, global deterioration of elements, or global overloading. It is important that local or global effects should be dealt with by different robustness approaches. For local effects a redistribution of loads to adjacent (undamaged) elements is preferable. Due to global effects the failures should be limited to a local level by e.g. determinate secondary systems with "weak/flexible" connections and seek the above mentioned compartmentalisation/segmentation. Therefore, there

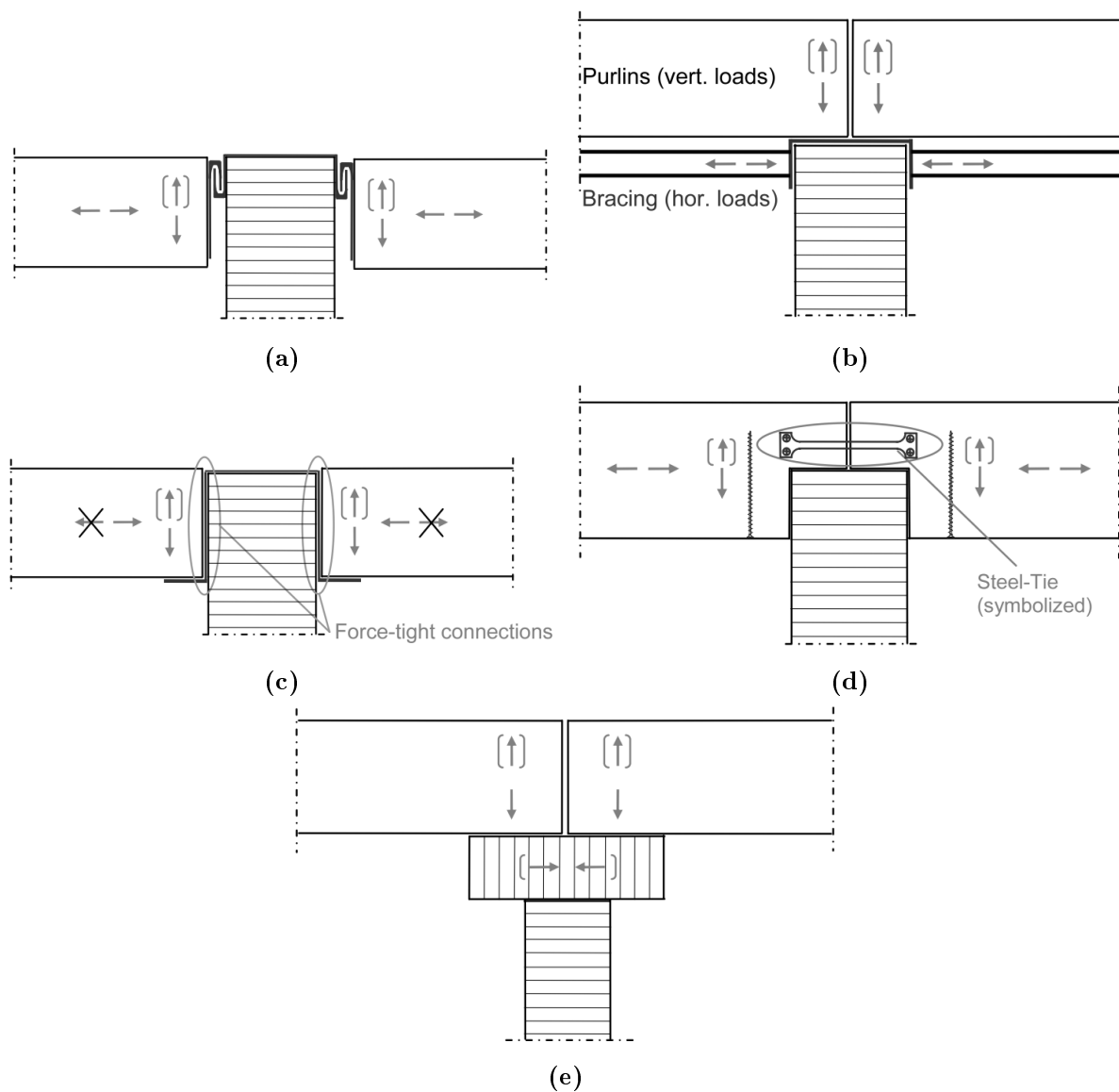


Fig. 2.30: Possible purlin to girder connection details enabling detachment according to [25]; (a) connection to transfer horizontal and vertical loads, potentially enabling detachment in case of failure; (b) separation of load bearing structure for horizontal and vertical loads, enabling detachment in case of failure; (c) connection to transfer axial compression forces and vertical loads, enabling detachment in case of failure; (d) connection to transfer axial tension and compression forces and vertical loads, enabling detachment in case of failure; (e) primary beam with cross-section to enable internal stability against lateral torsional buckling, also capable to transfer external horizontal loads (e.g. wind loads).

is no strategy for the structural designer which ensures robustness in all cases and when deciding on a strategy one has to consider different scenarios. [25]

2.8 Conclusions

It was shown that timber trusses as a beam typology can be used in a huge variety of structural systems. Nevertheless, they are mostly used as single-span beams. Furthermore, the well-established simplified design rules are only applicable for such systems. This is why these simple structural systems are ideal for further investigation.

The methodology of structural reliability was introduced with its manifold aspects such as design approaches, methods of structural reliability and target reliabilities. When combined with a state-of-the-art truss design approach and under the assumption of using appropriate models, this should allow calculating the resultant reliability of the structural system "1D-single-span beam". This value subsequently could be used as the so-called *target reliability* for trusses used as primary structures. This target reliability would therefore allow designing different structural systems for comparable applications, which are outside the boundaries of the simplified design rules.

Concerning dowelled steel-to-timber connections a gap between load-carrying capacity and load-deformation behaviour was highlighted and that so-far no conclusive load-deformation behaviour of dowelled steel-to-timber connections is provided neither in design codes, nor in literature. Therefore, later in this thesis the lately developed load-deformation behaviour from Manser (2021) [91] by means of regression analysis from existing test data is presented. Considering the load-carrying capacity an improved reduction factor due to eccentric loading is introduced that was also developed by [91].

The presented considerations of structural robustness for large-span hall and roof structures mostly make use of the principle of segmentation. Therefore, system effects are of less importance than they would be in cases where the method of alternative load paths is chosen for enhancing the robustness. The presented studies on positive system effects by introducing redundancies (parallel systems) were conducted on smaller trusses with minor distances between the trusses. For 1D-large-span systems the secondary structure obviously is not capable of redistributing loads in most cases. Therefore, within the scope of this thesis such considerations are neglected and the focus is on the behaviour of trusses acting as primary structures. The Weibull-weakest-link model adapted for truss chords under tension seems to be non-negligible and is therefore further addressed in this thesis.

Chapter 3

Mechanical modelling

3.1 Introduction

In this chapter, general aspects of modelling timber trusses are discussed concluding in the multi-scale modelling approach. Based on the multi-scale modelling approach, a framework is presented that considers all elements of a timber truss with dowelled steel-to-timber connections. An effective parametrisation methodology for modelling in a beam-based finite element program is explained and necessary details such as applied algorithms are provided. In addition to the resistance models for the beams, the above-mentioned newly developed load-deformation behaviour and reduction factor of the load-carrying capacity of eccentrically loaded connections by Manser (2021) [91] are presented. Finally, the developed truss design tool is explained, which applies parametrically the simplified design approach for timber trusses of SIA 265:2021 [121] (Sec. 2.3.3). This design tool was applied for designing most of the investigated trusses in Chapter 5.

A preliminary state of parts of this chapter has already been published in Schilling & Frangi (2020) [112]. Jonas Wydler, who is working on a doctoral thesis with a focus on the connections within the same project, was equally involved in the development of the overall multi-scale modelling approach and the principles of the modelling framework presented in Fig. 3.2 and 3.3, respectively.

3.2 Modelling of timber trusses

3.2.1 Introduction

Since the beams of timber trusses are slender elements, they are commonly modelled with beam-based finite element programs, i.e. with one dimensional (1D) finite elements. Regardless of whether trusses are assembled in two or three dimensions (2D or 3D), their single elements usually interact only within one plane. Out of plane, only stability issues need to be considered, which is part of the post-processing. For this reason, the modelling approaches focus on the following three degrees of freedom (dofs) or section forces: normal force N , shear force V_z and bending moment M_y . Further, as shown in Sec. 2.5, in the context of reliability analyses efficient models are of advantage. Therefore, higher dimensional finite elements should be avoided if

possible. In the following section, an overview of the modelling strategies of the single truss elements is presented concluding a so-called multi-scale modelling approach.

3.2.2 Modelling of timber beams

The timber beams within trusses can simply be modelled as linear elastic in all dofs. The non-linear behaviour of timber under compression along the grain cannot usually be activated in terms of the global load-deformation behaviour of a beam element for stability reasons. Therefore, simple stiffness matrices can be used as finite element representations. As resistance model the commonly known approaches from the design codes can be applied and for each beam the utilisation can be determined.

3.2.3 Modelling of truss joints

There are different modelling approaches to account for the detailing of the joints in timber trusses with dowelled steel-to-timber connections. Fig. 3.1a shows a schematic layout of a typical truss joint, from which the different models are derived. The simplest modelling approach is the ideal truss, with friction-free pinned connections between all beams, according to Culmann (1866) [22] (Fig. 3.1b), in which only axial forces occur.

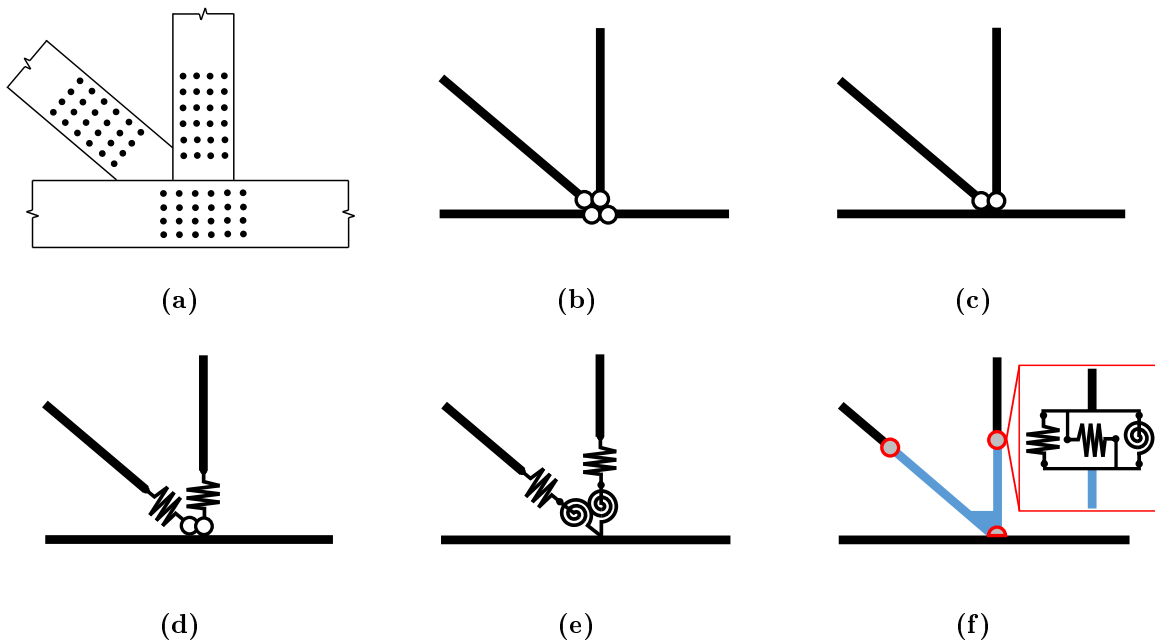


Fig. 3.1: Modelling approaches for timber trusses with dowelled steel-to-timber connections; (a) schematic truss joint layout; (b) pinned connections; (c) continuous chords and web members with pinned connections; (d) continuous chords and web members with pinned connections with axial stiffness; (e) continuous chords and web members with connections with axial and rotational stiffnesses; (f) continuous chords, web members and chords with connections with axial, transversal and rotational stiffnesses, and accounting for the position of each connection via steel elements.

To account for the continuity of the chords and the resulting occurrence of bending moments, the chords should indeed be modelled continuously (Fig. 3.1c). If the axial stiffness of the connections in the web members is considered by means of axial springs (Fig. 3.1d), the resulting overall deflections and the bending moments in the chords are larger due to the added flexibility. Taking also into account the rotational stiffness of dowelled connections leads to the model shown in Fig. 3.1e. These four models were presented in Sec. 2.3.2 and it was mentioned that the model according to Fig. 3.1e was recognised to be the best possible model in the 1980s. However, neglecting the connection in the chord is not on the conservative side, since the overall deflections are underestimated. Further, to take into account the rotational behaviour of each connection in the joint area, their behaviour should be concentrated in the centre of each dowel group (Fig. 3.1f). Therefore, the additional steel plates are additionally modelled as beams. This modelling approach considers the most relevant structural elements and besides neglecting the reduced cross-sections in the connections it is exhaustive, when applying a 1D finite element approach with regular beams and springs. To model the springs that represent the connections in the chords, spring elements with two nodes are necessary. Such elements might be unconventional but are available also in commercial software.

3.2.4 Modelling of connections

3.2.4.1 Load-deformation behaviour

The load-deformation behaviour of dowelled connections obviously depends on the load-deformation behaviour of their single dowels. Their load-deformation behaviour is typically strongly non-linear but is usually simplified as a linear-elastic behaviour. As discussed in Sec. 2.4, the state-of-the-art considerations are vague, and hence, this issue is addressed in more detail in Sec. 3.3.3.

For modelling the full connection behaviour, different approaches can be applied. The simplest one is to consider the dofs independently. Thus, the load-deformation behaviour of the lateral dofs can be specified as a multiple of the single dowels. For the rotational degree of freedom, the load-deformation characteristic can be determined via the polar moment of inertia.

The finite-element subroutine presented in Schweigler et al. (2018) [115] applies the same principles but combines the individual displacement vectors resulting in coupled section forces N - V_z - M_y . This model principally also allows to take into account the contact forces between the timber members, which can occur after some displacements of the connections. Due to complex geometries in the truss joints, a parametrised implementation is quite demanding though. Therefore, contact between timber members is neglected within the scope of this thesis.

3.2.4.2 Resistance models

In Sec. 2.4 it was concluded that for multiple-dowel connections under complex loading a proper resistance model is missing. This issue is addressed in more detail in Sec. 3.3.2.7.

3.2.5 Multi-scale modelling approach

In Fig. 3.2, the problem statement is transferred into a multi-scale modelling approach. The first scale represents the material behaviour, i.e. the timber embedment behaviour and the steel dowel properties. Via a beam on springs (BoS) model, the output of the first scale can be processed to the content of interest of the scale corresponding to the single-dowel connection, i.e. the load-deformation behaviour with its coherent load-to-grain angle dependency. This output can then be processed through the model developed by Schweigler et al. (2018) [115] to gain the load deformation behaviour of the entire connection and the coupled section forces N - V_z - M_y . On this scale also the load-deformation of the beams is considered. Both element types for the beams and the connections with their load-deformation behaviour finally can be processed through the 1D finite element model to gain the system behaviour. With resistance models for the beams and the connections, the failure behaviour can be assessed and the reliability of a truss or an entire structure can be determined. On all scales tests can be conducted to gather directly the content of interest or to update or validate the output of the model between the scale under consideration and the previous scale.

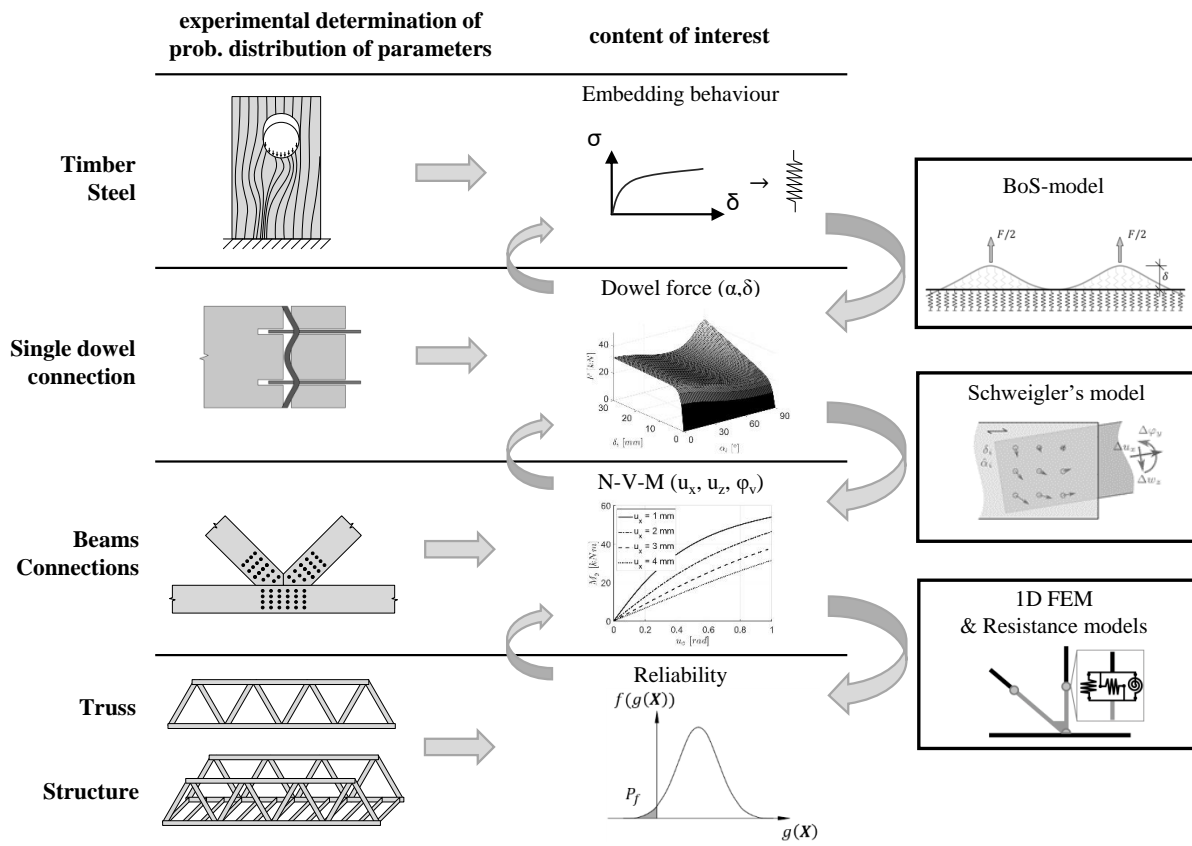


Fig. 3.2: Multi-scale modelling approach.

This multi-scale modelling approach can be used in a probabilistic context to assess the reliability of trusses and structures but it can also be used with deterministic inputs, e.g. following the code format.

On more basic scales, e.g. on the material scale, tests can be conducted in large numbers where entire structures are almost impossible to test due to costs and limitations of experimental set-ups. The understanding of the problem and the flexibility with respect to configurations is generally better when starting the approach on more basic scales. In contrast, the number of parameters that has to be investigated also increases when using a more basic scale as a starting point.

3.3 Framework

3.3.1 Introduction

The multi-scale modelling approach explained above (Fig. 3.2) contains all relevant models for the problem at hand. However, a framework had to be developed to implement this approach, which is shown in Fig. 3.3. It is structured into three main parts, i.e. the model as the central unit, the input and the output. In the following all sub-models and their input and output are presented in detail. All parts of the model were implemented in MATLAB vers. R2020a.

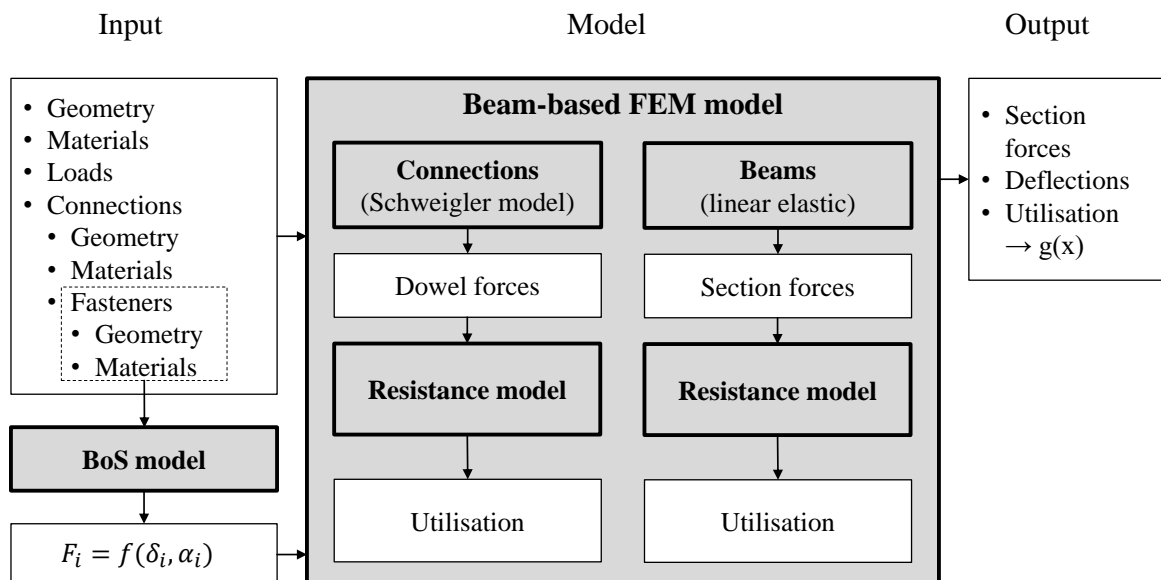


Fig. 3.3: Framework.

3.3.2 Beam-based finite element model

To build up a beam-based finite element model for a timber truss with dowelled steel-to-timber connections, the geometric layout of all parts need to be specified. Further inputs are the material

properties and the external loads. The developed model was implemented as a 3D model to allow for space structures of all kinds. All elements have two nodes and six dofs at each node, resulting in 12 dofs. For plane trusses and the beams of most space trusses, only three dofs are activated. Therefore, the other dofs only need to be specified to certain values for numerical reasons.

3.3.2.1 Joint typology

When studying Fig. 3.1f it is obvious that the actual modelling process within a finite element program is much more demanding than to model a truss with hinged connections as shown in Fig. 3.1b. Therefore, a joint typology and a coherent parametrisation were developed and implemented to automate the modelling process in order to achieve the model according to Fig. 3.1f while only modelling the beams according to Fig. 3.1b. Four different joint types should allow to model all possible 2D- and 3D-trusses with dowelled steel-to-timber connections. All joint types are described in the following list and the first three joint types are illustrated in Fig. 3.4.

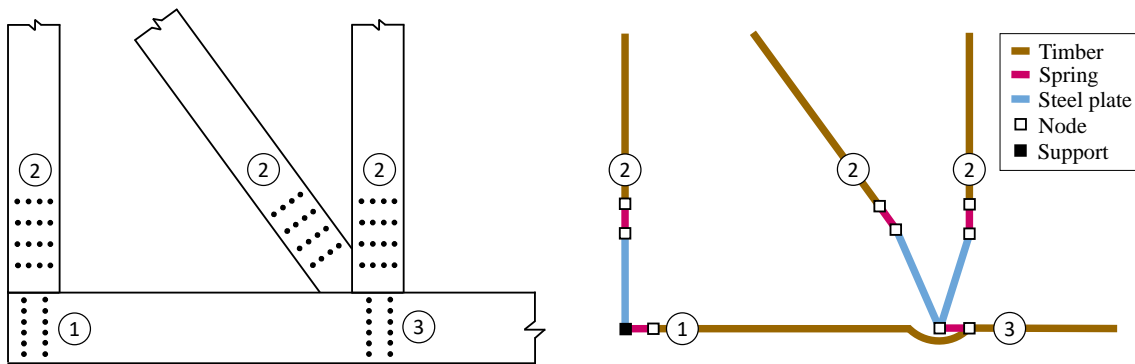


Fig. 3.4: Joint types 1-3 applied on a truss with continuous bottom chord and posts and diagonals.

Type 1 corresponds to the classical beam-end spring. It can be used at the beginning and at the end of the continuous chords, where they are connected to the supports.

Type 2 is used at both ends of web members, where the steel plates are added as beam elements. Their length corresponds to the distance between the centres of the dowel groups of the web member and the chord. The new nodes and the new steel beam elements are then added automatically. The spring representing the dowel group at the end of the timber beam is then added between the timber beam and the steel beam. Other applications of this type 2 are within jointed chords or space trusses where the plates have continuous bending stiffness.

Type 3 allows for representing the connections in the chords. The spring can be generated by the left or by the right beam element as a beam-end or beam-start spring, respectively. This spring does not act between two chord beam elements but between the chord and the steel plates. Therefore, the chord element needs to be linked to the adjacent chord element

again after the spring has been generated. The steel beams of the web members need to be linked to the other end of the spring. Hence, spring elements with two nodes are required for the connections in the chords.

Type 4 corresponds basically to type 2 but with an additional spring at the end of the steel beam. This type 4 is used in space trusses where the steel plates are centred and linked with an element allowing for a moment hinge. Instead of adding an additional finite element for modelling this hinge (which would enlarge the calculation time), the bending stiffness of the steel beams can be drastically reduced to avoid the transmission of bending moments.

3.3.2.2 Automation of the modelling process

The automation of the modelling process based on parametric inputs is shown in Fig. 3.5 and depends on the joint typology introduced above. First, the original timber beam elements are generated between the main truss nodes. Then nodes are added at the distance of the centres of the dowel groups on the axes of the web members and the steel elements are generated between these new and the original nodes. In the next step the beam mesh is produced, i.e. sub-elements with the same properties as the original timber beams are generated with the help of new nodes. Then all start- and end-springs of the timber beams are added. Finally the steel elements and the adjacent chord element are re-linked to the other node of the spring elements to guarantee continuous chord action and the spring acting between the chord and the steel plates.

3.3.2.3 Beam elements

All beams are modelled as beam elements with 12 dofs. The timber beams show linear-elastic behaviour in all dofs. This implementation is intuitive for all dofs of timber beams but for the ones where plastic deformations under compression forces could occur. Usually this limited plasticity cannot be reached due to stability issues. The steel plates might show certain local plastic deformations but their overall behaviour should be in the elastic state when properly designed. Therefore, all beam elements are represented by a 12-by-12 linear-elastic stiffness matrix. Due to low shear modulus of timber, a stiffness matrix which includes the shear stiffnesses is chosen (Eq. 3.1) [47].

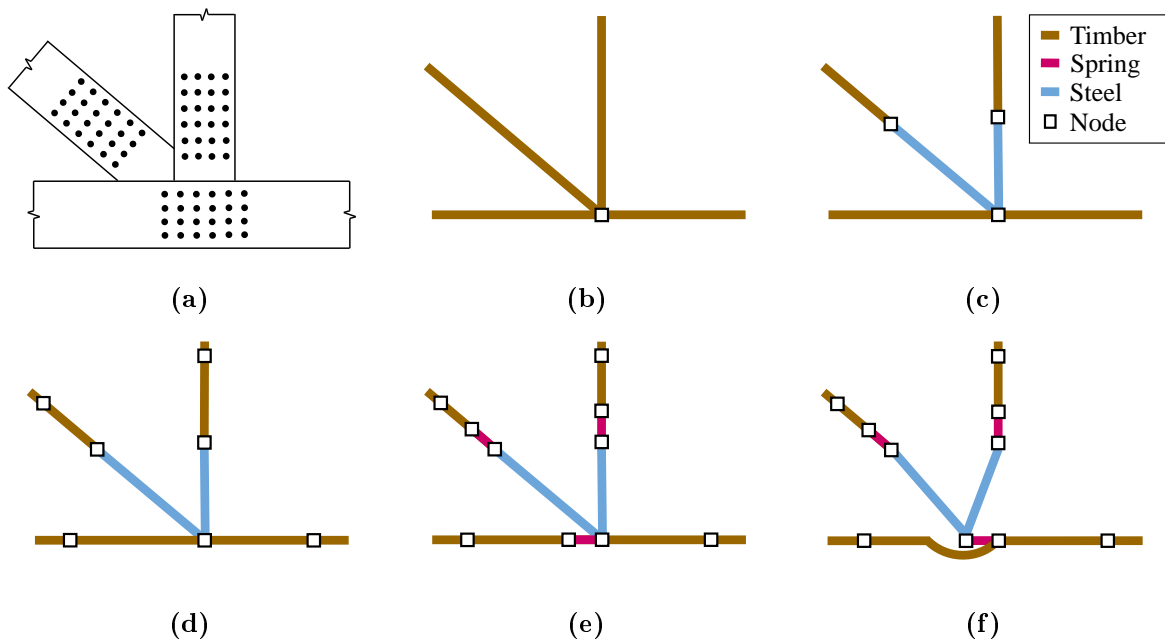


Fig. 3.5: Automated modelling process; (a) schematic truss joint area; (b) all beams are connected to one original node; (c) additional nodes are added at the specified distances along the timber beam axes and the steel elements are generated; (d) on the timber beam axes new nodes are generated for the meshing, i.e. subdivision of the original elements into new shorter beam elements; (e) the beam start and end springs are generated with additional nodes at a distance of 1 mm; (f) the steel elements and the adjacent chord elements are re-linked to the other node of the chord spring to assure continuous chords.

3.3.2.4 Spring elements

For ease of implementation all spring elements have two nodes. The computational effort of the solver is not effected since the 12-by-12 stiffness matrix only depends on the same six dofs that are needed also in a spring element with one node:

$$K_s = \begin{bmatrix} K & -K \\ -K & K \end{bmatrix}, \quad (3.2)$$

where K_s is the matrix of the spring element with two nodes and K corresponds to the 6-by-6 stiffness matrix of one node. These spring elements are modelled with a length of 1 mm which is small enough not to influence any results on truss scale but allows for an easy handling, since the geometrical properties can be dealt with in the same way as for the beams. The convention for the spring orientation in the implemented code is that all springs are directed away from the beam, i.e. beam-start springs are oriented opposite to the beam and beam-end springs are aligned with the beam.

Dowelled connections with independent degrees of freedom

When using independent dofs, both lateral dofs in x and z direction (corresponding to the normal force N and shear force V_z) in a dowelled connection can be represented by a multiple of the load-deformation behaviour of a shear plane of the single-dowel connection.

For the rotational behaviour (corresponding to the bending moment M_y) of the full connection, the polar moment of inertia can be applied to create one load-deformation behaviour based on the load-deformation behaviours of the shear planes of single-dowel connections:

$$K_{rot} = \sum_{i=1}^n K_i l_i^2, \quad (3.3)$$

where K_i is the stiffness of a single shear plane in dependence of the load-to-grain angle and l_i is the distance from the centre of the dowel group to the individual dowel. The stiffnesses of the other dofs (corresponding to V_y , M_x and M_z) can be fixed to any value greater than zero for numerical stability.

Within the framework, the independent load-deformation curves in all 6 dofs can be specified by polylines. This corresponds to a standard solution of commercial finite element software with non-linear solvers. In the most simple form, such a polyline can represent a linear-elastic behaviour and arbitrary curves can be approximated with several segments.

Dowelled connections with coupled degrees of freedom

The model developed by Schweigler et al. (2018) [115] combines the deformations of all individual dowels via vector addition for the dofs corresponding to N , V_z and M_y . The application of this model therefore allows a coupled consideration of these three dofs, which corresponds to a more realistic behaviour than an uncoupled one. The stiffnesses of the remaining dofs (corresponding to V_y , M_x and M_z) can be fixed to any value greater than zero to ensure numerical stability.

This semi-analytical model can be used as a subroutine in a beam-based finite element model. The necessary equations and the calculation procedure as well as a model validation were shown in detail in the original publication [115]. However, as described, there the model was not implemented as a subroutine but via a workaround by using the non-linear joint behaviour as an input into the structural analysis by an antecedent calculation of the joint behaviour for a set of relative deformation states. Within the framework of this thesis, a complete implementation as a subroutine is required though. This leads to a necessary correction of the calculation procedure for the stiffness matrix given in equation (16) of the original publication [115]. There, the individual entries were calculated based on the ratios between the differences of the section forces and the deformations of the actual and the antecedent calculation step. The herein proposed correction uses the central difference approximation to derive of the entries of the stiffness matrix:

$$f'(x) \approx \frac{f(x+h) - f(x-h)}{2h}, \quad (3.4)$$

where the approximation of the derivative $f'(x)$ is based on the secant between the responses of the values which are by an increment h larger or smaller than x . The tangent stiffness matrix K_{tan} then reaches the following form:

$$K_{tan} = \frac{\delta R}{\delta u} = \begin{bmatrix} \frac{\delta N}{\delta u_x} & \frac{\delta N}{\delta u_z} & \frac{\delta N}{\delta u_\varphi} \\ \frac{\delta V_z}{\delta u_x} & \frac{\delta V_z}{\delta u_z} & \frac{\delta V_z}{\delta u_\varphi} \\ \frac{\delta M_y}{\delta u_x} & \frac{\delta M_y}{\delta u_z} & \frac{\delta M_y}{\delta u_\varphi} \end{bmatrix}. \quad (3.5)$$

The procedure explained in [115] is adapted with the newly introduced correction for the implementation as a subroutine and shown in the following pseudo code. The code follows an object oriented approach where the class for the connection contains two methods, an initialisation method *initialiser* (Alg. 1) and a solver method *solver* (Alg. 2). The *initialiser* is used to construct the stiffness matrix based on small displacements and rotations before the first iteration of the first step of the solver. The *solver* is called in each iteration of each step of the finite element solver algorithm and gives the section forces based on the iterated displacements and rotations.

Algorithm 1 *initialiser*

- 1: $[u_x; u_z; u_\varphi] \leftarrow 10^{-6} \text{ArrayOfOnes}(3, 1)$
 - 2: $K_{tan} \leftarrow \text{CentralDifferenceGradient}$
 - 3: rearrange K_{tan} (3-by-3) into K (6-by-6)
 - 4: $K_s \leftarrow [K, -K; -K, K]$
-

Since the connection forces have to be calculated several times, a function *getConnectionForces* is implemented which takes the displacement vector (u_x , u_z and u_φ) of the connection as input and returns the connection force vector (N , V_z and M_y). The function *getConnectionForces* is shown in Alg. 3.

For the central difference gradient function Alg. 4 is provided. This algorithm determines the stiffness matrix according to Eq. 3.5 based on Alg. 3.

Algorithm 2 solver

- 1: $[u_x; u_z; u_\varphi]$ are calculated from the difference of the start and end nodes
 - 2: $[N_x; V_z; M_y] \leftarrow \text{getConnectionForces}$
 - 3: $K_{tan} \leftarrow \text{CentralDifferenceGradient}$
 - 4: rearrange K_{tan} (3-by-3) and assumed stiffness values for the remaining dofs into K (6-by-6)
 - 5: $K_s \leftarrow [K, -K; -K, K]$
 - 6: construct the 12 restoring forces from $[N_x; V_z; M_y]$ and the linear elastic relation for the remaining dofs
-

Algorithm 3 getConnectionForces

- 1: $[N_x; V_z; M_y] \leftarrow \text{ArrayOfZeros}(3, 1)$
 - 2: **for** $i = 1$ to n_{dowels} **do**
 - 3: $\delta_{x,i} \leftarrow z_i \tan(u_\varphi) + u_x$
 - 4: $\delta_{z,i} \leftarrow x_i \tan(u_\varphi) + u_z$
 - 5: $\delta_i \leftarrow \sqrt{\delta_{x,i}^2 + \delta_{z,i}^2}$
 - 6: **if** $\delta_i = 0$ **then**
 - 7: $\alpha_i \leftarrow 0$
 - 8: **else**
 - 9: $\alpha_i \leftarrow \arccos(\delta_{x,i}/\delta_i)$
 - 10: **end if**
 - 11: **if** $\delta_{z,i} < 0$ **then**
 - 12: $\alpha_i \leftarrow 2\pi - \alpha_i$
 - 13: **end if**
 - 14: **if** $\alpha_i \leq \pi/2$ **then**
 - 15: $\hat{\alpha}_i \leftarrow \alpha_i$
 - 16: **else if** $\alpha_i \leq \pi$ **then**
 - 17: $\hat{\alpha}_i \leftarrow \pi - \alpha_i$
 - 18: **else if** $\alpha_i \leq 3/2\pi$ **then**
 - 19: $\hat{\alpha}_i \leftarrow \alpha_i - \pi$
 - 20: **else**
 - 21: $\hat{\alpha}_i \leftarrow 2\pi - \alpha_i$
 - 22: **end if**
 - 23: $F_i = f(\delta_i, \hat{\alpha}_i)$
 - 24: $F_{x,i} = F_i \cos(\alpha_i)$
 - 25: $F_{z,i} = F_i \sin(\alpha_i)$
 - 26: $N_x \leftarrow N_x + F_{x,i}$
 - 27: $V_z \leftarrow V_z + F_{z,i}$
 - 28: $M_y \leftarrow M_y + F_{x,i} z_i - F_{z,i} x_i$
 - 29: **end for**
-

Algorithm 4 CentralDifferenceGradient

```

1:  $x_i \leftarrow [u_x; u_z; u_\varphi]$ 
2:  $\varepsilon \leftarrow 10^{-9} \text{ArrayOfOnes}(3, 1)$ 
3:  $\delta f = \text{ArrayOfZeros}(3, 3)$ 
4: for  $i = 1$  to  $3$  do
5:    $I \leftarrow \text{ArrayOfZeros}(3, 3)$ 
6:    $I(i, i) \leftarrow 1$ 
7:    $\delta f(1 : 3, i) \leftarrow (\text{getConnectionForces}(x_i + I \varepsilon) - \text{getConnectionForces}(x_i - I \varepsilon)) / (2\varepsilon)$ 
8: end for

```

3.3.2.5 Finite element solver

For the solver of the non-linear static analysis (force control) applied in the beam-based finite element program, a standard Newton-Raphson algorithm is used. It is applied on the following balance equation of restoring (inner) and imposed (outer) forces [21]:

$$r(u_j) - f_{j,ext} = 0, \quad (3.6)$$

where j is the analysis step index, u_j is the displacement vector, $r(u_j)$ is the restoring force vector and $f_{j,ext}$ is the imposed load vector. The Newton-Raphson algorithm minimizes the residual res until a tolerance Tol is reached. Therefore, in the non-linear static analysis (Alg. 5) the displacement vector u_j is updated in every iteration by means of a subtraction of the displacement residual, which corresponds to the inverse tangent stiffness matrix K_j^{-1} times the residual res . The variable Z_i is a matrix which selects the correct dofs for every element.

3.3.2.6 Resistance models for the truss members

For the timber members most parts of the resistance model corresponds to the classical design equations provided in SIA 265:2021 [121]. In the following paragraphs, the important equations are presented. The overall utilisation of a member can then be determined by the maximum utilisation factor from these equations.

Tension and bending

To determine the utilisation with respect to the interaction of tension forces N and both bending moments M_y and M_z Eq. 3.7 is applied in terms of stresses and strengths:

$$\frac{\sigma_{t,0}}{f_{t,0}} + \frac{\sigma_{m,y}}{f_{m,y}} + \frac{\sigma_{m,z}}{f_{m,z}} \leq 1, \quad (3.7)$$

where $\sigma_{t,0}$ is the tensile stress parallel to the grain, $f_{t,0}$ is the tensile strength parallel to the grain, σ_m is the bending stress for the y- and z-axis and f_m is the bending strength for the y- and z-axis.

Torsional buckling effects generally cannot occur in tension members within trusses, since the tensile stresses from N are larger than the compressive stresses from M_y and M_z . In tension

Algorithm 5 Non-linear static analysis

```

1: for  $j = 1$  to  $J$  do
2:    $u_j \leftarrow u_{j-1}$ 
3:   for  $i = 1$  to  $I$  do
4:      $[r_{i,j}, K_{i,j}] \leftarrow \text{element}\{i\}.\text{solver}(Z_i u_j)$ 
5:      $r_j \leftarrow r_j + Z_i^T r_{i,j}$ 
6:      $K_j \leftarrow K_j + Z_i^T K_{i,j} Z_i$ 
7:   end for
8:    $res \leftarrow r_j - f_{j,ext}$ 
9:   while  $\text{norm}(res) > Tol$  do
10:     $u_j \leftarrow u_j - K_j^{-1} res$ 
11:    for  $i = 1$  to  $I$  do
12:       $[r_{i,j}, K_{i,j}] \leftarrow \text{element}\{i\}.\text{solver}(Z_i u_j)$ 
13:       $r_j \leftarrow r_j + Z_i^T r_{i,j}$ 
14:       $K_j \leftarrow K_j + Z_i^T K_{i,j} Z_i$ 
15:    end for
16:     $res \leftarrow r_j - f_{j,ext}$ 
17:  end while
18: end for

```

members, M_z can generally not occur either, which is why the last part in Eq. 3.7 could be omitted.

Compression and bending

To determine the utilisation with respect to the interaction of compression forces N and both bending moments M_y and M_z Eq. 3.8 is applied:

$$\left[\frac{\sigma_{c,0}}{f_{c,0}} \right]^2 + \frac{\sigma_{m,y}}{f_{m,y}} + \frac{\sigma_{m,z}}{f_{m,z}} \leq 1, \quad (3.8)$$

where $\sigma_{c,0}$ is the compressive stress along the beam axis, $f_{c,0}$ is the compressive strength along the grain, σ_m is the bending stress for the y- and z-axis and f_m is the bending strength for the y- and z-axis.

Torsional buckling effects theoretically could occur within compression members in trusses. Due to buckling effects out-of-plane, the members (web members as well as compression chords) are supported in such small distances that torsional buckling effects can be neglected though. For trusses, out-of-plane bending moments M_z due to external loading do generally not occur. Furthermore, due to buckling effects for both axes in-plane and out-of-plane Eq. 3.8 cannot be decisive for the gross-cross-section. For the net-cross-sections (see below), it can be decisive though, i.e. the influence of the net-cross-sections can be more important than buckling effects.

Shear and torsion

To determine the utilisation with respect to the interaction of the shear forces V_y and V_z and torsional moment M_x Eq. 3.9 could be applied:

$$\frac{\tau_{tor}}{f_v} + \left[\frac{\tau}{f_v} \right]^2 \leq 1, \quad (3.9)$$

where τ_{tor} is the shear stress from torsion, f_v is the shear strength and τ is the shear stress. Torsion is not considered herein, since it should not occur in truss members. Therefore the simplified Eq. 3.10 can be applied:

$$\frac{\tau}{f_v} \leq 1. \quad (3.10)$$

Net-cross-sections

In the connection area, the utilisation of the three cases above is determined for the net-cross-sections. As prescribed in SIA 265:2021 [121], the slots for the plates and the holes for the dowels are subtracted from the gross-cross-section in the case of tension members (Fig. 3.6).

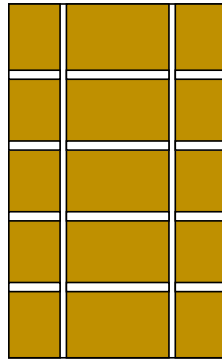


Fig. 3.6: Net-cross-section in the connection area for tension members.

In the case of compression members, according to [121], only the slots for the plates are subtracted from the gross-cross-section (Fig. 3.7).

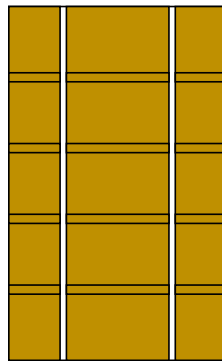


Fig. 3.7: Net-cross-section in the connection area for compression members.

For the moment of inertia in-plane I_y , the net-cross-section is calculated based on Fig. 3.7, i.e. the minor reduction due to the dowel-holes is neglected. For the shear area A_s , the net-

cross-section is calculated based on Fig. 3.6, as in the case of tension. As described above, no torsion and bending out-of-plane actions have to be considered within regular trusses.

General considerations of buckling

According to SIA 265:2021 [121], the buckling effect of timber beams under compression can be taken into account with the *effective length method*. A reduction factor k_c is determined which is applied on the compressive strength. This factor takes into account the geometrical properties of the beam, the buckling length, the modulus of elasticity (5% fractile value) and a differentiation between solid timber and GLT. In the case of a beam with an additional bending moment, the following Eq. 3.11 should be applied:

$$\frac{\sigma_{c,0}}{k_c f_{c,0}} + \frac{\sigma_m}{k_m f_m} \leq 1, \quad (3.11)$$

where $\sigma_{c,0}$ is the compressive stress along the beam axis, k_c the reduction factor of the compressive strength along the grain $f_{c,0}$ due to buckling, σ_m the bending stress and k_m the reduction factor of the bending strength f_m due to torsional buckling.

Theiler (2014) [127] showed that this *effective length method* is satisfactory for standard cases. However, in this thesis a procedure is needed which can be applied on probabilistic input. Therefore, an approach using second order theory has to be applied. As shown in [127], it can be insufficient to apply linear-elastic second order theory. The reduction of the stiffness due to plastification of wood under compression along the grain should be taken into account. In the following, the proposed procedure according to [127] is shown in terms of stresses and without specifications of a certain quantile (i.e. not on characteristic or design level):

$$\left(\frac{\sigma_{c,0}}{f_{c,0}} \right)^2 + \frac{\sigma_{m,II}}{f_m} \leq 1, \quad (3.12)$$

$$\sigma_{m,II} = \sigma_{m,I} \alpha, \quad (3.13)$$

$$\alpha = \frac{1}{1 - \frac{\sigma_{c,0}}{\sigma_{c,crit}}}, \quad (3.14)$$

$$\sigma_{c,crit} = \frac{\pi^2 T_k I}{l_k^2 A}, \quad (3.15)$$

$$T_k = \begin{cases} E & \text{for } \frac{\sigma_{c,0}}{f_{c,0}} \leq 0.5 \\ E \left[1 - \left(2 \frac{\sigma_{c,0}}{f_{c,0}} - 1 \right)^{\beta_T} \right] & \text{for } \frac{\sigma_{c,0}}{f_{c,0}} > 0.5 \end{cases}, \quad (3.16)$$

where $\sigma_{c,0}$ is the stress along the beam axis, $f_{c,0}$ the compressive strength along the grain, $\sigma_{m,II}$ the stress from bending according to second order theory, f_m the bending strength, $\sigma_{m,I}$ the stress from bending according to first order theory, α the enlargement factor, $\sigma_{c,crit}$ the critical buckling stress according to Euler, I the moment of inertia, l_k the buckling length, A the cross-section area, T_k the buckling modulus, E the modulus of elasticity and β_T a constant to determine the buckling modulus. The value for β_T is 4.0 in the case of GLT and 3.0 in the case of solid timber. $\sigma_{m,I}$ can be determined by the multiplication of the normal force N with the

imperfection $w_0 = l_k/500$ in case of GLT and $w_0 = l_k/300$ in case of solid timber according to SIA 265:2021 [121].

Although Theiler (2014) [127] proposed to consider the non-linear behaviour of the buckling modulus T_k , this part was not implemented in SIA 265:2012 [120]. A non-exhaustive parameter study for typical truss beam geometries with joints with slotted-in steel plates conducted within this study revealed that its influence is small indeed, especially due to the lowered buckling out-of-plane resistance. Nevertheless, within the framework the material non-linearity is considered.

Another non-exhaustive parameter study was herein conducted to compare the two design approaches, *effective length method* and second order theory, in the range of typical truss beams. It revealed only minor differences between the two approaches (also when considering the adaptation for buckling out-of-plane discussed below). The main difference is the behaviour of the utilisation factor (Eq. 3.11 and 3.12). In the case of the *effective length method* a linear relationship between applied normal force (or stress) and the resistance can be observed. In the case of the second order theory this relation is highly non-linear due to the enlargement factor α from Eq. 3.14, meaning that at levels only marginally under the critical buckling load the utilisation according to Eq. 3.12 can still be low. This non-linearity might effect reliability analyses where adaptive procedures are applied and complicates decision-making in the design process.

Buckling in-plane of truss members

Both web and chord members can be exposed to compression forces and therefore to buckling in-plane. The major differences are that chord members get larger bending moments at mid-span due to compliance and that they can be externally loaded when forces act between the truss nodes inducing additional bending moments. The continuity of the moment of inertia in chords is only partially decreased by the slots in the joints, since the slots are aligned with the beam height.

Theoretically, the buckling length of continuous chord members but also the buckling length of web members could be reduced due to partial clamping compared to hinged beams. E.g. [100] proposes $l_k = 0.8s$ for web members, where s is the truss node distance. [11] proposes an equation based on the rotational stiffness of dowelled connections to derive the buckling length reduction factor for web members.

However, to find the actual buckling lengths for all configurations is quite demanding. Therefore, the conservative assumption that all buckling lengths correspond to the member lengths is implemented in the framework. The influence of this assumption will be discussed in Chapter 6.

Buckling out-of-plane of truss beams

In Sec. 2.3.2, the topic of out-of-plane buckling was outlined in detail for both the symmetric and the antisymmetric buckling modes of chords depending on the support conditions and also for the web members. In [11], it was mentioned that the buckling length of web members can be longer than the distance between the intersection of axes of the chords and web members. This is an issue of detailing though, i.e. how the compression chords are linked to the stiffening system, and is therefore neglected herein. The weakening due to the slots for the steel plates is

taken into account via the model from Fig. 2.16 and the procedure proposed by Tölke (1929) [128].

In the following, additional information is provided for the actual use in practise and the implementation in the framework. The reduction factor of the buckling resistance φ_0 (the indices 0 follows the specifications from [128]) is applied on the critical buckling resistance according to Euler. For the sake of better readability a new plot for the reduction factor can be found in Fig. 3.8. Still, even in this enhanced plot the precision of the reading is limited due to steep curves. When using the relation $\varphi_0 = 1/\beta_0^2$ or rearranged as $\beta_0 = \varphi_0^{-0.5}$, a better readable version can be plotted (Fig. 3.9). When following Eq. 3.17 (which is based on the proposal from [128]), it can be seen that β_0 can be understood as an amplification factor of the buckling length to determine the critical buckling load according to Euler N_{cr} .

$$N_{cr} = \varphi_0 \frac{\pi^2 E I}{l_k^2} = \frac{1}{\beta_0^2} \frac{\pi^2 E I}{l_k^2} = \frac{\pi^2 E I}{(\beta_0 l_k)^2} \quad (3.17)$$

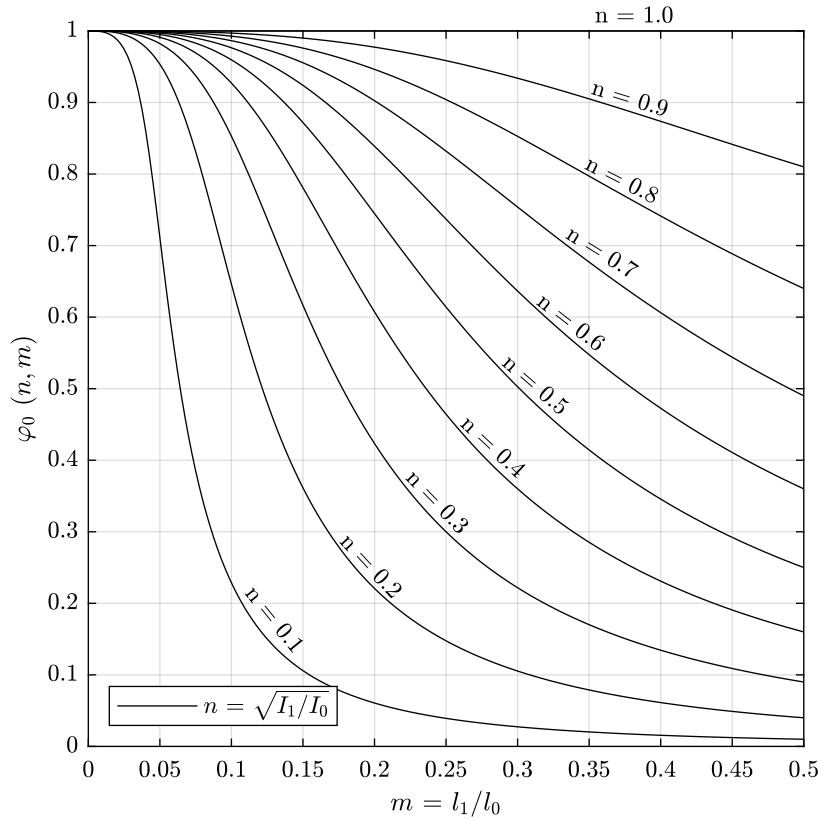


Fig. 3.8: Reduction factor φ_0 of buckling resistance due to slots in connection area.

In Sec. 2.3.2, it was mentioned that in Dubas et al. (1981) [26] it was recommended to simply use the reduction factor φ_0 directly on the buckling load. In Fig. 3.10, it can be observed that this simple reduction of the buckling reduction factor k_c according to SIA 265:2021 [121] with $\varphi_0 = 1/\beta_0^2$ is very conservative for low relative slenderness ratios λ_{rel} . It is therefore recommended to apply β_0 on the buckling length when using the *effective length method*.

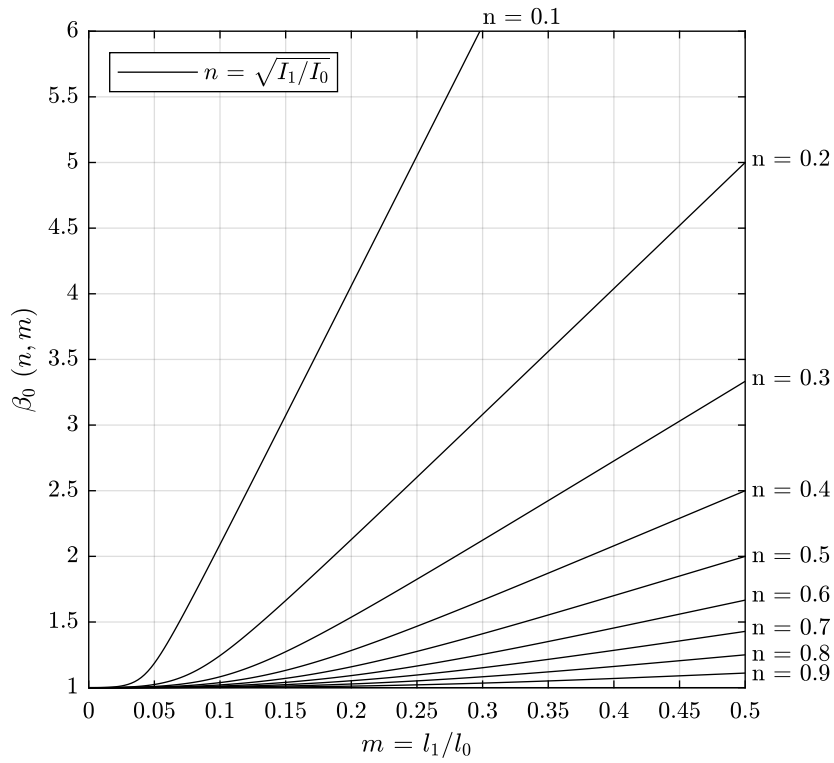


Fig. 3.9: Reduction factor β_0 of buckling resistance due to slots in connection area.

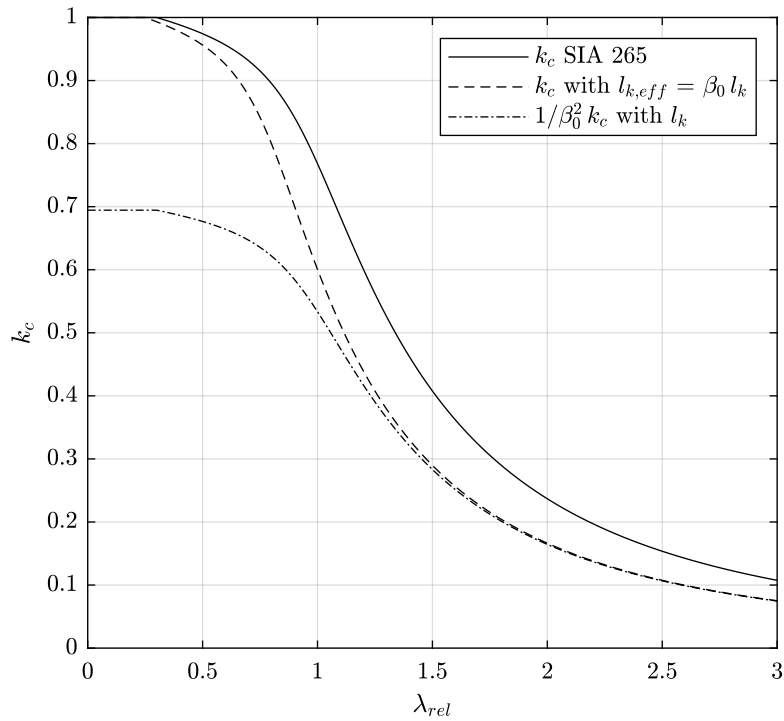


Fig. 3.10: Reduction factor k_c of the *effective length method* according to [121] combined with the reduction factor β_0 .

When using second order theory, φ_0 can be applied on the critical buckling stress according to Euler directly, which corresponds to an enlargement of the buckling length by β_0 . From the procedure explained above, only Eq. 3.15 has to be changed to:

$$\sigma_{c,crit} = \varphi_0 \frac{\pi^2 T_k I}{l_k^2 A} = \frac{\pi^2 T_k I}{(\beta_0 l_k)^2 A}. \quad (3.18)$$

Tölke (1929) [128] described the procedure how to determine φ_0 . He stated that for the transcendental equation Eq. 3.19 a solution can only be found by trials. Nowadays, one could possibly find approximate solutions by numerical or other methods. However, in this case a simple trick can be applied. When filling a table with φ_0 as the entries for the pairs of $n = \sqrt{I_1/I_0}$ in the columns in decreasing order from 1 to 0 and $m = l_1/l_0$ in the rows in increasing order from 0 to 0.50 each entry has to be smaller than the neighbours to the left and top (this format of the table was already presented by [128]). With such an algorithm a table with 201-by-201 entries was constructed. In the framework then for a pair of n and m simply the closest entry can be picked for a sufficient accuracy. The overall accuracy of this approach and its implementation in the framework is mainly dependent on the simplified modelling approach of the connection shown in Fig. 2.16.

$$\tan \left[\frac{1}{n} m \pi \sqrt{\varphi_0} \right] \tan \left[\left(\frac{1}{2} - m \right) \pi \sqrt{\varphi_0} \right] = \frac{1}{n} \quad (3.19)$$

3.3.2.7 Resistance models for the connections

Within this thesis, the resistance model for laterally loaded connections according to the design framework of SIA 265:2021 [121], which was presented in Sec. 2.4.2, is applied. For eccentric loading situations, which generally occur in connections of timber trusses, an additional reduction factor is introduced based on the master thesis of Manser (2021) [91].

Reduction of the load-carrying capacity for eccentrically loaded connections

Manser (2021) [91] used published test results from test configurations that allowed for testing laterally loaded connections with and without induced bending moments. In Gehri (1980) [48] and in Mischler (1998) [94], the test setup from Fig. 2.12 was used. Pedersen et al. (2001) [102] used another test setup where the bending moment was induced by a vertical load in mid-span of a simply supported beam as shown in Fig. 3.11. The resulting shear force was neglected by Manser and the derived model only considers the eccentricity of the bending moment in comparison to the normal force, i.e. the results were transformed into the form corresponding to the test configuration from Fig. 2.12.

In Fig. 3.12, the size proportions and the dowel layouts of the three connection configurations can be compared. This illustration shows that the reduction model should not take into account the eccentricity directly as used in Fig. 2.12 but a normalisation of the eccentricity by the connection height should be used instead. The connection height h_{conn} was introduced by Manser as the vertical distance of the two outer-most dowels. The absolute values for h_{conn} are the following: in Gehri 45 mm, in Mischler 160 mm and in Pedersen et al. 252 mm.

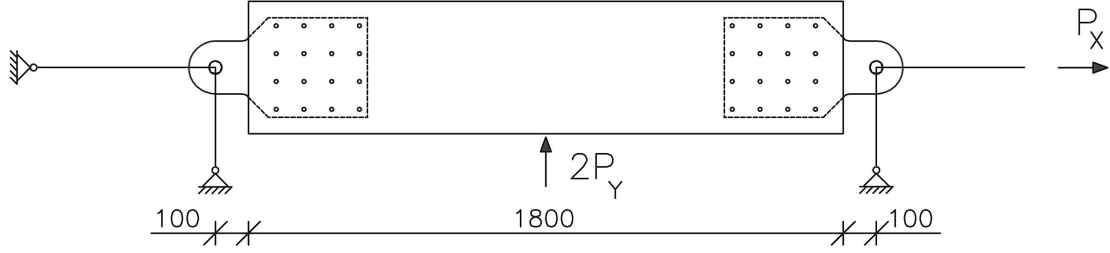


Fig. 3.11: Test setup from Pedersen et al. (2001) [102].

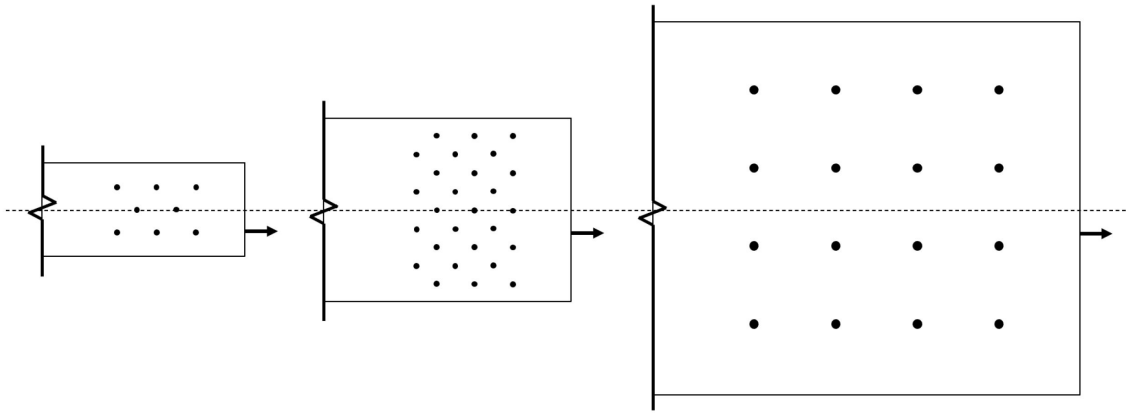


Fig. 3.12: Illustration of the size proportions of the three connection configurations from [91]. From left to right: Configuration of Gehri (1980) [48], Mischler (1998) [94] and Pedersen et al. (2001) [102].

Manser (2021) [91] found the following non-linear regression model for the reduction factor due to eccentric loading k_e with a coefficient of determination $R^2 = 0.88$:

$$k_e = \frac{F_{u,e}}{F_{u,0}} = 1 - 1.56 \left(\frac{e}{h_{conn}} \right)^{1.25}, \quad (3.20)$$

where $F_{u,e}$ is the ultimate load with applied eccentricity, $F_{u,0}$ the ultimate load without eccentricity, e the applied eccentricity and h_{conn} the connection height.

In Fig. 3.13, the used test results and the models from Gehri (1980) [48] (Fig. 2.12), SIA 265:2021 [121] (Sec. 2.3.3) and the proposal from Manser (2021) [91] (Eq. 3.20) are shown. When observing the intersection of the SIA 265:2021 model and the model from Eq. 3.20, it can be concluded that on mean level the reduction factor of 0.75 specified in SIA 265:2021 is conservative up to a relative eccentricity of 0.23 (intercept of *Model SIA 265* and *Regression improved*).

In future research it has to be clarified whether the simple combination of the used test data is accurate and conservative. From Fig. 3.13 one can observe that the model developed by Manser (2021) [91] is at least more conservative with respect to the normalised eccentricity than the original approach from Gehri (1980) [48].

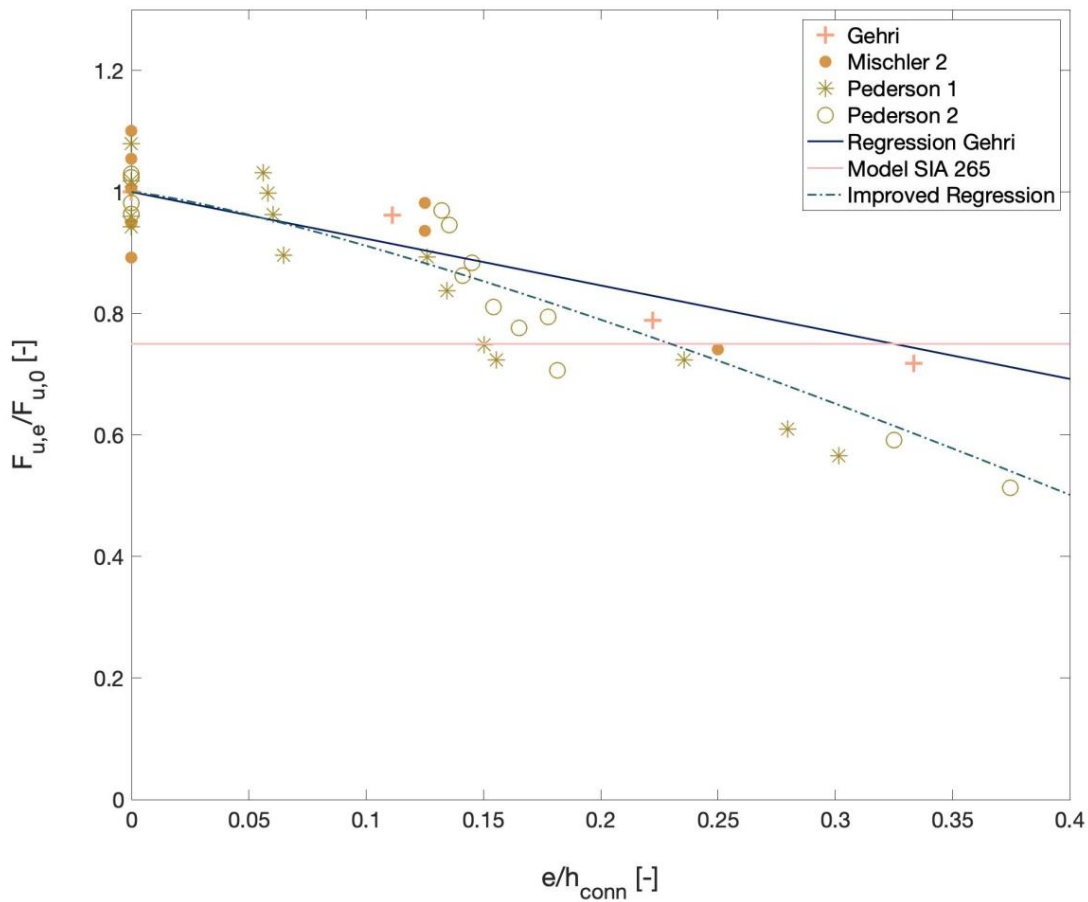


Fig. 3.13: Illustration of the reduction factor with respect to the normalised eccentricity with the used test data from Gehri (1980) [48], Mischler (1998) [94] and Pedersen et al. (2001) [102] and the models from Gehri (1980) [48], SIA 265:2021 [121] and Manser (2021) [91] according to [91].

3.3.3 Load-deformation behaviour of dowelled steel-to-timber connections

As shown in Fig. 3.2, the load-deformation behaviour per single dowel was intended to be derived from a BoS model. The development of an according model was taken care of by the doctoral thesis within this project conducted by Jonas Wydler. Since the derivation of the respective input parameters in the BoS model and with it the derivation of the load-deformation behaviour per single dowel is not finished until now, an alternative derivation took place. In the master thesis of Manser (2021) [91], the load-deformation behaviour of steel-to-timber connections per dowel and shear plane was investigated based on multi-dowel connection tests with dowel diameters between 6-12 mm. For this purpose she used load-deformation curves from literature (Mischler (1998) [94], Erchinger (2009) [32], Sandhaas (2012) [108], Langedijk (2007) [87] and van Groesen & Kranenburg (2007) [129]) and evaluated the data by means of an extended version of the parametric curve described by Richard & Abbott (1975) [107]. This approach allowed her to fit regression functions for the single parameters of the extended Richard & Abbott curve that take

into account various connection parameters. The curve is described by seven parameters which are illustrated and described in Fig. 3.14.

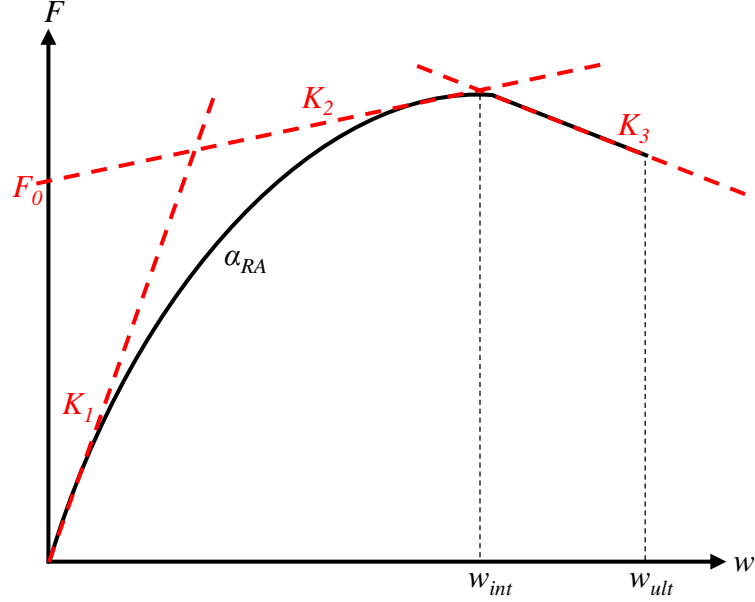


Fig. 3.14: Illustration of the curve characterising parameters of the extended Richard & Abbott curve, where K_1 [N/mm] is the initial stiffness, K_2 [N/mm] is the secondary stiffness, K_3 [N/mm] is the tertiary (decreasing) stiffness, F_0 [N] is the intersection of K_2 and the vertical axis, w_{int} [mm] is the deformation at the transition point of K_2 and K_3 , w_{ult} [mm] is the ultimate deformation and α_{RA} [-] is a parameter to control the curvature.

The load-deformation curve can be described by Eq. 3.21, where in the second case the deformation w_{int} is applied for the part similar to the first case:

$$F = \begin{cases} \frac{(K_1 - K_2)w}{\left(1 + \left(\frac{(K_1 - K_2)w}{F_0}\right)^{\alpha_{RA}}\right)^{\frac{1}{\alpha_{RA}}}} + K_2 w & \text{for } 0 \leq w \leq w_{int} \\ \frac{(K_1 - K_2)w_{int}}{\left(1 + \left(\frac{(K_1 - K_2)w_{int}}{F_0}\right)^{\alpha_{RA}}\right)^{\frac{1}{\alpha_{RA}}}} + K_2 w_{int} - K_3 (w - w_{int}) & \text{for } w > w_{int}, \end{cases} \quad (3.21)$$

where w is the deformation and F the force.

For the regression functions of all seven parameters a power function was chosen by [91]:

$$y = A n_{row}^B n_{col}^C d^D f_u^E \rho^F \left(\frac{t_1}{d}\right)^G \left(\frac{t_2}{d}\right)^H \left(\frac{a_1}{d}\right)^I \left(\frac{a_2}{d}\right)^K \left(\frac{a_3}{d}\right)^L \left(\frac{a_4}{d}\right)^M, \quad (3.22)$$

where the dependent variable y represents any of the seven curve characterising parameters from above. The independent parameters representing the connection parameters are listed below:

n_{row} [-]	Number of dowel rows
n_{col} [-]	Number of dowels in a row
d [mm]	Dowel diameter

f_u [N/mm ²]	Ultimate tensile strength of steel
ρ [kg/m ³]	Timber density
t_1/d [–]	Normalised thickness of side members
t_2/d [–]	Normalised thickness of middle members
a_1/d [–]	Normalised dowel-to-dowel distance
a_2/d [–]	Normalised dowel-to-dowel distance \perp
a_3/d [–]	Normalised dowel-to-end distance
a_4/d [–]	Normalised dowel-to-edge distance \perp .

In Tab. 3.1, the mean values of all data and the coefficient of determination R^2 of the regression functions are listed for the seven curve characterising parameters according to the values from [91]. The R^2 values indicate that for K_1 , K_2 , F_0 and w_{int} the regressions are well-applicable. w_{ult} is still acceptable to use. K_3 and α_{RA} are critical though, i.e. their regression functions can explain only a quarter of the variation. Since w_{ult} is not applied in the framework and the specific value of K_3 is of minor importance, only the vague results for α_{RA} might be of concern though.

Tab. 3.1: Mean values, coefficients of determination R^2 of the regressions and standard deviations of the Normal distributed error terms σ_ϵ of the regressions for the curve characterising parameters [91].

Parameter	mean values	R^2
K_1	4205 N/mm	0.92
K_2	165 N/mm	0.81
K_3	652 N/mm	0.24
F_0	6160 N	0.98
w_{int}	5.13 mm	0.71
w_{ult}	8.34 mm	0.59
α_{RA}	2.18	0.26

In Tab. 3.2, the coefficients A to M determined by Manser by means of non-linear regression for Eq. 3.22 are presented.

Since insufficient information on the load-deformation behaviour of connections loaded under other load-to-grain angles than 0° can be found in literature, Manser (2021) [91] evaluated the ratios between the curve characterising parameters for 0° and 90° load-to-grain angles of test series on single-dowel connections with a dowel diameter $d = 10$ mm and *Kerto S* LVL from the master thesis of Eschmann (2021) [33]. To obtain the curve characterising parameters perpendicular to the grain, the values based on the regression functions from above can be multiplied by the conversion factors specified in Tab. 3.3. For K_3 and w_{ult} no factors could be determined in [91].

Tab. 3.2: Coefficients of the regressions of Eq. 3.22 for the curve characterising parameters [91].

y	A	B	C	D	E	F	G	H	I	K	L	M
K_1	5.65	-0.68	-0.51	0.56	0.14	0.91	0.03	0.40	0.12	-0.09	0.09	-0.49
K_2	10.4	3.73	1.64	3.89	-0.50	-0.33	1.77	-4.30	-0.58	2.37	0.42	-5.25
K_3	10547	0.65	0.42	-0.38	-0.05	-0.01	-0.25	-1.23	-0.16	0.22	-0.27	0.03
F_0	29.6	-0.44	-0.26	1.00	-0.25	0.84	0.17	0.25	0.09	-0.27	0.10	-0.13
w_{int}	573	-0.62	-0.72	-0.32	-0.41	-0.25	0.31	0.74	0.06	-0.92	0.12	0.36
w_{ult}	0.21	-0.91	-1.20	-0.94	-0.33	1.35	0.25	0.83	0.50	-0.73	-0.21	0.33
α_{RA}	1.45	0.37	0.25	0.25	0.00	-0.05	0.05	-0.45	-0.15	0.25	-0.10	0.20

Tab. 3.3: Conversion factors between the values of the single-dowel load-deformation behaviour per shear plane for 0° and 90° load-to-grain angle based on [91].

K_1	K_2	F_0	w_{int}	α_{RA}
0.33	2.0	0.61	1.4	1.4

For parallel-to-the-grain loading, the load-deformation behaviour developed by Manser (2021) [91] can be compared to the specifications of EN 1995:2004 [31] and SIA 265:2021 [121]. The following parameters are compared:

- Slip modulus K_{ser} of EN 1995:2004, i.e. twice the value of Eq. 2.12 (adaption for steel-to-timber connections).
- Slip modulus K_{ser} of SIA 265:2021, i.e. Eq. 2.13.
- Connection load-carrying capacity on design level of SIA 265:2021, i.e. Eq. 2.11.
- Connection load-carrying capacity on mean level based on SIA 265:2021, i.e. Eq. 2.11 where the safety factors were removed from the individual parameters as it is explained in the subsequent Chapter in Sec. 4.4.2.1.
- Initial stiffness K_1 based on Manser (2021). i.e. Eq. 3.22.
- Non-linear load-deformation curve based on Manser (2021), i.e. Eq. 3.21.

The comparison considers all connection parameters as listed above and takes place for the load-displacement behaviour of a single dowel with four shear planes due to two slotted-in steel plates, i.e. the force per dowel F_i and the displacement per dowel δ_i , as they are applied in the algorithms presented in Sec. 3.3.2.4. In Fig. 3.15 the load-deformation behaviour of connections with different amounts of dowels with $d = 6$ [mm] are visualised. While K_{ser} from the design standards remain unaffected, the initial stiffness K_1 by Manser shows a softer behaviour for connections consisting of more dowels. The non-linear model by Manser changes considerably with respect to the dowel force and the transition point w_{int} . For only one dowel, the discrepancy of the non-linear model to the dowel load-carrying capacity according to SIA 265:2021 is large. No single-dowel connections with a dowel diameter of only 6 mm are in the database underlying the regression model, and hence, this case is an extrapolation of the model. Therefore, most likely this load-deformation behaviour is too optimistic. As single-dowel connections are practically irrelevant and are omitted in the further investigations of this thesis, this circumstance should not induce further issues. Generally, a certain discrepancy between the models by Manser and SIA 265:2021 can be explained e.g. by the negligence of the rope effect in SIA 265:2021. Comparing Fig. 3.15 (d) and (e), one can observe that the enlargement of the timber member thickness and the dowel spacings along the grain have a positive influence on the initial stiffness and the non-linear curve by Manser. Investigating the entries in Tab. 3.2, these physically logical findings are in line with the regression coefficients. For enlarged dowel spacings vertical to the

grain, a negative influence on the non-linear model results though, which physically is illogical. In the investigations of this thesis, these parameters are not further addressed (the same for all cases) and hence, no issues are expected to result. For other studies, these aspects have to be considered carefully though. Changes in the density or the steel strength cannot be considered independently, since they affect the selection of the member thickness. Further, in the scope of this thesis, these parameters are not specifically chosen to influence the load-deformation behaviour and hence, no special investigations are conducted herein for these parameters.

In Fig. 3.16 the results of similar investigations are presented for a dowel diameter of $d = 12$ [mm]. Again, for only one dowel, a major discrepancy in the load-carrying capacity can be observed. For larger connections, once more, a significant aggravation of the load-deformation behaviour can be observed. With that large diameters it is practically not desirable to enlarge the timber member thickness. Comparing Fig. (d) (e), one can observe that enlarging the parallel-to-grain spacings is enhancing the load-deformation behaviour, but only marginally. In comparison to the case with $d = 6$ [mm], in the case with $d = 12$ [mm], the K_{ser} of both design standards EN 1995:2004 [31] and SIA 265:2021 [121] are better aligned. Still, a large discrepancy can be found comparing them to K_1 , which is dependent on the actual connection configuration.

Investigating both Fig. 3.15 and 3.16, a clear conclusion can be drawn: according to the regression model developed by Manser (2021) [91] the actual connection configuration influences the load-deformation behaviour strongly with respect to the connection load-carrying capacity, the initial stiffness and also the shape and transition of the curve. In the design standards, the connection load-carrying capacity is only dependent on the number of dowels in a row and the slip modulus K_{ser} is assumed to be independent (Sec. 2.4). This discrepancy calls for further investigations in future publications.

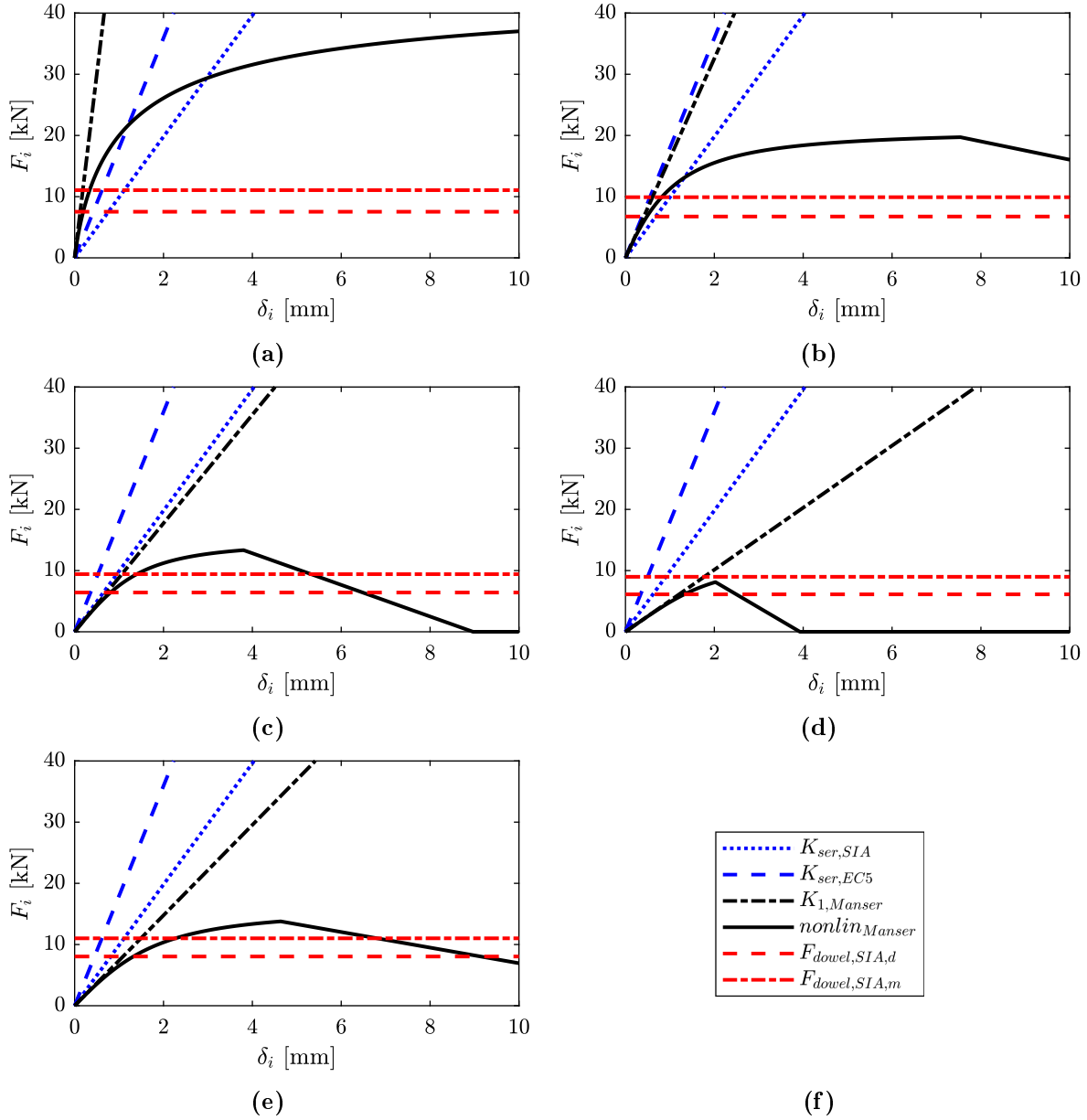


Fig. 3.15: Comparison of the load-deformation behaviour per dowel for dowelled steel-to-timber connections with the following specifications: $d = 6$ [mm], $\rho_m = 420$ [kg/m³], $f_u = 510$ [N/mm²], $t_1/d = 3.3$, $t_2/d = 8.3$, $a_1/d = 7$, $a_2/d = 3$, $a_3/d = 7$, $a_4/d = 4$; (a) $n_{col} = 1$, $n_{row} = 1$; (b) $n_{col} = 3$, $n_{row} = 3$; (c) $n_{col} = 5$, $n_{row} = 5$; (d) $n_{col} = 8$, $n_{row} = 8$; (e) $n_{col} = 8$, $n_{row} = 8$ and enlarged member thickness and spacings along the grain: $t_1/d = 7.5$, $t_2/d = 17$, $a_1/d = 10$, $a_3/d = 10$; (f) legend.

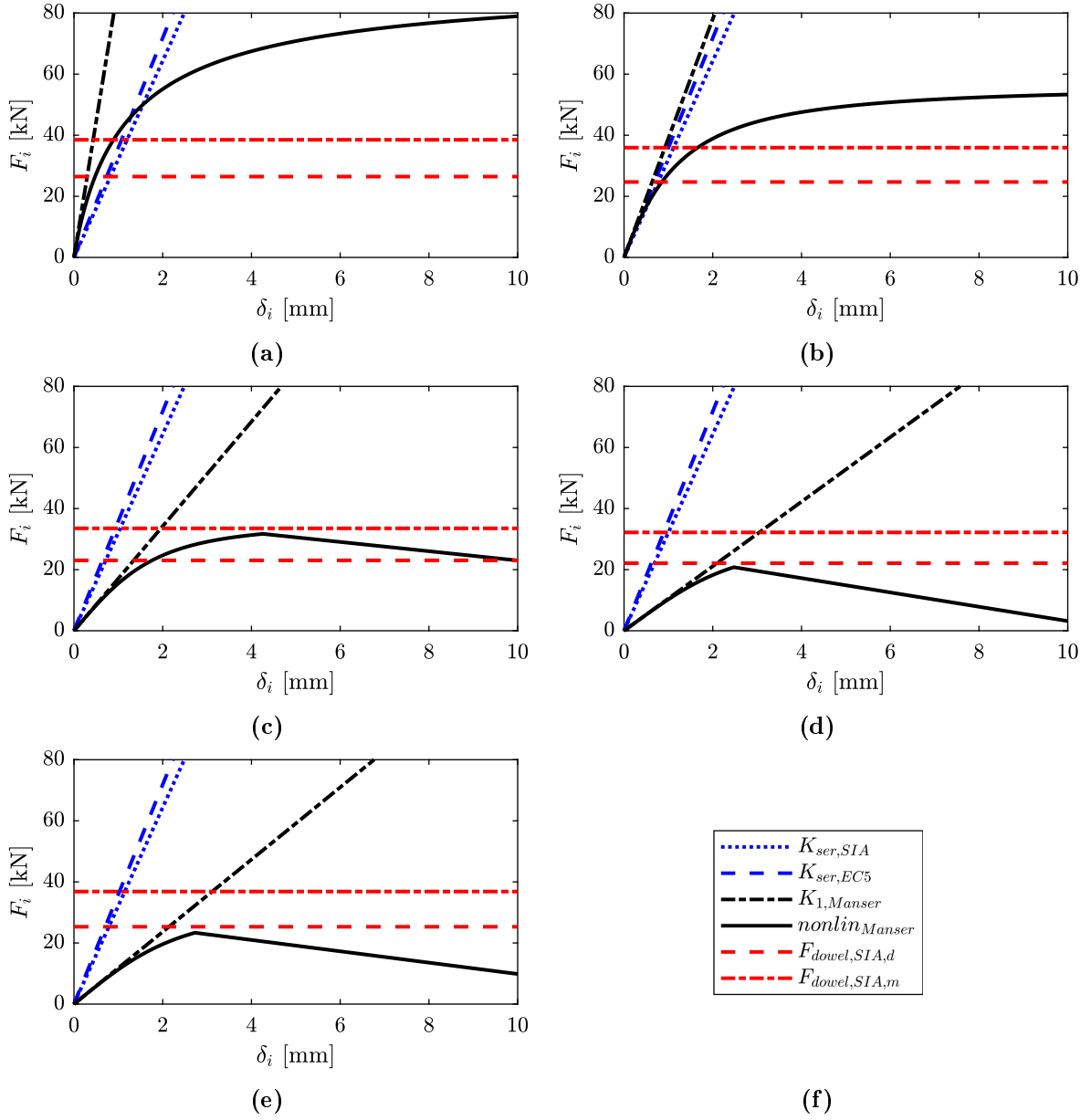


Fig. 3.16: Comparison of the load-deformation behaviour per dowel for dowelled steel-to-timber connections with the following specifications: $d = 12$ [mm], $\rho_m = 420$ [kg/m³], $f_u = 510$ [N/mm²], $t_1/d = 3.8$, $t_2/d = 8.3$, $a_1/d = 7$, $a_2/d = 3$, $a_3/d = 7$, $a_4/d = 4$; (a) $n_{col} = 1$, $n_{row} = 1$; (b) $n_{col} = 2$, $n_{row} = 2$; (c) $n_{col} = 4$, $n_{row} = 4$; (d) $n_{col} = 6$, $n_{row} = 6$; (e) $n_{col} = 6$, $n_{row} = 6$ and enlarged spacings along the grain: $a_1/d = 14$, $a_3/d = 14$; (f) legend.

3.4 Truss design tool

3.4.1 Introduction

A truss design tool was developed in MATLAB vers. R2020a in order to efficiently design timber trusses with dowelled steel-to-timber connections according to the simplified design approach from SIA 265:2021 [121] (Sec. 2.3.3). Therefore, the truss and web layout, the basic geometric properties (of the truss and the hall) as well as the timber properties, and the reference height for the snow load have to be chosen. Then, the connections and the member heights are generated. The fulfilment of the design approach requirements are then checked and one can choose whether the input file for the framework with all possibilities of the load-deformation behaviour of the connections should be generated. The selection of alternative GLT strength class, beam width and dowel diameter is left to the user.

3.4.2 Input

The following list of input has to be provided for the truss constructor. The input of the number of segments of the bottom chord is used as the key element for the automated generation of the nodes and beams of the respective truss shapes with corresponding web layouts under the given geometric inputs.

- truss shape
 - triangular truss
 - parallel chord truss
 - duopitch roof truss with raised eaves
 - bowstring truss
 - bowstring truss with raised eaves
 - monopitch roof truss
 - monopitch roof truss with raised eave
- web layout
 - falling and rising diagonals
 - rising and falling diagonals
 - falling and rising diagonals with mid-post
 - falling and rising diagonals with posts
 - rising and falling diagonals with posts
 - falling diagonals with posts
 - rising diagonals with posts

- length of the truss
- height of the truss
- eave height if existent
- distance between trusses
- reference height for snow load
- number of segments of the bottom chord
- dowel diameter
- beam width
- GLT strength class
- whether self-weight is considered

3.4.3 Ultimate limit state

The loading for the dimensioning of the truss is based on the ultimate limit state loading conditions according to SIA 260:2013 [117] and follows the provisions from Sec. 4.6. The characteristic snow load is determined by Eq. 4.32 and then multiplied by the accumulation area of the purlin distance times the truss distance and the partial safety factor of 1.5. Eq. 4.34 is used to determine the load of the super structure $F_{pur,tilt}$ acting in the truss nodes and multiplied by the partial safety factor of 1.35. Generally, not all load introduction points have the same accumulation area. Hence, in all cases half of the distance to the neighbouring load introduction points are used. The normal forces of the beams are then determined by a simple linear elastic finite element code applied with truss beams (assumptions postulated by Culmann [22]).

If the self-weight is considered (what generally should be done), an iterative procedure is applied. The dimensioning of the components (see next section) is done based on the external loading and the self-weight, which depends on the cross-sections from the iteration before, until no changes occur any more. The self-weight in the design tool is considered by means of concentrated nodal forces in the main truss nodes.

3.4.4 Connection and beam dimensions

For all cases, connections with two steel plates of 5 mm thickness with an additional gap of 1 mm are applied. With the selected dowel diameter, beam width and GLT strength class the resistance of a single dowel is determined for the case of parallel to the grain and perpendicular to the grain loading. Then, for all beams the minimal net-cross-sections (Sec. 3.3.2.6) are determined according to the simplified design approach of SIA 265:2021 [121] (Sec. 2.3.3), i.e. the resistances are multiplied by the reduction factors of 2/3 or 0.75, respectively. The normal forces of the chord-connections are determined from the difference of the neighbouring chord segments, the

connection forces in the web members coincide with the member forces. The connection configurations are determined iteratively within given layout choices, where the minimum connection has two dowels in one column. For larger forces, the layout is found iteratively by means of a number of columns which is equal to the number of rows minus two under consideration of the reduction factor for the number of dowels in a row from Eq. 2.10.

For the height of the bottom chord and the web members, the number of dowel rows together with the provisions from SIA 265:2021 [121] for the minimum distances and the beforehand calculated minimum net-cross-section are sufficient to determine the beam height. In the case of the top chord, the load introduction has to be considered additionally. The load generally acts on the top chord directly, which is then supported by the web members via the steel plates and the chord connections. Therefore, the determined connection layout is checked, whether the vector sum of the induced load and the acting normal force can be carried, and enlarged if necessary.

After the determination of the connections, the stability of the compressive members is checked and if necessary the member heights are enlarged. The basic buckling length herein coincides with the member length. In all cases, the *effective length method* according to SIA 265:2021 [121] is applied and out-of-plane the buckling length is enlarged by the factor β_0 (Sec. 3.3.2.6). For the determination of l_1 (Fig. 2.16) the effective angles between the web members and the chords and the connection geometries are respected, but a possible inclination of the top chord is neglected. The derived equations are expected to deliver realistic results, although in some cases additional constraints might occur, leading to small errors. In practice the effective truss joint geometry can be respected easily by drafting exact connection details, but for the amount of trusses considered herein this effort would be infeasible. The possible heights of the chord members are restricted arbitrarily to a ratio of the height divided by the width equals to 4 and for the web members this ratio is restricted to 3. Otherwise, a flag is risen and the user should select a larger member thickness or GLT strength class and possibly adapt the dowel diameter. The user should select beam widths in increments of 20 mm and the determined heights are automatically rounded up to increments of 40 mm (lamella thickness) [64].

3.4.5 Serviceability limit state

In a next step, the linear elastic finite element code is applied again to determine the deflections under serviceability limit state loading conditions. The found result is then compared to the provisions from SIA 265:2021 [121] and SIA 260:2013 [117], i.e. the user is informed whether the deflections are within the limits of 2/3 of the admissible deflections which are herein chosen to 1/350 (for *functionality with ductile installations*) times the truss length. The SLS design load (Eq. 3.23) is determined under consideration of the creep factor of $\varphi = 0.6$ and the respective reduction factors ψ_1 and ψ_2 for the characteristic snow load $Q_{s,k}$. Conservatively, the entire self-weight G and weight of the super structure $F_{pur,tilt}$ is considered for the deflection checking, although in dependence of the construction process some parts could be neglected.

$$E_d = (1 + \varphi) (G + F_{pur,tilt} + \psi_2 Q_{s,k}) + (\psi_1 - \psi_2) Q_{s,k} \quad (3.23)$$

3.4.6 Output

After the design and determination of the deflections, the user is informed about geometric details such as the chord-to-truss slenderness. In case of too slender cross-sections due to buckling, a flag is risen to advise the user to change the input. If the user is satisfied with the received truss, a table is provided with all the output in a format which can be used directly as input for the developed framework (Sec. 3.3). Additionally, different load-deformation behaviour approaches are provided, which can be easily selected for parametric studies (Sec. 5.2).

3.5 Conclusions

Different aspects of modelling timber trusses were discussed such as the modelling of the joints and the connection behaviour. The developed multi-scale modelling approach intends to provide a show-case on how a structure can holistically be investigated.

Subsequently, a framework that takes into account all elements of timber trusses with dowelled steel-to-timber connections was developed. The introduced joint typology allows for an effective automation of the modelling process and a convenient usability by parametrisation. The finite elements were explained in detail and a necessary update for the implementation of the joint model derived in Schweigler et al. (2018) [115] as a subroutine was presented with corresponding algorithms. The resistance models for the timber members were described in detail with a special focus on the buckling behaviour based on the cross-section weakening due to the slots for the steel plates. The procedure developed by Tölke (1929) [128] was discussed and the calculation of the reduction factor was explained. Both models derived by Manser (2021) [91] for the load-deformation behaviour and the reduction factor for the load-carrying capacity under eccentric loading were presented with all necessary details for an implementation.

Finally, a truss design tool was presented which makes use of the simplified design approach from SIA 265:2021 [121]. It allows for a parametrised design of various truss layouts in combination with web member layouts. Further details such as the length, height, dowel diameter, etc. can be specified and thanks to the built-in finite element code the normal forces and deformations according to the assumptions postulated by Culmann (1866) [22] can be processed for the design of the individual beams and connections. Further, the necessary input for the above-introduced framework is provided as an output of the design tool.

Chapter 4

Probabilistic modelling

4.1 Introduction

As already described in Sec. 2.5.1.1 for reliability analyses the variability of model input parameters has to be taken into account. In this section these probabilistic models are presented for timber products, especially glued laminated timber (GLT), steel products and for the actions imposed on the structures. Next to these inherent variabilities, model uncertainties are introduced for the resistance models of the timber members, the load-carrying capacity and the load-deformation behaviour of the connections and the snow loads. For many aspects in this chapter, a combination of findings from literature and own investigations is presented.

Generally, the selection of probability density functions (PDF) can rely on different aspects. One can apply pure statistical inference and hence, select the best model according to mathematics. Another possibility is to consider fundamental physical behaviour, e.g. certain properties can only take positive values. For certain test evaluations in engineering, standards are available that regulate which distribution types should be selected to guarantee e.g. comparability between test series conducted at different institutions. Other reasons, such as compatibility with size-effect models may also influence the model selection. Further, in certain situations the entity of data is applied to fit a distribution and in others, only a specific range of quantiles are selected. E.g. in code calibration, the lower tail of a PDF is most important to fit the data and hence, lower-tail fitting is conducted. In this study, the overall approach was to fit distribution functions to entire data sets. Herein, but also in related fields such as structural robustness (Sec. 2.7), the system behaviour is of utmost importance. This is why the probabilistic description of the properties has to be evenly accurate in the entire range. The complexity of the proposed models might be higher than it typically is in the scope of standardisation of design codes. Especially the nowadays available methods of structural reliability (Sec. 2.5.3), software packages and computational power justify the slightly more complex but more accurate probabilistic models than they were sought some decades ago. These considerations lead to the following selection principle within this study: for physical reasons, some PDF were excluded a priori; the statistical inference was usually conducted based on a maximum likelihood approach over the entire data sets; and some considerations of standards were applied, but often different PDF were selected and size-effect models were applied that nowadays can be applied easily within software packages.

Some of the discussed aspects in this chapter are not applied in the further investigations of this thesis such as GLT strength and stiffness properties perpendicular to the grain, the mixed mode fracture energy or part of the steel properties. Within the scope of the underlying research project, ongoing developments of enhanced connection resistance models indicate that these properties are fundamental though and therefore they were derived and are presented in this thesis.

4.2 Timber products

4.2.1 Overview of timber products

A huge variety of timber products exists. Herein the focus is on engineered structures, for which the most simple product is solid timber, which is basically a prismatic cut-out of timber logs. For more information about the characteristics and the probabilistic model of solid timber, the interested reader is referred to [71] and [82].

Apart from this almost raw use, a variety of so-called engineered timber products exist. An overview of the production process and the end products is given in Fig. 4.1. Three major production principles exist: sawing of boards, peeling of veneers, and stranding. From these three base products different end products can be produced by using different arrangements, orientations and bonding techniques.

The characteristics of the end products can be manipulated by choosing an adequate base product and configuration of it. For instance the orientation of the single base products is decisive for the structural behaviour of the product in these respective orientations. Further, the smaller or thinner the single base products are, the more homogeneous the end product is.

For engineered timber trusses, mainly two product categories are used: glued laminated timber (GLT) and laminated veneer lumber (LVL). Nowadays, the market share for GLT is bigger. Both products are available from coniferous (softwood) and deciduous (hardwood) species. For LVL, it is possible to choose a configuration with all the veneers oriented along the beam axis or with a certain amount of veneers orthogonal to it. With the latter solution, some capacity towards the main loading direction may be lost, when used with dowelled connections, a reinforcement against splitting is achieved though [80]. Apart from the production method, the main difference between GLT and LVL is the thickness of the lamellas. For GLT, it can vary between 6 and 45 mm (regular: 40 mm) and for LVL, a maximum of 6 mm is prescribed (regular: 3 mm) [64]. The single boards or veneers can be jointed endlessly along their axis. That is why length-restrictions of the end products exist mainly due to transportation and manufacturing. Strength grading of the single lamellas or veneers allows for a categorisation into strength classes of the end products. Concerning the strength grading of GLT, the interested reader is referred to [37].

In the scope of this thesis, it was decided to focus on GLT. In the following section, the relevant GLT properties are discussed and respective probabilistic models are presented.

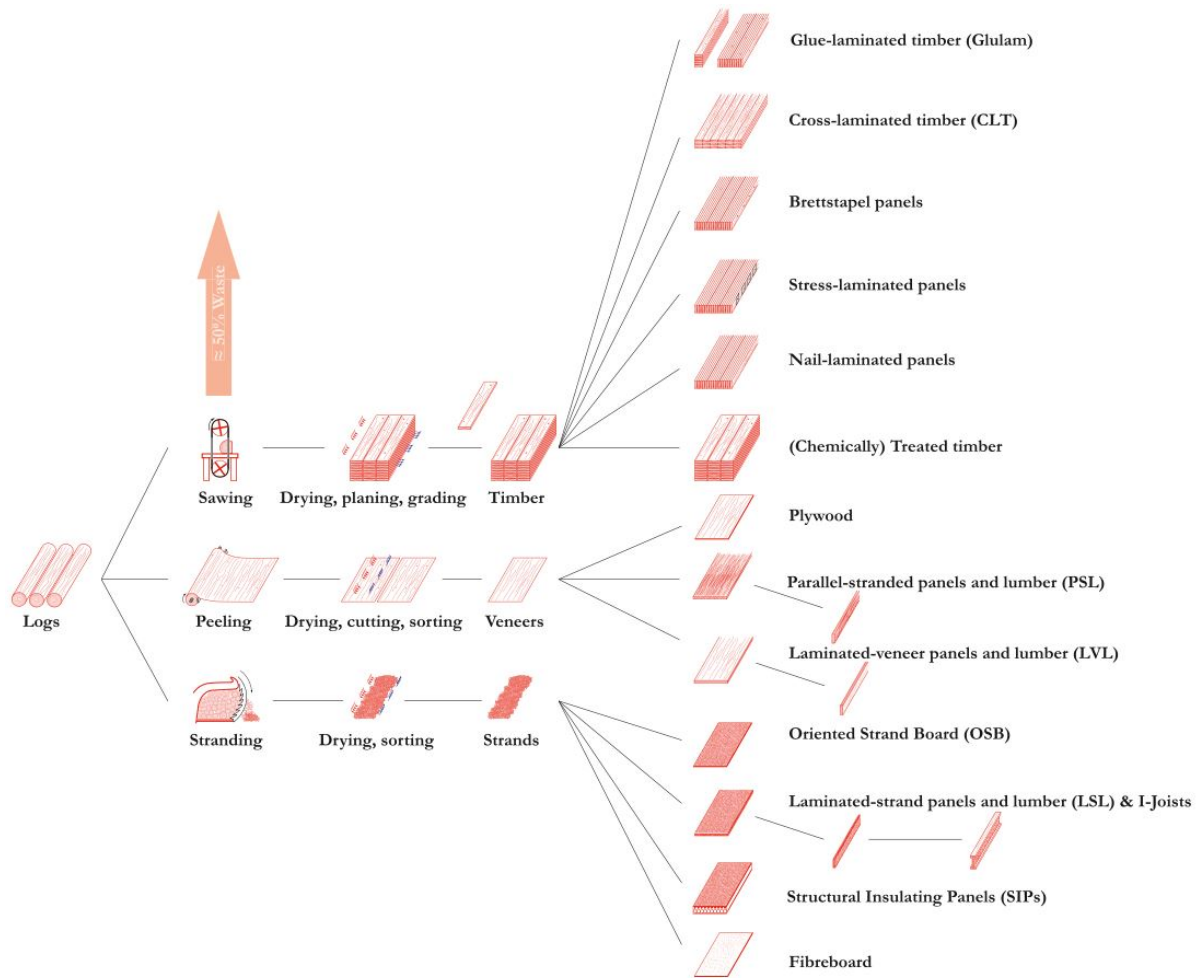


Fig. 4.1: The processing chain of engineered timber products [104].

4.2.2 Glued laminated timber

4.2.2.1 Introduction

To the knowledge of the author, no document exists that summarises all properties of GLT with respect to a full probabilistic description. Therefore, results from literature are presented, discussed and further evaluated for the most relevant properties.

Major parts of this section have been already published in Schilling et al. (2021) [113]. Herein, the intention is to provide a stand-alone section for each property. In each section, code provisions and relevant literature are presented and critically discussed, and the derivation of the proposed distribution functions with coherent size-effect models are explained. The derived probabilistic models are presented and referenced concisely in Tab. 4.1. The focus of the chapter is solely on homogeneous GLT due to the scope of the thesis, which deals with trusses. Their members are mostly stressed in axial direction and hence, combined GLT is of minor interest.

Tab. 4.1: Summary of proposed probabilistic models for GLT properties.

property	distribution function	parameters	size-effect model
f_m [N/mm ²]	2-p Weibull	Tab. 4.7	Eq. 4.1, 4.2
E_0 [kN/mm ²]	Lognormal	Tab. 4.9	Eq. 4.5
$f_{t,0}$ [N/mm ²]	2-p Weibull	Tab. 4.13	Eq. 4.6, 4.7, 4.8, 4.9
$f_{c,0}$ [N/mm ²]	Lognormal	Tab. 4.14	-
f_v [N/mm ²]	2-p Weibull	$a = 4.63, b = 8.31$	Eq. 4.10
G_v [N/mm ²]	Lognormal	$\lambda = 6.47, \zeta = 0.0513$	Eq. 4.5
$f_{t,90}$ [N/mm ²]	2-p Weibull	$a = 0.848, b = 3.688$	Eq. 4.12 / 4.11
$f_{c,90}$ [N/mm ²]	Lognormal	$\lambda = 1.05, \zeta = 0.0959$	-
E_{90} [N/mm ²]	Lognormal	$\lambda = 5.70, \zeta = 0.107$	-
ρ [kg/m ³]	Log-/Normal	Tab. 4.15	-

4.2.2.2 Code provision

In the JCSS PMC (2006) [71] for GLT, a prior probabilistic model is presented (Tab. 4.2) and part of the given values are indicative [83]. For most properties, only the type of distribution function is provided. These might be understood as recommendations where further knowledge is missing.

Tab. 4.2: Probabilistic models for properties for GLT according to [71].

	Distribution	COV
Bending strength: R_m	Lognormal	0.15
Bending MOE: E_m	Lognormal	0.13
Tension strength par. to the grain: $R_{t,0}$	Lognormal	
Tension strength perpendicular to the grain: $R_{t,90}$	2-p Weibull	
MOE - tension par. to the grain: $E_{t,0}$	Lognormal	
MOE - tension perpendicular to the grain: $E_{t,90}$	Lognormal	
Compression strength parallel to the grain: $R_{c,0}$	Lognormal	
Compression strength perpendicular to the grain: $R_{c,90}$	Normal	
Shear modulus: G_v	Lognormal	
Shear strength: R_v	Lognormal	
Density: ρ_{den}	Normal	0.1

Characteristic strength and stiffness properties as well as densities for different strength classes of homogeneous GLT are provided in EN 14080:2013 [29] (Tab. 4.3). The characteristic values are indicated by the index k and correspond to 5% quantiles.

Tab. 4.3: Characteristic strength and stiffness properties in N/mm² and densities in kg/m³ for homogeneous GLT according to EN 14080:2013 [29].

Symbol	Festigkeitsklasse von Brettschichtholz						
	GL 20h	GL 22h	GL 24h	GL 26h	GL 28h	GL 30h	GL 32h
$f_{m,g,k}$	20	22	24	26	28	30	32
$f_{t,0,g,k}$	16	17,6	19,2	20,8	22,3	24	25,6
$f_{t,90,g,k}$	0,5						
$f_{c,0,g,k}$	20	22	24	26	28	30	32
$f_{c,90,g,k}$	2,5						
$f_{v,g,k}$	3,5						
$f_{r,g,k}$	1,2						
$E_{0,g,mean}$	8 400	10 500	11 500	12 100	12 600	13 600	14 200
$E_{0,g,05}$	7 000	8 800	9 600	10 100	10 500	11 300	11 800
$E_{90,g,mean}$	300						
$E_{90,g,05}$	250						
$G_{g,mean}$	650						
$G_{g,05}$	540						
$G_{r,g,mean}$	65						
$G_{r,g,05}$	54						
$\rho_{g,k}$	340	370	385	405	425	430	440
$\rho_{g,mean}$	370	410	420	445	460	480	490

4.2.2.3 Selection of probabilistic models

Probability density functions (PDF) are used to describe single properties probabilistically. Most of them have two distribution parameters, which are usually derived from the mean value μ (or some specific quantile) and the standard deviation σ . In civil engineering it is common to introduce the normalisation of the standard deviation σ , i.e. the coefficient of variation CoV which is the ratio of σ/μ . It is one of the most important parameters when discussing the reviewed literature.

The authors of Frese (2016) [43], Frese & Blaß (2016) [44] and Frese et al. (2017) [45] kindly provided the data of interest from their simulation studies based on the "Karlsruher Rechenmodell". These data sets are used in many of the following chapters, hence, some considerations are presented here. For all data, the following distribution functions were fitted by means of maximum likelihood estimation (e.g. [114]): Lognormal, Gamma, Beta, two parameter (2-p) Weibull, and three parameter (3-p) Weibull. The Beta and 3-p Weibull distributions were used in the original publications and are well-suited to describe the data. The behaviour of their bounds are not or only limited suitable for reliability analysis. For the same reason the Normal distribution was excluded a priori. The Gamma distribution showed in most cases very similar characteristics

as the Lognormal distribution and since it is uncommon in timber engineering, it was excluded for further considerations. Tools like plots with the different probability density functions (PDF) over histograms, quantile-quantile-plots (QQ-plots) and the Bayesian information criterion (BIC) were applied to compare the different distribution functions (statistical inference). This analysis revealed that most of the data could be represented satisfactorily by either Lognormal $\mathcal{LN}(\lambda, \zeta)$ or 2-p Weibull $\mathcal{W}(a, b)$ distributions. The skewness of the data sets revealed itself to be a good indicator which of both is most suitable.

The statistical inference process of the data of Frese & Blaß (2016) [44] and Frese et al. (2017) [45] revealed that with changing specimen size also the fundamental behaviour, such as the skewness, changes. Since these changes occurred for small specimen sizes, satisfactory results could be achieved by describing the data size-independently by 2-p Weibull distributions. Another possibility to achieve more accurate models is the use of more powerful but also more complex distribution functions, e.g. the generalised lambda distribution. To the knowledge of the author, this function is unknown in timber engineering and therefore it is not proposed herein. For more information about generalised lambda distribution, the interested reader is referred to [131].

For other data sets used herein, that were provided by the authors in their publications, the inference process considered the same distribution functions and tools for comparison.

Whenever possible, the size effect of the structural members was taken into account directly within the probability density functions, i.e. separate size-effect models were applied to each parameter of the distribution function. This allowed describing separately the size effect on the location and on the scatter of the properties. In other cases, global size-effect factors were applied on the full distribution functions. These size-effect models therefore allow to shift the location of the probability density functions, but not their shape. For properties with brittle failure modes, the pure shift in location leads to minor errors when considering that for perfectly brittle materials the variability is a material constant and hence, the shape is not influenced by size effects [54, 130, 133]. The format of all size-effect models was chosen similar to Weibull-weakest-link models (Sec. 2.6.6), i.e. power functions in which the base is normalised to a reference size. All size-effect models were fitted with the MATLAB vers. R2020a function "nlinfit", i.e. an iterative least square estimation.

4.2.2.4 Bending strength

For the bending strength f_m the JCSS PMC (2006) [71] proposes a Lognormal distribution with a CoV of 15%. Compared to a CoV of 25% for structural timber the order of the value seems correct, when considering homogenisation effects from the assembly of the lamellas. In EN 14080:2013 [29] only the characteristic bending strength values are provided that correspond to the number within the strength class name by definition. Brandner & Schickhofer (2008) [14] concluded that the CoV of GLT is around 15%, more or less independent of the CoV of the tensile strength of the lamellas.

Fink (2014) [37] estimated the bending strength f_m and the modulus of elasticity (MOE) in bending E_m for GL24h and GL36h based on visual grading (Tab. 4.4) and machine grading (Tab. 4.5). For all simulations, a height of 0.6 m and a length of 10.8 m was selected which corresponds to a ratio of 1:18. This ratio corresponds to the specifications of EN 384 [2] which describes the procedure to determine characteristic values of mechanical properties. For GL24h, the required characteristic bending strength of 24 MPa was not reached in both grading schemes. The actual mean value should therefore be higher than the ones provided, i.e. probably higher than 30 MPa. The CoV seem to be plausible compared to the findings above. It also appears plausible that the scattering for visual-graded GLT is higher and that the scattering is higher for lower strength classes with less strict grading criteria. In the case of GL24h with non-shortened timber boards, the CDF of the empirical simulation data were plotted together with the fitted Lognormal distribution (Fig. 4.2, right). In both the lower and upper tail, a certain overestimation of the Lognormal distribution can be observed.

Tab. 4.4: Estimated material properties in bending [MPa] according to Fink (2014) [37].

Strength class	Board length	$f_{m,g}$			$E_{m,g}$	
		$f_{m,g,mean}$	$f_{m,g,k}$	COV	$E_{m,g,mean}$	COV
GL24h	shorted	27.1	21.1	0.14	10'700	0.03
	non-shorted	27.7	21.4	0.15	10'600	0.04
GL36h	shorted	42.2	33.9	0.13	15'200	0.03
	non-shorted	44.6	35.0	0.13	15'100	0.04

Tab. 4.5: Estimated material properties in bending [MPa] using machine-grading indicators according to Fink (2014) [37].

Strength class	Board length	$f_{m,g}$			$E_{m,g}$	
		$f_{m,g,mean}$	$f_{m,g,k}$	COV	$E_{m,g,mean}$	COV
GL24h	shorted	28.6	22.4	0.12	10'700	0.03
	non-shorted	29.0	22.7	0.13	10'700	0.04
GL36h	shorted	44.4	36.7	0.11	15'000	0.03
	non-shorted	45.5	38.0	0.11	14'900	0.04

The data sets of Frese (2016) [43] derived from simulations of the bending strength for visually graded GL24h and GL28h and for machine graded GL32h and GL36h were evaluated (Tab. 4.6). The simulated beams have a height of 0.6 m and a span of 10.8 m which corresponds to a ratio of 1:18. The tabulated mean values, standard deviations and CoV are empirical statistical estimates. The characteristic values are first provided empirically, i.e. the 50th value of 1'000, and for the 2-p Weibull distribution. For all strength classes the 2-p Weibull is an appropriate fit, despite a certain underestimation of the values in the lower tails. In contrast to the findings of

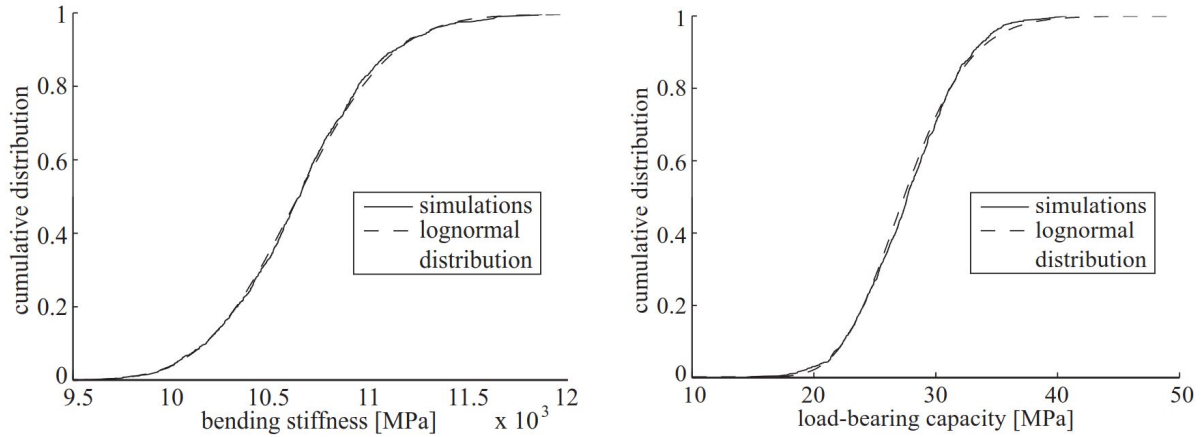


Fig. 4.2: Estimated bending stiffness (left) and estimated load-bearing capacity (right) of GL24h, non-shorted timber boards, number of simulations = 10^3 (Fink (2014) [37]).

Fink (2014) [37] in Tab. 4.6 no clear influence of the CoV with respect to the strength class can be observed. This agrees with the above-mentioned findings of Brandner & Schickhofer (2008) [14]. Therefore, the use of a CoV = 15% is proposed independently of the strength class.

Tab. 4.6: Statistical parameters for the bending strength f_m of GLT according to the data of Frese (2016) [43].

	GL24h	GL28h	GL32h	GL36h
$f_{m,mean}$ [N/mm ²]	33.3	38.1	43.5	47.1
$f_{m,k}$ [N/mm ²]	24.2/23.5	28.7/27.4	32.1/30.9	36.3/34.6
σ [N/mm ²]	5.21	5.50	6.64	6.56
CoV [%]	15.7	14.4	15.3	13.9
a [–]	35.5	40.5	46.3	50.0
b [–]	7.20	7.60	7.37	8.11

Frese & Blaß (2016) [44] conducted a size-effect study for the bending strength. For this purpose they simulated 10 different specimen sizes with heights between 0.3 m and 3.0 m and with a constant ratio of height to length of 1:18. These data sets were further evaluated by the author of this thesis. In Fig. 4.3 the skewness can be observed. As mentioned, for small specimen sizes the skewness is positive. The statistical inference further revealed that for the small specimen sizes, the 2-p Weibull is not a perfect fit, like it is undoubtedly for the large specimen sizes. For a specimen height of 0.6 m the Lognormal and the 2-p Weibull distribution show a similar BIC value and when plotted against the data, both show deficiencies. Therefore, a Lognormal distribution is the better choice only for small specimens. In the context of reliability analyses the use of the 2-p Weibull distribution is somehow on the safe side, since it underestimates the values in the lower tail, which are most critical for the reliability.

For all specimen sizes the two distribution parameters a and b of the 2-p Weibull are shown against the specimen heights in Fig. 4.4. For both, a clear trend can be observed. Since the

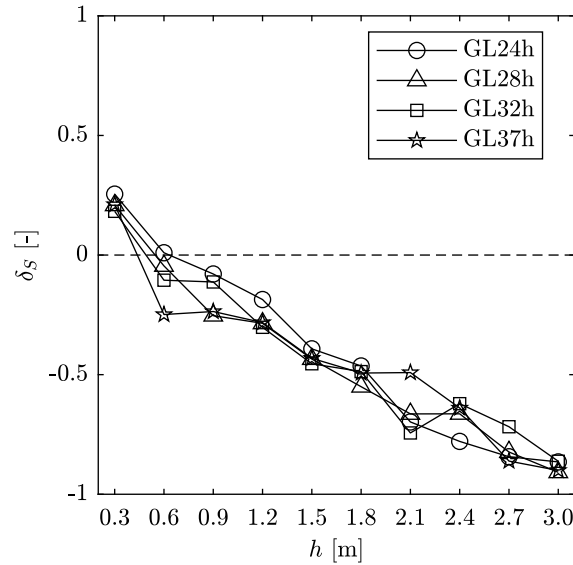


Fig. 4.3: Skewness δ_S of simulated bending strengths f_m vs. beam height h according to the data of Frese & Blaß (2016) [44].

strength classes do not correspond to the ones of Frese (2016) [43], a relative model is sought which uses 0.6 m as the reference height. Eq. 4.1 & 4.2 represent the individual size-effect factors for both Weibull parameters, where h is the beam height in [m]. It has to be kept in mind that since a constant ratio of 1:18 of height to length was used, the size effect is not a pure height but a height-length effect, i.e. the effect of both measures are included. Graphically the two functions are shown in dashed lines in Fig. 4.4. For ease of use and since the shapes are similar, the models consider all strength classes at once.

$$k_{m,y,h,a} = \left(\frac{0.6}{h}\right)^{0.18} \quad (4.1)$$

$$k_{m,y,h,b} = \left(\frac{0.6}{h}\right)^{-0.36} \quad (4.2)$$

In both simulation studies the characteristic values, which characterise the strength classes, are not exactly met for the reference height of 0.6 m. Therefore, the following values from Tab. 4.7 are proposed for the probabilistic representation of the bending strength. The underlying assumptions are the characteristic values of the corresponding strength classes and a CoV of 15% for all classes. From these two values and the assumption of a 2-p Weibull distribution all other values are derived. For the consideration of the size effect, the models according to Eq. 4.1 and 4.2 are proposed.

4.2.2.5 Modulus of elasticity

The JCSS PMC (2006) [71] proposes a Lognormal distribution with a CoV of 13% for the MOE in bending E_m . This is the same value as for structural timber, but due to homogenisation the value for GLT is expected to be lower. Fink (2014) [37] discussed this issue as well and found

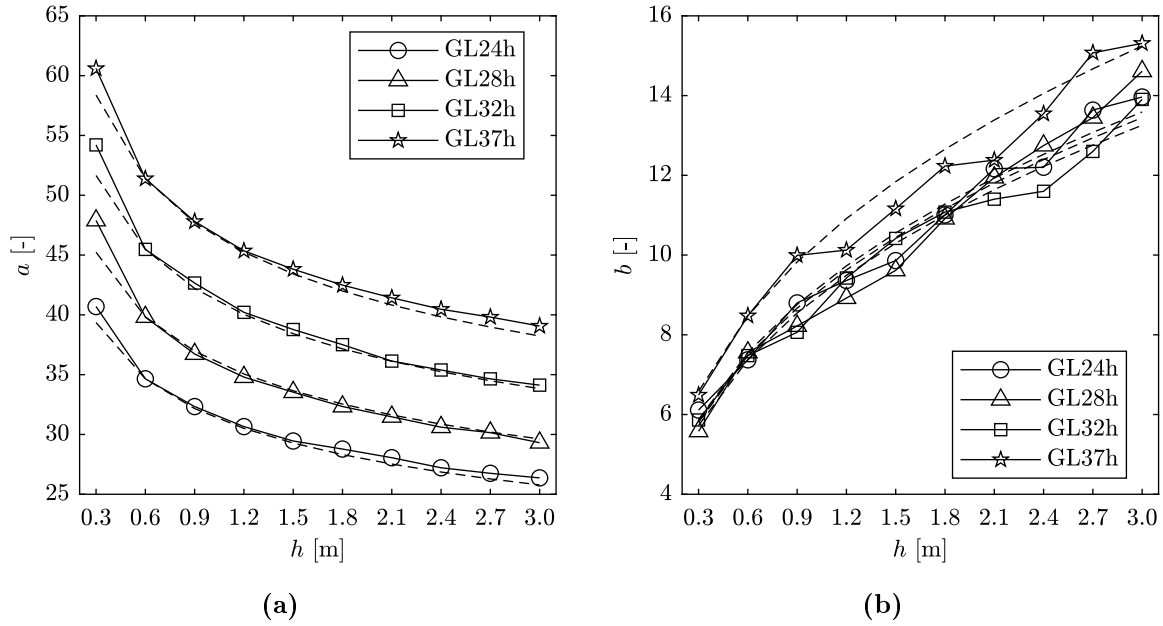


Fig. 4.4: Weibull distribution parameters of the bending strength f_m vs. height h according to the data of Frese & Blaß (2016) [44]; (a) parameter a (b) parameter b . The dashed lines represent the respective height effect models from Eq. 4.1 and 4.2.

Tab. 4.7: Proposed statistical parameters for the bending strength f_m of GLT for the reference height $h = 0.60$ m.

	GL20h	GL22h	GL24h	GL26h	GL28h	GL30h	GL32h	GL36h
$f_{m,mean}$ [N/mm ²]	27.4	30.1	32.9	35.6	38.4	41.1	43.9	49.3
$f_{m,k}$ [N/mm ²]	20	22	24	26	28	30	32	36
σ [N/mm ²]	4.11	4.52	4.93	5.34	5.76	6.17	6.58	7.40
CoV [%]	15	15	15	15	15	15	15	15
a [-]	29.1	32.0	34.9	37.9	40.8	43.7	46.6	52.4
b [-]	7.91	7.91	7.91	7.91	7.91	7.91	7.91	7.91

CoV in experimental campaigns from literature between 4% and 7.5%. From Tab. 4.4 & 4.5 it can be seen that he found simulated values of CoV in the range of 3% to 4%. For the case of GL24h with non-shortened timber boards the CDF of the empirical simulation data were plotted together with the fitted Lognormal distribution (Fig. 4.2, left). The Lognormal distribution is an appropriate selection.

When using a Lognormal distribution to determine the CoV of the different GLT classes according to EN 14080:2013 [29], a value of roughly 11% can be found (Tab. 4.8). That is why these provisions are not further considered.

The data sets of Frese (2016) [43] derived from the simulations of the MOE in bending, tension and compression for visually graded GL24h and GL28h and for machine graded GL32h and GL36h were evaluated. The results of these own investigations are presented in Tab. 4.9, 4.10

Tab. 4.8: Statistical parameters for the MOE in bending E_m of GLT according to EN 14080:2013 [29].

	GL20h	GL22h	GL24h	GL26h	GL28h	GL30h	GL32h
$E_{m,mean}$ [kN/mm ²]	8.40	10.5	11.5	12.1	12.6	13.6	14.2
$E_{m,k}$ [kN/mm ²]	7.00	8.80	9.60	10.1	10.5	11.3	11.8
σ [kN/mm ²]	0.904	1.10	1.23	1.29	1.36	1.49	1.55
CoV [%]	10.8	10.4	10.7	10.7	10.8	10.9	10.9
λ [-]	2.12	2.35	2.44	2.49	2.53	2.60	2.65
ζ [-]	0.107	0.104	0.106	0.106	0.107	0.109	0.109

and 4.11. All three configurations have a height of 0.6 m. In bending the span was chosen to a ratio of 1:18, i.e. 10.8 m, in tension the length was chosen to a ratio 1:9, i.e. 5.4 m and in compression a square of 0.6 m times 0.6 m was used. The tabulated mean values, standard deviations and CoV are empirical statistical estimates. The characteristic values are first provided empirically, i.e. the 50th value of 1'000, and for the Lognormal distribution. In all cases a good agreement can be found between the empirical and Lognormal characteristic values. When comparing the three loading situations, it can be observed that the tensile values are highest and the ones under compression are lowest. The scattering is smallest for compression and highest for bending. When comparing the values derived from the data of Frese (2016) [43] to the findings above, higher values were achieved along with more reasonable values for the CoV.

For ease of use, especially when applying finite element software, the provision of one data set for all loading situations is sought. It seems appropriate to use the data for the MOE in bending E_m , since their mean values are in-between the others but the CoV are the largest.

Tab. 4.9: Statistical parameters for the MOE in bending E_m of GLT for the reference height $h = 0.60$ m according to the data of Frese (2016) [43].

	GL24h	GL28h	GL32h	GL36h
$E_{m,mean}$ [kN/mm ²]	12.8	14.0	16.5	17.4
$E_{m,k}$ [kN/mm ²]	11.8/11.8	12.8/12.9	15.8/15.7	16.7/16.6
σ [kN/mm ²]	0.661	0.679	0.463	0.475
CoV [%]	5.15	4.87	2.82	2.73
λ [-]	2.55	2.63	2.80	2.86
ζ [-]	0.0513	0.0487	0.0281	0.0272

For the size effect of the MOE, Brandner et al. (2007) [16] and Brandner et al. (2008) [15] proposed two models, a simple linear one and a more sophisticated non-linear model. They describe the characteristic value in relation to the mean value in dependence of the quantity of lamellas n . The ratio of 67% is related to the value for solid timber ($n = 1$) and 90% is related to the reference height of 0.6 m with $n = 15$ for lamellas of 40 mm height:

$$E_k = E_{mean} \cdot \min \left[\frac{1}{60}(n - 1) + 0.67; 0.9 \right], \quad (4.3)$$

Tab. 4.10: Statistical parameters for the tensile MOE E_t of GLT for the reference height $h = 0.60$ m according to the data of Frese (2016) [43].

	GL24h	GL28h	GL32h	GL36h
$E_{t,mean}$ [kN/mm ²]	13.0	14.1	16.9	17.8
$E_{t,k}$ [kN/mm ²]	12.0/12.1	13.1/13.2	16.3/16.3	17.2/17.2
σ [kN/mm ²]	0.580	0.594	0.354	0.367
CoV [%]	4.45	4.21	2.10	2.06
λ [–]	2.57	2.65	2.83	2.88
ζ [–]	0.0446	0.0421	0.0209	0.0206

Tab. 4.11: Statistical parameters for the compressive MOE E_c of GLT for the reference height $h = 0.60$ m according to the data of Frese (2016) [43].

	GL24h	GL28h	GL32h	GL36h
$E_{c,mean}$ [kN/mm ²]	12.1	13.0	14.9	15.7
$E_{c,k}$ [kN/mm ²]	11.3/11.3	12.3/12.3	14.3/14.3	15.2/15.2
σ [kN/mm ²]	0.468	0.452	0.358	0.368
CoV [%]	3.88	3.48	2.41	2.33
λ [–]	2.49	2.56	2.70	2.76
ζ [–]	0.0387	0.0348	0.0240	0.0233

$$E_k = E_{mean} \cdot \min \left[1 - 1.645 \frac{0.20}{\sqrt{n}}; 0.9 \right]. \quad (4.4)$$

Further evaluation of the data of Frese & Blaß (2016) [44] showed that Lognormal distributions are an appropriate model for all different heights. Therefore, the height effect can be described via the distribution parameters directly. In Fig. 4.5a it can be seen that the first parameter λ is only slightly size-dependent, and hence, $k_{E,h,\lambda} = 1$ is proposed. The second parameter ζ is described by an equation of the typical format (power function) from Weibull's weakest link theory. The resultant model can be seen in dashed lines in Fig. 4.5b. For ease of use, the influence of the strength classes was neglected and considers all four classes at once in the fitted Eq. 4.5, where h is the beam height in [m]:

$$k_{E,h,\zeta} = \left(\frac{0.6}{h} \right)^{\frac{1}{1.28}}. \quad (4.5)$$

From the two models of Eq. 4.3 & 4.4 the corresponding ζ values of the Lognormal distribution were determined for all heights between 40 mm and 600 mm and in Fig. 4.6 compared to the proposed height model from Eq. 4.5 based on the values for GL24h. It is important to note that the model based on the data of Frese & Blaß (2016) was fitted to data between 0.3 m and 3 m and forced through the value of ζ at 0.6 m. That is why the model tends to fit better to larger beams than to the small ones, as shown in Fig. 4.6. Further, the GLT configurations used by

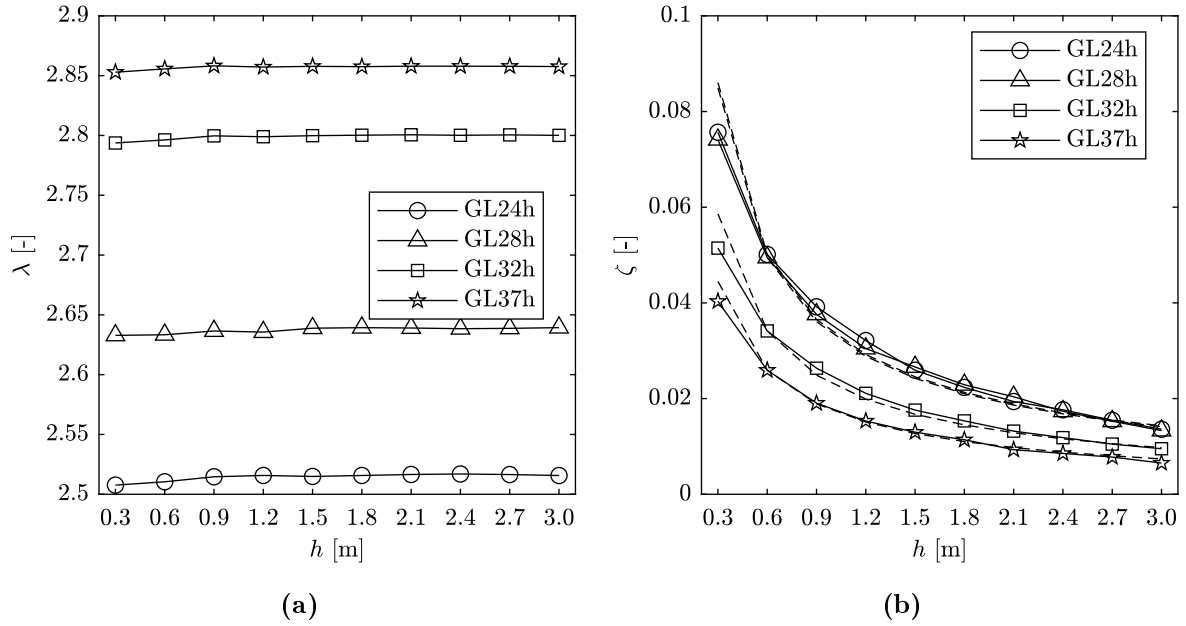


Fig. 4.5: Lognormal distribution parameters of the MOE in bending E_m vs. height h according to the data of Frese & Blaß (2016) [44]; (a) parameter λ ; (b) parameter ζ with the height effect model from Eq. 4.5 in dashed lines.

Frese & Blaß (2016) have a lamella thickness of only 30 mm. Still, the proposed model from Eq. 4.5 fits also for small beam heights.

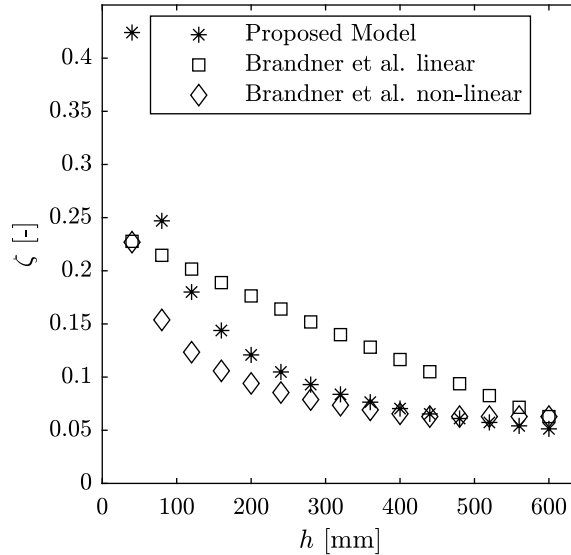


Fig. 4.6: Comparison of the height effect models for the second Lognormal distribution parameter ζ of the MOE from Eq. 4.5, 4.3 and 4.4.

Within the scope of this thesis, no table with values for all possible strength classes is proposed. The four grading classes presented in Tab. 4.9 are sufficient herein. Frese (2016) [43]

investigated more strength classes and hence, more data is available which should be evaluated in the context of another publication.

4.2.2.6 Tensile strength

A Lognormal distribution without a CoV for the tensile strength $f_{t,0}$ is proposed in the JCSS PMC (2006) [71]. EN 14080:2013 [29] provides only the characteristic tensile strength values. These values correspond to 80% of the characteristic bending strength, i.e. 0.8 times the number of the according strength class. The ratio is valid independently of the strength class. Frese (2016) [43] found the ratio between the characteristic tensile strength and the characteristic bending strength to be 88% and no dependence with respect to the strength classes. For his simulation study, the specimen height was chosen to 0.6 m and the length to 5.4 m, corresponding to a ratio of 1:9. The herein conducted statistical inference revealed the 2-p Weibull distribution to be appropriate. Heavy left tails and negative skewness are clear indicators. In Tab. 4.12 the mean values, the standard deviations and the CoV are empirical statistical estimates. The characteristic values are first provided empirically, i.e. the 50th value of 1'000, and for the 2-p Weibull distribution. Although the CoV shows a slightly decreasing behaviour for higher strength classes, it still seems appropriate to use a constant CoV of 11% independently of the strength class.

Tab. 4.12: Statistical parameters for the tensile strength $f_{t,0}$ of GLT for the reference length $l = 5.40$ m and the reference height $h = 0.60$ m according to the data of Frese (2016) [43].

	GL24h	GL28h	GL32h	GL36h
$f_{t,0,mean}$ [N/mm ²]	26.7	30.8	35.8	38.6
$f_{t,0,k}$ [N/mm ²]	21.3/20.8	24.6/24.5	28.2/29.1	32.0/31.6
σ [N/mm ²]	3.02	3.33	3.79	3.87
CoV [%]	11.3	10.8	10.6	10.0
a [–]	28.0	32.2	37.4	40.3
b [–]	10.1	10.8	11.8	12.3

Frese et al. (2017) [45] conducted a size-effect study for the tensile strength of GLT beams of lengths between 150 mm and 108 m, heights between 120 mm and 600 mm and two grading schemes, which resulted in GL23h and GL33h. In the herein conducted data evaluation, smaller lengths than 1.35 m were neglected due to practical irrelevance. The influence of the height was herein investigated based on three different heights of 120 mm, 360 mm and 600 mm. The statistical inference process showed that beams with short lengths and small heights can be described with a Lognormal distribution, where medium sized and large beams are clearly 2-p Weibull distributed. The plot of the skewness in Fig. 4.7 revealed itself to be a good indicator for the distinction of which distribution is a well-suited fit. When the skewness is positive, a Lognormal distribution is a good fit and around the value of zero the transition is made towards 2-p Weibull for clearly negative values. Hence, for increasing height, lengths and strength classes, 2-p Weibull is describing the data better. Since the practically relevant lengths only start from

around 2.7 m and heights of 120 mm are rare, only a small error is introduced, when all sizes are described by the 2-p Weibull distribution.

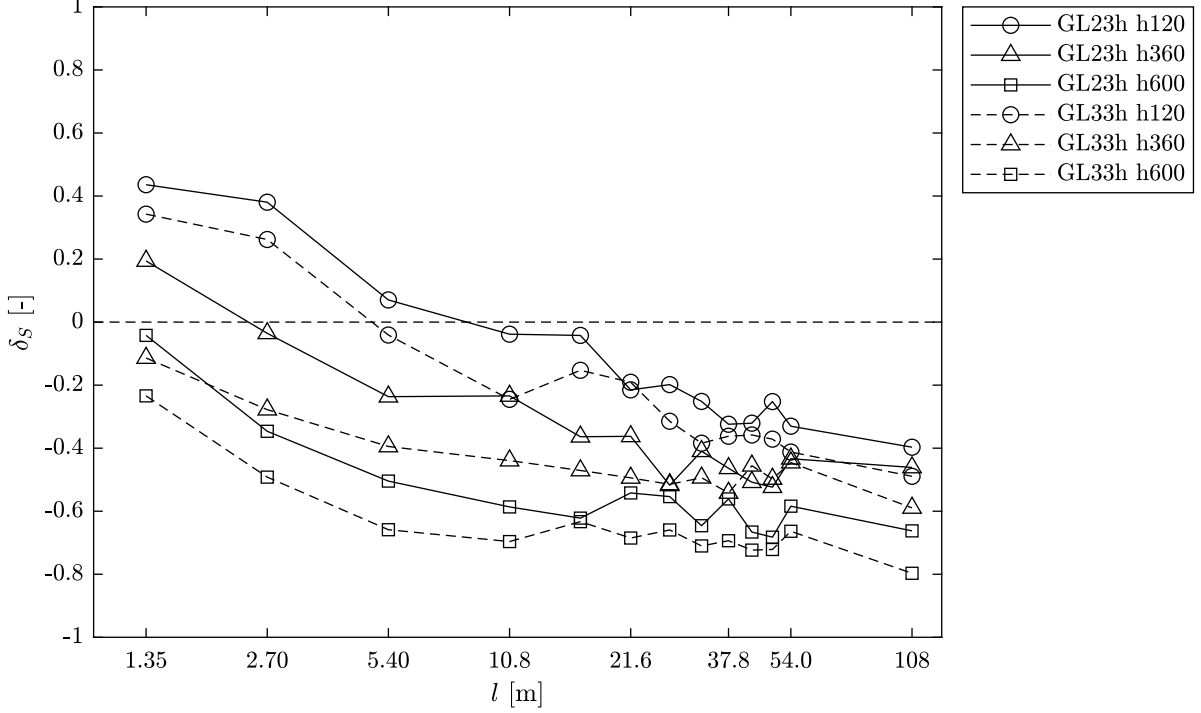


Fig. 4.7: Skewness δ_S of simulated tensile strengths $f_{t,0}$ vs. beam length l according to the data of Frese et al. (2017) [45]. (Attention has to be paid to the logarithmic axis for the length.)

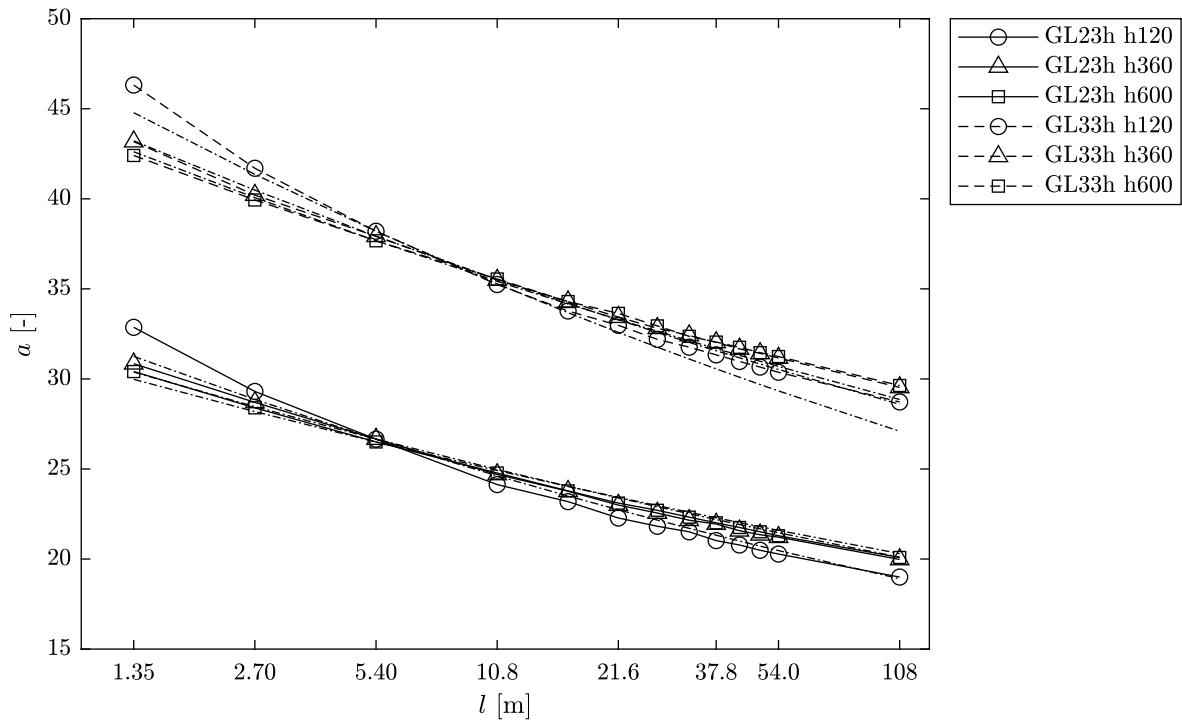
In Fig. 4.8 it can be seen that both parameters of the 2-p Weibull distribution are strongly length dependent. For both parameters, correction factors in the format of Weibull's weakest link theory were fitted, which can be seen in Eq. 4.6 and 4.8. Both equations have an individual correction of the exponent, which stems from the height influence, that was again described in the format of Weibull's weakest link theory provided in Eq. 4.7 and 4.9. In Fig. 4.9 both height correction models can be seen that are forced through the value at $h = 600$ mm. For ease of use the influence of the strength classes was neglected and the fitted functions consider both strength classes at once. In the four equations, l and h respectively denote the beam length and height in [m].

$$k_{t,0,l,a} = \left(\frac{5.4}{l}\right)^{\frac{1}{k_{t,0,h,a} \cdot 11.2}} \quad (4.6)$$

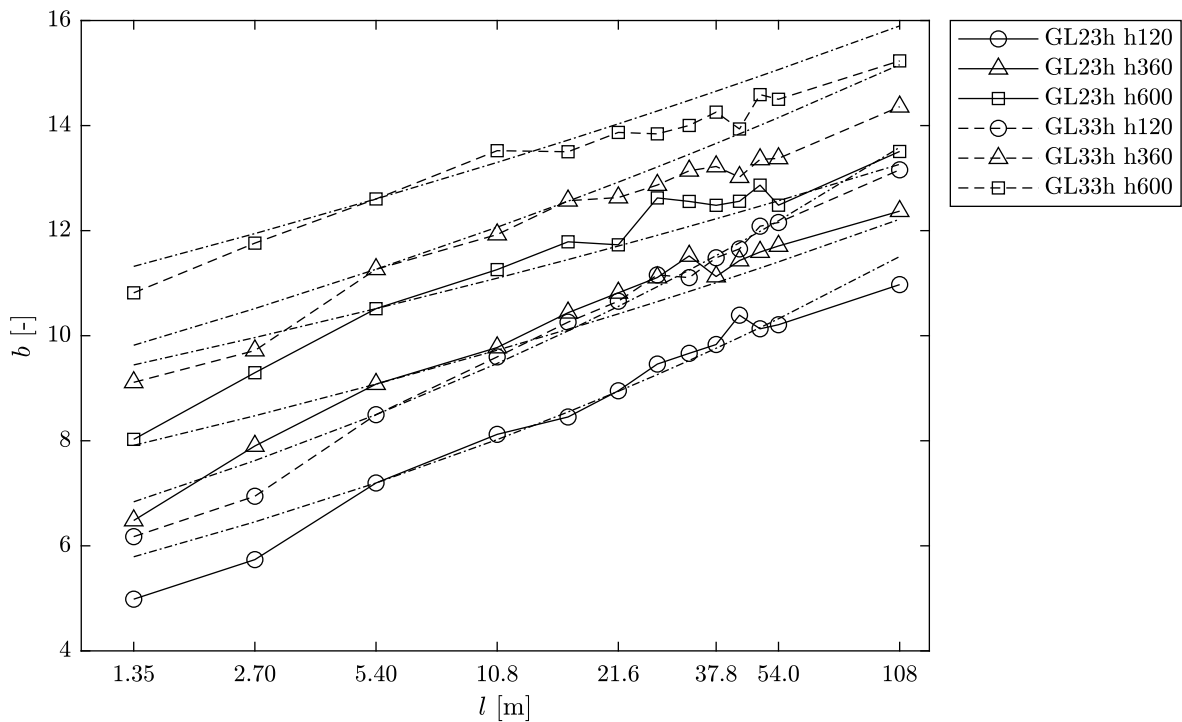
$$k_{t,0,h,a} = \left(\frac{0.6}{h}\right)^{\frac{-1}{6.56}} \quad (4.7)$$

$$k_{t,0,l,b} = \left(\frac{5.4}{l}\right)^{\frac{-1}{k_{t,0,h,b} \cdot 12.9}} \quad (4.8)$$

$$k_{t,0,h,b} = \left(\frac{0.6}{h}\right)^{\frac{-1}{2.24}} \quad (4.9)$$



(a)



(b)

Fig. 4.8: 2-p Weibull distribution parameters of tensile strengths $f_{t,0}$ vs. length l according to the data of Frese et al. (2017) [45]; (a) parameter a with the length effect model from Eq. 4.6 in chain dotted lines; (b) parameter b with the length effect model from Eq. 4.8 in chain dotted lines.

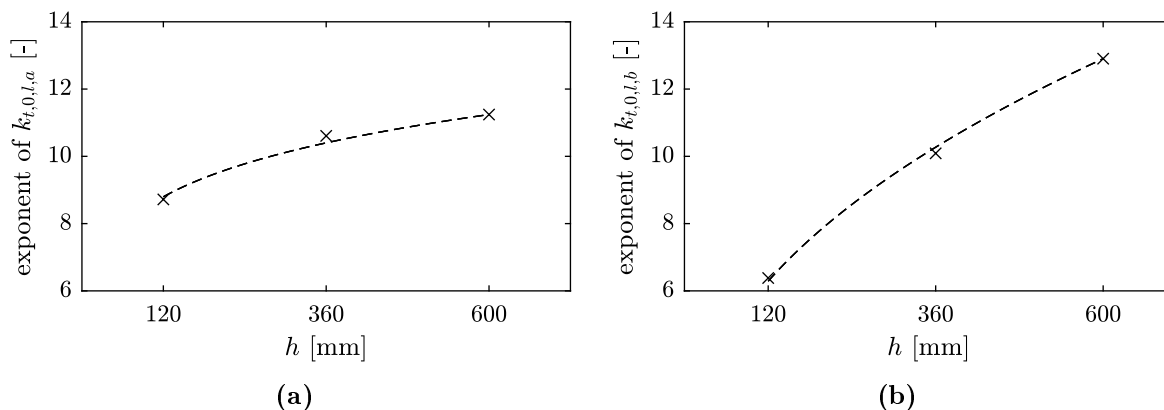


Fig. 4.9: Height effect models for the exponent of the length effect models of $k_{t,0,l,a}$ and $k_{t,0,l,b}$ with respect to the height h for the 2-p Weibull distribution parameters of the tensile strengths $f_{t,0}$ according to the data of Frese et al. (2017) [45]; (a) height effect model $k_{t,0,h,a}$ from Eq. 4.7; (b) height effect model $k_{t,0,h,b}$ from Eq. 4.9.

The finally proposed statistical parameters of the tensile strength are summarised in Tab. 4.13. The three underlying assumptions are the following: 88% relationship between the characteristic tensile to bending strengths, a constant CoV of 11% and that the 2-p Weibull distribution is valid for all cases. For the consideration of the size effect, the models from Eq. 4.6 to 4.9 are proposed.

Tab. 4.13: Proposed statistical parameters for the tensile strength $f_{t,0}$ of GLT for the reference length $l = 5.40$ m and the reference height $h = 0.60$ m.

	GL20h	GL22h	GL24h	GL26h	GL28h	GL30h	GL32h	GL36h
$f_{m,mean}$ [N/mm ²]	22.0	24.2	26.4	28.6	30.8	33.0	35.2	39.6
$f_{m,k}$ [N/mm ²]	17.6	19.4	21.1	22.9	24.6	26.4	28.2	31.7
σ [N/mm ²]	2.42	2.66	2.91	3.15	3.39	3.63	3.88	4.36
CoV [%]	11	11	11	11	11	11	11	11
a [–]	23.1	25.4	27.7	30.0	32.3	34.6	36.9	41.5
b [–]	11.0	11.0	11.0	11.0	11.0	11.0	11.0	11.0

4.2.2.7 Compressive strength

The compressive strength $f_{c,0}$ is proposed to be modelled Lognormally distributed by the JCSS PMC (2006) [71], but no CoV is provided. EN 14080:2013 [29] provides only the characteristic compressive strength values. These values correspond to the characteristic bending strength, i.e. the number of the strength class name. Frese (2016) [43] found considerably higher values though. The herein conducted analysis of his data is summarised in Tab. 4.14. The mean values, the standard deviations and the CoVs are empirical statistical estimates. The characteristic value are first provided empirically, i.e. the 50th value of 1'000, and for the Lognormal distribution.

For the simulation study both, the specimen height and the length, were chosen to be 0.6 m. The statistical inference process revealed the Lognormal distribution to be appropriate.

Tab. 4.14: Statistical parameters for the compressive strength $f_{c,0}$ of GLT for the height and length $h = l = 0.60$ m according to the data of Frese (2016) [43].

	GL24h	GL28h	GL32h	GL36h
$f_{c,0,mean}$ [N/mm ²]	40.4	43.7	50.2	53.1
$f_{c,0,k}$ [N/mm ²]	37.5/37.7	40.9/41.1	48.0/48.0	50.9/50.9
σ [N/mm ²]	1.68	1.63	1.38	1.39
CoV [%]	4.16	3.72	2.76	2.62
λ [–]	3.70	3.78	3.92	3.97
ζ [–]	0.0416	0.0373	0.0277	0.0262

When comparing the characteristic compressive strength from Tab. 4.14 to the values of EN 14080:2013 [29], i.e. 24, 28, 32 and 36, roughly a ratio of 1.5 results.

Within the scope of this thesis no table with values for all possible strength classes is proposed. The four grading classes shown in Tab. 4.14 are sufficient and there is more data available that should be evaluated properly in the context of another publication.

No size effects are expected, since the failure behaviour of slender compression members is governed by buckling and for buckling-restrained members the failure mode is ductile.

4.2.2.8 Shear strength

The JCSS PMC (2006) [71] proposes a Lognormal distribution without a CoV for the shear strength f_v and EN 14080:2013 [29] provides only one characteristic compressive strength value independent of the strength class of 3.5 MPa. Schickhofer (2001) [111] tested 80 I-shaped GLT beams in an optimised three point bending test for which the data is provided in the appendix of his publication. Visually and machine graded lamellas were considered in the tests. A slightly negative correlation between the strength classes and the shear strength was observed. For standardisation an at least constant value for all strength classes was proposed together with a characteristic shear strength value of 3.50 MPa.

The statistical inference process of the data of [111] revealed that the 2-p Weibull distribution is appropriate. The empirical 5% quantile value is 3.24 MPa and the value from the 2-p Weibull distribution is 3.43 MPa. Overall a shear failure rate of 80% was achieved. Therefore, in 20% of the cases the provided strength values are assumed to be higher. When conducting a right-censored 2-p Weibull analysis with a 95% significance level for the confidence intervals, the scatter increases and the resulting 5% quantile value is 3.38 MPa. The coherent CoV according to the fitted Weibull distribution is 10.4%.

Kloeck (2005) [79] conducted 30 shear tests with beams of combined GLT, where the outer lamellas consisted of a higher strength class to reduce the probability of getting bending failure. Still, only 60% of the specimens failed in shear. The empirical 5% quantile is 3.64 MPa. From

a simple right censored analysis with a 95% significance level and a 2-p Weibull distribution the 5% quantile is 4.03 MPa and the CoV is 11.1%. Kloeck (2005) [79] processed the data further and came up with a final 5% quantile of 3.63 MPa on a 95% significance level.

Foschi & Barrett (1980) [40] provided a volume effect model for the longitudinal shear strength of uncracked beams. For the exponent a value of $\frac{1}{6}$ is recommended species-independently. Although in their investigation solid timber was used, the same model is applied for GLT until new data is provided.

Neither Schickhofer (2001) [111], nor Kloeck (2005) [79] provided the effectively stressed volume in their publications. In Steiger & Gehri (2011) [124] it can be seen that in case no glued-in rods were applied in their experimental campaigns, the stressed volume is likely to be smaller than when they would have applied such reinforcements. Due to a lack of information of the compressive stresses in the shear fields, the data is treated as it would have been derived from specimens reinforced with glued-in rods. As shown in Fig. 4.10, in the case of the I-shaped beam of Schickhofer (2001) [111] twice the free length between the loading and support plates times the web cross-section was applied, resulting in 0.082 m^3 . In the case of the rectangular beam of Kloeck (2005) [79] twice the free length between the loading and support plates times the width times 60% of the height was used, resulting in 0.070 m^3 . The application of 60% of the height was recommended in Ehrhart (2019) [27].

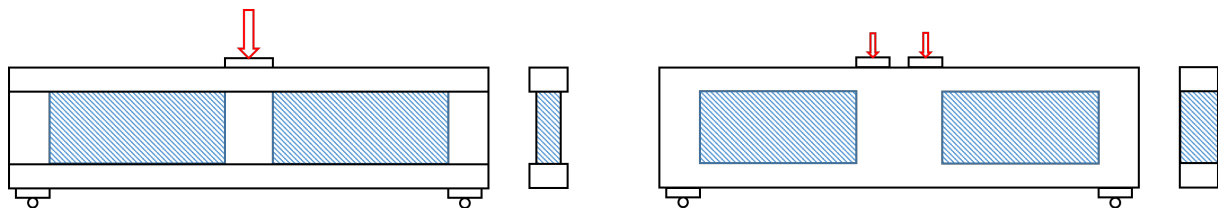


Fig. 4.10: Schematic representation of the determination of the stressed volumes of the I-shaped GLT beams from Schickhofer (2001) [111] on the left and of the combined GLT beams from Kloeck (2005) [79] on the right.

Finally, the data sets from Schickhofer (2001) [111] and Kloeck (2005) [79] were merged. Since Schickhofer (2001) provided more data it was used as the reference volume. The values from Kloeck (2005) were therefore modified by the volume correction provided in Eq. 4.10, where V denotes the volume in $[\text{m}^3]$. Since the volumes are in a similar range, only a small correction factor of $k_v = 1.03$ results. Since the volume of Kloeck (2005) is smaller, the strength values were divided by this factor before merging.

$$k_v = \left(\frac{0.082}{V} \right)^{\frac{1}{6}} \quad (4.10)$$

A right censored fitting of the 2-p Weibull distribution with a significance level of 95% was used on the merged data set, resulting in the distribution parameters $a = 4.63$ and $b = 8.31$. This corresponds to a 5% quantile of 3.24 MPa and a CoV of 14.3%. As expected, the resulting CoV is larger, since both individual data sets showed similar CoV but different mean values. The difference might be explained on the one hand by different growth regions of the trees used

for the lamellas and on the other hand by differences in the applied strength grading rules. The remaining question is whether or not these two data sets are enough to cover for the fundamental variation due to these reasons.

The resulting characteristic value is lower than all proposals from above. Therefore the question arises, if the value from EN 14080:2013 [29] is on the safe side. The answer to this question would need further consideration of the actual loading situations, which is related to the stressed volume as well. This problem is out of the scope of this publication but should be discussed further.

4.2.2.9 Shear modulus

The JCSS PMC (2006) [71] proposes a Lognormal distribution without a CoV for the shear modulus G_v . In EN 14080:2013 [29] a mean value of $G_{v,mean} = 650$ MPa and a characteristic value of $G_{v,k} = 540$ MPa are provided independent of the strength class. Under the assumption of a Lognormal distribution this corresponds to a standard deviation of $\sigma = 71.1$ MPa and hence a CoV of 10.9%. The distribution parameters are $\lambda = 6.47$ and $\zeta = 0.109$.

Brandner et al. (2007) [16] showed that the test method has a strong influence on the results concerning both, mean values and scatter. Finally, they proposed the mean value $G_{v,mean} = 650$ MPa and the same height effect, as they provided for the MOE (section 4.2.2.5 and Eq. 4.3) for all strength classes of homogeneous and heterogeneous GLT made from softwood.

As a consequence of this strong relation to the MOE, the herein proposed statistical parameters for the shear modulus are based on the following: Lognormal distribution, $G_{v,mean} = 650$ MPa, and the second distribution parameter $\zeta = 0.0513$ based on E_m of GL24h (Tab. 4.9). From this the characteristic value $G_{v,k} = 590$ MPa and the first distribution parameter $\lambda = 6.47$ can be derived. The height correction factor $k_{hl,\zeta}$ is then consequently inherited from the MOE according to Eq. 4.5.

4.2.2.10 Tensile strength perpendicular to the grain

For the tensile strength perpendicular to the grain $f_{t,90}$ in the JCSS PMC (2006) [71] a 2-p Weibull distribution is proposed but no CoV is provided. In EN 14080:2013 [29] a characteristic value of $f_{t,90,k} = 0.5$ MPa is provided independently of the strength class.

Mistler (1998) [95] conducted a meta-study of various test series of different specimen sizes between 27 cm^3 and 0.153 m^3 . He also argued that a pure volume-dependent size effect, like it was provided in design codes, is inaccurate. He instead used a rope-chain model, which he adopted to the two parameters a and b of a 2-p Weibull distribution. The rope can be understood as a parallel system and accounts for load-redistribution effects in the area perpendicular to the force. The chain can be understood as a series system which accounts for a weakest-link model along the force direction. This approach is very promising, since it takes into account a logical and physical background and provides a full probabilistic model depending only on the area perpendicular to the loading and the height of a specimen.

Aicher & Dill-Langer (1997) [4], Ranta-Maunus (1998) [106] and Aicher et al. (1998) [3] investigated the duration of load effect on $f_{t,0}$ for prismatic specimens and curved beams. They confirmed the pure volume effect in the manner of a Weibull-weakest-link model provided in the codes with a differentiation of the exponent for short-term and long-term loading. For short-term loading the exponent is 0.3 and for long-term loading it is 0.2, where the latter was adopted in the design codes. For the prismatic specimens, lamellas from one spruce stand of very high strength classes were used, and hence, low CoV of 10 – 11% arose for the single test series.

Blaß & Schmid (1999) [12] conducted a test series with 153 specimens for the so-called reference volume of $V_0 = 0.01 \text{ m}^3$ with GLT from different producers and from different strength classes. No clear influence of the strength class could be observed. They fitted two and three parameter Weibull distributions to the results from the single strength classes but also for all specimens. For the overall resulting 2-p Weibull distribution the parameters are $a = 0.848$ and $b = 3.688$, which is associated with a CoV = 30%. Further, they performed another 155 tests with smaller volumes (between 912 and 2195 cm^3) and discussed also the volume effect. They found the exponent of the Weibull-weakest-link model to be in the range of the above provision for short-term loading of approximately 0.3.

Aicher et al. (2002) [5] evaluated different size-effect models with the data sets of Mistler (1998) [95] that have at least ten specimens and additional data from Aicher et al. (1998) [3], i.e. a total of 20 test series. The data sets from Blaß & Schmid (1999) [12] were not included, although some of these data were already included in the data collection of Mistler (1998) [95] from a preliminary research report. The four investigated size-effect models were: volume model; depth model; cross-section model; and a combined cross-section/length model, which uses two separate exponents. The rope-chain model developed by Mistler (1998) [95] was reduced to the depth model, although a certain load-redistribution effect, especially along the grain was acknowledged. In their own proposal, the combined cross-section/length model, this effect is included since for the length a less severe exponent was found than for the cross-section. For all four models for the 5% quantile level and the median level the exponents are provided together with a coefficient of correlation. The best results were found when applying the combined cross-section/length model.

Mistler (2016) [96] included the data of Aicher et al. (1998) [3] and repeated the analysis from Mistler (1998) [95]. Therefore, the rope-chain model was presented with slightly different coefficients. The updated data set of Blaß & Schmid (1999) [12] was not included and the findings from Aicher et al. (2002) [5] were not discussed.

Due to this situation of having several publications with three different size-effect models without a complete mutual comparison, the author of this thesis did some minor investigations based on the statistical parameters provided in Aicher et al. (2002) [5]. When the rope-chain model from Mistler (2016) [96] is applied on the smallest and largest area of the data, the second Weibull parameter is $b = 2.05$ and $b = 4.45$, respectively. Due to the direct link between this parameter and the CoV a bandwidth of CoV between 25% and 51% could be concluded. The CoV of the single data sets are between 9% and 36%, which reveals a major difference between the model and the underlying data. Further, for this data set the two Weibull parameters were

investigated with respect to all possible combinations of length, width and height of the specimen. For the first parameter a , which corresponds to the 63.2% quantile value, a more or less clear negative trend with increasing geometry of any kind could be observed. The issue comes with the second parameter b , which is directly related to the CoV. Visually, no clear trend can be observed with respect to any geometric quantity. When having a closer look at the geometries of the specimen of the single test series together with the CoV several observations can be made:

- Some test series show systematic changes in only one dimension, which allows for a specific observation of that influence. When considering only such sub-series of two or three different sizes at once, no clear trend for the CoV can be detected. E.g. for a changing height but constant area perpendicular to the load sometimes the smallest series has the smallest CoV but in other cases it has the largest CoV.
- The height is the only quantity for which multiple systematic changes in the measure exist. Therefore, it seems unlikely to find a clear trend for changes in the other two dimensions from the underlying data sets.
- For most test series the GLT configurations are unknown to the author. In the publication of Blaß & Schmid (1999) [12] and Aicher et al. (1998) [3] the reference volume of 0.01 m³ was tested. As stated earlier, the values of the CoV are roughly 30% vs. 11%. The larger one is affiliated with timber from various producers and the smaller one only with one spruce stand. It has to be assumed that similar problems exist for the other data sets.

For all these reasons, it is questionable, if the conducted meta-studies are capable of precisely describing the volume effect after all. Therefore, until more conclusive investigations are available, it is proposed herein to apply the 2-p Weibull distribution from Blaß & Schmid (1999) [12] with $a = 0.848$ and $b = 3.688$ for the following reasons: (1) the GLT selection which is representative of the basic population, (2) the number of tests, and (3) that the reference volume according to the design codes was used. For the volume effect, the pure volume-based models with consideration of the duration of load are proposed:

$$k_{t,90,0} = \left(\frac{0.01}{V} \right)^{\frac{1}{3.33}}, \quad (4.11)$$

$$k_{t,90,\infty} = \left(\frac{0.01}{V} \right)^{\frac{1}{5}}, \quad (4.12)$$

where V is the volume in [m³]. The statistical parameters are $f_{t,90,mean} = 0.765$ MPa, $f_{t,90,k} = 0.379$ MPa, $\sigma = 0.231$ MPa and $CoV = 30.2\%$.

4.2.2.11 Compressive strength perpendicular to the grain

The JCSS PMC (2006) [71] specifies a Normal distribution without a CoV for the compressive strength perpendicular to the grain $f_{c,90}$. EN 14080:2013 [29] provides a strength class independent characteristic value of $f_{c,90,k} = 2.5$ MPa.

Damkilde et al. (1998) [23] conducted 120 tests with GLT cutoffs with a height of 200 mm and different widths. The lengths were adjusted to a resultant constant area of 25'000 mm². The specimens were gathered over several production days from one Danish and three Swedish GLT producers. The quality of the GLT represents normal Nordic GLT quality (presumably GL 24). Since no actual failure was reached, a strain-based criterion was defined. They found the following empirical statistical estimates: $f_{c,90,mean} = 2.87$ MPa, $f_{c,90,k} = 2.44$ MPa, and $CoV = 9\%$. No distribution function was fitted.

As mentioned above, a Normal distribution can cause problems for reliability analyses due to possible negative values, and hence, a Lognormal distribution is proposed. For $f_{c,90}$ no true failure occurs and therefore the failure criterion is defined deformation-based. Hence, the Lognormal distribution is a reasonable selection. The following distribution parameters are found based on the mean and the characteristic value: $\lambda = 1.05$ and $\zeta = 0.0959$. For the Lognormal distribution a $CoV = 9.61\%$ results, which is a further indicator for an adequate choice.

Due to the ductile failure behaviour, there is no size effect.

4.2.2.12 Modulus of elasticity perpendicular to the grain

For the tensile MOE perpendicular to the grain $E_{t,90}$, in the JCSS PMC (2006) [71] a Lognormal distribution is proposed but no CoV is specified. EN 14080:2013 [29] provides a mean value of $E_{90,mean} = 300$ MPa and a strength class independent characteristic value of $E_{90,k} = 250$ MPa. From this the following statistical parameters and Lognormal distribution parameters can be calculated: $CoV = 10.8\%$, $\sigma = 32.3$ MPa, $\lambda = 5.70$ and $\zeta = 0.107$. The findings from the tests under compression of Damkilde et al. (1998) [23] with a proposed $E_{c,90,mean} = 300$ MPa support the values from EN 14080:2013 [29].

Aicher & Dill-Langer (1997) [4] found higher values in the tensile perp. to the grain tests. For the reference volume of 0.01 m³: $E_{t,90,mean} = 446$ MPa, $E_{t,90,k} = 398$ MPa, and $CoV = 6.8\%$. For the volume of 0.03 m³: $E_{t,90,mean} = 419$ MPa, $E_{t,90,k} = 375$ MPa, and $CoV = 6.5\%$. Since these two test series stem from very high strength classes, i.e. GL32h and GL36h, this arises the question, if the MOE perp. to the grain really is strength class independent. Another explanation for the difference between the results of [23] and [4] could lie in the loading direction, i.e. compression vs. tension.

4.2.2.13 Density

The JCSS PMC (2006) [71] proposes a Normal distribution with a CoV of 10% for the density ρ . This is the same value as proposed for structural timber. Due to homogenisation, the value for GLT is expected to be lower though. A Normal distribution is an intuitive choice for the natural occurrence and the simple piling of lamellas. A proper truncation should be performed or a Lognormal distribution could be selected, since in a Normal distribution negative values are not excluded, which might lead to problems related to reliability analyses.

Using a Normal distribution to determine the CoV of the different GLT classes according to EN 14080:2013 [29], the values vary roughly between 5% and 6% without a clear trend (Tab. 4.15).

Intuitively, for higher classes a lower scattering was expected due to more strict grading criteria. Nevertheless, the values seem more reasonable than the assumption in the JCSS PMC (2006) of generally 10%. In Damkilde et al. (1998) [23] for normal Nordic GLT quality a CoV of 4.8% was found, which supports the values of EN 14080:2013. For GL36h the characteristic density can be found in SIA 265:2012 [120] and its mean value can be estimated from the general trend (Tab. 4.15).

To use a Normal distribution for a specific strength class the values for ρ_{mean} and σ can be used from Tab. 4.15. For a Lognormal distribution the values of the two dimensionless parameters λ and ζ can be used.

Tab. 4.15: Statistical parameters for the density of GLT according to EN 14080:2013 [29] and SIA 265:2012 [120].

	GL20h	GL22h	GL24h	GL26h	GL28h	GL30h	GL32h	GL36h
ρ_{mean} [kg/m ³]	370	410	420	445	460	480	490	500
ρ_k [kg/m ³]	340	370	385	405	425	430	440	450
σ [kg/m ³]	18.2	24.3	21.3	24.3	21.3	30.4	30.4	30.4
CoV [%]	4.93	5.93	5.07	5.46	4.63	6.33	6.20	6.08
λ [–]	5.91	6.01	6.04	6.10	6.13	6.17	6.19	6.21
ζ [–]	0.0506	0.0613	0.0521	0.0563	0.0474	0.0656	0.0642	0.0629

4.2.2.14 Edgewise loading

Brandner & Schickhofer (2006) [17] discussed system effects of structural elements such as GLT in edgewise loading situations. From their investigations and comparison of different prescriptions from design codes, a clear positive effect with increasing number of lamellas can be concluded. For small beams Rammer (1996) [105] found opposite results though, but clearly stated that these were only preliminary results. Due to the lack of a full probabilistic description of this effect in literature, herein the bending and the shear strength under edgewise loading are simply assumed to be 1.2 times (based on SIA 265:2021 [121]) larger than the respective values from flatwise loading described above.

4.2.2.15 Correlations

The correlation between the different GLT properties should not generally be neglected in probabilistic modelling. No investigations or hints could be found in literature though and the collected data sets did not allow for a corresponding evaluation. The use of the correlation coefficients provided in the JCSS PMC (2006) [71], that were estimated for solid timber, are not recommended by the author of this thesis to be used for GLT properties for the following reasons. The only correlation coefficients that could be derived from own investigations are based on the data of Frese (2016) [43] for the correlation between the moduli of elasticity and the respective strength values under bending, tension and compression. While in the provisions from the JCSS PMC

(2006) [71] in the case of bending and tension they are assumed *high* with a value of 0.8, based on the data of Frese (2016) [43] they are only in the range of 0.1 – 0.3. In the case of compression, high values in the range of 0.6 – 0.8 can be found, but their correlation is non-existent in the JCSS PMC (2006) [71]. Most likely, the described deviations stem from the fundamental differences in the composition of GLT compared to solid timber.

It seems unclear, whether any high correlations exist for GLT properties, due to the assembly of single boards. Only for the relations between the moduli of elasticity and the respective strength values under compression parallel and perpendicular to the grain high values are expected. Therein, the high correlation is introduced by the very definition (deformation criteria for the strength values). As described above, the three distinguished moduli of elasticity are further smeared into one value for practical applications. Due to these considerations, within the scope of this thesis no correlations of GLT properties are taken into account.

4.2.2.16 Weibull-weakest-link model for truss chord members

For the Weibull-weakest-link model for truss chord members derived by Lam (2000) [86] (Sec. 2.6.6.4), the exponent has to be determined for GLT. When considering the exponents proposed in [86] for Canadian solid timber strength classes in the range of 4.4 – 8.8, it seems reasonable to assume the second 2-p Weibull parameter $b = 11$ of Tab. 4.13 as exponent of the weakest-link model.

4.3 Resistance models for truss members

4.3.1 Introduction

In Sec. 3.3.2.6 the different resistance models for the members of timber trusses with dowelled steel-to-timber connections are presented and discussed. According to the JCSS PMC (2006) [71] and Köhler (2006) [82] (compare Tab. 4.18), deviations and simplifications related to the probabilistic modelling and the limit state equations have to be taken into account by introducing model uncertainties (Tab. 4.16). These model uncertainties depend on the limit state, e.g. combined stress effects, and on the deviation between actual conditions and the standard test conditions.

Tab. 4.16: Model uncertainties X_M for component load bearing capacity according to [71].

	Mean	Standard deviation	Distribution
Without load duration effects	1	0.05 – 0.10	Lognormal
With load duration effects, eq. (16)-(17)	1	0.10	Lognormal

4.3.2 Applied model uncertainties for truss members

In trusses the loading per member depends on the system behaviour, which itself depends on various aspects such as geometric layout, clamping stiffness in the joints, etc. Therefore, it

generally deviates from standard testing configurations. That is why even for simple cases without combination of stress effects, model uncertainties have to be considered. For more complex situations with combined stress, the scattering has to be increased. For the checking of stress effects in net-cross-sections, the model uncertainties also have to be increased. The net-cross-sections might lead to stress peaks and the determination of stresses based on the moment of inertia or the shear area as described in Sec. 3.3.2.6 is clearly simplified. For the buckling resistance according to second order theory, a model uncertainty is introduced e.g. to cover for variations in the imperfections. For the buckling out-of-plane an additional model uncertainty has to be introduced to the reduction factor according to Tölke (1929) [128] for the consideration of the bottleneck effect. Since this uncertainty is multiplied with the one for buckling out-of-plane, instead of explicitly applying it, the scatter is enlarged. For both buckling modes, the model uncertainty of the bending resistance is implicitly included. Hence, for these models the scatter has to be chosen larger than for e.g. pure bending.

The spatial variation of the model uncertainties is taken into account by using a different set of model uncertainties for each truss member, i.e. a member between two truss joints. This choice might be enhanced or at least will need to be clarified in future research or codification. With this choice, the resistance within the two net-cross-section areas at each side of a web member have the same set of model uncertainties. Within chord members, the set can be the same or different, in dependence of the association of the connections to one or the other adjacent member (compare Sec. 3.3). However, assigning different sets of model uncertainties to one member would also be inconsistent. Generally, in the gross-cross-sections in the middle of the members other failure modes are decisive than for the net-cross-section at the member ends. Therefore, no differentiation between the two cases is made and the scatter is chosen on the larger spectrum of the recommendations from Tab. 4.16. The herein applied model uncertainties per member are stated in Tab. 4.17.

Tab. 4.17: Mean values μ_ϵ and standard deviations σ_ϵ of the model uncertainties for the different resistance models of the truss members.

Parameter	μ_ϵ	σ_ϵ
$X_{t,0}$	1	0.1
$X_{c,0}$	1	0.1
$X_{m,y}$	1	0.1
$X_{v,z}$	1	0.1
$X_{P-\Delta,y}$	1	0.15
$X_{P-\Delta,z}$	1	0.20

The probabilistic representations of the equations from Sec. 3.3.2.6 are given in the following. Eq. 3.7 for combined tension and bending in-plane changes to:

$$X_{t,0} \frac{\sigma_{t,0}}{f_{t,0}} + X_{m,y} \frac{\sigma_{m,y}}{f_{m,y}} \leq 1. \quad (4.13)$$

For combined compression and bending effects Eq. 3.8 changes to:

$$\left(X_{c,0} \frac{\sigma_{c,0}}{f_{c,0}}\right)^2 + X_{m,y} \frac{\sigma_{m,y}}{f_{m,y}} \leq 1. \quad (4.14)$$

Since shear forces out-of-plane are generally very small or even in-existent in trusses, only the shear forces in-plane are considered. Eq. 3.10 then takes the following form:

$$X_{v,z} \frac{\tau}{f_v} \leq 1. \quad (4.15)$$

Eq. 3.12 for in-plane and out-of-plane buckling finally takes the following format with consideration of the respective model uncertainty:

$$\left(X_{c,0} \frac{\sigma_{c,0}}{f_{c,0}}\right)^2 + X_{P-\Delta} \frac{\sigma_{m,II}}{f_m} \leq 1. \quad (4.16)$$

The adaptation of the Weibull-weakest-link model for tension chord members with scattering tensile strengths for the individual chord members is shown in Eq. 2.52. When the model uncertainty of the tensile strength $X_{t,0}$ is considered, it changes to:

$$S = \min \left(\frac{S_i}{X_{t,0,i} \lambda_i} \right), (i = 1, \dots, n), \quad (4.17)$$

where $X_{t,0}$ has to be introduced in the denominator, since it is applied on the strength directly instead of the stress index as it is used in Eq. 4.13. Finally, the combined stress index for tension and in-plane bending under consideration of the Weibull-weakest-link model and inherit model uncertainties takes the following format:

$$\frac{\sigma_{t,0}}{S} + X_{m,y} \frac{\sigma_{m,y}}{f_{m,y}} \leq 1. \quad (4.18)$$

4.4 Dowelled connections

4.4.1 Introduction

In this section first the probabilistic aspects of the model of the load-carrying capacity of axially loaded and eccentrically loaded connections are presented with respective model uncertainties. Then the model uncertainties belonging to the load-deformation behaviour model described in Sec. 3.3.3 are introduced.

4.4.2 Load-carrying capacity

As shown in Sec. 2.4, the load-carrying capacity of dowelled connections can be determined based on only two material properties: the embedment strength of the timber members and the tensile strength of the steel dowels. The other parameters are of geometric nature and are fabricated precise enough to neglect their variability a priori. To be able to use the model from SIA 265:2021 [121] within a probabilistic framework, the safety factors applied on different parameters have to be eliminated and proper model uncertainties have to be introduced. The reduction model for

eccentrically loaded connections from Manser (2021) [91] was derived with a coherent error term that is further evaluated herein.

4.4.2.1 Adaptations of the load-carrying capacity model under lateral loading

In the design approach of SIA 265:2021 [121], presented in Sec. 2.4.2.1, the timber member thicknesses have been enlarged by the following combination of safety factors:

$$\sqrt{\frac{\gamma_{M,timber}}{k_{mod} \gamma_{M,steel}}} = \sqrt{\frac{1.3}{0.9 \cdot 1.1}} \approx 1.15. \quad (4.19)$$

The factor k_{β} corresponding to failure mode II was further reduced by the following ratio of safety factors:

$$\frac{\gamma_{M,steel}}{\gamma_{M,timber}} = \frac{1.1}{1.3} \approx 0.85. \quad (4.20)$$

According to Fuhrmann (2011) [46], the safety and modification factors in the design approach of SIA 265:2021 [121] are chosen following the specifications from DIN 1052:2004-08 and its introduction document [9]. These two adaptations with the resultant factors from Eq. 4.19 and 4.20 have to be reversed, which leads to different coefficients in Eq. 2.4-2.9 resulting in the following equations:

$$t_{1,1} = 0.78 \sqrt{\frac{f_{u,k}}{f_{h,k}}} d^{0.8}, \quad (4.21)$$

$$k_{\beta 1,1} = \sqrt{2}, \quad (4.22)$$

$$t_{1,2} = 2.20 \sqrt{\frac{f_{u,k}}{f_{h,k}}} d^{0.8}, \quad (4.23)$$

$$k_{\beta 1,2} = 2, \quad (4.24)$$

$$t_{2,2} = 2.20 \sqrt{\frac{f_{u,k}}{f_{h,k}}} d^{0.8}, \quad (4.25)$$

$$k_{\beta 2,2} = 2. \quad (4.26)$$

4.4.2.2 Model uncertainty of the load-carrying capacity model for uni-axial loading

Köhler (2006) [82] discussed several aspects of applying model uncertainties within a probabilistic design framework to model the load-carrying capacity of dowelled timber-to-timber connections. He further made proposals for the JCSS PMC [71], but only the ones for the timber members were adopted, i.e. in [71] no model uncertainties are proposed for the load-carrying capacity of connections. The proposals from [82] (Tab. 4.18) for the connections are in the form of Lognormal distributions and are based on "model a)" described in Table 5-4 of the original publication [82]. This model has the same fundamental assumptions as the one applied in this thesis. The mean values deviate from one, since Köhler considered a bias in the design models

that he found from comparison to test data. The mean values and the standard deviations both differ amongst the failure modes and for the consideration of multiple fastener connections. The correct determination of these parameters for steel-to-timber connections is out of scope of this thesis. Hence, the parameters are estimated based on the ones for timber-to-timber connections and further considerations discussed in the following paragraphs.

Tab. 4.18: Model uncertainties X_M for the member load-carrying capacity and for dowelled timber-to-timber connections according to [82].

		mean	st.dev.	Distribution	
Component, e.g. Eq. (6.4)	Short term	1	0.05 – 0.10	Lognormal	
Component, e.g. Eq. (6.13)	Long term	1	0.10	Lognormal	
Dowel Type Connection, section 5.3.3.					
Single Fastener (Failure Mode I, II, III)	}	X_{MI}	0.8	0.12	Lognormal
		X_{MII}	1.2	0.15	Lognormal
		X_{MIII}	1.3	0.20	Lognormal
Multiple Fastener	X_M	1.25	0.3	Lognormal	

In both Franke & Franke (2019) [42] and Schweigler et al. (2021) [116], it is stated that experiments on dowelled steel-to-timber connections showed a 20% higher load-carrying capacity than the European Yield Model. In both publications the authors assume that this difference stems mainly from the missing consideration of the rope effect for steel dowel connections that are forming plastic hinges. As mentioned above, the practical guidelines [63] discourage the use of connections failing in mode I. Further, in this thesis only connections with two steel plates are considered, whereby the middle member is dominating the connection behaviour over the side members. This results in a predominant failure mode III for the middle member and a less important failure mode II or III in the side members. Therefore, for the single fasteners only one model uncertainty $X_{M,III}$ is applied in the framework of this thesis. A Lognormal distribution with $\mu_\epsilon = 1.2$ and $\sigma_\epsilon = 0.20$ is applied. For the model uncertainty $X_{k_{red}}$ for multiple fasteners, i.e. for k_{red} specified in Eq. 2.10, the model from Tab. 4.18 with $\mu_\epsilon = 1.25$ and $\sigma_\epsilon = 0.3$ is applied. In the implementation of the framework the resultant k_{red} was limited to a maximum of 1.0, to omit a positive group effect.

4.4.2.3 Embedment strength

Köhler (2005) [81] applied Eq. 2.2 for the embedment strength for probabilistic considerations, independent of the characteristic values. Under this assumption with the distribution characteristics for the density from Tab. 4.15 the embedment strength can be modelled probabilistically.

It is assumed that the model uncertainty of this embedment strength model is covered by the model uncertainty applied on single-dowel connections from the previous section.

In SIA 265:2021 [121] a linear interpolation for other load-to-grain angles is proposed. Since this is only a simplification, herein the well-known approach developed by Hankinson (1921) [55] is used, which is also specified in EN 1995-1-1:2004 [31]:

$$f_{h,\alpha} = \frac{f_{h,0} f_{h,90}}{f_{h,0} \sin^2(\alpha) + f_{h,90} \cos^2(\alpha)}. \quad (4.27)$$

When considering the fact that in GLT each single dowel row is embedded in another lamella, depending on the perspective, the density for GLT or solid timber has to be inserted respectively. Inserting the value for GLT implies assuming the same embedment strength for all dowels of a full connection. Inserting the value for solid timber therefore corresponds to taking into account the between-lamella variability. Both options have been implemented in the framework of this thesis. Due to the fact that the load-deformation behaviour was derived from experiments on full connections, in the subsequent investigations only the perspective of GLT is applied, i.e. all dowels have the same embedment strength.

Further, as an alternative the full probabilistic embedment strength model according to Leijten et al. (2004) [88] and Köhler (2006) [82] has been implemented. For the subsequent investigations it is not applied, since with this change also the respective model uncertainties would need to be adapted. This model which was derived from single-dowel connections embedded in solid timber has the format of a power function:

$$f_h = A \rho^B d^C \epsilon, \quad (4.28)$$

where A , B and C are the model parameters and ϵ is the model error. When rewriting the equation in an exponential form and using $A^* = \ln(A)$ the following equation can be derived:

$$f_h = \exp(A^* + B \ln(\rho) + C \ln(d) + \epsilon). \quad (4.29)$$

For softwood the parameters for the normal distributions from Tab. 4.19 with inherit correlations from Tab. 4.20 and 4.21 can be used. The indices indicate whether the values are valid along the grain or perpendicular to it. For the interpolation for arbitrary load-to-grain angles it is again proposed to use the approach from Eq. 4.27.

When neglecting the model variability and uncertainty, one could also use the mean values from Tab. 4.19. The format then is comparable to the approach from Eq. 2.2. As shown in [82], Eq. 2.2 delivers systematically smaller embedment strength values.

4.4.2.4 Model uncertainty of the reduction factor for eccentrically loaded connections

The reduction factor of the load-carrying capacity for eccentrically loaded connections according to Manser (2021) [91] was presented in Sec. 3.3.2.7. In the present study, the corresponding model uncertainty X_{k_e} was derived based on the data collected by [91]. The same format as proposed in the JCSS PMC (2006) [71] and Köhler (2006) [82] is chosen, i.e. the model uncertainty is

Tab. 4.19: Marginals for embedment strength model according to [82, 88].

Parameter	μ	σ
A_0^*	-2.33	0.232
B_0	1.07	0.0380
C_0	-0.253	0.0120
ϵ_0	0	0.107
A_{90}^*	-2.55	0.309
B_{90}	1.10	0.0520
C_{90}	-0.432	0.0210
ϵ_{90}	0	0.129

Tab. 4.20: Correlation matrix for embedment strength parameters parallel to the grain according to [82, 88].

	A_0^*	B_0	C_0	ϵ_0
A_0^*	1	-0.991	-0.235	0
B_0		1	0.105	0
C_0			1	0
ϵ_0				1

Tab. 4.21: Correlation matrix for embedment strength parameters perpendicular to the grain according to [82, 88].

	A_{90}^*	B_{90}	C_{90}	ϵ_{90}
A_{90}^*	1	-0.984	-0.0550	0
B_{90}		1	-0.126	0
C_{90}			1	0
ϵ_{90}				1

represented by a Lognormal distribution and then is multiplied with the reduction factor. The error ϵ between the regression model y' and the actual test data y can be expressed as follows:

$$\epsilon = \frac{y}{y'} = \frac{y}{y - r}, \quad (4.30)$$

where r is the residual vector of the regression function. The statistical evaluation of ϵ reveals a mean value $\mu_\epsilon = 1$ (neglecting some minor numerical error) and a standard deviation $\sigma_\epsilon = 0.08$. By means of the method of moments, the Lognormal distribution parameter of the model uncertainty X_{k_e} can be estimated.

Within the modelling framework of this thesis, k_e is limited by a lower bound of 0.1 and an upper bound of 1. The lower bound is introduced, since connections without or with very small normal forces get huge eccentricities from minor bending moments and therefore could indicate

failure of connections that are barely stressed. The upper bound prevents the connection from being stronger than without eccentricity due to the model uncertainty.

4.4.2.5 Mixed mode fracture energy

Köhler (2006) [82] presented a simplified model for the mixed mode fracture energy which is dependent on the density and is compatible with the assumptions from Jorissen (1998) [75] who used it within a model to calculate the load-carrying capacity of dowelled connections:

$$G_c = 0.0013 \rho - 0.1918 [\text{Nmm/mm}^2], \quad (4.31)$$

where ρ is the density. Since this model has been only applied to solid timber connections, it is unclear how to apply it to connections in GLT. One possibility is to use it with CoV = 10% valid for solid timber. The other possibility is to use it with CoV \approx 5% based on Tab. 4.15. This issue is related to the actual layout of the connection within the different lamellas.

4.4.3 Load-deformation behaviour

4.4.3.1 Model uncertainty of the load-deformation behaviour of single-dowel steel-to-timber connections

The determination of the individual curve characterising parameters of the load-deformation behaviour according to Manser (2021) [91] was presented in Sec. 3.3.3. In this thesis, the same procedure was applied as shown in Sec. 4.4.2.4 to derive the model uncertainties. The corresponding mean values and standard deviations of the individual model uncertainties are shown in Tab. 4.22. As described above, by means of the method of moments the Lognormal distribution parameters can be estimated based on these pairs.

For the secondary stiffness K_2 , in some cases, the individual error terms were in the same range as the respective model answers, leading to large values of ϵ from Eq. 4.30. The presented value of the standard deviation was derived iteratively by neglecting the cases with large ϵ until a mean value $\mu_\epsilon \approx 1$ was reached. Therefore, only 223 out of 272 test results could be used for its determination.

Tab. 4.22: Mean values μ_ϵ and standard deviations σ_ϵ of the model uncertainties of the curve characterising parameters according to the data collected by [91].

Parameter	μ_ϵ	σ_ϵ
X_{K_1}	1	0.16
X_{K_2}	1	0.78
X_{K_3}	1	0.87
X_{F_0}	1	0.12
$X_{w_{int}}$	1	0.40
$X_{w_{ult}}$	1	0.45
$X_{\alpha_{RA}}$	1	0.12

To visualise the scatter due to these model uncertainties, in Fig. 4.11 the resulting load-deformation curves per dowel of a Monte Carlo Simulation with 10'000 samples for the case of a connection with a dowel diameter $d = 6$ [mm] and 25 dowels is presented. Only the first part of the curve according to the first case of Eq. 3.21 is shown. The decreasing behaviour is not shown, since it is of lesser importance for this study and would compromise the readability of the graph. The large scatter of w_{int} leads to immense differences of the reached deformations per dowel, i.e. from very brittle to very ductile behaviour.

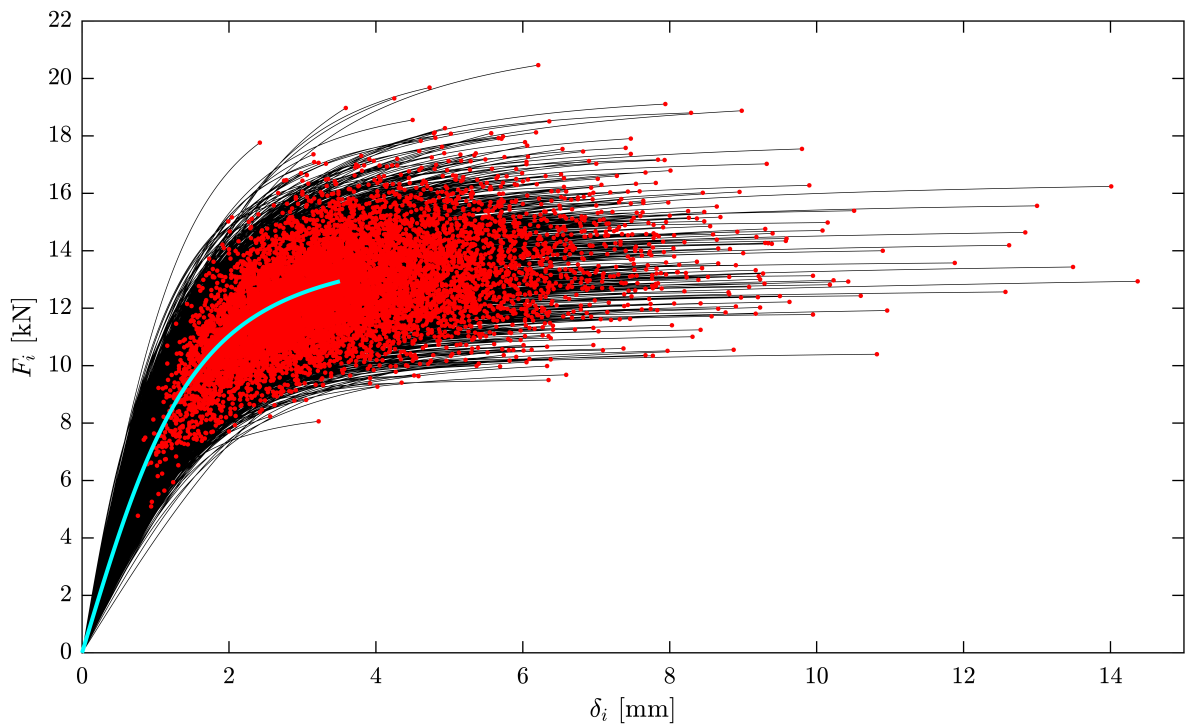


Fig. 4.11: Scatter of the load-deformation behaviour per dowel described in Sec. 3.3.3 by means of 10'000 Monte Carlo Simulations on the example of a dowelled steel-to-timber connection with four shear planes under consideration of the model uncertainties (X_{K_1} , X_{K_2} , X_{F_0} , $X_{w_{int}}$ and $X_{\alpha_{RA}}$) from Tab. 4.22. The connection specifications are: $d = 6$ [mm], $n_{col} = 5$, $n_{row} = 5$, $\rho_m = 420$ [kg/m³], $f_u = 510$ [N/mm²], $t_1/d = 3.3$, $t_2/d = 7.5$, $a_1/d = 7$, $a_2/d = 3$, $a_3/d = 7$, $a_4/d = 4$. The red markers indicate the transition point at w_{int} and the line in cyan represents the load-deformation curve without scattering.

4.4.3.2 Model uncertainty of the load-deformation behaviour of multi-dowel steel-to-timber connections

The model from Schweigler et al. (2018) [115] described in Sec. 2.4.3.3 and 3.3.2.4 combines the load-deformation curves from the single dowels into the load-deformation behaviour of a full connection. The uncertainty of the single-dowel behaviour is respected with the considerations from above. However, the combination is based on the balance between inner and outer forces of the entire structure by means of the finite element solver. The outputs are the load-deformation curves of the single dofs and the section forces of the full connection. None of these properties

can be affected by a model uncertainty without disturbing the balance of the system. The typical considerations of model uncertainties deal only with single number model answers. The inclusion of the load-deformation behaviour in the ultimate limit state needs therefore further considerations.

Undoubtedly there are several reasons to introduce model uncertainties due to the necessary simplification of the approach mentioned in Sec. 2.4.3.3. However, within the scope of this thesis no model uncertainties are applied to this model. Further investigations are clearly necessary to deal with such complex models in general but also for the model at hand, comparisons to experiments will be necessary for a proper evaluation.

4.5 Steel products

4.5.1 Introduction

In the scope of this thesis two steel products are used: steel plates, made from flat steel and steel dowels. Both products have been used most commonly in the steel quality classes S235 and S355. In Switzerland, it is common knowledge that S235 basically is non-existent, i.e. when ordering S235 the actual quality upon delivery is much higher. Hence, only S355 is used herein. Even for S355 the only guarantee upon delivery is that the characteristic yield strength is at least 355 MPa. Since the actual strength of dowels plays a crucial role in activating plastic deformations in connections, in praxis it can be necessary to conduct tests of each batch after delivery and adapt the planned structure corresponding to the results.

4.5.2 Steel S355

4.5.2.1 Modulus of elasticity (MOE)

SIA 263:2013 [119] provides a MOE of $E = 210 \text{ kN/mm}^2$ and the JCSS PMC (2001) [70] proposes a Lognormal distribution function with a CoV = 0.03 which results in the distribution parameters $\lambda = 5.35$ and $\zeta = 0.0300$.

4.5.2.2 Yield strength

SIA 263:2013 [119] provides a characteristic yield strength of S355 $f_{y,k} = 355 \text{ kN/mm}^2$ and the JCSS PMC (2001) [70] proposes a Lognormal distribution function with a CoV = 0.07 which results in the distribution parameters $\lambda = 5.99$ and $\zeta = 0.0699$.

4.5.2.3 Ultimate tensile strength

SIA 263:2013 [119] provides a characteristic ultimate tensile strength of S355 $f_{u,k} = 510 \text{ kN/mm}^2$ and the JCSS PMC (2001) [70] proposes a Lognormal distribution function with a CoV = 0.04 which results in the distribution parameters $\lambda = 6.30$ and $\zeta = 0.0400$.

4.5.2.4 Correlation matrix

The JCSS PMC (2001) [70] proposes a correlation matrix, of which the herein relevant part is shown in Tab. 4.23.

Tab. 4.23: Correlation matrix for steel according to [70].

	f_y	f_u	E
f_y	1	0.75	0
f_u		1	0
E			1

4.5.2.5 Density

According to SIA 263:2013 [119] the mean density of steel is 7850 kg/m³. [7] provides the CoV = 4% and a Normal distribution. For the same reasons as explained in Sec. 4.2.2.13 a Lognormal distribution is proposed herein. The two distribution parameters are then: $\lambda = 8.97$ and $\zeta = 0.0400$.

4.5.2.6 Shear modulus

SIA 263:2013 [119] provides a shear modulus of $G_v = 81$ kN/mm². Since the JCSS PMC (2001) [70] does not provide any details for the shear modulus, the same distribution characteristics as for the MOE are assumed: Lognormal distribution function with a CoV = 0.03, resulting in $\lambda = 4.39$ and $\zeta = 0.0300$.

4.5.2.7 Shear yield strength

SIA 263:2013 [119] provides a ratio between shear yield strength and yield strength of $\tau_y = f_y/\sqrt{3}$. Since the JCSS PMC (2001) [70] does not provide any details for the shear yield strength, this constant ratio is assumed.

4.6 Actions

4.6.1 Introduction

The probabilistic modelling of actions can be quite demanding when considering the temporal and spatial variabilities [69]. Within the scope of this thesis only timber trusses for large-span roof structures in Switzerland are studied. Their design typically is dominated by snow loads. Combinations with wind loads are neglected due to an immense increase of complexity. For the intended parameter studies within the scope of this thesis, the benefit would be low. The self-weights of the trusses and of the roof structures are also considered.

4.6.2 Snow loads

Sanpaolesi (1996) [109] stated various encountered problems and proposals in the process of finding adequate snow load models for the Eurocode. Several interesting statements are briefly summarised: In regions whose maximum snow cover usually consists of an accumulation of several snow falls, the Gumbel distribution is well-suited to describe snow loads. For regions whose maximum amount of snow is determined by single snow fall events, the Lognormal distribution is better suited. The CoV of snow loads is notably higher than for imposed or wind loads and is smallest in mountainous regions where snow falls quite regularly and is accumulated during winter. An annual probability of exceedance of 0.02, resulting in a mean recurrence interval of 50 years, is applied to the characteristic snow load on the ground.

According to Baravalle (2017) [7] the yearly maxima of snow loads on roofs can be modelled by a Gumbel distribution and a CoV = 0.40. He also indicated that the usual characteristic value corresponds to the 98% fractile value. He further introduces a model uncertainty that takes into account the uncertainty of the model itself and the shape coefficient. He proposes a Lognormal distribution with mean value of 1.00 and a CoV = 0.30.

In SIA 260:2013 [117] it is stated that for variable loads under normal conditions a temporal reference period of one year with a 98% probability can be selected, which refers to a 50-year return period. The following equation from SIA 261:2020 [118] represents the characteristic snow load s_k in dependence of the reference height h_0 , which is valid for structures placed to heights up to 2000 m above sea level:

$$s_k = \left[1 + \left(\frac{h_0}{350} \right)^2 \right] 0.4 \text{ kN/m}^2 \geq 0.9 \text{ kN/m}^2. \quad (4.32)$$

The proposed conversion factors with respect to thermal conditions and wind exposition are both assumed to be 1.0. Different models exist to take into account the shape of the distributed snow in dependence of the roof shape. Herein, only *load model 1* for uniformly distributed snow is taken into account. When considering roofs with inclinations up to 30°, no correction is proposed. No size-correction needs to be applied, since at least one of the sides of the herein considered hall structures is assumed to be larger than 25 m.

Accounting for Swiss topology and the correction of the reference height due to local differences with respect to the model from Eq. 4.32, four different reference heights are considered within the scope of this thesis: 500 m, 1000 m, 1500 m and 2000 m. In Tab. 4.24 the resulting characteristic snow loads and the two Gumbel parameters μ and β are provided.

4.6.3 Self-weight of timber trusses

Within this thesis GLT is used for the members of the timber trusses. The probabilistic models of the density of the different GLT strength classes was presented in Tab. 4.15. Within the used framework (Sec. 3.3) the geometry of each GLT beam is captured as a cuboid with a specific cross-section and the length of the corresponding finite elements. The steel plates in the truss

Tab. 4.24: Characteristic snow loads and Gumbel parameters for different heights according to [118] and [7].

h_0 [m]	s_k [kN/m ²]	μ [-]	β [-]
500	1.22	0.490	0.186
1000	3.67	1.48	0.561
1500	7.75	3.12	1.19
2000	13.5	5.42	2.06

joints are also considered as cuboids and the probabilistic model for their density was presented in Sec. 4.5.2.5.

4.6.4 Self-weight of roof structures

For roof structures, many solutions are available on the market. In the case of flat roofs, gravel or soil is often put on top of the roof. Nevertheless, within the scope of this thesis the same type of roof structure was selected for all cases without additional weight from gravel or soil. A non-exhaustive review in the world wide web showed that the load from the non-bearing structure is in the range of 0.35 kN/m². Additional weight often comes from photovoltaic panels of roughly 0.15 kN/m², which can be applied on flat or inclined roofs and is therefore considered in all cases.

The load-bearing structure herein consisting of purlins and panels must be adapted to the individual structures. As shown in Sec. 2.2.4 typical distances between girders are 4-10 m, the distance between the purlins is in the range of 1.0-2.5 m and roof inclinations of up to 30° are common. In Sec. 2.7.4 it was shown that for robust design of large-span timber halls compartmentalisation is proposed for which the secondary structure, i.e. the purlins, should be single-span beams.

Hence, for the superstructure, single-span purlins made from GL24h are applied together with LVL panels, i.e. Kerto Q. For these elements, that support the non-bearing structure and the photovoltaic panels, a parameter study was conducted. With the derived equation, the point loads on the top chords of the investigated trusses can be determined. The following ranges of parameters were investigated:

- roof inclination between 0 – 30° in steps of 10°;
- snow loads for the reference heights 500 m, 1000 m, 1500 m and 2000 m in Switzerland according to [118];
- girder distances between 4-10 m in steps of 1 m;
- purlin distances between 0.5-2.5 m in steps of 0.5 m. For reference heights 500 m distances up to 4.0 m and for 1000 m distances up to 3.0 m were considered, since reasonable results could be found.

For both the purlins made from GL24h and the Kerto Q panels the relevant SLS and ULS were checked including long-term behaviour according to the Swiss codes[121, 122]. The sizes and the material parameters of the elements were chosen according to the typical layouts provided in [64]. Generally, it is unclear over how many spans the individual panels are applied. Therefore, conservative assumptions with respect to the number of spans were considered for both limit states.

When putting the purlins on inclined top chords, the purlins are tilted. Therefore, with increasing angle of the top chords, the loading out-of-plane in the purlins increases. Where for the construction process of the roof structure this might be ideal, for purlins made from GLT this tilting is of concern. The production process of GLT allows for large heights but only for limited widths. The widths are essential for the loading out-of-plane. Therefore, both possibilities were investigated. i.e. tilted and non-tilted purlins, where in the latter case, additional elements have to be applied. For high snow loads, large distances between girders and large distances between purlins, the cross-section sizes reach a range where two GLT beams need to be glued edgewise, i.e. the production gets very intensive and shrinkage / swelling problems can arise for such large cross-sections.

From the parameter-studies of both possibilities equations were fitted that yield the point loads in [kN] acting on the girders at each girder-purlin crossing. Eq. 4.33 is valid for non-tilted purlins and Eq. 4.34 is valid for tilted purlins.

$$F_{pur,0} = -0.880 + \frac{0.0346 \left(10.1 + (h_0/350)^2\right)^{0.408} (2.73 + d_{gir})^{1.63} (0.705 + d_{pur})^{1.50}}{0.533 + \cos(\alpha)^{1.47}} \quad (4.33)$$

$$F_{pur,tilt} = -1.66 + \frac{0.0110 \left(10.2 + (h_0/350)^2\right)^{0.451} (5.03 + d_{gir})^{2.19} (1.06 + d_{pur})^{1.51}}{2.65 + \cos(\alpha)^{18.0}} \quad (4.34)$$

Within both equations h_0 is the reference height for the determination of the snow load in [m], d_{gir} is the distance between the girders in [m], d_{pur} is the distance between the purlins in [m] and α is the inclination angle of the top chord of the trusses in [°].

In Tab. 4.25 exemplary values are provided for both cases to show the difference between the two approaches in terms of the point loads in [kN], which increases for larger inclinations. As it can be seen, without inclination there are minor differences which stem from a certain error introduced by the fitting process. As discussed above, for high snow loads and long spans, tilted purlins can be of concern. Still, in most cases the purlins might be worth being applied tilted to ease the construction process. Within this thesis, the approach from Eq. 4.34 is used.

Concerning the scattering of the self-weight of such structures assumptions have to be made, since no data is available. In Sec. 4.2.2.13 it was shown that the CoV of the density of GLT for the standard sizes is in the order of 5%. For the Kerto Q panels the CoV should be even lower due to high numbers of veneer layers used (homogenisation). The non-bearing roof structure and the photovoltaic panels are industrialised products. That is why their CoV is expected to be in the range of some percent. Overall, CoV = 5% seems to be an adequate selection. Since this chapter only intends to provide a reasonable estimate, no size-effect study is conducted. For

Tab. 4.25: Point loads from roof structure at girder-purlin intersections according to Eq. 4.33 and 4.34.

α [°]	h_0 [m]	d_{gir} [m]	d_{pur} [m]	$F_{pur,0}$ [kN]	$F_{pur,tilt}$ [kN]
0	500	6	1.0	3.89	3.65
0	500	10	2.5	21.9	22.2
0	1500	4	1.0	3.54	3.36
0	1500	8	2.5	23.5	24.0
10	1000	6	1.0	4.84	5.17
10	1000	10	2.5	26.4	29.0
10	2000	4	1.0	4.41	4.80
10	2000	8	2.5	28.3	31.3
20	500	6	1.0	4.18	4.85
20	500	10	2.5	23.2	27.6
20	1500	4	1.0	3.80	4.50
20	1500	8	2.0	25.0	29.8
30	1000	6	1.0	5.55	6.88
30	1000	10	2.5	29.8	36.8
30	2000	4	1.0	5.08	6.43
30	2000	8	2.5	32.0	39.6

the same reasons as explained in Sec. 4.2.2.13 a Lognormal distribution is proposed. The second parameter ζ can be determined by the following equation, using CoV = 5% [125]:

$$\zeta = \sqrt{\ln(\text{CoV}^2 + 1)} = 0.0500. \quad (4.35)$$

The first parameter λ can be determined by the combination of Eq. 4.34 and Eq. 4.36 [125]:

$$\lambda = \ln(F_{pur,tilt}) - \frac{\zeta^2}{2} = \ln(F_{pur,tilt}) - 0.00125. \quad (4.36)$$

4.7 Conclusions

For GLT properties, a fundamental and long-necessary update of the provisions from the JCSS PMC (2006) [71] could be derived based on literature and collected data sets that were evaluated by the author of this thesis. Many of these new provisions are in need of validation and complementation by experimental campaigns or non-accessible existing data sets. Nevertheless, the presented collection is believed to be a reasonable probabilistic description allowing to assess the correct order of reliability of GLT structures such as timber trusses. The newly introduced complexity due to considerations of size effects is of no concern when utilising parametrised models. Correlations of the properties and edgewise loading conditions have to be addressed in future research – within the scope of this thesis they are neglected or taken into account in a simplified manner.

Model uncertainties have been introduced for the resistance models of the timber members following the provisions from the JCSS PMC (2006) [71]. The magnitude of the variability in general but especially the values for second order effects had to be chosen based on judgement by the author of this thesis. For the model uncertainties of the European Yield Model reasonable assumptions could be derived based on literature, nevertheless a derivation from experimental data would be preferable. For the newly introduced load-deformation behaviour and the reduction factor for eccentric loading of connections by Manser (2021) [91] model uncertainties were derived herein. The magnitude of the variability of some of these parameters is quite large, implying that the approach is in need of more data sets to improve the regression functions.

Next to these considerations, the adaptation of the European Yield Model according to SIA 265:2021 [121] to the level of mean values was presented, the variability of the steel products was shown, for the self-weight of roof structures a parametrised approach was derived, and the probabilistic aspects of the snow loads were discussed.

Although many of the provisions from this chapter will have to be updated in future research, reasonable models and assumptions could be derived for most properties allowing for an assessment of the reliability of timber trusses used in hall and roof structures under the described limitations.

Chapter 5

Structural behaviour of timber trusses

5.1 Introduction

In this chapter, the focus lies on the structural behaviour of timber trusses. In the first section, four exemplary trusses are used to compare different models for the truss joints and the load-deformation behaviour of the connections with respect to different relevant design aspects.

Subsequently, the simplified design approach of SIA 265:2021 [121] is evaluated. Four different truss layouts and many different web member layouts and chord slenderness ratios are investigated based on the most accurate model discussed in the first section. The results based on the developed modelling framework are compared to the design rules. Conclusions are drawn regarding the validity of the design approach.

Finally, the potential of the herein developed modelling framework is illustrated on a showcase structure and various aspects of a system-based design approach are discussed.

5.2 Modelling of timber trusses

5.2.1 Introduction

The different modelling approaches of the truss joints presented in Sec. 3.2.3 are first compared on the example of four trusses. An additional refinement of the modelling details from Fig. 3.1 is applied and different assumptions for the load-deformation behaviour of the single dowels are compared. To exclude the influence of distributed loads, the self-weight of the trusses is neglected in this part. The introduction of the self-weight as point loads was not considered, since the snow reference height is already chosen arbitrarily and the considerations in this section are of relative nature.

5.2.2 Investigated trusses

Four trusses, designed with the truss design tool presented in Sec. 3.4, were investigated with respect to the modelling details: a parallel chord truss with rising and falling diagonals with a constant dowel diameter of 12 mm (Fig. 5.1 and Tab. 5.1); the same layout with a constant dowel diameter of 6 mm (Fig. 5.1 and Tab. 5.2) (note the different web member heights); a duopitch roof truss with raised eaves and falling and rising diagonals with posts (Fig. 5.2 and Tab. 5.3); and a triangular truss with falling diagonals with posts (Fig. 5.3 and Tab. 5.4). All

four trusses were designed according to the simplified design approach defined in SIA 265:2021 [121] (Sec. 2.3.3) by means of the truss design tool presented in Sec. 3.4. The measures of the trusses were chosen to represent roughly medium dimensions provided in Tab. 2.3 and to fit closely the critical chord slenderness of 1/7 to be applied with the simplified design approach. From the options shown in Tab. 2.3, the chosen layouts are the most common ones. With these layouts the most relevant aspects of the truss joint models can be discussed and hence, no further layouts were considered.

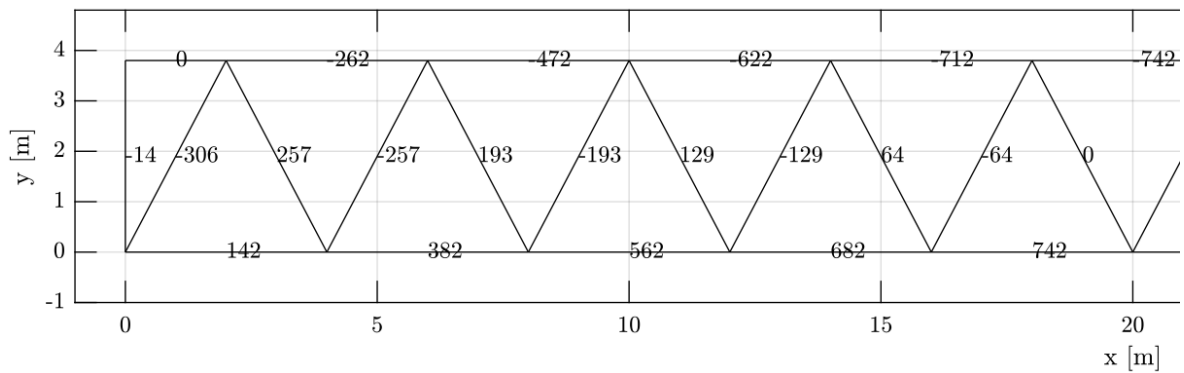


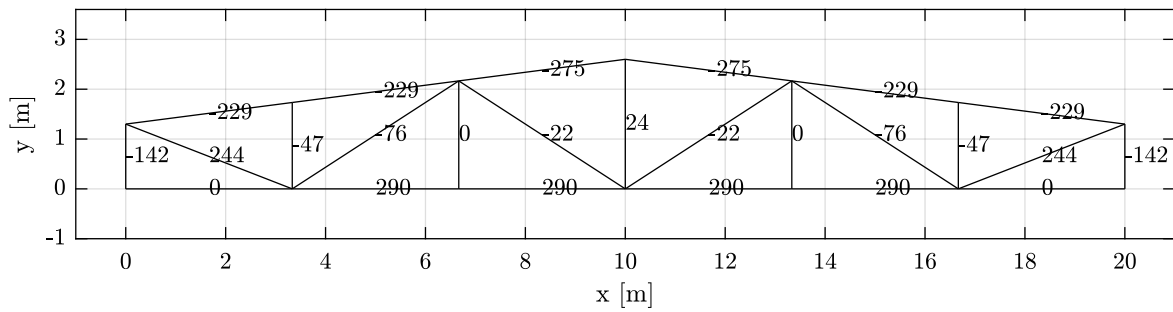
Fig. 5.1: Parallel chord trusses (a) and (b) with rising and falling diagonals: Normal forces in [kN] for ULS loading conditions. Only the left half of the truss is shown for better readability.

Tab. 5.1: Characteristics of truss (a).

parameter	value	parameter	value
type	parallel chord truss	bottom chord segments	10
web layout	rising and falling diagonals	dowel diameter	12 mm
span-width	40 m	member width	200 mm
truss height	3.8 m	GLT class	GL24h
truss slenderness	10.5	bottom chord height	520 mm
girder distance	5 m	top chord height	400 mm
purlin distance	4 m	chord slenderness	7.3
reference snow height	500 m	web member heights	160 - 360 mm

Tab. 5.2: Characteristics of truss (b). (The differences to truss (a) are highlighted in bold.)

parameter	value	parameter	value
type	parallel chord truss	bottom chord segments	10
web layout	rising and falling diagonals	dowel diameter	6 mm
span-width	40 m	member width	200 mm
truss height	3.8 m	GLT class	GL24h
truss slenderness	10.5	bottom chord height	520 mm
girder distance	5 m	top chord height	400 mm
purlin distance	4 m	chord slenderness	7.3
reference snow height	500 m	web member heights	80 - 320 mm

**Fig. 5.2:** Duopitch roof truss (c) with raised eaves and falling and rising diagonals with posts: Normal forces in [kN] for ULS loading conditions.**Tab. 5.3:** Characteristics of truss (c).

parameter	value	parameter	value
type	duopitch roof truss with raised eaves	purlin distance	3.33 m
web layout	falling and rising diagonals with posts	reference snow height	500 m
span-width	20 m	bottom chord segments	6
truss height	2.6 m	dowel diameter	12 mm
eave height	1.3 m	member width	200 mm
roof inclination	7.4°	GLT class	GL24h
truss slenderness	10.3	bottom chord height	280 mm
girder distance	5 m	top chord height	240 mm
		chord slenderness	7.0
		web member heights	160 - 240 mm

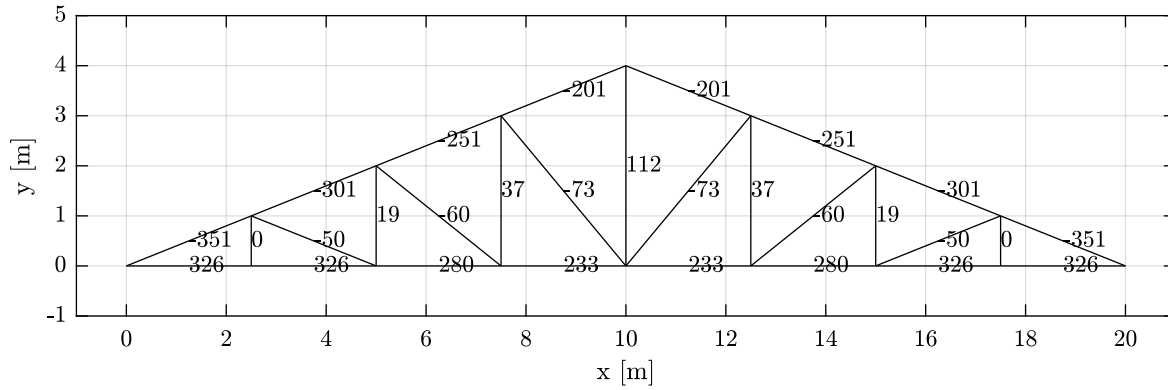


Fig. 5.3: Triangular truss (d) with falling diagonals with posts: Normal forces in [kN] for ULS loading conditions.

Tab. 5.4: Characteristics of truss (d).

parameter	value	parameter	value
type	triangular truss	bottom chord segments	8
web layout	falling diagonals with posts	dowel diameter	12 mm
span-width	20 m	member width	200 mm
truss height	4 m	GLT class	GL24h
roof inclination	21.8°	bottom chord height	280 mm
truss slenderness	10.0	top chord height	280 mm
girder distance	5 m	chord slenderness	7.1
purlin distance	2.5 m	web member heights	160 - 200 mm
reference snow height	500 m		

5.2.3 Modelling details

As presented in Sec. 3.2.3, different degrees of complexity can be considered to model truss joints. The herein considered models are illustrated in Fig. 5.4, where also their names are introduced. Further, these models are combined with three different models for the load-deformation behaviour of the dowelled connections: K_{ser} according to SIA 265:2021 [121] (Eq. 2.13 and 2.14); the initial stiffness K_1 of the approach developed by Manser (2021) [91] (Sec. 3.3.3); and the full non-linear model (n-1) by Manser (2021) [91] (Sec. 3.3.3). Finally, these three approaches of the load-deformation behaviour are considered with coupled dofs based on the model published by Schweigler et al. (2018) [115]. Altogether, these combinations led to 21 models that are investigated in the following.

5.2.4 Results

Fig. 5.5 shows that for the trusses (a), (b) and (c) the decrease in normal force compared to ideal, pin-jointed trusses [22] is in the range of 1-2%. In the case of the triangular truss (d), the reduction is up to 9%. This reduction increases for the models which include the chord springs and is more severe when the load-deformation of the single dowels is modelled with the initial stiffness K_1 or the full non-linear approach based on Manser (2021) [91].

In Fig. 5.6, the maximum deflections of the trusses from SLS loading conditions are normalised by the deflections determined with the *Culmann* model. The first observation is that the *rigid* and the *Culmann, cont.* models show very similar deflections as the *Culmann* model. The load-deformation behaviour according to Manser (2021) generally shows a softer behaviour than when using K_{ser} and, as expected, even more when the non-linear behaviour is considered. Models that take into account the springs in the chords clearly show a softer behaviour than when only considering the web springs. In some cases, the influence of the chord springs is even larger than the one from the web springs. Especially for the trusses (c) and (d), they have a very strong influence. The introduction of the steel plates, and with it the correct consideration of the location of the web springs, has a minor but an increasing influence on the deflections. When the coupling of the dofs is considered, only minor changes occur.

For the ULS loading conditions in Fig. 5.7, very similar observations can be made for the relative truss deflections. As expected, due to the non-linear load-deformation behaviour, in the respective models a certain increase in the relative deflections can be observed compared to the SLS loading conditions.

In Fig. 5.8 - 5.10, the maximum stress increase of the bottom chord, the top chord and the web members, respectively, are shown. This stress increase factor is basically determined by division of the maximum stress in a cross-section divided by its stress in the center, where the stress state relates to pure normal force action. As shown in Fig. 5.5, the normal forces show certain decreases compared to the *Culmann* model. Hence, the results are corrected by the respective ratios. Since the chords are continuous, the stress increase in most cross-sections is of minor importance because their absolute stress level cannot be decisive. Therefore, the relevant stress increase factor for a chord is determined by the division of the maximum absolute stress

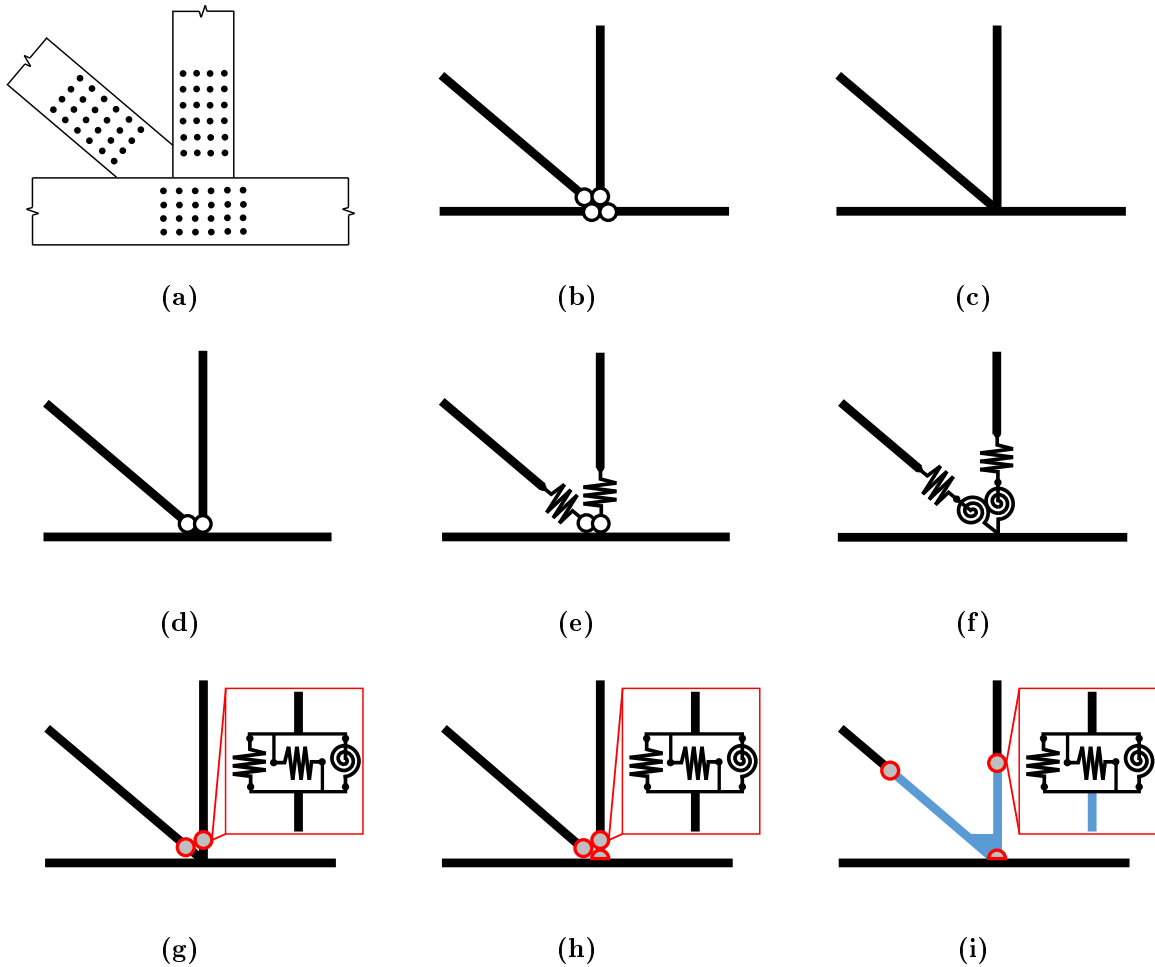


Fig. 5.4: Investigated models for the joints of timber trusses with dowelled steel-to-timber connections on the example of the layout in (a); (b) *Culmann*: friction free hinges; (c) *rigid*: fully rigid beam connections; (d) *Culmann, cont.*: continuous chords and friction free hinges at both ends of web members; (e) *web N*: continuous chords, normal force springs and friction free hinges at both ends of web members; (f) *web N-M*: continuous chords, normal force and moment springs at both ends of web members; (g) *web N-V-M*: continuous chords, normal force, shear force and moment springs at both ends of web members; (h) *chord N-V-M*: continuous chords, normal force, shear force and moment springs at both ends of web members and in the chords; (i) *full N-V-M*: continuous chords, normal force, shear force and moment springs at both ends of web members and in the chords with steel plates between the web and chord springs.

by the maximum absolute stress from pure normal forces. These stress maxima generally do not spatially coincide. Therefore, local stress increase factors can be larger than the global value but are irrelevant. In the case of the bottom chord, the nine models including the chord springs are evaluated twice. The lower values marked in colour correspond to the results from net-cross-section analysis. The grey markers represent the results from gross-cross-section analysis. The difference comes from the stronger reduction of the net-cross-section under tension than in bending (Sec. 3.3.2.6). When strongly reduced net-cross-sections do not spatially coincide with

large bending stresses, the difference of both results increases further. (Since in the first twelve models the connections are not considered in the framework, their stress increase factors cannot be evaluated automatically. A similar difference is expected as for the last nine models.) In the top chord, all members suffer from the same cross-section reduction, since the holes for the dowels are not subtracted (Sec. 3.3.2.6), and therefore, the results are independent of the selected cross-section analysis.

In both the bottom and top chord a major part of the stress increase stems, as expected, from the continuous chords themselves. With added flexibility there is a trend towards higher stress increases. For the trusses (c) and (d) the stress increase in the bottom chord is stronger influenced by the introduction of the flexibility in the chord connections than by the flexibility of the web connections. For truss (d) the same is true for the top chord.

For the stress increase factors of the web members, obviously, there is no influence for models with friction free hinges other than the effect of the normalisation by the ratio of the maximum normal forces, as explained above. The parallel chord trusses (a) and (b) show larger stress increase factors for the models that do not consider the chord springs and the steel plates. Further, softer load-deformation behaviour leads to lower stress increase. For truss (c), the most accurate model with consideration of all parts leads to the overall largest stress increase. In the case of truss (d), the differences are more moderate. The influence of the coupled dofs is more pronounced for the stress increase factors of the web members than for the chords. The *rigid* model leads to much higher results that are out of the axes limits.

The reduction of the load-carrying capacity for eccentrically loaded connections according to Eq. 3.20 is evaluated again separately for the bottom chord, top chord and the web members in Fig. 5.11 - 5.13, respectively. When very small normal forces occur in a connection, the reduction factor is very sensitive to the bending moment. Therefore, a lower limit has been introduced to exclude low reduction factors that occur in connections which cannot be decisive for the design, i.e. reduction factors are excluded from this analysis when the respective normal force is lower than half of the smallest introduced load. For most cases the *rigid* model shows reduction values that are outside the selected axis limits. Only in the top chord of truss (d), its value is in the same order as the values from the other models. Generally, in the chords the reduction is smaller than 10%, but in the top chord of truss (d) up to 40% is reached. The coupling of the dofs has a significant influence, especially for the non-linear load-deformation model. For the web connections, the reduction is less than 15% in all cases. No obvious tendency can be concluded with respect to the different load-deformation models. In certain cases stiffer behaviour is of advantage, while in other cases the opposite can be observed. The inclusion of the chord springs in some cases introduces further complexity. With respect to the coupling of the dofs a certain effect can be noted.

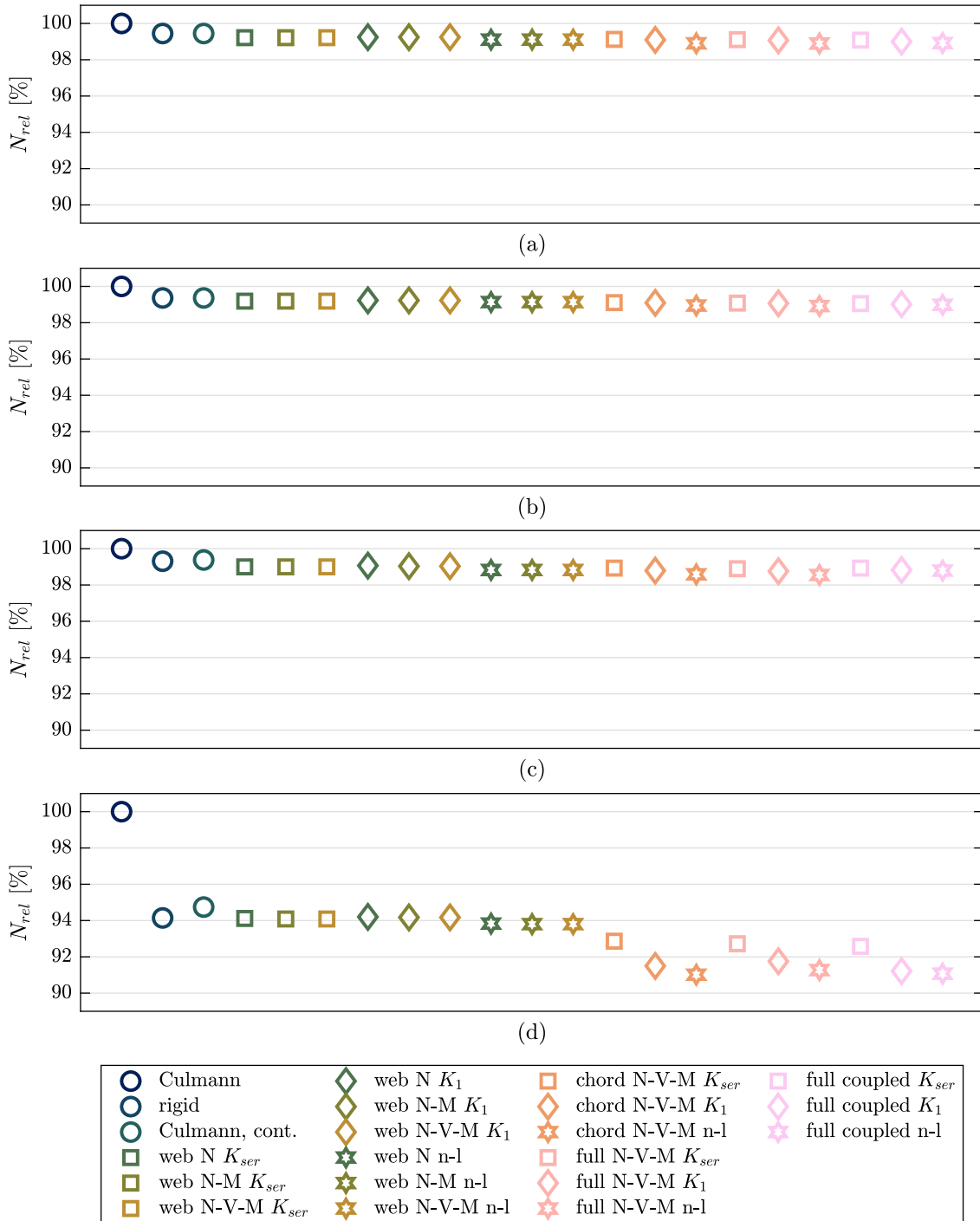


Fig. 5.5: Maximum relative normal force (in comparison to the *Culmann* model) of trusses (a) to (d) for the 21 modelling approaches.

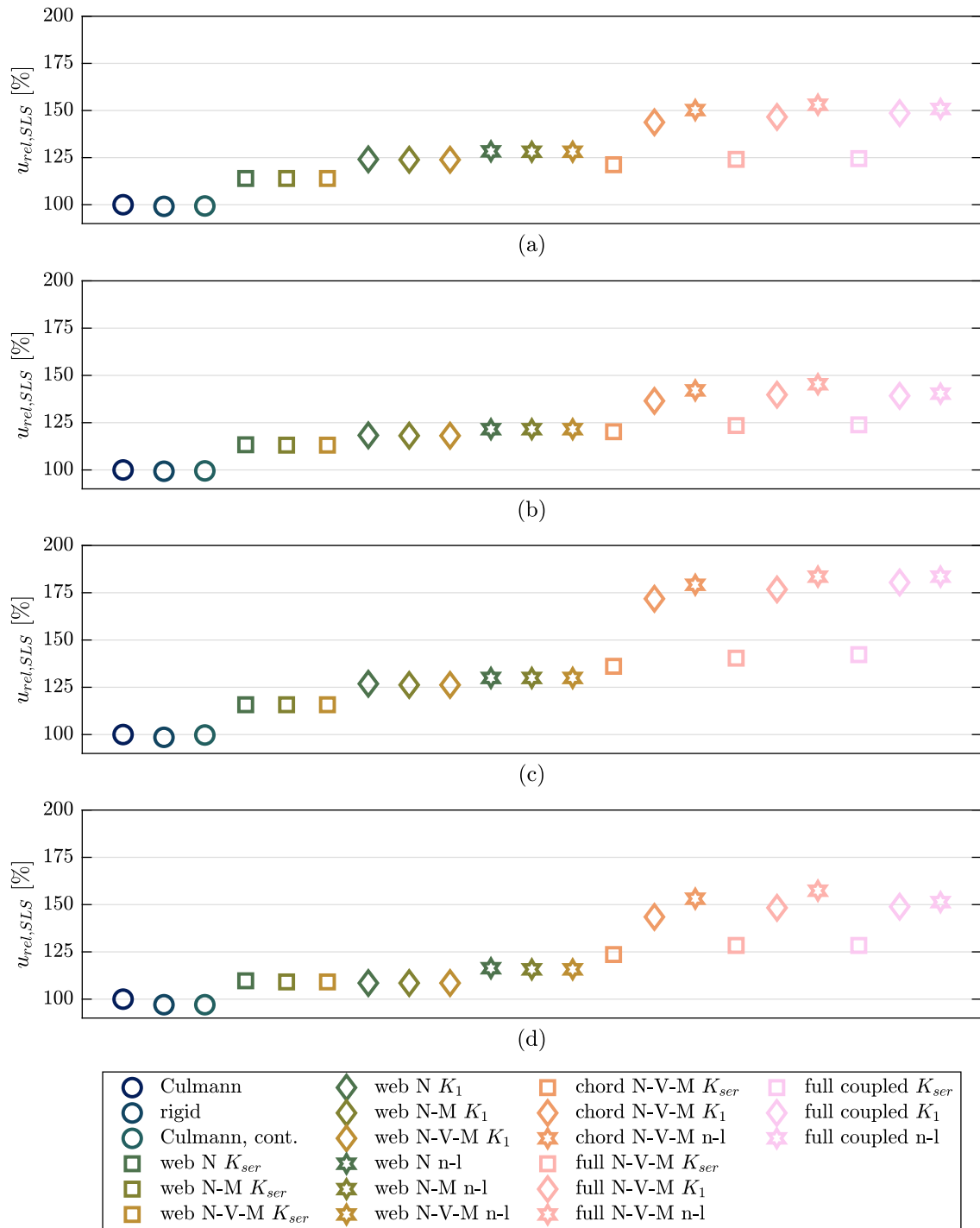


Fig. 5.6: Maximum relative deflection (in comparison to the *Culmann* model) of trusses (a) to (d) for the 21 modelling approaches under SLS loading conditions.

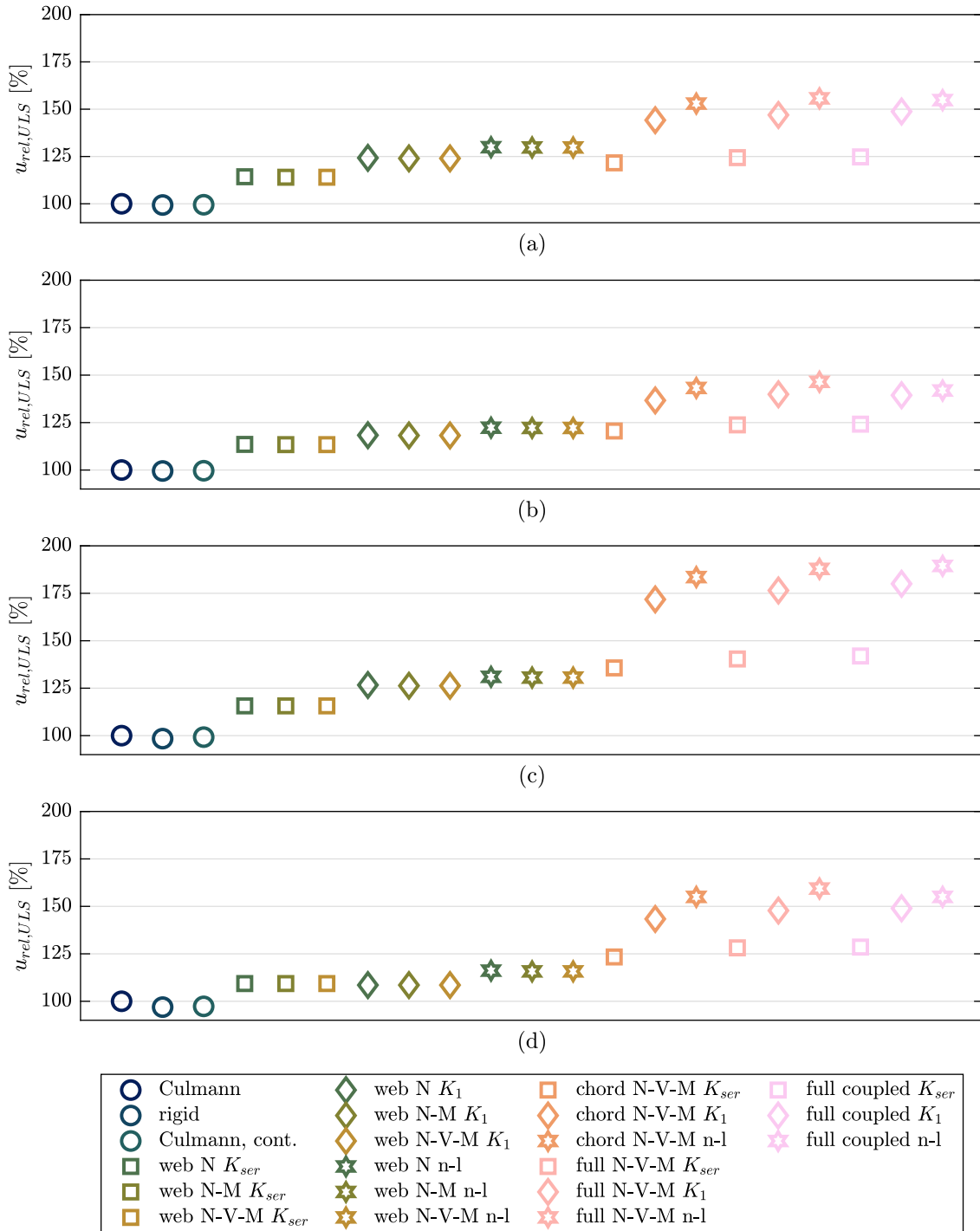


Fig. 5.7: Maximum relative deflection (in comparison to the *Culmann* model) of trusses (a) to (d) for the 21 modelling approaches under ULS loading conditions.

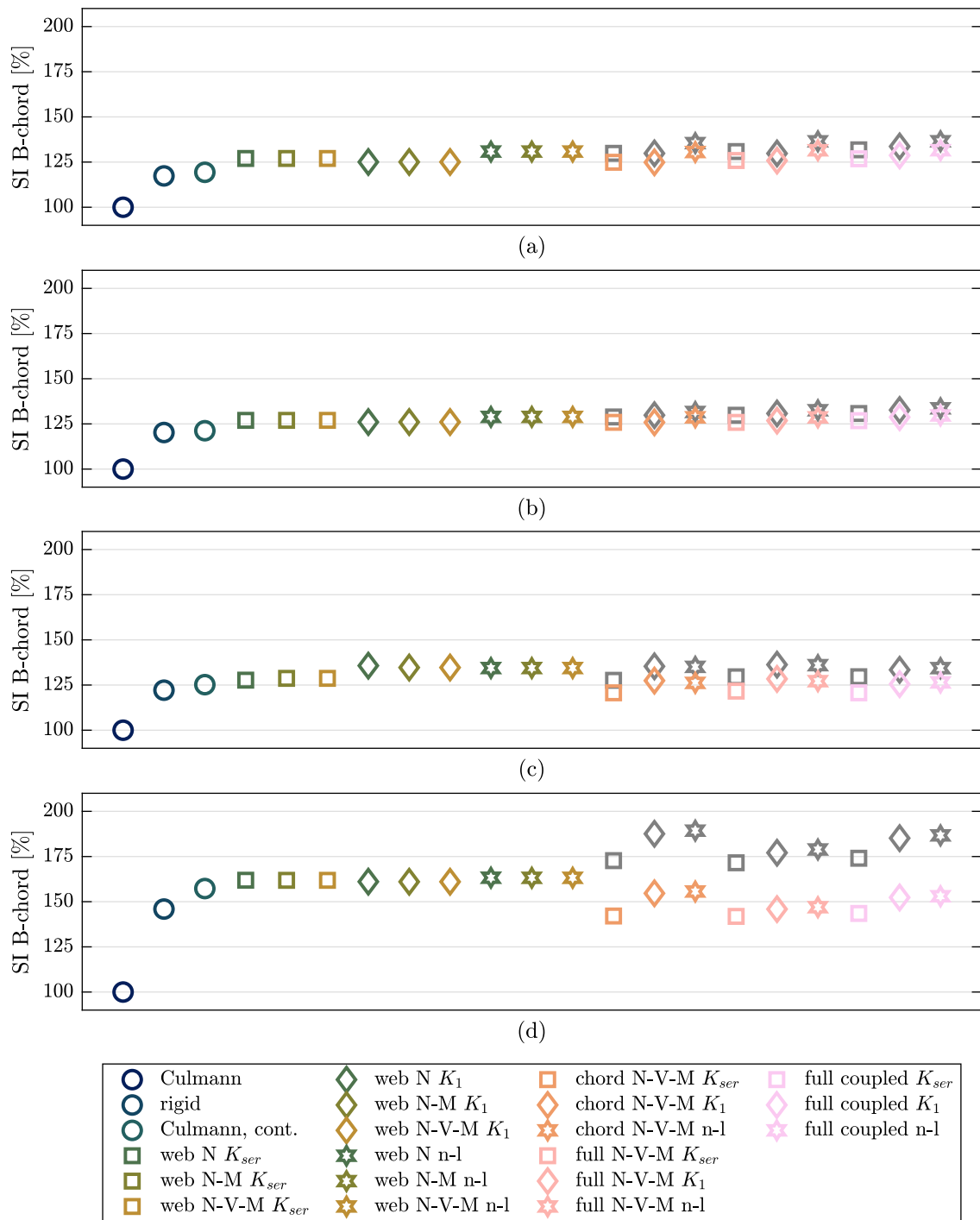


Fig. 5.8: Maximum relative stress increase (SI) in the bottom chord (in comparison to the *Culmann* model) of trusses (a) to (d) for the 21 modelling approaches.

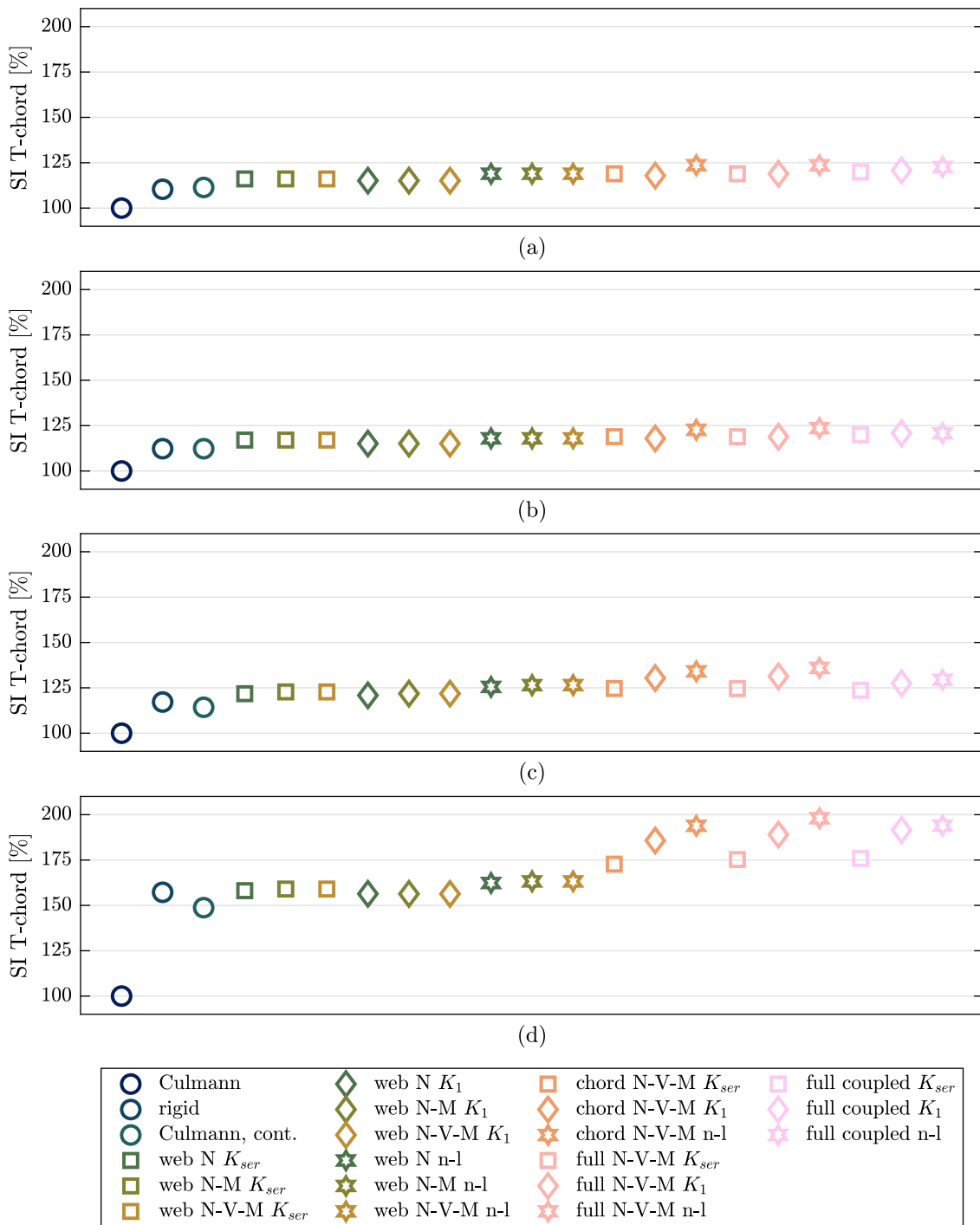


Fig. 5.9: Maximum relative stress increase (SI) in the top chord (in comparison to the *Culmann* model) of trusses (a) to (d) for the 21 modelling approaches.

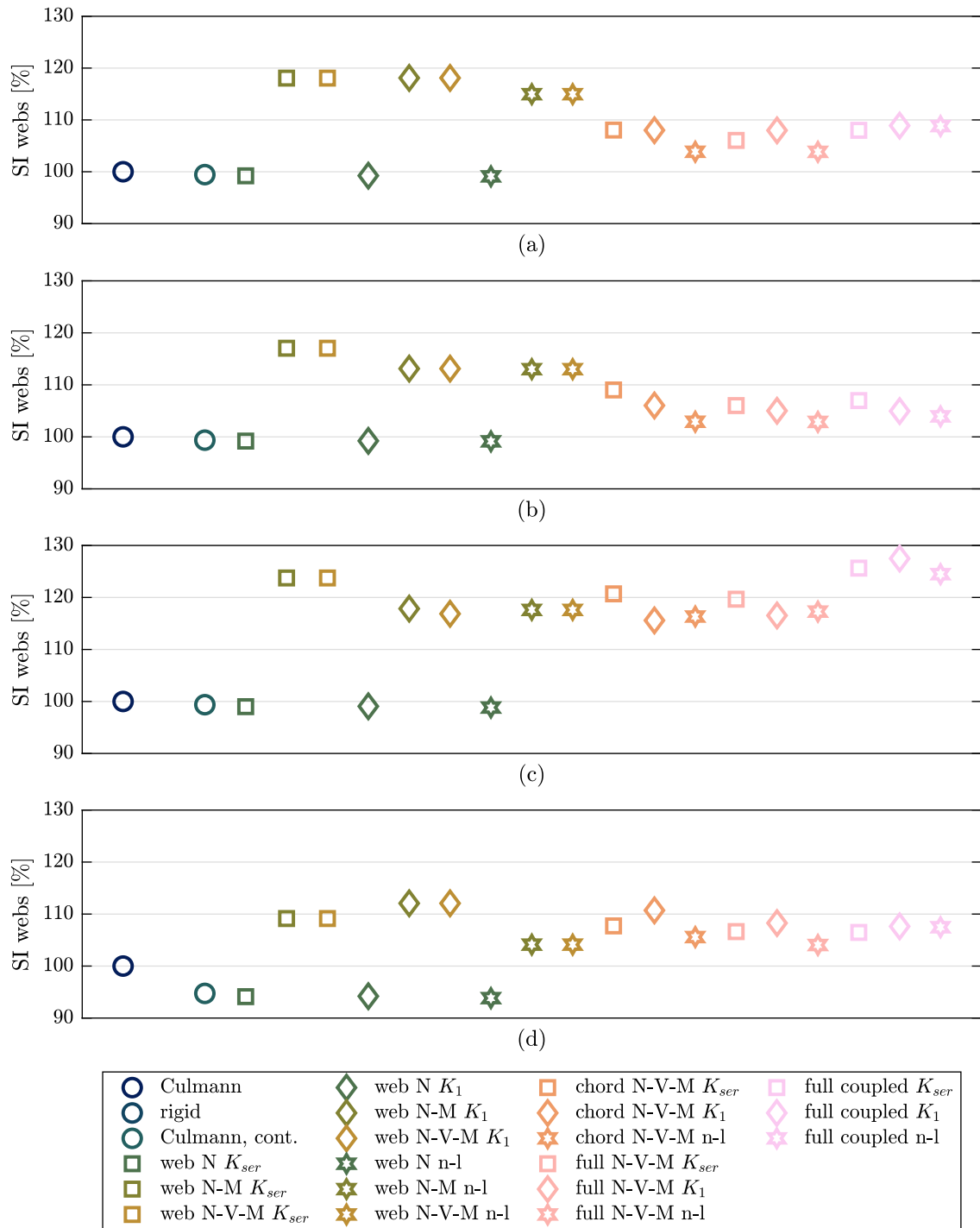


Fig. 5.10: Maximum relative stress increase (SI) in the web members (in comparison to the *Culmann* model) of trusses (a) to (d) for the 21 modelling approaches.

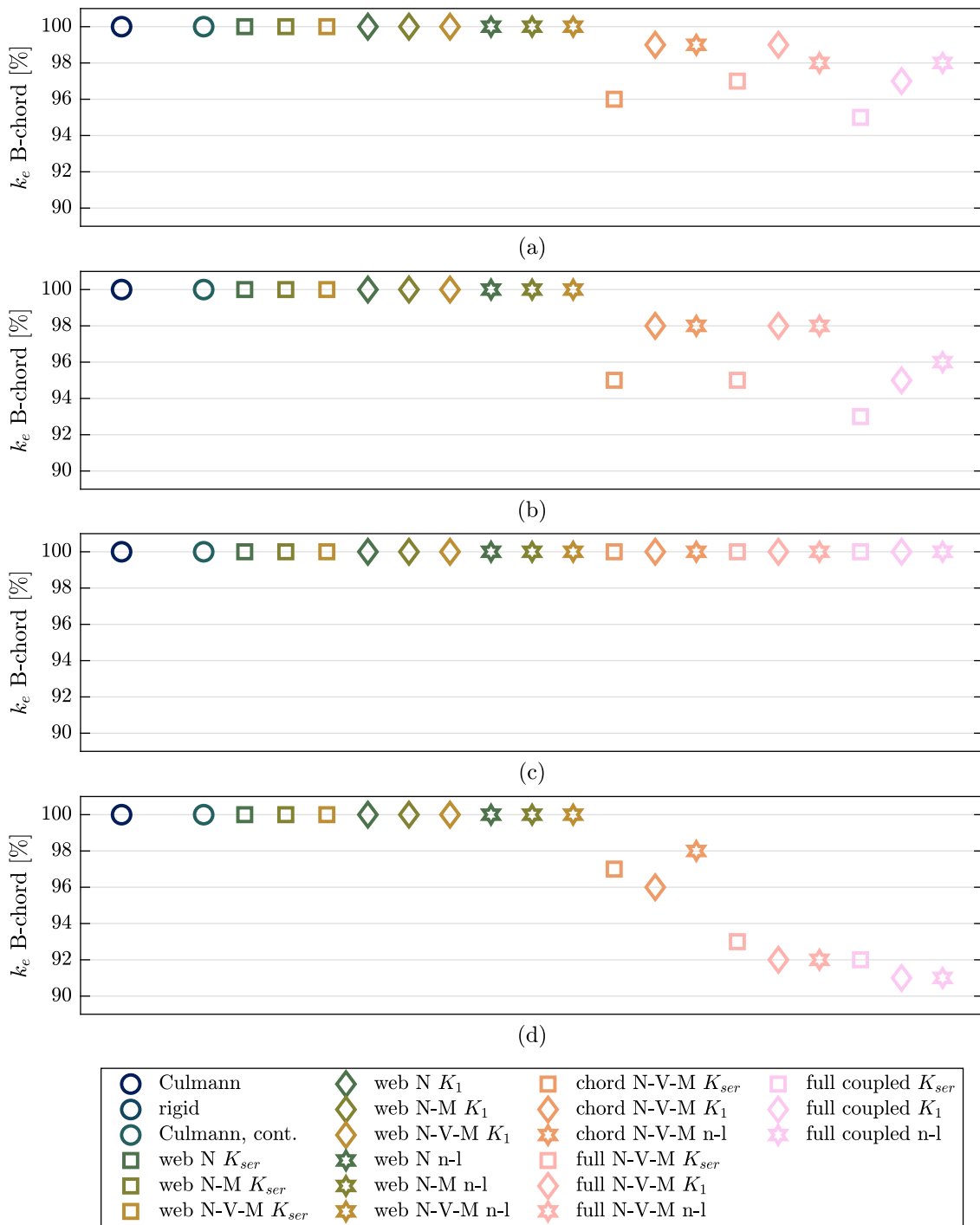


Fig. 5.11: Minimum reduction factor k_e due to eccentricity in the connections of the bottom chord of trusses (a) to (d) for the 21 modelling approaches.

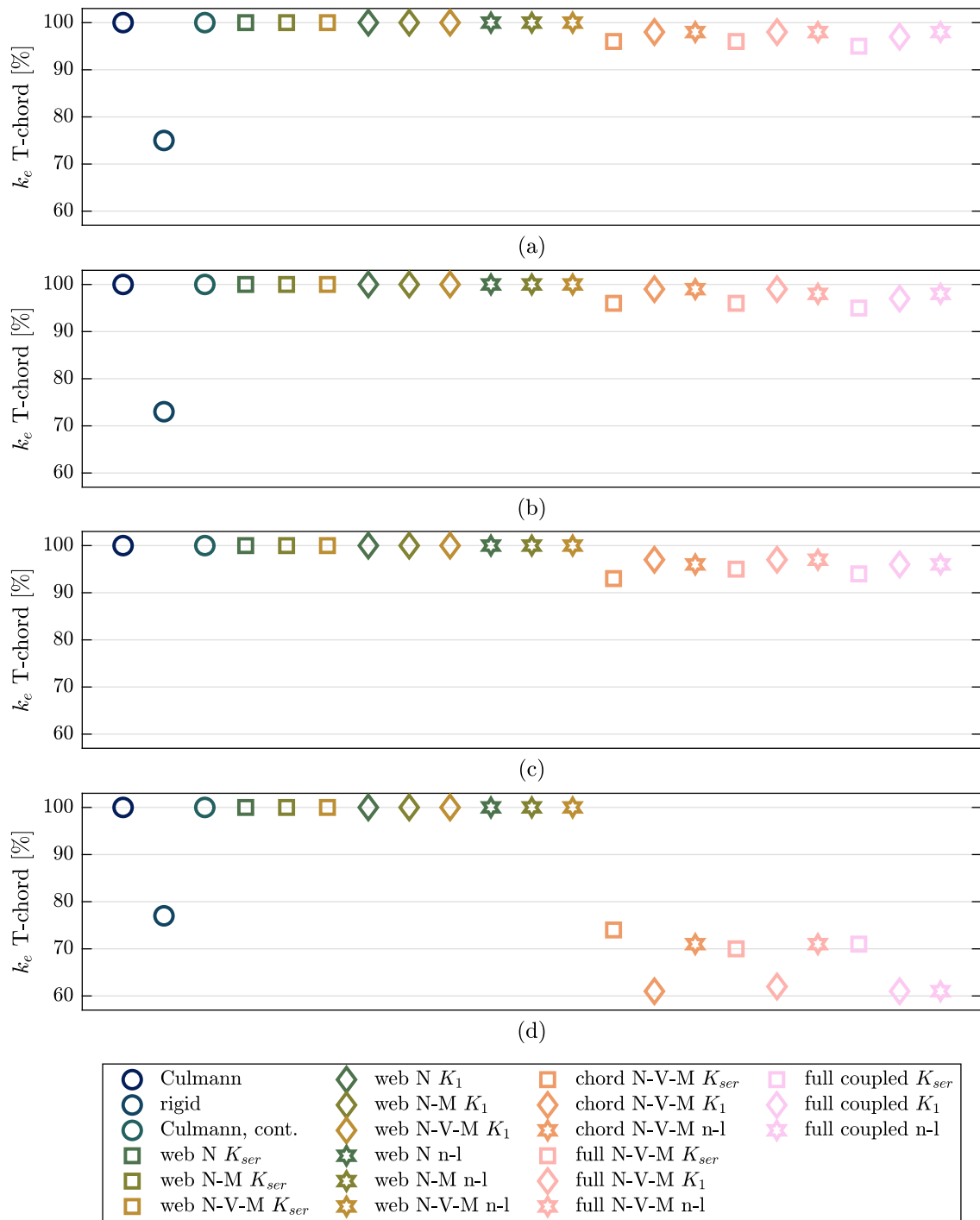


Fig. 5.12: Minimum reduction factor k_e due to eccentricity in the connections of the top chord of trusses (a) to (d) for the 21 modelling approaches.

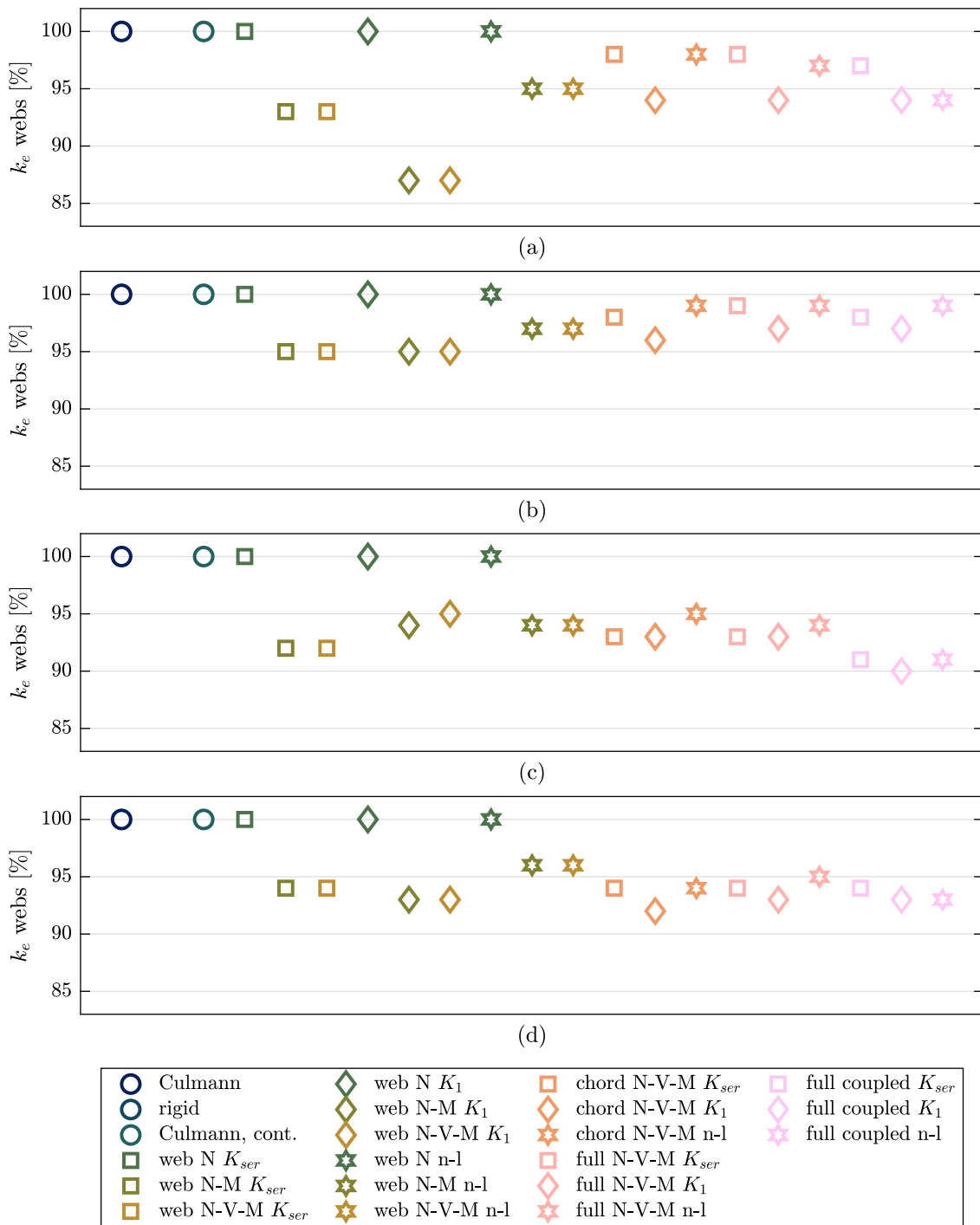


Fig. 5.13: Minimum reduction factor k_e due to eccentricity in the connections of the web members of trusses (a) to (d) for the 21 modelling approaches.

5.2.5 Discussion

As shown in Sec. 2.3.2, Scheer & Golze (1981) [110] found 1-2% lower normal forces for the model *Culmann, cont.* than for the pure *Culmann* truss. When studying Fig. 5.5, it can be seen that this statement holds for all models of the trusses (a), (b) and (c). For the triangular truss (d), the reduction is up to 9% though and a clear influence from the considered chord connections can be observed.

The comparison of the models with respect to the relative deflections for both SLS and ULS loading conditions reveals clearly the importance of the consideration of the chord connections for all trusses. Further, the choice of the load-deformation behaviour has a major influence, where the influence of the initial stiffness is much more pronounced than the non-linearity. In Sec. 3.3.3 the differences in the load-deformation behaviour were shown on the level of single-dowel connections within multi-dowel connections. There it could be observed, that for larger dowel groups both load-deformation approaches based on Manser (2021) [91] (K_1 and non-linear curve) show softer behaviour than K_{ser} from SIA 265:2021 [121]. Hence, for the large dowel groups in the considered trusses these discrepancies are significant. According to the design rules from SIA 265:2021 [121], the admissible deflections need to be restricted to 2/3 when only the normal forces are considered. Vice-versa, the relative deformations should not be larger than 150% of the value from the *Culmann* model. For trusses (a), (b) and (d), this assumption holds. For truss (c), where the deflections reach 180% of the *Culmann* model, this restriction is insufficient.

With respect to the stress increase factors in the chords, the importance of the model selection depends on the truss layout. In the case of the parallel chord trusses (a) and (b), only a minor influence can be observed, where for truss (c) and especially for the triangular truss (d) the influence is pronounced. The consideration of the net-cross-section is important in the lower chord under tension, since the absolute maximum stress and the maximum stress from pure normal force spatially generally do not coincide and hence, more beneficial values can be found. For the stress increase factors in the web members, no clear tendency with respect to the models can be derived when considering all four trusses. Neither the load-deformation behaviour, nor the model complexity reveal a clear trend.

The prescribed restriction of the resistance of the chords to 2/3 according to SIA 265:2021 [121] corresponds to a limit of the stress increase factor of 150%. This limit is met by trusses (a), (b) and (c), but clearly not in the top chord of truss (d), where almost 200% is reached. This calls for further investigations of the validity of the approach with respect to the truss and web layouts. Further, the stress increase factor of the web member of truss (c) reaches the limit of the design rule, and therefore, for this rule further investigations are necessary.

With respect to the reduction factor due to eccentric loading, it is interesting to note that the minimum value did not occur in a web member but in the top chord of truss (d) and that the value of 0.75 prescribed in SIA 265:2021 [121] is exceeded.

The study of all these aspects clearly shows the need of an accurate modelling. None of the simplifications reveals conservative results with respect to all considerations. However, the

selection of the load-deformation behaviour and the inclusion of the chord connections both show a major influence on various aspects. The coupling of the dofs for certain aspects has an influence that generally should not be neglected either. Finally, it can be concluded that for further investigations the most comprehensive model *full Schweigler n-l* should be used.

The comparison of the results to the simplified design approach from SIA 265:2021 [121] reveals drawbacks with respect to the truss layout. The design rule considering the deflections is non-conservative for the duopitch truss (c) and the reduction of the stress increase in the chords and the reduction of the connection resistance are insufficient in the case of the triangular truss (d). Although the rules are exceeded in some cases, it has to be stated that the design verification by means of the developed framework (Sec. 3.3) was still fulfilled in all cases. This can be explained by rounding up member heights to full lamellas and number of dowels in connections to certain connection layouts. Further, in dependence of the truss slenderness, the deflections are hardly ever decisive.

5.3 Evaluation of the simplified design approach according to SIA 265:2021

5.3.1 Introduction

Preliminary results from Sec. 5.2 revealed certain deficiencies of the simplified design approach of SIA 265:2021 [121]. Hence, it is further reviewed in the context of its applicability to single span beams using various truss and web layouts. All trusses were designed with the truss design tool presented in Sec. 3.4. The same properties are investigated as in Sec. 5.2, although with a focus on the truss characteristics in contrast to the modelling details.

5.3.2 Investigated trusses

For the evaluation of the validity of the simplified design approach from SIA 265:2021 [121], four different truss layouts are studied: parallel chord trusses, duopitch roof trusses with raised eaves, triangular trusses and monopitch roof trusses. The first three cover the most common structures and the monopitch roof truss represents the largest deviation between form and forces. The remaining static systems from Tab. 2.3 (e.g. bowstring trusses) are expected to show similar or less severe results than the ones being investigated. The web layouts are selected from the following list: falling and rising diagonals, rising and falling diagonals, falling and rising diagonals with mid-post, falling and rising diagonals with posts, rising and falling diagonals with posts, falling diagonals with posts and rising diagonals with posts.

For the first three types (parallel chord truss, duopitch roof truss with raised eaves and triangular truss) a span-width of 20 m and a truss slenderness ratio of 1 : 10 is selected. The span-width of the monopitch roof truss is only 15 m, since for the chosen loading conditions of a reference snow height $h_0 = 500$ m and a girder distance of 5 m the detailing with standard GLT of up to a strength class of GL32h did not work for the intended chord slenderness ratios (1 : 5.6

to 1 : 8.3). The truss slenderness ratios further had to be limited to 1 : 7.5. For all trusses, the resulting purlin distance (acting in the truss joints only) are in the range of 2 m. The modelling details correspond to the case *full coupled n-l* described in Sec. 5.2.3.

In the case of the parallel chord trusses the same layouts are chosen also for trusses with span-widths of 40 m and chord slenderness ratio of 1 : 7.1, i.e. each truss member is twice as long. This configuration should allow for an evaluation of the influence of absolute measures in contrast to relative ratios. The application of the non-linear load-deformation relation according to Manser (2021) [91] did not allow for an investigation of other truss types with doubled span-widths. The regression functions prevent the usage of the necessary number of dowels in such compact connections. Due to this issue, but also due to sufficient insight from the remaining trusses, no further cases are investigated.

The beam widths and the GLT strength classes are selected in such a way that the intended chord to truss slenderness ratios result. It is pointed out that generally only one of the two chords corresponds to the slenderness ratio and the other one is smaller, i.e. the two chord heights are selected individually, as it is usually done in practice. Aside the focus on practically relevant configurations, an equalisation of the truss chord height would influence the stiffness and with it the deflections of the truss. Hence, for the higher chord the stress increase factors would be non-conservative.

5.3.3 Results

Fig. 5.14 shows that for the parallel chord trusses and the duopitch roof trusses with raised eaves the relative change in normal forces compared to the modelling approach from *Culmann* is in the range of a few percent. For the triangular trusses, the reduction is more severe with roughly 10 – 15% and for the monopitch roof trusses the reduction is up to 25%.

The relative deflections under SLS loading conditions roughly meet the design rules of $3/2 = 150\%$ (dashed line) in the case of the triangular trusses and the parallel chord trusses with a span-width of 40 m. For all other cases, the relative increase in deflections is higher and in the case of the monopitch roof trusses values up to 185% occur. Next to a noteworthy influence of the web layouts, it can be observed that higher chord slenderness ratios lead to a larger increase in deflections. In the case of ULS loading conditions, only slightly higher values are achieved with the same tendencies as under SLS loading conditions.

In Fig. 5.15, the stress increase (SI) due to additional bending moments in comparison to the modelling approach from *Culmann* with pure axial forces is displayed for the bottom chord (B-chord), the top chord (T-chord), the web members in general, and the web members in the connection areas (web-conn). In the bottom chord, the stress increase is below the design provisions (dashed line) for the prescribed minimum chord slenderness ratio of 1 : 7. No significant difference between the parallel chord trusses with 20 m and 40 m span-width can be observed for the chord slenderness 1 : 7.1. For lower slenderness ratios, the limit of $3/2 = 150\%$ is slightly surpassed.

For the top chord, the limit (dashed line) is clearly surpassed by the triangular trusses and even more by the monopitch roof trusses. For the parallel chord trusses, the limit holds and for the duopitch roof trusses, in dependence of their web layouts, the limit holds or is surpassed. For these two truss layouts, no clear trend can be observed with respect to their chord slenderness ratios.

The general stress increase in the web members is larger or equal (by definition) than it is for their connection areas. In the connection areas, the limit $133\% = 1/0.75$ holds in all cases and is almost met in some cases of the duopitch roof trusses with raised eaves. For the generally higher stress increase in mid-span of the web members, no design rules exist. It has to be kept in mind that in the figure only the maximum values are displayed and that they might occur in web members that inherit only small stresses from normal forces.

The reduction factors of the connection capacity k_e are shown in Fig. 5.16 for the bottom chord, the top chord and the web members. No general trends with respect to the chord slenderness ratios can be observed when considering all truss layouts. For the monopitch roof trusses, the design rule is exceeded in various cases for all beam types. For the other three truss types, the limit (dashed lines) is exceeded only slightly in the web members for a chord slenderness ratio of 1 : 8.3. By definition, this reduction factor is very sensitive to the magnitude of the normal force (compare Sec. 5.2.4). Still, all connections are designed individually and therefore all can be decisive for the overall capacity including connections with relatively small normal forces. Hence, all connections must be covered by the design rule.

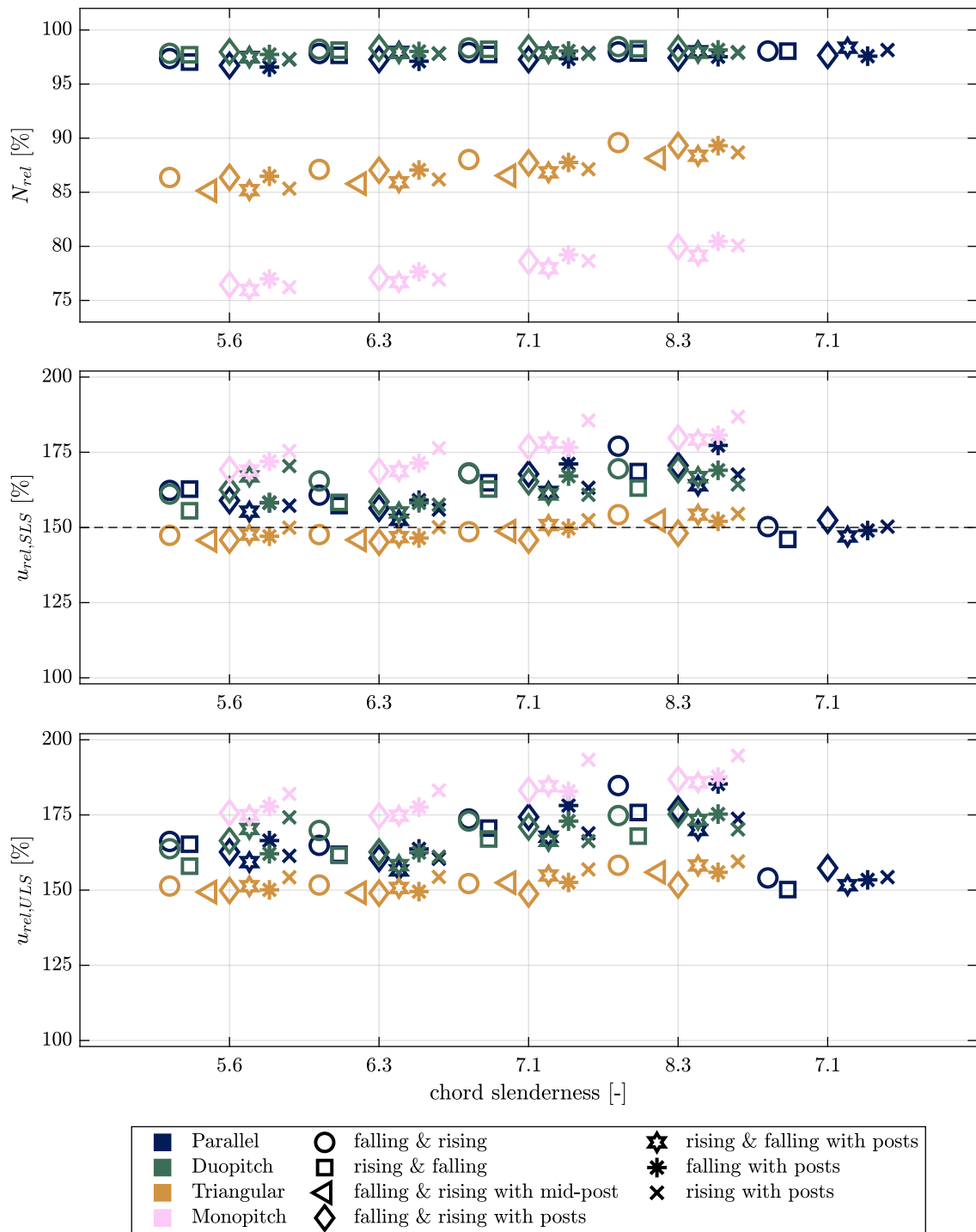


Fig. 5.14: Relative normal force and deflections in the SLS and ULS compared to the *Culmann* model. The first four chord slenderness ratios are associated with trusses with the originally selected span-widths of 20 m and 15 m, respectively. The results shown at the right end for a chord slenderness of 7.1 refer to parallel chord trusses with a span-width of 40 m. In the case of $u_{rel,SLS}$, the dashed line represents the design rule according to SIA 265:2021 [121].

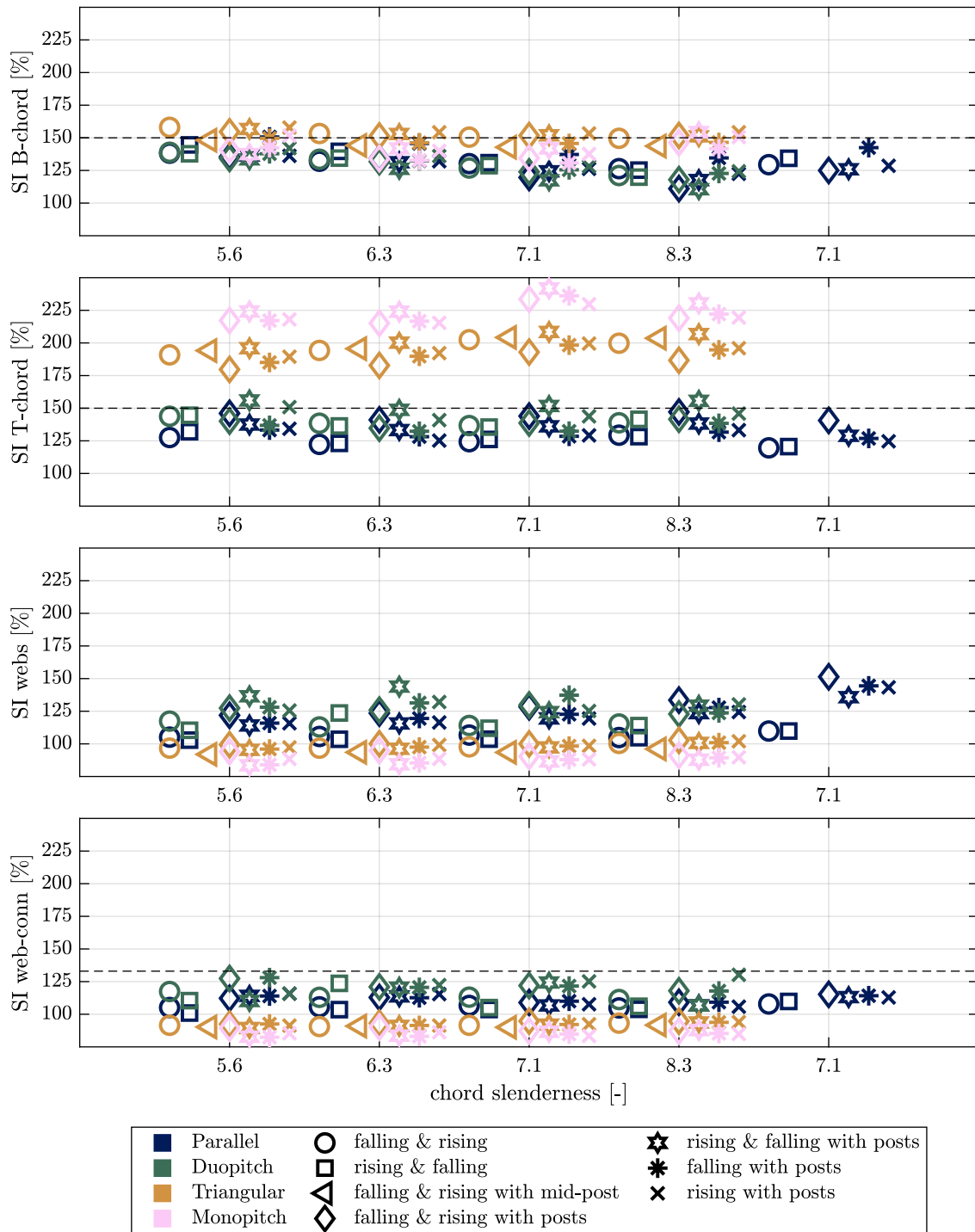


Fig. 5.15: Maximum stress increase (SI) in the bottom chord, top chord, web members and in the connection areas of the web members compared to the *Culmann* model. The first four chord slenderness ratios are associated with trusses with the originally selected span-widths of 20 m and 15 m, respectively. The results shown at the right end for a chord slenderness of 7.1 refer to parallel chord trusses with a span-width of 40 m. In the case of the bottom chord, the top chord and the web member connection areas, the dashed lines represent the design rules according to SIA 265:2021 [121].

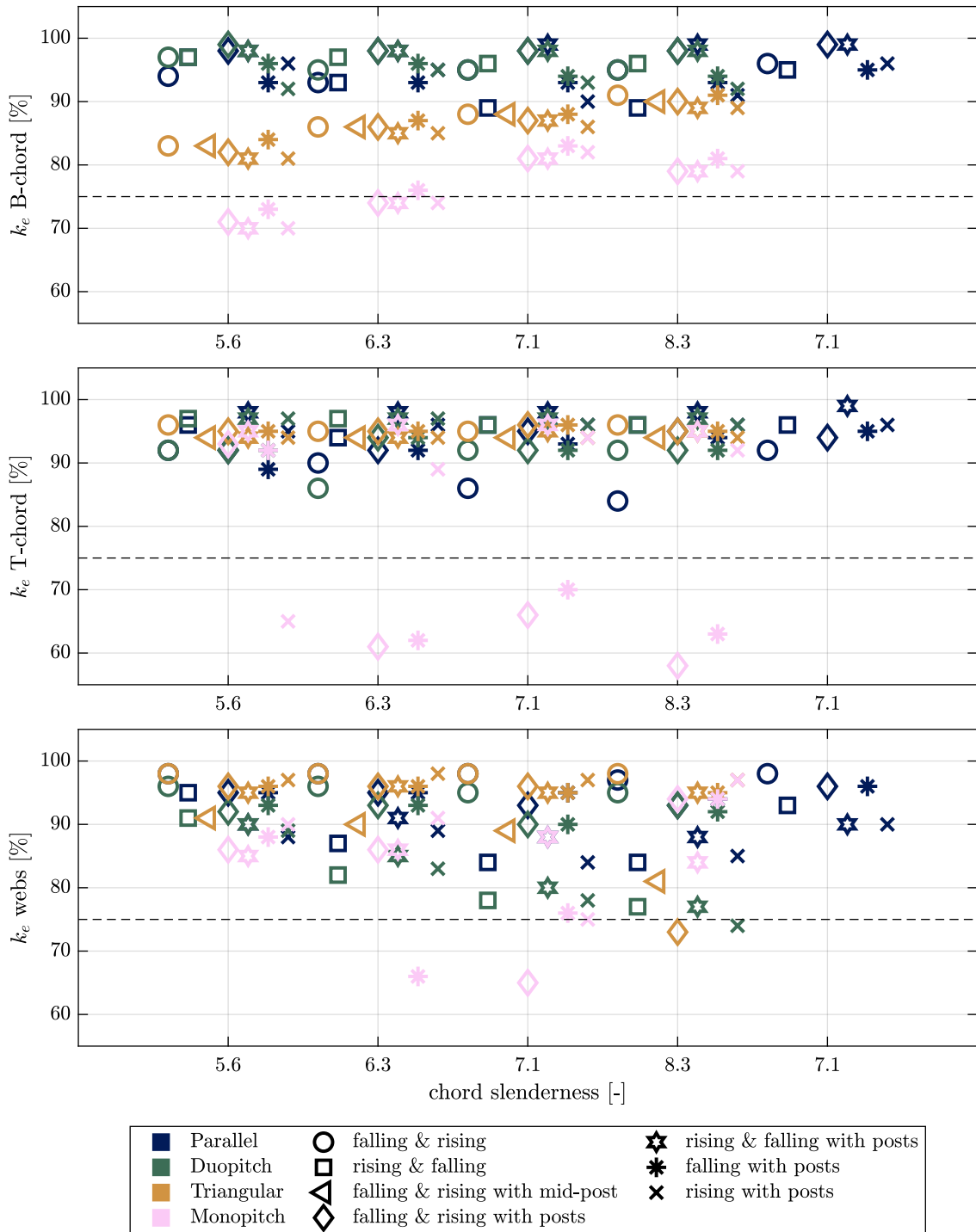


Fig. 5.16: Minimum reduction factor k_e due to eccentricity in the connections of the bottom chord, top chord and the web members. The first four chord slenderness ratios are associated with trusses with the originally selected span-widths of 20 m and 15 m, respectively. The results shown at the right end for a chord slenderness of 7.1 refer to parallel chord trusses with a span-width of 40 m. In all three cases, the dashed lines represent the design rule according to SIA 265:2021 [121].

5.3.4 Discussion

For the relative change in normal forces compared to the modelling approach from *Culmann*, the same observation can be made as pointed out in Sec. 5.2.5 that for the parallel chord trusses and the duopitch roof trusses with raised eaves, the values are in the range of a few percent. In the case of the triangular trusses and especially for the monopitch roof trusses, the deviations are quite pronounced though. These high values indicate that a considerable load share is transferred via the chords directly.

The increase in deflections compared to the modelling approach from *Culmann* under SLS loading conditions clearly surpasses the design rule of $3/2 = 150\%$ for many trusses. In contrast to the models which were applied to derive the design rules, the applied framework considers the chord connections, and hence the deflections are larger. As it could be seen in the previous section (Fig. 5.6), the applied load-deformation model per shear plane and fastener developed by Manser (2021) [91] leads to larger deformations than when the stiffness K_{ser} from SIA 265:2021 [121] is applied. While applying the truss design tool for this study (Sec. 3.4), in no case the absolute deflection limit was met. Therefore, on the one hand the deviations with respect to the design rules are considerable for the applied truss and chord slenderness ratios but on the other hand the deformation criterion is non-decisive.

Although the absolute deflections (not provided herein) are considerably larger for the ULS than for the SLS loading conditions, the consideration of the connections leads to a similar relative increase compared to the *Culmann* model. The slightly higher increase results from the flattening of the non-linear load-deformation behaviour of the connections under larger displacements (Fig. 3.14).

The design rule regarding the stress increase in the chords compared to the *Culmann* model stays within the limits of the design approach for the bottom chords. It is clearly exceeded in the top chords of the triangular and the monopitch roof trusses though. Still, during the investigations the utilisation of the top chord members was in the acceptable range. The reason why despite the exceedance of the limit no failure occurred is most likely to be found in the buckling out-of-plane behaviour, i.e. for the top chords, obviously, the buckling out-of-plane was decisive. Therefore, despite the clear overstep of this design rule, the designed trusses can still take up the induced stress increase. Further, as mentioned above, some over-design is commonly introduced by rounding up the member height to full lamellas and certain connection configurations.

As explained above, for the general stress increase in the web members, no design rule exists and for design only the connection areas might be decisive. The design limit of $1/0.75 = 133\%$ for the wood in the connection areas holds in all cases and is utilised most for the duopitch roof trusses with raised eaves. No general trend can be observed with respect to the chord slenderness ratio. Overall, this design rule seems to be appropriate.

The reduction factor of the connection capacity k_e due to eccentric loading is observed to be well-applicable to the parallel chord trusses, the duopitch roof trusses with raised eaves and the triangular trusses. Since in some cases the design rule with a reduction of 0.75 is met or slightly

exceeded, no generalised and concluding statement can be given though. The clear overstep of the design rule in the case of the monopitch roof trusses reveals a limitation of the simplified design approach.

As a summary it can be stated that the specifications according to the simplified design approach from SIA 265:2021 [121] are exceeded in many cases of the herein conducted investigations. The deflection criterion for the negligence of the connections is exceeded for three out of four investigated truss shapes. The rule concerning the stress increase in the chords is well-applicable to the bottom chord but is clearly exceeded in the top chord in the case of the triangular trusses and the monopitch roof trusses. The reduction factor for the wood in the connection area is observed to be well-chosen, but for the connection capacity it does not hold for the monopitch roof trusses. Still, when observing the utilisation of the individual members and connections by means of the developed framework no failure occurred. Three explanations can be given: (1) the chosen truss slenderness ratios lead to significantly smaller deflections than allowed, (2) the stress increase factors are mostly exceeded in the top chord where buckling out-of-plane might be decisive and (3) the rounding up of the cross-section heights to full lamellas of 40 mm thickness and the completion of the rectangular dowel layouts lead to over-designed elements.

5.4 Potential of the modelling framework

5.4.1 Introduction

The potential of the developed modelling framework (Sec. 3.3) lies in the design of diverse structures which can be built from timber trusses (Tab. 2.1 & 2.2). This means that restrictions of the simplified design approaches available in design codes can be omitted. Load introduction points between the main truss joints can be considered correctly, multi-span beams can be modelled, and the design of 2D-spanning and even space structures can be verified. In this section, for the sake of inspiration, an example beam grid structure is shown and various aspects are discussed on its basis.

5.4.2 Example truss structure: beam grid

For the investigation of a beam grid, a truss configuration was chosen that shares no beams with the crossed trusses. The sub-configurations of this 3-by-3 beam grid will be investigated with regard to their reliability in Chapter 6. Therefore, the details of the underlying single-span trusses with a span-width of 16 m are presented herein, before the whole structure is presented. The single trusses consist of parallel chords and falling and rising diagonals. The only two actions that are considered are the self-weight of the trusses and snow loads. For better comparability of the sub-configurations, only the three joints towards the center in the top chords are loaded (Fig. 5.17) by an arbitrary load-introduction area of 25 m² and a reference snow height $h_0 = 500$ m (information about the actions is provided in Sec. 4.6). In Fig. 5.18, the reactions

in the supports at the beam ends are provided, considering the self-weight and external loading from the arbitrarily chosen snow loads.

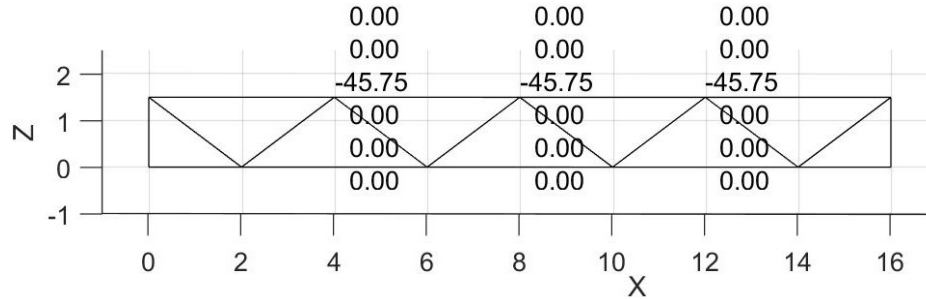


Fig. 5.17: External loading of the single trusses.

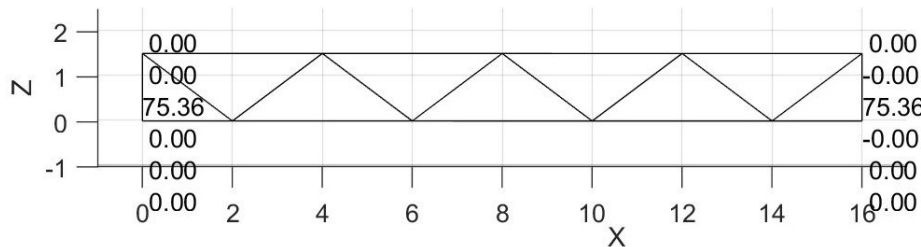


Fig. 5.18: Reactions of the single trusses.

In Fig. 5.19 & 5.20 the maximum utilisation of the member cross-sections and the connections are illustrated, respectively. This truss was not designed with the truss design tool (Sec. 3.4) following the simplified design approach of SIA 265:2021 [121], but by changing the inputs of the developed framework (Sec. 3.3) iteratively. When designing such a truss without underlying design approach, the engineer has to follow certain intentions. Here, the intention was to have two distinct kinds of limit state functions that are maximally utilised. This selection should allow for a valuable comparison in terms of reliability in contrast to the answers for trusses designed according to the simplified design approach. Subsequently, a very high cross-section utilisation of 0.97 in the bottom chord could be reached together with very high utilisations of the connections in the chords up to the maximum allowable utilisation of 1.00. If simultaneously a high utilisation of the web members and their connections would have been sought, the overall deflections would have increased. This would have consequently led to larger induced bending moments in the chords and with it to larger necessary chord cross-sections and connections. Based on this example, one can see that the design of an entire system, such as a truss, is complex and hence, as much automation as possible is needed. Further, it illustrates what drawbacks an element-by-element design with simplified rules can have by neglecting important interrelations of the load-deformation behaviour of the single elements.

Next to the single trusses of the beam grid, combinations of trusses can be investigated. The most simple one is to consider two or three trusses next to each other. As expected, in Fig. 5.21 three times exactly the same results are achieved as in the case of a single truss (Fig. 5.19).

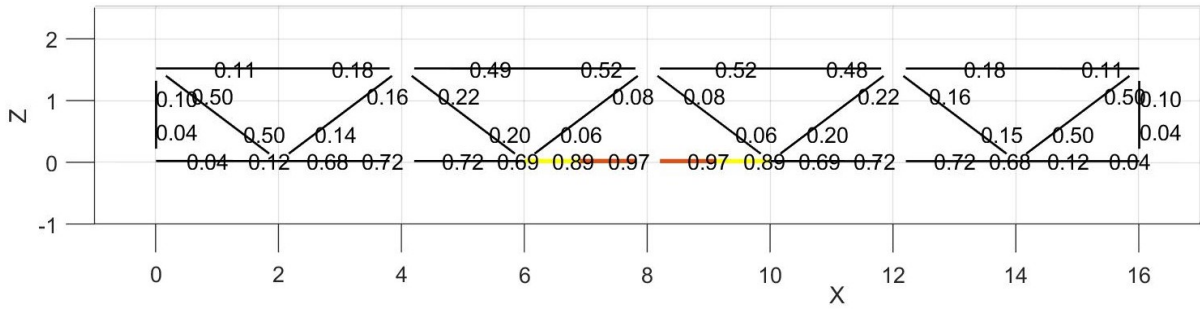


Fig. 5.19: Utilisation of the members of the single trusses.

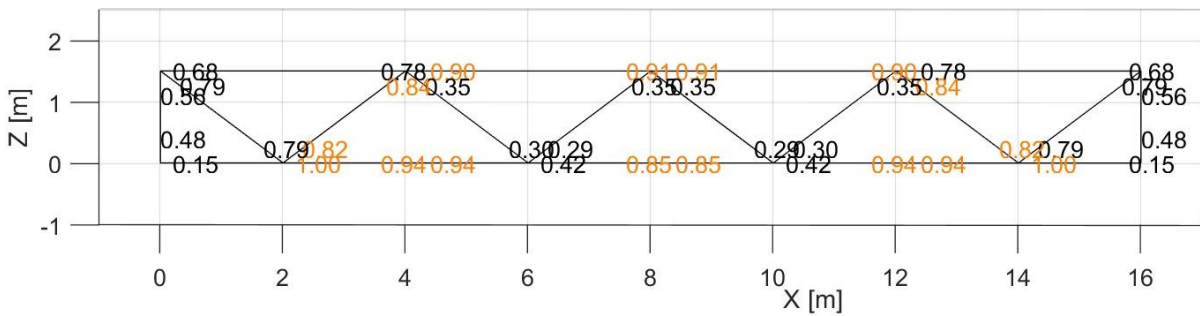


Fig. 5.20: Utilisation of the connections of the single trusses.

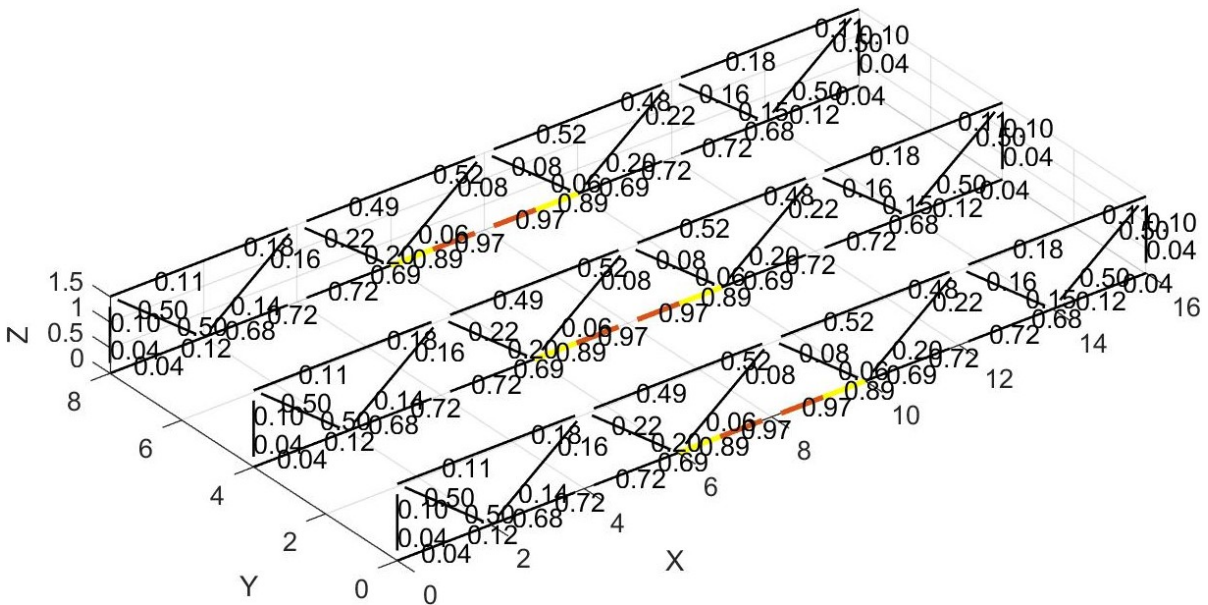


Fig. 5.21: Utilisation of the members of the three trusses next to each other.

The most simple beam grid consists of only one truss at each side. For the sake of comparability, the imposed snow load at the truss crossing has to be doubled. Hence, the same loading conditions are achieved as for the individual trusses above. Consequently, the same utilisation (Fig. 5.22) is achieved as for a single truss (apart from some numeric errors for small utilisations).

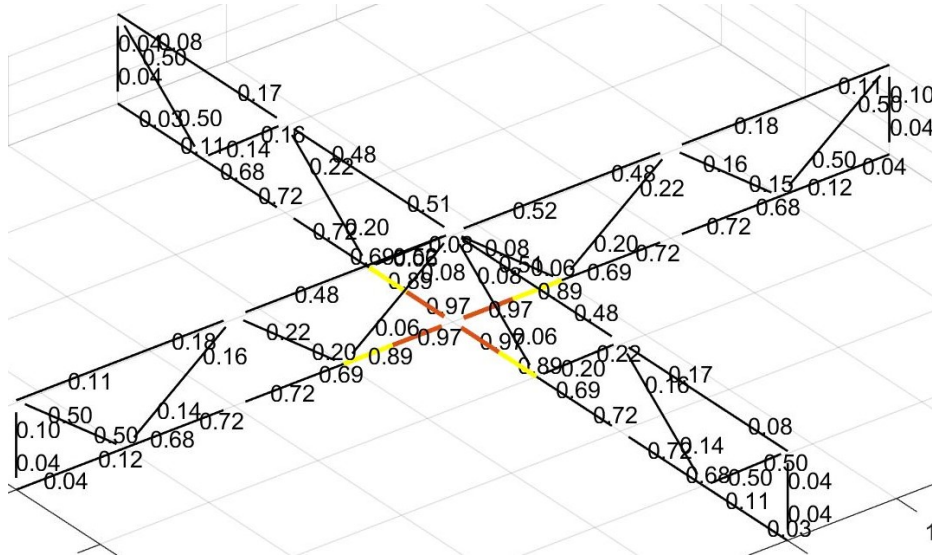


Fig. 5.22: Utilisation of the members of the 1-by-1 beam grid.

The same procedure can be followed for a 2-by-2 beam grid, i.e. at the crossing points the loads are doubled and hence, the exact same utilisation (Fig. 5.23) is reached as for a single truss.

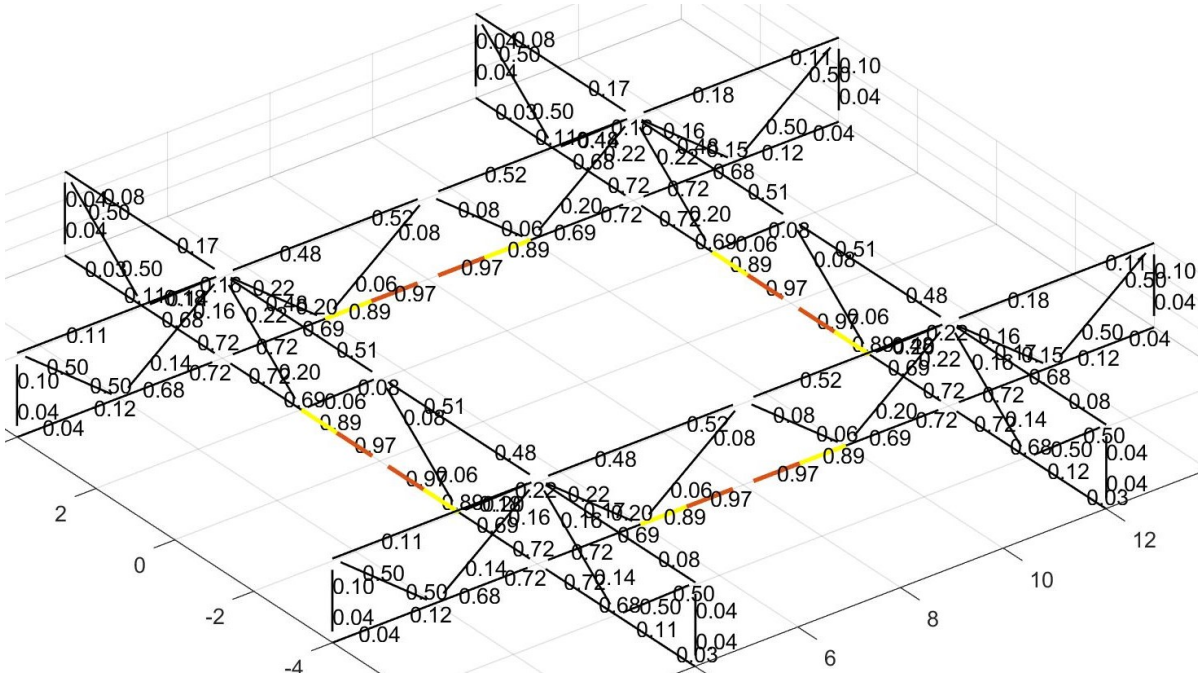


Fig. 5.23: Utilisation of the members of the 2-by-2 beam grid.

When finally considering the 3-by-3 beam grid with twice the snow load at each beam crossing, different utilisation factors of the beams (Fig. 5.24) and connections (Fig. 5.25) can be observed. This results from compatibility, initiated by different deflections of the single beams. For a proper design of such a structure, the individual members and connections of the individual trusses need

to be adapted. The changes would consequently lead to new section forces due to the change of the load-deformation behaviour of the single components, and therefore, this procedure again would be iteratively.

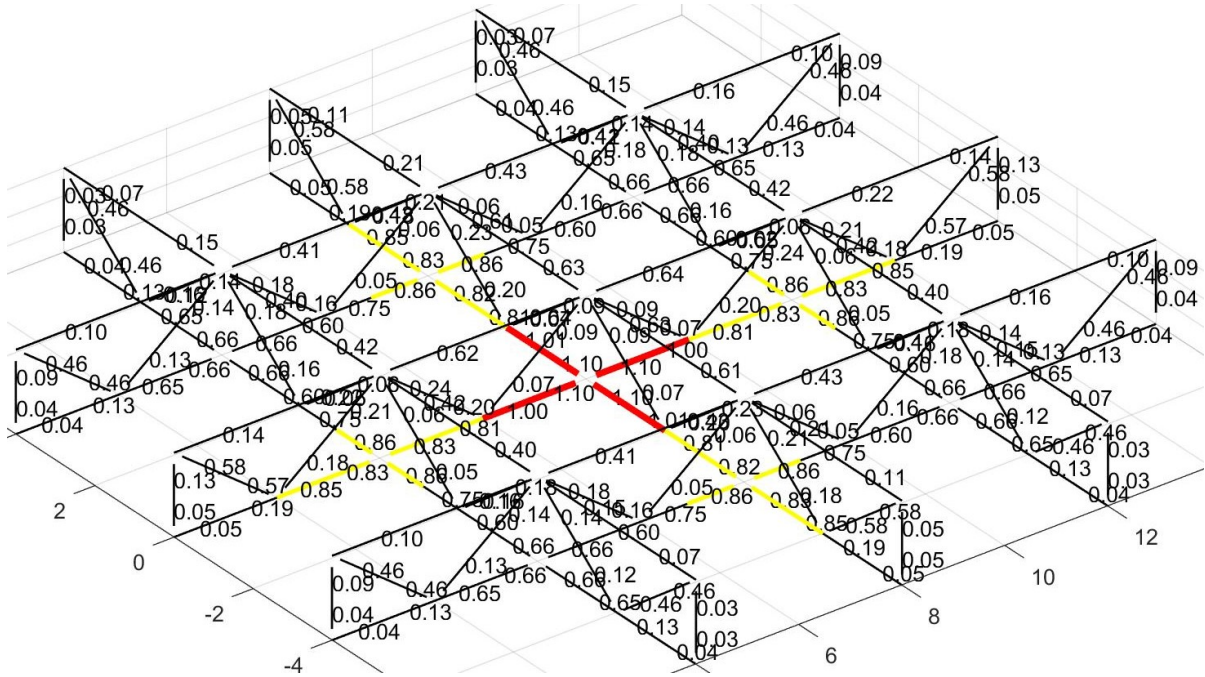


Fig. 5.24: Utilisation of the truss members of a 3-by-3 beam grid structure.

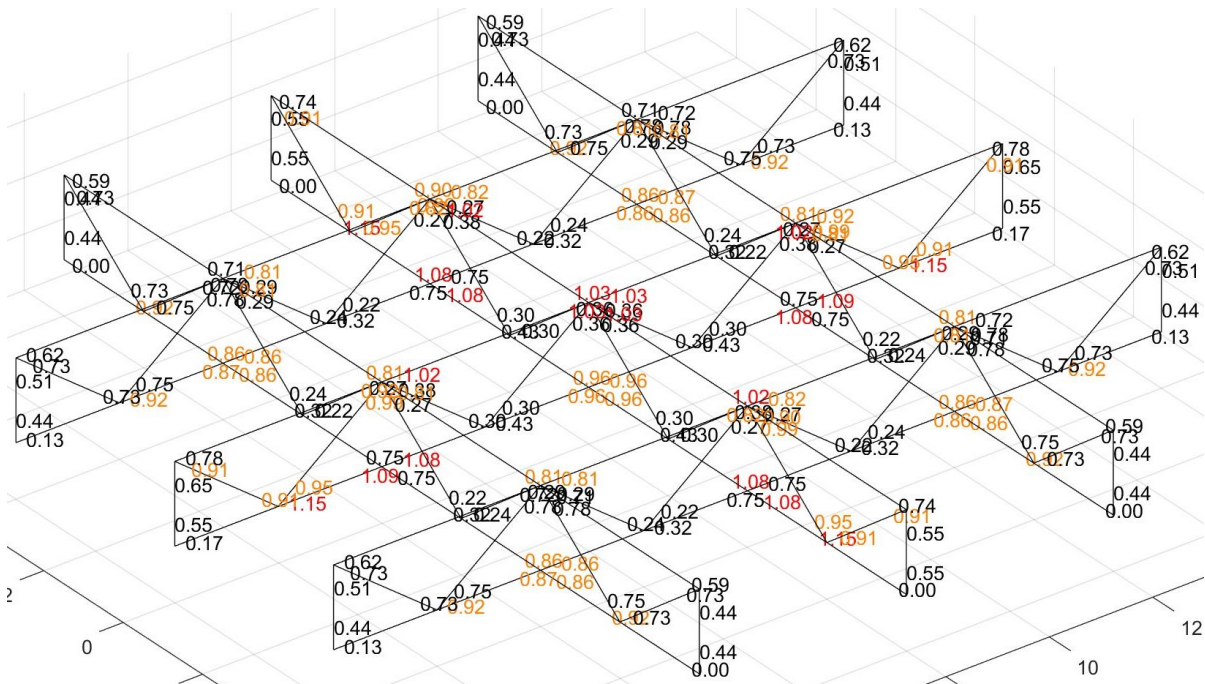


Fig. 5.25: Utilisation of the connections in the truss members of a 3-by-3 beam grid structure.

Based on this 3-by-3 beam grid and its sub-systems, considerations of a system-based design approach could be illustrated. Further considerations are addressed in the following list:

- For the design of larger and more complex structures with more components and interrelations, further development of the framework will be necessary. One of the most important advancements would be an automated process that selects member cross-sections, dowel configurations and the materialisation of the single components, i.e. cost functions with an optimisation procedure need to be developed. A further issue will be the correct consideration of the Weibull-weakest-link model in complex truss structures.
- The introduced parametrisation for the consideration of all connections and steel plates presented in Sec. 3.3 could be combined with similar parametric approaches used for the truss design tool in Sec. 3.4 that allow for a simple modelling process of complex truss structures.
- The consideration of the non-linearity of the load-deformation behaviour of the connections seems to be promising, but it comes with a major increase in calculation time. For large systems, calculation times of several hours to days might be necessary. Therefore, computational optimisation will be a constant companion in further explorations of system-based design approaches.
- Alongside the future development of appropriate procedures, a holistic model for the load-deformation behaviour and the resistance of the connections has to be sought. It is pointed out that the herein applied models are only valid for cases where normal forces dominate the connection behaviour.

5.5 Conclusions

The main conclusion with respect to the modelling details of the truss joints is that all additionally introduced elements and considerations induce non-negligible changes in at least some aspects of truss design. The often neglected consideration of the chord connections are of similar importance as the consideration of the web connections. Both selections of the initial stiffness as well as the non-linearity of the load-deformation behaviour have a huge impact on various aspects. Of less, but still non-negligible importance is the consideration of the steel plates and the coupling of the dofs in the connections.

The evaluation of the simplified truss design approach from SIA 265:2021 [121] revealed various oversteps of the design rules for the investigated trusses. Still, the accordingly designed trusses did not lead to any failure. It is assumed, that (1) with established truss slenderness ratios the deflections generally are not of concern, (2) other failure modes are decisive for the critical cross-sections under compression where the rules were non-conservative and (3) that the rounding up of the member heights to full lamellas and to specified connection layouts leads to hidden reserves.

On the example of a beam grid structure, the potential of the modelling framework was explored and discussed. Aspects of the design process without an underlying design approach were addressed and the necessity of the consideration of the interrelations between the different components and their load-deformation behaviour was highlighted. Finally, a brief outlook with respect to the necessary developments of the framework for truly system-based design approaches was provided.

Chapter 6

Reliability of timber trusses

6.1 Introduction

In this chapter, first the subset simulation as the selected method of structural reliability is evaluated regarding the applicability for the problem at hand and different aspects such as the influence of the model uncertainties are discussed. Then, the probability of failure is determined for the trusses investigated in Sec. 5.3. Based on these results, a possible derivation of the target reliability for timber trusses is discussed. Finally, for the sub-systems of the beam grid structure presented in Sec. 5.4, the probability of failure is evaluated and the potential of system-based design approaches is discussed.

Most of the evaluated trusses were designed with the truss design tool presented in Sec. 3.4. Therefore, they are designed according to the Swiss codes [117, 118, 121] and hence, they resemble trusses as they are built in Switzerland. The drawback of this approach is that, as shown in Chapter 4, there are discrepancies in the material property models of the codes and the newly derived models in this thesis. Subsequently, the values of the probability of failure do not allow for absolute but only for relative considerations and only allow for comparisons within this thesis. As described e.g. in Fahrni (2021) [35], the nature of the applied models are not expected to reveal the "true probability of failure" and hence, this relative consideration is sufficient for the scope of this thesis.

6.2 Applied models and limit states

In Sec. 3.3.2.6 various limit states for truss members are presented. Each single limit state allows for the determination of a utilisation factor and hence, by means of the developed framework (Sec. 3.3), the overall utilisation per member can be determined (Sec. 5.4). Model uncertainties are added to these resistance models in Sec. 4.3 in order to account for deviations and simplifications related to the probabilistic modelling and the limit-state equations.

The connection load-carrying capacity is principally determined by the procedure explained in Sec. 2.4.2. Necessary adaptations for probabilistic considerations are presented in Sec. 4.4.2. Although two possibilities for the determination of the embedment strength are shown and were implemented in the framework, in the subsequent investigations only the equations based on SIA 265:2021 [121] were applied. Additionally, the model presented in Sec. 3.3.2.7 is used to account for eccentric loading of the connections. The model uncertainty of this model is presented

in Sec. 4.4.2.4. The ratio of the normal force acting in a connection over the connection load-carrying capacity reduced by the factor accounting for eccentricities allows for the determination of the utilisation of each connection in a truss (Sec. 5.4).

Subsequently, the overall utilisation of a truss can be determined as the maximum utilisation of all members and connections. This overall utilisation can then be applied to pose the limit-state function in terms of realisations as follows:

$$g(\mathbf{x}) = 1 - \max(\text{utilisation}). \quad (6.1)$$

For the load-deformation behaviour of the single dowels of the steel-to-timber connections, the model presented in Sec. 3.3.3 is applied with the corresponding model uncertainties derived in Sec. 4.4.3.1. The ultimate deformation of this approach is not considered in the framework, since the decreasing stiffness after the transition point leads to failure of the connection anyway. This additional option for failure in the connections has to be considered separately. It is not possible to directly determine a utilisation factor for this failure, since the finite element solver (Sec. 3.3.2.5) does not find equilibrium and hence, cannot converge to a solution. Therefore, in case of no equilibrium the value of -1 is assigned to the limit-state function. Hence, the connection limit state is two-part and takes into account the classical view point of resistance as it is applied in the design codes and also the newly introduced approach, which considers the load-deformation behaviour.

Next to the discussed model uncertainties, the following inherent variabilities and models are considered for the truss members consisting of GLT:

- f_m , E_0 , $f_{t,0}$, $f_{c,0}$, f_v , G_v and ρ as summarised and referenced in Tab. 4.1.
- Under edgewise loading the properties are assumed to be 1.2 times larger than the respective values from flatwise loading (Sec. 4.2.2.14).
- The properties are assumed to be independent (Sec. 4.2.2.15).
- If stated, the Weibull-weakest-link model for truss chord members is applied (Sec. 4.2.2.16).

For the steel dowels, the scattering of the ultimate tensile strength Sec. 4.5.2.3 is of relevance for the resistance and the load-deformation behaviour of the dowelled connections. The steel plates are not checked for the load-carrying capacity, and hence, in these investigations only the scattering of the MOE (Sec. 4.5.2.1), the shear modulus (Sec. 4.5.2.6) and the density (Sec. 4.5.2.5) are considered.

The main loading of the trusses is the snow load. Its probabilistic model and the respective model uncertainty are described in Sec. 4.6.2. For all investigations uniform snow loads are assumed, i.e. the same snow load per load-catchment area is applied on all load introduction points. Next to the snow load, the self-weight of the roof structure is modelled probabilistically as described in Sec. 4.6.4.

From this overview it can be concluded that timber trusses with dowelled steel-to-timber connections comprise hundreds or even thousands of uncertain parameters. Different components

of the trusses and different limit states per component can lead to failure and therefore various of these parameters can be decisive. Subsequently, possible model simplifications (i.e. setting non-decisive parameters to deterministic values) are case-sensitive and therefore not pursued in this thesis.

6.3 Evaluation of the method of structural reliability

6.3.1 Introduction

As presented in Sec. 2.5.3, different methods of structural reliability exist to estimate the probability of failure. In the master thesis of Zimmermann (2020) [132], reliability analyses of timber trusses were conducted based on a preliminary state of the framework (Sec. 3.3) and the probabilistic models (Chapter 4). He concluded that the first order reliability method (FORM), the second order reliability method (SORM) and importance sampling (IS) are incapable of determining the probability of failure for the problem at hand, due to the number of limit state functions and their non-linear behaviour. Further, no adaptive procedures could be applied due to the number of input parameters. He finally recommended to apply the subset simulation (SS). Preliminary investigations by the author of this thesis confirmed the findings of Zimmermann. Au & Beck (2001) [6], who first introduced the subset simulation, promoted their approach to be robust to the number of uncertain parameters and efficient in computing small probabilities. In an example, they applied the method to a problem including 1501 uncertain parameters, which is in the same order as used herein.

In this section, first preliminary investigations are presented, where the general behaviour of the subset simulation is explored. Then, the influence of the introduced model uncertainties is investigated and followed by considerations of the single limit state functions. Finally, the scatter of the resulting probabilities of failure is discussed with a focus on the number of samples per subset.

6.3.2 Preliminary investigations

Preliminary investigations of the reliability were conducted on the trusses (a) to (d) presented in Sec. 5.2.2. They were investigated with regard to the influence of the modelling uncertainties (MU) and in the case of the duopitch roof truss with raised eaves (c) the Weibull-weakest-link model (WWL) for the consideration of the length effect for truss chord members with an exponent of $b = 11$ (Sec. 2.6.6.4, 4.2.2.16 and 4.3). The absolute values of the results are expected to be generally conservative, since the self-weight was included in the reliability analyses, but not in the truss design (Sec. 5.2). All calculations were conducted with the reliability module of UQLab [92] for subset simulations with a batch size (Batch) of 1000. The number of subsets (#sub) and the number of model evaluations (Eval) are chosen automatically. The resulting probability of failure P_f and the reliability index $\beta = -\Phi^{-1}(P_f)$, where Φ is the standard normal cumulative density function [92], are provided in Tab. 6.1 together with the coefficient of variation (CoV).

Tab. 6.1: Results of the subset simulations for the preliminary investigations. The abbreviations in the column headers are: model uncertainty (MU), Weibull-weakest-link model (WWL), batch size per subset (Batch), number of evaluated subsets ($\#_{\text{sub}}$), number of considered model evaluations (Eval), probability of failure (P_f), reliability index (β) and coefficient of variation (CoV). In the two columns for the MU and the WWL, the capital letters indicate whether they are considered.

truss	MU	WWL	Batch	$\#_{\text{sub}}$	Eval	P_f	β	CoV
(a)	-	-	1000	7	6400	$1.39 \cdot 10^{-7}$	5.14	0.48
(a)*	M	-	1000	3	2800	$5.58 \cdot 10^{-3}$	2.54	0.22
(b)	-	-	1000	8	7300	$4.17 \cdot 10^{-8}$	5.36	0.49
(b)	M	-	1000	3	2800	$1.96 \cdot 10^{-3}$	2.88	0.22
(c)	-	-	1000	8	7300	$2.58 \cdot 10^{-8}$	5.45	0.50
(c)	-	W	1000	8	7300	$3.86 \cdot 10^{-8}$	5.37	0.48
(c)	M	-	1000	3	2800	$1.40 \cdot 10^{-3}$	2.99	0.26
(c)	M	W	1000	3	2800	$1.32 \cdot 10^{-3}$	3.01	0.25
(d)	-	-	1000	5	4600	$1.48 \cdot 10^{-5}$	4.18	0.39
(d)	-	W	1000	6	5500	$5.25 \cdot 10^{-6}$	4.41	0.37
(d)	M	-	1000	3	2800	$1.74 \cdot 10^{-3}$	2.92	0.24
(d)	M	W	1000	3	2800	$1.31 \cdot 10^{-3}$	3.01	0.23

* Numeric errors occurred, i.e. too conservative result.

The first observation is that for all trusses P_f increases by several orders of magnitude, when MU are considered. The comparison of the different trusses shows that without consideration of MU the P_f is scattering more, than with consideration of MU. For trusses (b), (c) and (d), a similar P_f results, when MU are considered. In the case of truss (a), under consideration of MU numeric errors occurred such that the finite element solver did not converge even for a step size that corresponds to 1% of the loads. Hence, the respective result is too conservative. Due to the nature of the subset simulation, which derives the samples of a new subset from the failure region of the previous subsets, the propagation of the principally rare numeric error can lead to a significant increase of P_f . The consideration of the WWL in trusses (c) and (d) does not provide distinct results. Two possible reasons can be provided: (1) the limit state function of the lower chord elements under combined tension and bending effects is not decisive in these trusses; or (2) the effect has a smaller impact than the scatter of the results. Due to the small member lengths of the bottom chord segments, the WWL effect, indeed is small, i.e. in the deterministic case the utilisation of the bottom chord elements increases only in the range of 1% for truss (c) and even less for truss (d).

The calculation time of these models evaluated on standard personal computers varied in the range of hours to days in dependence of the number of finite elements and dowels in the

connections. The higher number of dowels for truss (b) with $d = 6$ mm led to twice the calculation time in comparison to truss (a) with $d = 12$ mm.

Overall, it can be concluded that the subset simulation is the adequate selection from the variety of methods of reliability. The example trusses demonstrate the importance of the MU. Further, with consideration of MU, the resulting P_f are in the same order of magnitude for the different trusses, which were designed according to the simplified design approach of SIA 265:2021 [121]. The consideration of WWL partly led to illogical results, i.e. P_f decreased with consideration of WWL. Therefore, the magnitude of the scatter of the results will be investigated later in this section. The runtime of the subset simulation per truss in the range of hours to days seems feasible for future applications.

6.3.3 Influence of the model uncertainties

The influence of the different model uncertainties are investigated further, by means of a duopitch roof truss with raised eaves (Fig. 6.1 and Tab. 6.2) and a triangular truss (Fig. 6.2 and Tab. 6.3). These trusses were selected, since it was possible to find relatively small configurations (little amount of finite elements) while reaching high utilisations in different elements. The MU are grouped into three classes: (1) the model uncertainties of the timber members (MU-T), which include all limit state functions from Sec. 3.3.2.6 with their respective MU from Sec. 4.3; (2) the model uncertainties of the connections (MU-C), which include the resistance models according to Sec. 3.3.2.7 and the load-deformation behaviour shown in Sec. 3.3.3 with their respective model uncertainties presented in Sec. 4.4; and (3) the model uncertainties of the snow loads (MU-S) presented in Sec. 4.6.2.

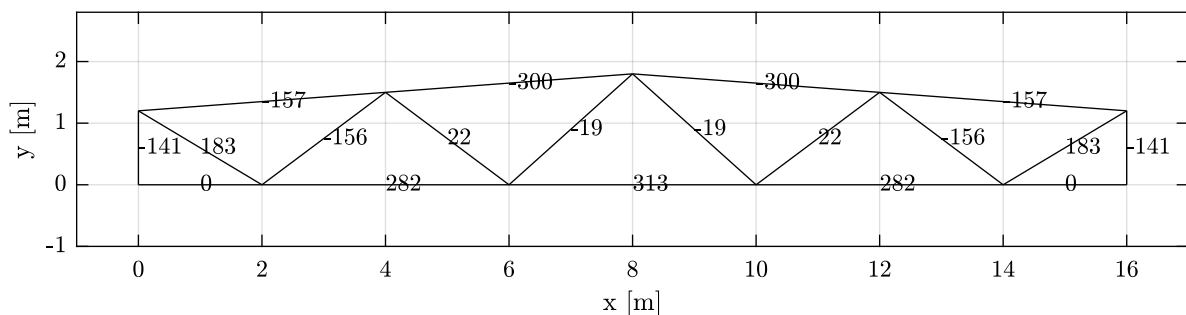
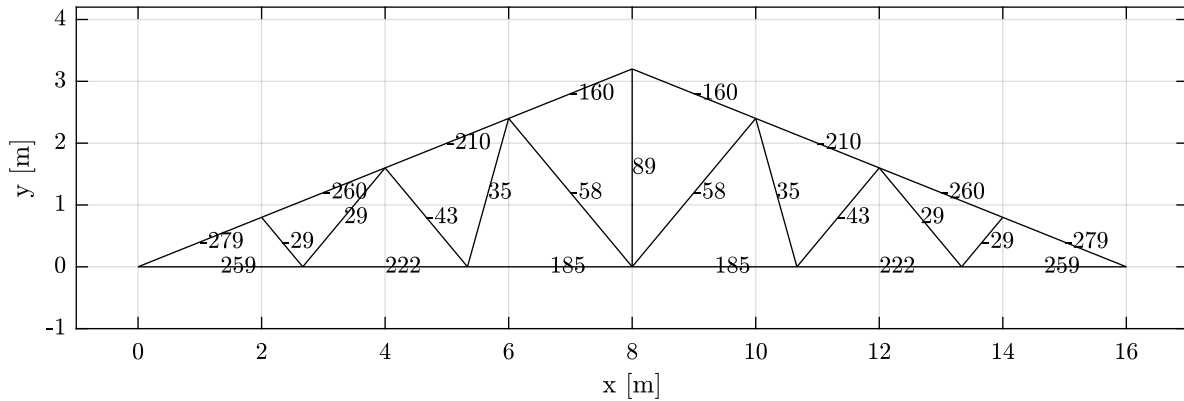


Fig. 6.1: Normal forces in [kN] of the duopitch roof truss with raised eaves for ULS loading conditions.

In Tab. 6.4, the results of the reliability analyses of the duopitch roof truss with raised eaves and the triangular truss are presented. For the duopitch roof truss, all three classes of MU lead to a decrease of P_f by several orders of magnitude, where the influence of MU-C is most significant. In the case of the triangular truss, also MU-C is most influential, but all results are within only one order of magnitude. When considering the different combinations of MU, a general trend can be observed that MU-C is most important before MU-S and only then MU-T follows. Generally, the resulting P_f for both trusses under consideration of all MU are in the same range, as found in the section above.

Tab. 6.2: Characteristics of the duopitch roof truss with raised eaves.

parameter	value	parameter	value
type	duopitch roof truss	purlin distance	4 m
	with raised eaves	reference snow height	500 mm
web layout	falling and rising	bottom chord segments	5
	diagonals	dowel diameter	12 mm
span-width	16 m	member width	220 mm
truss height	1.8 m	GLT class	GL24h
eave height	1.2 m	bottom chord height	240 mm
roof inclination	4.3°	top chord height	240 mm
truss slenderness	10.7	chord slenderness	6.25
girder distance	6 m	web member heights	160 - 240 mm

**Fig. 6.2:** Normal forces in [kN] of the triangular truss for ULS loading conditions.**Tab. 6.3:** Characteristics of the triangular truss.

parameter	value	parameter	value
type	triangular truss	bottom chord segments	6
web layout	falling and rising	dowel diameter	12 mm
	diagonals with mid-post	reference snow height	500 mm
span-width	16 m	member width	200 mm
truss height	3.2 m	GLT class	GL24h
roof inclination	21.8°	bottom chord height	240 mm
truss slenderness	10.0	top chord height	240 mm
girder distance	5 m	chord slenderness	6.7
purlin distance	2 m	web member heights	160 - 200 mm

For the duopitch roof truss, the highest value of P_f was found for the combination of MU-C and MU-S, which again rises the question of the scatter of the results. Therefore, this simulation with only MU-C and MU-S was repeated several times and the results are presented in Tab. 6.5.

From these results it can be concluded that the scatter of the subset simulations is large indeed and that this high value might have been an outlier.

With respect to the WWL, again, unclear results were found. In the deterministic case, for the duopitch roof truss an increase of the utilisation due to WWL was found to be in the range of 3%, where for the triangular truss no influence was observed. For the duopitch roof truss, in the cases where WWL and MU-T are considered and in the case where WWL and all MU are considered, P_f decreases in comparison to the results without WWL, which generally is illogical. In all the other cases where WWL is considered, an increasing tendency can be observed. Therefore, the influence of the scatter of the results is larger than the influence of the WWL and no final conclusions can be drawn.

Tab. 6.4: Results of the subset simulations for the investigations with respect to the influence of the model uncertainties. The abbreviations in the column headers are: model uncertainty (MU) with respect to the timber members (MU-T), the connections (MU-C) and the snow loads (MU-S), Weibull-weakest-link model (WWL), batch size per subset (Batch), number of evaluated subsets (#sub), number of considered model evaluations (Eval), probability of failure (P_f), reliability index (β) and coefficient of variation (CoV). In the four columns for the MU and the WWL, the capital letters indicate whether they are considered.

truss	MU-T	MU-C	MU-S	WWL	Batch	#sub	Eval	P_f	β	CoV
duopitch	-	-	-	-	1000	11	10000	$3.23 \cdot 10^{-11}$	6.53	0.59
duopitch	T	-	-	-	1000	8	7300	$4.57 \cdot 10^{-08}$	5.34	0.47
duopitch	-	C	-	-	1000	5	4600	$7.88 \cdot 10^{-05}$	3.78	0.33
duopitch	-	-	S	-	1000	6	5500	$2.38 \cdot 10^{-06}$	4.58	0.37
duopitch	T	C	-	-	1000	5	4600	$7.19 \cdot 10^{-05}$	3.80	0.31
duopitch	T	-	S	-	1000	6	5500	$1.83 \cdot 10^{-06}$	4.63	0.38
duopitch	-	C	S	-	1000	4	3700	$9.82 \cdot 10^{-04}$	3.10	0.27
duopitch	T	C	S	-	1000	4	3700	$3.23 \cdot 10^{-04}$	3.41	0.26
duopitch	-	-	-	W	1000	8	7300	$2.48 \cdot 10^{-08}$	5.45	0.50
duopitch	T	-	-	W	1000	9	8200	$5.14 \cdot 10^{-09}$	5.73	0.52
duopitch	T	C	S	W	1000	4	3700	$2.64 \cdot 10^{-04}$	3.47	0.26
triangular	-	-	-	-	1000	6	5500	$2.32 \cdot 10^{-06}$	4.58	0.39
triangular	T	-	-	-	1000	6	5500	$6.03 \cdot 10^{-06}$	4.38	0.37
triangular	-	C	-	-	1000	5	4600	$7.17 \cdot 10^{-05}$	3.80	0.31
triangular	-	-	S	-	1000	5	4600	$3.86 \cdot 10^{-05}$	3.95	0.34
triangular	T	C	-	-	1000	4	3700	$1.83 \cdot 10^{-04}$	3.56	0.31
triangular	T	-	S	-	1000	5	4600	$2.10 \cdot 10^{-05}$	4.10	0.34
triangular	-	C	S	-	1000	4	3700	$1.65 \cdot 10^{-04}$	3.59	0.27
triangular	T	C	S	-	1000	4	3700	$3.04 \cdot 10^{-04}$	3.43	0.26
triangular	-	-	-	W	1000	6	5500	$9.41 \cdot 10^{-06}$	4.28	0.39
triangular	T	-	-	W	1000	6	5500	$8.66 \cdot 10^{-06}$	4.30	0.38
triangular	T	C	S	W	1000	4	3700	$3.44 \cdot 10^{-04}$	3.39	0.26

Tab. 6.5: Results of the repeated subset simulations for the duopitch roof truss with raised eaves under consideration of the model uncertainties for the connections and snow loads. The mean value and CoV are highlighted in bold. The abbreviations in the column headers are: model uncertainty (MU) with respect to the timber members (MU-T), the connections (MU-C) and the snow loads (MU-S), Weibull-weakest-link model (WWL), batch size per subset (Batch), number of evaluated subsets (#sub), number of considered model evaluations (Eval), probability of failure (P_f), reliability index (β) and coefficient of variation (CoV). In the four columns for the MU and the WWL, the capital letters indicate whether they are considered.

truss	MU-T	MU-C	MU-S	WWL	Batch	#sub	Eval	P_f	β	CoV
duopitch	-	C	S	-	1000	4	3700	$9.82 \cdot 10^{-4}$	3.10	0.27
duopitch	-	C	S	-	1000	4	3700	$2.73 \cdot 10^{-4}$	3.46	0.24
duopitch	-	C	S	-	1000	4	3700	$3.69 \cdot 10^{-4}$	3.38	0.26
duopitch	-	C	S	-	1000	4	3700	$2.34 \cdot 10^{-4}$	3.50	0.26
duopitch	-	C	S	-	1000	4	3700	$2.96 \cdot 10^{-4}$	3.44	0.24
								mean	$4.31 \cdot 10^{-4}$	3.33
								CoV	65%	

6.3.4 Combination of the single limit states

For both the duopitch roof truss with raised eaves and the triangular truss presented in Sec. 6.3.3 the individual limit state functions (LSF) are investigated further due to two reasons. On the one hand, this investigation should simply allow for a deeper insight into the behaviour of the LSF. On the other hand, Li et al. (2015) [90] raised concerns about the capability of the subset simulation with respect to the consideration of LSF in one simulation. They argued that with standard subset simulation only single LSF can be evaluated and proposed a new procedure that applies a unified intermediate event, to resolve the sorting difficulty arising in the standard subset simulation.

In principle, the individual LSF for the members and the connections form a series system, in which every element can be decisive. Therefore, the resulting P_f of the individual LMS can be added by Eq. 2.35 and the overall P_f should be equal to the application of all LMS within one run of subset simulation. This principle could even be followed for the consideration of every limit state function for all individual elements. Due to the high number of elements and very low expected P_f of certain limit states in various elements, this approach is not feasible. The results of the individual LSF evaluations are provided in in Tab. 6.6, where the combinations are printed in bold. Two errors are introduced in the procedure: (1) The limit state resulting from the load-deformation curve (l-d) was excluded in the other cases by omitting its decreasing part, i.e. only the first part of Eq. 3.21 without limits for the deformation was applied. Still, some failure events occurred due to the load-deformation behaviour. (2) In the case of the elements in the bottom chord, the limit state with regard to the interaction of tension and bending (t-b) is redundant with the limit state including WWL. Therefore, the combined P_f found by this approach is generally conservative. The remaining limit state functions in Tab. 6.6 are: compression and bending (c-b), stability in-plane (s-in), stability out-of-plane (s-out) and the resistance of the

connections (con). As expected, the limit state considering shear stresses lead to such small P_f that the calculations were aborted.

Tab. 6.6: Results of the subset simulations for the investigations with respect to the combination of the individual limit state functions (LMS). For all four cases the results from the combinations by Eq. 2.35 are provided in bold. The abbreviations in the column headers are: model uncertainty (MU), Weibull-weakest-link model (WWL), limit state function (LMS) batch size per subset (Batch), number of evaluated subsets (#sub), number of considered model evaluations (Eval), probability of failure (P_f), reliability index (β) and coefficient of variation (CoV). In the two columns for the MU and the WWL, the capital letters indicate whether they are considered.

truss	MU	WWL	LMS	Batch	#sub	Eval	P_f	β	CoV
duopitch	-	-	t-b	1000	8	7300	$2.17 \cdot 10^{-8}$	5.48	0.48
duopitch	-	-	c-b	1000	8	7300	$1.26 \cdot 10^{-8}$	5.57	0.49
duopitch	-	-	s-in	1000	7	6400	$1.15 \cdot 10^{-7}$	5.17	0.44
duopitch	-	-	s-out	1000	8	7300	$2.16 \cdot 10^{-8}$	5.48	0.47
duopitch	-	-	con	1000	11	10000	$1.08 \cdot 10^{-11}$	6.69	0.63
duopitch	-	-	l-d	1000	10	9100	$1.32 \cdot 10^{-10}$	6.32	0.58
comb.							$1.71 \cdot 10^{-7}$	5.10	
duopitch	M	W	t-b	1000	6	5500	$2.76 \cdot 10^{-6}$	4.54	0.37
duopitch	M	W	WWL	1000	5	4600	$3.43 \cdot 10^{-5}$	3.98	0.34
duopitch	M	W	c-b	1000	6	5500	$1.05 \cdot 10^{-6}$	4.74	0.42
duopitch	M	W	s-in	1000	7	6400	$5.31 \cdot 10^{-7}$	4.88	0.42
duopitch	M	W	s-out	1000	7	6400	$2.74 \cdot 10^{-7}$	5.01	0.42
duopitch	M	W	con	1000	4	3700	$1.54 \cdot 10^{-4}$	3.61	0.28
duopitch	M	W	l-d	1000	4	3700	$1.17 \cdot 10^{-4}$	3.68	0.32
comb.							$3.10 \cdot 10^{-4}$	3.42	
triangular	-	-	t-b	1000	6	5500	$1.12 \cdot 10^{-6}$	4.73	0.40
triangular	-	-	c-b	1000	5	4600	$1.16 \cdot 10^{-5}$	4.23	0.38
triangular	-	-	s-in	1000	5	4600	$1.67 \cdot 10^{-5}$	4.15	0.38
triangular	-	-	s-out	1000	6	5500	$2.01 \cdot 10^{-6}$	4.61	0.41
triangular	-	-	con	1000	11	10000	$2.85 \cdot 10^{-11}$	6.55	0.61
triangular	-	-	l-d	1000	11	10000	$3.01 \cdot 10^{-11}$	6.54	0.60
comb.							$3.14 \cdot 10^{-5}$	4.00	
triangular	M	W	t-b	1000	6	5500	$8.06 \cdot 10^{-6}$	4.31	0.37
triangular	M	W	WWL	1000	6	5500	$4.35 \cdot 10^{-6}$	4.45	0.34
triangular	M	W	c-b	1000	5	4600	$2.27 \cdot 10^{-5}$	4.08	0.33
triangular	M	W	s-in	1000	5	4600	$1.80 \cdot 10^{-5}$	4.13	0.32
triangular	M	W	s-out	1000	7	6400	$8.23 \cdot 10^{-7}$	4.79	0.39
triangular	M	W	con	1000	5	4600	$9.02 \cdot 10^{-5}$	3.74	0.30
triangular	M	W	l-d	1000	5	4600	$6.62 \cdot 10^{-5}$	3.82	0.30
comb.							$2.10 \cdot 10^{-4}$	3.53	

The very low P_f for the duopitch roof truss without consideration of MU and WWL in Tab. 6.4 could not be replicated with the approach of combined LMS functions shown in Tab. 6.6. In the case with MU and WWL, for the duopitch roof truss, both respective results are similar. For the triangular truss without consideration of MU and WWL, the combination approach is more conservative. In the case with MU and WWL, the order of both results is similar, but the consideration of all LMS at once revealed more conservative results. Therefore, the results under consideration of MU and WWL again might indicate a large scatter of the results. A very interesting observation is that without consideration of MU and WWL for both trusses the stability in-plane LMS is most critical, but with consideration of MU and WWL a drastic change towards the two connection limit states occurs. Therefore, this result is a further indication that the investigation of the connection behaviour must be one of the most important aspects in future research activities. Further, the statement from Dubas et al. (1981) [26] (Sec. 2.3.2), that in comparison to the in-plane stability in the vast majority of the cases the stability out-of-plane is decisive, is questionable.

In contrast to the concerns raised by Li et al. (2015) [90], it seems that the applied subset simulation algorithm implemented in UQLab [92] is capable of determining P_f for various LMS within one subset simulation.

6.3.5 Scatter of the results

As discussed above and shown in Tab. 6.5, the scatter of the results based on the subset simulations is non-negligible and partly prevents clear conclusions. Therefore, based on the above-presented duopitch roof truss with raised eaves, the influence of the batch size per subset was investigated. The investigation included batch sizes of 1000, 2000 and 4000 under consideration of all MU and WWL. For each batch size, nine subset simulations were conducted. The results are summarised in Tab. 6.7, where for each batch size the mean value and the respective CoV are provided. The resulting P_f are illustrated in the scatter plot in Fig. 6.3.

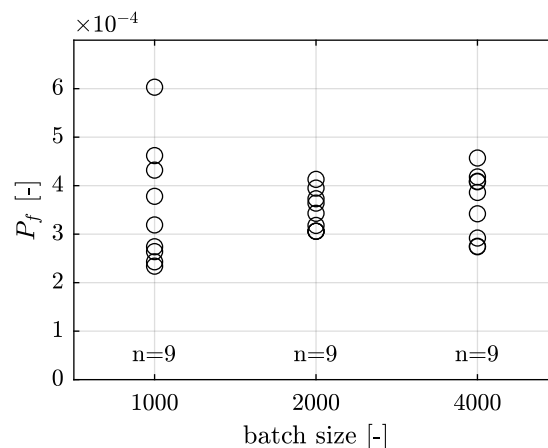


Fig. 6.3: Scatter of P_f of the duopitch roof truss considering MU and WWL for different batch sizes.

As expected, a tendency can be found that the scatter decreases with larger batch size. Since for a batch size of 2000 the results are better than for a batch size of 4000, no final conclusions are possible though. Furthermore, the results would be even closer to each other, if one would exclude the highest value of P_f for a batch size of 1000. Overall, it can be concluded that the subset simulation is an equitable choice, but the scatter is in a range that prevents a proper evaluation of effects with small impacts.

6.4 Target reliability

6.4.1 Introduction

For trusses with connections that exhibit a non-negligible rotational stiffness, the simplified design approach is the only SIA 265:2021 [121] (Sec. 2.3.3) conform way for design. As presented in Sec. 2.3.2, the development of these established rules did not include any calculatory assessment of the structural reliability. Therefore, a direct link to the target reliabilities presented in Sec. 2.5.4 is missing. Further, most probabilistic models applied herein have not been compared to the ones considered for the development of the target reliabilities presented in Sec. 2.5.4. Consequently, the reliability of trusses that are at the limit of the rules from the simplified design approach are evaluated in order to derive a target reliability for further usage of the herein applied models. The intention of this chapter resembles the conducted soft-calibration for the transition of design code formats (Sec. 2.5.1.2). For this purpose, the 28 trusses with a chord slenderness ratio of 7.1 from Sec. 5.3 are investigated. Based on the findings from Sec. 6.3.5 and the model runtimes for all subset simulations, a batch size of 2000 was selected. Since the importance and the exponent of the WWL is not properly evaluated yet, this limit state was excluded for the following investigations.

6.4.2 Results

As discussed in Sec. 6.3.2, numeric errors can occur such that the finite element solver does not converge. Due to the propagation of these failure events in the subset simulation, the respective results are too conservative. In the case of the 28 trusses with a chord slenderness ratio of 7.1 from Sec. 5.3, this issue occurred 14 times, i.e. only half of the results can be used. These results are listed in Tab. 6.8, where also the mean values per truss layout are provided.

The two parallel chord trusses with a span-width of 20 m exhibit the smallest mean P_f , where for the parallel chord trusses with a span-width of 40 m, the highest mean P_f was found. For the duopitch roof trusses and the triangular trusses, similar results can be observed. In the case of the monopitch roof trusses, no valid result could be retrieved.

6.4.3 Discussion

Although half of the results cannot be used due to numeric errors, clear tendencies can be observed from the remaining results. The scatter due to the influence from the web member

layouts is small in comparison to the influence of the truss layout. The order of magnitude is similar in all cases and comparable to the results from the sections above. A tendency of larger trusses being less reliable can be observed. Several reasons might explain this circumstance:

- The hidden reserves from rounding up the member height to full lamellas are smaller for larger cross-sections in a relative view-point.
- The discrepancy between the design without consideration of the load-deformation behaviour and the evaluation by means of the framework is likely to be larger for trusses with higher connection forces, since in the load-deformation behaviour larger number of dowels are generally penalised (Sec. 3.3.3).
- The increase in absolute measures leads to more pronounced limit states with respect to buckling.
- For the load-deformation behaviour, the error terms of the regression functions of the curve characterising parameters were transformed into a relative format (Eq. 4.30). Therefore, the sampled parameters scatter more for larger absolute values. Although this behaviour is realistic, further evaluations are necessary to determine whether this probabilistic consideration of the error terms truly fits the data.
- Since the simplified design approach does not consider the actual utilisation of the elements, by chance, the utilisations within different truss types can be different.

In the case of the triangular trusses (Sec. 5.3), the design rule with respect to the stress increase in the top chord was clearly surpassed. Still, their P_f is in the same order as for the other truss layouts. This circumstance can be explained by the observations in Sec. 6.3.4 that under consideration of the MU, the connection limit states are dominating the overall reliability. Further, aside the monopitch roof trusses (Fig. 5.16) the lowest reduction factor k_e for a chord slenderness of 7.1 was found for the duopitch roof trusses. This might, at least partly, explain why the duopitch roof trusses exhibit the largest P_f , compared to the parallel chord trusses and triangular trusses of the same span-width.

Overall, the range of P_f varies by one order of magnitude for the investigated trusses designed by means of the simplified design approach from SIA 265:2021 [121]. That is why no final conclusions for the determination of the target reliability of timber trusses can be made herein. The found range again deviates roughly by one order of magnitude compared to the target reliabilities presented in Sec. 2.5.4. Future research must clarify, whether this discrepancy stems from the considered example structures with respective modelling approaches or from the underlying assumptions (Chapter 4).

6.5 Potential of system-based design approaches

6.5.1 Introduction

In this section, the sub-systems of the beam grid structure introduced in Sec. 5.4 are evaluated with respect to their reliability. Based on these findings, the full potential of system-based design approaches is discussed.

6.5.2 Reliability of beam grid sub-systems

In Tab 6.9 the results of the reliability assessment of the beam grid sub-systems introduced in Sec. 5.4 are presented. Further, in Fig. 6.4 P_f of these sub-systems beam grid structure are illustrated. The most simple sub-system is the single truss, presented in Fig. 5.17 to 5.20. The next sub-systems are the cases with two or three trusses side by side, as shown in Fig. 5.21. Further, the results for the 1-by-1 beam grid (Fig. 5.22) and the 2-by-2 beam grid (Fig. 5.23) sub-systems are presented. For the first four cases, three subset simulations were conducted per case and their respective mean values are shown.

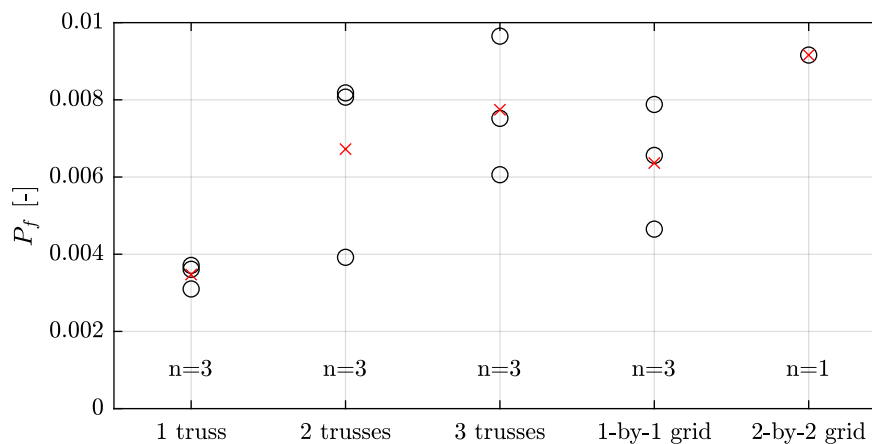


Fig. 6.4: P_f of the sub-systems of the show-case beam grid structure presented in Sec. 5.4. Next to the data points also the mean values are shown (red crosses).

Although in the deterministic considerations, the exhibited utilisation was the same in all five cases, the results presented in Fig. 6.4 show a clear trend of increasing P_f with increasing number of trusses. In spite of the large scatter, the mean values indicate what was expected: Trusses used side by side form a series system, where the number of trusses corresponds roughly to the multiplication factor of P_f of a single truss. This finding arises the question, if in design codes like the Eurocode 5 [31] next to the modification factors to account for positive system effect (k_{sys}) additional ones should be introduced for such negative system effects. The large scatter does not allow for a proper comparison between the two single trusses and the 1-by-1 grid though. The only obvious conclusion is that there is no big influence of the intersection. The result of the 2-by-2 grid has to be interpreted carefully, but it indicates that P_f is in the range of three or four trusses arranged side by side.

In comparison to the above-discussed trusses with similar absolute measures, the single truss exhibits a larger P_f , i.e. is less reliable. The obvious reason is that the truss was designed by means of the framework (Sec. 3.3) directly, where the other trusses were designed by the truss design tool (Sec. 3.4) applying the simplified design approach from SIA 265:2021 [121]. Therefore, hidden reserves were excluded in this rather academic example, where both the detailing and the loading situation were manipulated in order to achieve a very high utilisation of the members and the connections. Nevertheless, such high utilisations are achievable or even sought in practice. That is why the approach to determine the target reliability based on the simplified design approach from SIA 265:2021 [121] might be questionable after all.

For the first four cases, the runtime per subset simulation on standard personal computers varied in the range of one to three days. For the 2-by-2 beam grid, more than six days were necessary and a more powerful computer was needed due to memory-consumption. That is why only one subset simulation was conducted in the latter case.

As a concluding remark of these investigations it can be stated that the proof of concept was successful. The probabilistic approach captured the reduced reliability due to serial combinations of the single trusses, where for the deterministic evaluations the same utilisation was reached in all sub-systems. Although the system effects could be introduced manually for such simple combinations (pure series system), methods of reliability must be applied for more complex systems. For such complex systems, the process of validation of the system effects seems to be infeasible though. Therefore, to validate the applied framework with respect to positive system effects (parallel systems) future studies should investigate systems where a plausibility check is possible.

6.6 Conclusions

On the one hand, the subset simulation is an accurate selection to determine the probability of failure of systems such as single trusses and more complex structures consisting of multiple trusses. On the other hand, the precision must be further evaluated and enhanced in order to correctly capture system effects and to allow for a probabilistic assessment of the design. Herein, no final conclusions can be drawn whether this issue can be solved by simply enlarging the batch size per subset, although a positive tendency was found. Still, it was demonstrated that fundamental effects are captured correctly, such as the serial combination of the individual limit state functions or the reliability assessment of multiple trusses arranged side by side.

The attempt to derive the target reliability based on the state-of-the-art truss design approach from SIA 265:2021 [121] revealed uneven reliability levels for different trusses. At least partly, the reason stems from the probabilistic modelling approach, rather than from the true behaviour. For clarification, further investigations will be needed that go hand in hand with the development of a holistic connection model.

The runtimes of the subset simulations for single trusses are in the range of hours to days. For larger systems, the runtime is in the range of weeks though and memory issues occurred for standard personal computers. That is why for future investigations, computational optimisation

is a necessity and the usage of supercomputers might be indispensable. Still, the benefit of accounting system effects correctly seems to be worth of corresponding investments. Although the potential is promising, the herein developed mechanical and probabilistic models do not allow yet for an application in engineering practice.

Tab. 6.7: Results of the subset simulations for the investigations with respect to the influence of the batch size. The mean values and CoV per batch size are highlighted in bold. The abbreviations in the column headers are: model uncertainty (MU), Weibull-weakest-link model (WWL), batch size per subset (Batch), number of evaluated subsets (#sub), number of considered model evaluations (Eval), probability of failure (P_f), reliability index (β) and coefficient of variation (CoV). In the two columns for the MU and the WWL, the capital letters indicate whether they are considered.

truss	MU	WWL	Batch	#sub	Eval	P_f	β	CoV
duopitch	M	W	1000	4	3700	$2.64 \cdot 10^{-4}$	3.47	0.26
duopitch	M	W	1000	4	3700	$2.74 \cdot 10^{-4}$	3.46	0.26
duopitch	M	W	1000	4	3700	$2.43 \cdot 10^{-4}$	3.49	0.26
duopitch	M	W	1000	4	3700	$4.32 \cdot 10^{-4}$	3.33	0.26
duopitch	M	W	1000	4	3700	$6.03 \cdot 10^{-4}$	3.24	0.27
duopitch	M	W	1000	4	3700	$2.34 \cdot 10^{-4}$	3.50	0.25
duopitch	M	W	1000	4	3700	$3.78 \cdot 10^{-4}$	3.37	0.25
duopitch	M	W	1000	4	3700	$4.62 \cdot 10^{-4}$	3.31	0.25
duopitch	M	W	1000	4	3700	$3.19 \cdot 10^{-4}$	3.41	0.25
						mean	$3.57 \cdot 10^{-4}$	3.38
						CoV	33%	
duopitch	M	W	2000	4	7400	$3.06 \cdot 10^{-4}$	3.43	0.19
duopitch	M	W	2000	4	7400	$3.73 \cdot 10^{-4}$	3.37	0.19
duopitch	M	W	2000	4	7400	$3.64 \cdot 10^{-4}$	3.38	0.18
duopitch	M	W	2000	4	7400	$3.06 \cdot 10^{-4}$	3.43	0.19
duopitch	M	W	2000	4	7400	$3.95 \cdot 10^{-4}$	3.36	0.19
duopitch	M	W	2000	4	7400	$3.06 \cdot 10^{-4}$	3.43	0.18
duopitch	M	W	2000	4	7400	$4.13 \cdot 10^{-4}$	3.34	0.18
duopitch	M	W	2000	4	7400	$3.18 \cdot 10^{-4}$	3.42	0.18
duopitch	M	W	2000	4	7400	$3.43 \cdot 10^{-4}$	3.40	0.18
						mean	$3.47 \cdot 10^{-4}$	3.39
						CoV	11%	
duopitch	M	W	4000	4	14800	$4.09 \cdot 10^{-4}$	3.35	0.13
duopitch	M	W	4000	4	14800	$2.74 \cdot 10^{-4}$	3.46	0.13
duopitch	M	W	4000	4	14800	$4.08 \cdot 10^{-4}$	3.35	0.13
duopitch	M	W	4000	4	14800	$2.92 \cdot 10^{-4}$	3.44	0.13
duopitch	M	W	4000	4	14800	$2.75 \cdot 10^{-4}$	3.46	0.13
duopitch	M	W	4000	4	14800	$4.18 \cdot 10^{-4}$	3.34	0.13
duopitch	M	W	4000	4	14800	$3.42 \cdot 10^{-4}$	3.40	0.13
duopitch	M	W	4000	4	14800	$4.57 \cdot 10^{-4}$	3.32	0.13
duopitch	M	W	4000	4	14800	$3.86 \cdot 10^{-4}$	3.36	0.13
						mean	$3.62 \cdot 10^{-4}$	3.38
						CoV	18%	

Tab. 6.8: Results of the subset simulations for the investigations with respect to the target reliability. The mean values per truss layout are highlighted in bold. The abbreviations in the column headers are: model uncertainty (MU), Weibull-weakest-link model (WWL), batch size per subset (Batch), number of evaluated subsets (#sub), number of considered model evaluations (Eval), probability of failure (P_f), reliability index (β) and coefficient of variation (CoV). In the two columns for the MU and the WWL, the capital letters indicate whether they are considered.

truss	MU	WWL	Batch	#sub	Eval	P_f	β	CoV
Par_FaRi	M	-	2000	4	7400	$4.40 \cdot 10^{-4}$	3.33	0.18
Par_FaPo	M	-	2000	4	7400	$5.69 \cdot 10^{-4}$	3.25	0.16
					mean	$5.04 \cdot 10^{-4}$	3.29	
Par_FaRi_L40	M	-	2000	3	5600	$4.36 \cdot 10^{-3}$	2.62	0.13
Par_FaPo_L40	M	-	2000	3	5600	$8.25 \cdot 10^{-3}$	2.40	0.14
					mean	$6.30 \cdot 10^{-3}$	2.49	
Duo_FaRi	M	-	2000	3	5600	$2.01 \cdot 10^{-3}$	2.88	0.16
Duo_RiFa	M	-	2000	3	5600	$2.23 \cdot 10^{-3}$	2.84	0.16
Duo_FaRiPo	M	-	2000	3	5600	$1.59 \cdot 10^{-3}$	2.95	0.16
Duo_FaPo	M	-	2000	3	5600	$1.29 \cdot 10^{-3}$	3.01	0.16
Duo_RiPo	M	-	2000	3	5600	$2.33 \cdot 10^{-3}$	2.83	0.15
					mean	$1.89 \cdot 10^{-3}$	2.90	
Trian_FaRi	M	-	2000	3	5600	$1.35 \cdot 10^{-3}$	3.00	0.17
Trian_FaRiMid	M	-	2000	3	5600	$1.37 \cdot 10^{-3}$	3.00	0.16
Trian_FaRiPo	M	-	2000	3	5600	$1.08 \cdot 10^{-3}$	3.07	0.17
Trian_FaPo	M	-	2000	3	5600	$1.60 \cdot 10^{-3}$	2.95	0.18
Trian_RiPo	M	-	2000	3	5600	$1.40 \cdot 10^{-3}$	2.99	0.18
					mean	$1.36 \cdot 10^{-3}$	3.00	

Tab. 6.9: Results of the subset simulations for the investigations of the sub-system of the show-case beam grid structure presented in Sec. 5.4. For each sub-system the mean value is provided in bold. The abbreviations in the column headers are: model uncertainty (MU), Weibull-weakest-link model (WWL), batch size per subset (Batch), number of evaluated subsets (#sub), number of considered model evaluations (Eval), probability of failure (P_f), reliability index (β) and coefficient of variation (CoV). In the two columns for the MU and the WWL, the capital letters indicate whether they are considered.

sub-system	MU	WWL	Batch	#sub	Eval	P_f	β	CoV
1 truss	M	-	1000	3	2800	$3.71 \cdot 10^{-3}$	2.68	0.22
1 truss	M	-	2000	3	5600	$3.61 \cdot 10^{-3}$	2.69	0.15
1 truss	M	-	2000	3	5600	$3.10 \cdot 10^{-3}$	2.74	0.15
					mean	$3.47 \cdot 10^{-3}$	2.70	
2 trusses	M	-	1000	3	2800	$3.92 \cdot 10^{-3}$	2.66	0.20
2 trusses	M	-	1000	3	2800	$8.07 \cdot 10^{-3}$	2.41	0.19
2 trusses	M	-	1000	3	2800	$8.18 \cdot 10^{-3}$	2.40	0.22
					mean	$6.72 \cdot 10^{-3}$	2.47	
3 trusses	M	-	1000	3	2800	$9.65 \cdot 10^{-3}$	2.34	0.20
3 trusses	M	-	1000	3	2800	$6.06 \cdot 10^{-3}$	2.51	0.19
3 trusses	M	-	1000	3	2800	$7.52 \cdot 10^{-3}$	2.43	0.20
					mean	$7.74 \cdot 10^{-3}$	2.42	
1-by-1 grid	M	-	1000	3	2800	$6.56 \cdot 10^{-3}$	2.48	0.20
1-by-1 grid	M	-	1000	3	2800	$7.88 \cdot 10^{-3}$	2.41	0.20
1-by-1 grid	M	-	1000	3	2800	$4.65 \cdot 10^{-3}$	2.60	0.22
					mean	$6.36 \cdot 10^{-3}$	2.49	
2-by-2 grid	M	-	1000	3	2800	$9.16 \cdot 10^{-3}$	2.36	0.21

Chapter 7

Conclusions and outlook

7.1 Conclusions

In this thesis, a novel modelling approach for timber trusses with dowelled steel-to-timber connections was developed and embedded into a probabilistic environment to assess the reliability of such trusses. The holistic approach builds the basis for a transition from element-by-element design approaches towards a system-based design. First, fundamentals of various aspects were presented in an extensive state-of-the-art report. Then, the mechanical modelling approach was presented, including details such as a correction of the joint model from Schweigler et al. (2018) [115] for the implementation as a finite element subroutine or the applied limit state functions. Subsequently, the applied probabilistic models were presented, that are based on findings from literature and own investigations. For glued laminated timber, new probabilistic models for the most relevant mechanical properties were derived from own investigations based on findings from literature. Further, adaptations and models needed for a probabilistic assessment were presented for the connection behaviour, the steel products and the actions. Finally, deterministic and probabilistic investigations were conducted with respect to the structural behaviour and the reliability, respectively. Thereby, first the fundamental behaviour of the models was investigated. Then, assessments were conducted with respect to the simplified truss design approach from SIA 265:2021 [121]. In the end, based on a show-case structure, aspects of a system-based design were discussed.

The main conclusions per chapter were already presented at their end. In the following, the conclusions are stated from a more holistic view-point.

Structural behaviour

- The developed multi-scale modelling approach was successfully translated into a modelling framework. For future extensions or adaptations, single elements can be exchanged.
- The modelling framework was applied with different degrees of modelling complexity of the truss joints. Thereby it could be confirmed that all structural elements should be considered. Neglecting details such as the chord springs or the steel plates lead to non-negligible deviations.

- The introduced parametrisation and automation allow for an efficient modelling of all parts of timber trusses with dowelled steel-to-timber connections.
- It could be confirmed that the coupling of the degrees of freedom with respect to the normal force, shear force and bending moment in-plane according to the joint model from Schweigler et al. (2018) [115] generally should be considered.
- Since the herein applied modelling framework consists of extended considerations of the background of the simplified truss design approach from SIA 265:2021 [121], it can be applied for design directly.
- On the basis of example trusses it was shown that the simplified design approach from SIA 265:2021 [121] seems to hold for parallel chord trusses and duopitch roof trusses with raised eaves. For triangular and monopitch roof trusses the limits were exceeded though. The rule concerning the deflections in the serviceability limit state was overstepped in most cases. Nevertheless, none of the example trusses did show a critical utilisation of their components.
- Based on a show-case beam grid structure it was demonstrated that the developed modelling framework can be applied to design complex trusses. The design process still needs an iterative procedure though.

Reliability

- With respect to the probabilistic modelling of glued laminated timber, fundamentals were missing. Herein, new models were derived for the most relevant mechanical properties with the strategy of an overall best fit, in order to correctly capture system effects. Next to the provided models for specified reference sizes, corresponding size-effect models were derived.
- The resistance model for eccentrically loaded connections and the load-deformation behaviour developed by Manser (2021) [91] were successfully applied and the respective probabilistic consideration of the model uncertainties could be derived. Nevertheless, further investigations will be needed to harmonise the introduced limit states based on the respective models. Alongside, the numeric stability of the load-deformation behaviour under consideration of the model uncertainties must be enhanced.
- The subset simulation revealed itself to be an accurate method to determine the reliability of full trusses with numerous uncertain parameters and limit state functions. Further, it is capable to consider system effects. Still, the evaluation of the method revealed certain drawbacks with respect to the precision. No final conclusions could be drawn, whether the precision can be enhanced solely by enlarging the batch size per subset.
- The investigations of the reliability with respect to the individual limit state functions revealed the connection load-deformation behaviour and the connection resistance model to

be most important. Therefore, future attempts should focus on connections. On the one hand, the models have to be improved for better accuracy. On the other hand, the consequences of design decisions such as introducing enhanced ductility should be evaluated.

- Although under deterministic consideration the Weibull-weakest-link model showed a non-negligible influence, in the probabilistic assessments, its influence could not be confirmed. Two explanations can be provided: (1) the low precision of the applied subset simulations lead to too large scatter; and (2) the connection behaviour was dominating the reliability assessments.
- The intended derivation of the target reliability based on the simplified design approach from SIA 265:2021 [121] revealed uneven levels of reliability amongst the different truss layouts and their absolute sizes. At least partly, the reasons might stem from the underlying probabilistic models.
- In terms of structural robustness, the presented system-based design approach allows for the strategy of *reducing vulnerability* by means of identifying key elements and their proper design. Within one segment of a larger structure, necessary reliability assessments can be conducted to consider system effects. To follow the approach of *enhancing robustness* for complex trusses by means of providing alternative load-paths, further developments are needed though, such as the consideration of geometric non-linearities and the definition of according scenarios.
- For simple trusses, the model runtime is in the order of seconds to minutes. For complex structures, several hours can be necessary though. Subsequently, for subset simulations on standard personal computers, days to weeks are needed. Further, the memory consumption can be of concern. Therefore, currently the application for complex structures is limited to research applications, where supercomputers can be applied. To allow for applications in practice, computational optimisation is of utmost importance.

7.2 Outlook

In this chapter, an overview of further considerations is provided that could not be investigated within the scope of this thesis. They will be hopefully addressed in future research projects in this promising field, which would allow for a holistic consideration of structural systems.

Connection behaviour

- The gap between the consideration of the load-deformation behaviour and the resistance model for connections must be closed and a holistic connection model should be derived.
- Herein, the load-deformation behaviour derived by Manser (2021) [91] was applied, that follows a top-down approach, where the load-deformation behaviour per dowel and shear

plane was derived based on full connection tests. Actually, dowelled connections in glued laminated timber under multi-axial loading build complex systems, since most dowels are embedded in different lamellas and each dowel is loaded individually with respect to magnitude and direction. When the mentioned top-down approach is combined with a bottom-up approach starting from single-dowel connections, systematic deviations might be derived, and hence, a semi-empirical approach could be developed. To investigate the differences between top-down and bottom-up approaches, the joint model derived in Schweigler et al. (2018) [115] can be applied, since it is capable of considering individual load-deformation paths for all dowels.

- In principle, the probabilistic consideration of the model error by means of a relative consideration of the model uncertainties works. The accuracy of the approach should be further investigated though, since for trusses with large connections a decreased reliability was found.
- The load-deformation behaviour model derived by Manser (2021) [91] builds a solid basis. On this basis, load-deformation curves could be adapted artificially to represent e.g. more ductile or less scattering behaviour and hence, their influence on the system behaviour could be studied or the demand on specific aspects could be derived.
- The joint model derived in Schweigler et al. (2018) [115] allows for the consideration of contact between truss members. A parametric and automated procedure should be developed in order to efficiently apply this extension.
- For the joint model derived in Schweigler et al. (2018) [115], respective model uncertainties should be developed. The derivation must respect the balance of the system, i.e. the section forces, and is most likely dependent on the applied load-deformation approach.

Probabilistic modelling

- The developed probabilistic models for glued laminated timber (GLT) cover the most relevant mechanical properties. Still, models for the properties under edgewise loading and parameters applied in fracture mechanics approaches have to be developed.
- Some of the developed models for GLT are strongly based on simulation data. These models should be validated or updated with results from experimental campaigns.
- For some GLT properties, further data should be collected to enhance the statistical relevance of the probabilistic models and to cover the variability that stems from different growth regions and differences in the strength grading methods.
- As discussed in this thesis, the correlation between different properties of GLT might be lower than for solid timber. Still, their influence might be crucial for probabilistic assessments and hence, they should be derived. For bending, tension and compression

along the grain, the respective values could be derived from simulations (e.g. based on the "Karlsruher Rechenmodell").

- In this thesis, only snow loads on roof structures were considered as external loading. Wind loads and imposed loads have to be introduced to the framework in order to assess full structures.
- Model uncertainties should be attempted to be minimised. As shown in this thesis, their influence is crucial and their variability directly interferes with the reliability.

Weibull-weakest-link model

- Lam (2000) [86] derived a Weibull-weakest-link model for truss chord members under tension and calibrated the exponent for some Canadian solid timber grading classes. For glued laminated timber, the respective exponent is yet to be determined.
- In a probabilistic context, its importance could not be clarified, due to the large scatter of the results. Therefore, before the determination of the exponent, it should be investigated how large the influence is, where the exponent is expected to be in the range of 8-11.

Optimisation

- In order to efficiently apply the developed framework to the design of trusses, optimisation procedures based on cost-functions have to be developed which allow for an automated selection of cross-sections, connection layouts and the materialisation.
- To allow for better performance with respect to reliability analyses, the application of surrogate modelling techniques should be aspired.
- If both steps can be achieved, reliability based design optimisation schemes could be applied, which could spark a revolution with respect to design methodologies.

Nomenclature

Abbreviations

#sub	Number of subsets in a subset simulation
Batch	Batch size of subset simulation
CC	Consequence class
CDF	Cumulative distribution function
CoV	Coefficient of variation
dofs	Degrees of freedom
Eval	Number of evaluations in a subset simulation
GIR	Glued-in rods
GLT	Glued laminated timber
LVL	Laminated veneer lumber
MOE	Modulus of elasticity
MU	Model uncertainty
MU-C	Model uncertainty for connections
MU-S	Model uncertainty for snow loads
MU-T	Model uncertainty for timber beams
PDF	Probability density function
RC	Reliability class
SLS	Serviceability limit state
ULS	Ultimate limit state
WWL	Weibull-weakest-link model

Upper-case Roman letters

A	Cross-section area
A_s	Shear area
A_{sy}	Shear area with respect to y-axis
A_{sz}	Shear area with respect to z-axis
D_f	Failure domain
D_s	Safe domain
$D_{\mathbf{X}}$	Domain of random vector
E	Modulus of elasticity
E_0	Modulus of elasticity parallel to the grain
E_{90}	Modulus of elasticity perpendicular to the grain
$E_{90,mean}$	Mean value of modulus of elasticity perpendicular to the grain
$E_{90,k}$	Characteristic value of modulus of elasticity perpendicular to the grain
E_c	Modulus of elasticity in compression

$E_{c,90,mean}$	Mean value of the modulus of elasticity perpendicular to the grain in compression
$E_{c,mean}$	Mean value of the modulus of elasticity in compression
$E_{c,k}$	Characteristic value of the modulus of elasticity in compression
E_d	Load combination
E_k	Characteristic value of the modulus of elasticity (general)
E_m	Modulus of elasticity in bending
$E_{m,mean}$	Mean value of the modulus of elasticity in bending
$E_{m,k}$	Characteristic value of the modulus of elasticity in bending
E_{mean}	Mean value of the modulus of elasticity (general)
E_t	Modulus of elasticity in tension
$E_{t,90}$	Modulus of elasticity perpendicular to the grain in tension
$E_{t,90,mean}$	Mean value of the modulus of elasticity perpendicular to the grain in tension
$E_{t,90,k}$	Characteristic value of the modulus of elasticity perpendicular to the grain in tension
$E_{t,mean}$	Mean value of the modulus of elasticity in tension
$E_{t,k}$	Characteristic value of the modulus of elasticity in tension
F	Force
F_0	Intersection of K_2 and the vertical axis
F_i	(Connection sub-routine related:) Force per dowel
F_i	(System related:) Component failure
F_i	(Weibull related:) Force per link
F_k	Limit stress
F_{max}	Maximum force in all links
$F_{parallel}$	Failure of a parallel system
$F_{pur,0}$	Load imposed at purlin-girder crossing for horizontally applied purlins
$F_{pur,tilt}$	Load imposed at purlin-girder crossing for tilted purlins
F_{series}	Failure of a series system
$F_{u,0}$	Ultimate load without eccentricity
$F_{u,e}$	Ultimate load with applied eccentricity
$F_X(x)$	Cumulative distribution function
$F_{x,i}$	Force per dowel in x-direction
$F_{z,i}$	Force per dowel in z-direction
FS	Factor of safety
G	Self-weight
G_c	Mixed mode fracture energy
G_v	Shear modulus
$G_{v,mean}$	Mean value of the shear modulus
$G_{v,k}$	Characteristic value of the shear modulus
I	(Algorithm related:) Index matrix
I	(Civil engineering related:) Moment of inertia
I_0	Moment of inertia out-of-plane of gross-cross-section
I_1	Moment of inertia out-of-plane of net-cross-section
I_x	Moment of inertia around x-axis
I_y	Moment of inertia around y-axis
I_z	Moment of inertia around z-axis

K	Stiffness matrix of one node
K_1	Initial stiffness
K_2	Secondary stiffness
K_3	Tertiary (decreasing) stiffness
K_e	Stiffness matrix of beam elements
K_i	Stiffness of a single shear plane in dependence of the load-to-grain angle
K_s	Stiffness matrix of spring elements
K_{ser}	Slip modulus under service loads
$K_{ser,0}$	Slip modulus under service loads parallel to the grain
$K_{ser,90}$	Slip modulus under service loads perpendicular to the grain
K_{rot}	Polar moment of inertia
K_{tan}	Tangent stiffness matrix
K_u	Slip modulus under ultimate loading
L_i	Length of individual chord elements
L	Member length
L_{ref}	Reference length
M	Model
$M_{u,k}$	Characteristic plastic bending capacity
M_x	Torsion
M_y	Bending moment around y-axis
M_z	Bending moment around z-axis
N	(Civil engineering related:) Normal force
N	(Reliability related:) Sample size
N_{cr}	Critical buckling load according to Euler N_{cr}
N_f	Number samples in failure domain
N_{rel}	Relative normal force compared to <i>Culmann</i> model
N_x	Normal force
P_f	Probability of failure
$P_{f,MC}$	Probability of failure determined by Monte Carlo simulation
$P_{f,parallel}$	Probability of failure of a parallel system
$P_{f,series}$	Probability of failure of a series system
$Q_{s,k}$	Characteristic snow load
R	Resistance parameter
$R_{d,con}$	Resistance of a dowel-type connection
S	(Reliability related:) Demand parameter
S	(Weibull weakest link related:) Strength
SI	Stress increase factor
T_k	Buckling modulus
V	Volume
V_0	Reference volume
V_{ref}	Reference volume
V_y	Shear force in y-direction
V_z	Shear force in z-direction
\mathbf{X}	Random vector
$X_{\alpha RA}$	Model uncertainty of the parameter to control the curvature

X_{F_0}	Model uncertainty of the intersection of K_2 and the vertical axis
X_{K_1}	Model uncertainty of the initial stiffness
X_{K_2}	Model uncertainty of the secondary stiffness
X_{K_3}	Model uncertainty of the tertiary stiffness
$X_{M,III}$	Model uncertainty for failure mode III
$X_{P-\Delta,y}$	Model uncertainty for second order effect in-plane
$X_{P-\Delta,z}$	Model uncertainty for second order effect out-of-plane
$X_{c,0}$	Model uncertainty of the compressive strength parallel to the grain
X_{k_e}	Model uncertainty of the reduction factor due to eccentric loading
$X_{k_{red}}$	Model uncertainty for the reduction factor due to multiple dowels on an axis
$X_{m,y}$	Model uncertainty of the bending strength around the y-axis
$X_{t,0}$	Model uncertainty of the tensile strength parallel to the grain
$X_{v,z}$	Model uncertainty of the shear strength
$X_{w_{int}}$	Model uncertainty of the deformation at the transition point of K_2 and K_3
$X_{w_{ult}}$	Model uncertainty of the ultimate deformation
Z_i	Matrix which selects the correct dofs for every element
δR	Incremental restoring forces
δN	Incremental normal force
δV_z	Incremental shear force in z-direction
δM_y	Incremental bending moment around y-axis
δu	Incremental displacements
δu_x	Incremental displacements in x-direction
δu_z	Incremental displacements in z-direction
δu_φ	Incremental rotations
dV	Incremental volume
ΔV	Incremental volume

Lower-case Roman letters

a	First Weibull distribution parameter
a_1	Dowel-to-dowel distance \parallel
a_2	Dowel-to-dowel distance \perp
a_3	Dowel-to-end distance \parallel
a_4	Dowel-to-edge distance \perp
b	Second Weibull distribution parameter
d	Dowel diameter
d_{gir}	Girder distance
d_{pur}	Purlin distance
e	Eccentricity
$f()$	Function (in general)
$f'()$	Derivative of a function
$f_{c,0}$	Compressive strength parallel to the grain
$f_{c,0,mean}$	Mean value of compressive strength parallel to the grain
$f_{c,0,k}$	Characteristic value of compressive strength parallel to the grain
$f_{c,90}$	Compressive strength perpendicular to the grain

$f_{c,90,mean}$	Mean value of compressive strength perpendicular to the grain
$f_{c,90,k}$	Characteristic value of compressive strength perpendicular to the grain
f_h	Embedment strength
$f_{h,0,k}$	Characteristic value of embedment strength parallel to the grain
$f_{h,90,k}$	Characteristic value of embedment strength perpendicular to the grain
$f_{h,\alpha}$	Embedment strength for specific load-to-grain angle
$f_{h,k}$	Characteristic value of embedment strength
$f_{j,ext}$	Imposed load vector
f_m	Bending strength
$f_{m,mean}$	Mean value of bending strength
$f_{m,k}$	Characteristic value of bending strength
$f_{m,y}$	Bending strength for the y-axis
$f_{m,z}$	Bending strength for the z-axis
$f_{t,0}$	Tensile strength parallel to the grain
$f_{t,0,mean}$	Mean value of tensile strength parallel to the grain
$f_{t,0,k}$	Characteristic value of tensile strength parallel to the grain
$f_{t,90}$	Tensile strength perpendicular to the grain
$f_{t,90,mean}$	Mean value of tensile strength perpendicular to the grain
$f_{t,90,k}$	Characteristic value of tensile strength perpendicular to the grain
f_u	Steel strength
$f_{u,k}$	Characteristic value of ultimate tensile strength of steel
f_v	Shear strength
$f_{y,k}$	Characteristic value of yield strength of steel
$g()$	Limit state function
h	(Size related:) Height
h	(Math related:) Increment
h_0	Reference snow height
h_{conn}	Connection height
j	Analysis step index
k	Order of magnitude of the probability of failure
k_α	Safety factor for dowel-type connections
k_β	Coefficient of all members to determine connection resistance
$k_{\beta 1,1}$	Coefficient of side member to determine connection resistance in failure mode II
$k_{\beta 1,2}$	Coefficient of side member to determine connection resistance in failure mode III
$k_{\beta 2,2}$	Coefficient of middle member to determine connection resistance in failure mode III
$k_{E,h,\lambda}$	Size effect factor for the first Lognormal distribution parameter for the modulus of elasticity
$k_{E,h,\zeta}$	Size effect factor for the second Lognormal distribution parameter for the modulus of elasticity
k_c	Reduction factor of the compressive strength along the grain
k_e	Reduction factor due to eccentric loading
k_m	Reduction factor of the bending strength
$k_{m,y,h,a}$	Size effect factor for the first Weibull distribution parameter for the bending strength

$k_{m,y,h,b}$	Size effect factor for the second Weibull distribution parameter for the bending strength
k_{mod}	Modification factor of timber
k_{red}	Reduction factor of connection resistance in dependence of the dowels on one axis
$k_{t,0,l,a}$	Length effect factor for the first Weibull distribution parameter for the tensile strength parallel to the grain
$k_{t,0,l,b}$	Length effect factor for the second Weibull distribution parameter for the tensile strength parallel to the grain
$k_{t,0,h,a}$	Height effect factor for the first Weibull distribution parameter for the tensile strength parallel to the grain
$k_{t,0,h,b}$	Height effect factor for the second Weibull distribution parameter for the tensile strength parallel to the grain
$k_{t,90,0}$	Size effect factor for the Weibull distribution for the tensile strength perpendicular to the grain for short term loading
$k_{t,90,\infty}$	Size effect factor for the Weibull distribution for the tensile strength perpendicular to the grain for long term loading
k_v	Size effect factor for the Weibull distribution for the shear strength
l_0	Beam length
l_1	Length of weak zone
l_i	Distance from the centre of a dowel group to the individual dowel
l_k	Buckling length
m	Ratio of length of weak zone divided by beam length
n	Square root of the ratio of moments of inertia
n_{col}	Number of dowels in a row
n_{row}	Number of dowel rows
p	Number of shear planes
p_i	Component probability
r	Realisation of a resistance parameter R
r_k	Characteristic member resistance
$r(u_j)$	Restoring force vector
s	(Reliability related:) Realisation of a demand parameter S
s	(Geometric properties:) Truss node distance
$s_{G,k}$	Characteristic dead load effects
$s_{Q,k}$	Characteristic live load effects
s_k	Characteristic snow load
t_1	Thickness of side members
$t_{1,1}$	Minimal side member thickness to reach failure mode II
$t_{1,2}$	Minimal side member thickness to reach failure mode III
t_2	Thickness of middle members
$t_{2,2}$	Minimal middle member thickness to reach failure mode III
u_j	Displacement vector
$u_{rel,SLS}$	Relative deflections compared to <i>Culmann</i> model under SLS loading
$u_{rel,ULS}$	Relative deflections compared to <i>Culmann</i> model under ULS loading
w	Deformation of load-displacement relation

w_0	Imperfection
w_{int}	Deformation at the transition point of K_2 and K_3
w_{ult}	Ultimate deformation
\mathbf{x}	Realisation of random vector
x_i	Lever arm in x-direction
y	(Generally:) Model response
y	(Regression related:) Data
y'	Regression model
z_d	Design variable
z_i	Lever arm in z-direction
δf	Derivative of function

Upper-case Greek letters

Φ_y	Shear correction factor with respect to y-axis
Φ_z	Shear correction factor with respect to z-axis
Φ	Standard Normal cumulative distribution function

Lower-case Greek letters

α	(Timber engineering related:) Load-to-grain angle
α_i	Angle per dowel
$\hat{\alpha}_i$	Load-to-grain angle per dowel
α_{RA}	Parameter to control the curvature
β	Reliability index
β_0	Amplification factor of the buckling length
β_T	Constant to determine the buckling modulus
δ_S	Skewness
δ_i	Displacement per dowel
$\delta_{x,i}$	Displacement per dowel in x-direction
$\delta_{z,i}$	Displacement per dowel in z-direction
ϵ	Error (term)
φ	Creep factor
φ_0	Reduction factor of the buckling resistance
γ_G	Partial factors of characteristic dead load effects
γ_M	Partial factor on r_k
$\gamma_{M,steel}$	Safety factor for steel
$\gamma_{M,timber}$	Safety factor for timber
γ_Q	Partial factors of characteristic live load effects
λ	First Lognormal distribution parameter
λ_i	Proportionality factor
μ	Mean value
μ_ϵ	Mean value of model uncertainty
ψ_1	Reduction factor 1 for snow load
ψ_2	Reduction factor 2 for snow load
ρ	(Reliability related:) Consequences
ρ	(Material related:) Density

ρ_m	Mean value of the density
ρ_{mean}	Mean value of the density
ρ_k	Characteristic value of the density
σ	(Probability related:) Standard deviation
σ	(Civil engineering related:) stress
σ_ϵ	Standard deviation of model uncertainty
$\sigma_{c,0}$	Compressive stress along the beam axis
$\sigma_{c,crit}$	Critical buckling stress according to Euler
$\sigma_{m,I}$	Bending stress according to first order theory
$\sigma_{m,II}$	Bending stress according to second order theory
$\sigma_{m,y}$	Bending stress for the y-axis
$\sigma_{m,z}$	Bending stress for the z-axis
σ_{max}	Maximum stress
$\sigma_{t,0}$	Tensile stress parallel to the grain
τ	Shear stress
τ_{tor}	Shear stress from torsion
$\tau_{y,k}$	Characteristic shear yield strength of steel
ξ	Tensile length adjustment factor
ζ	Second Lognormal distribution parameter
α	(Second order theory related:) Enlargement factor

Special characters

\mathbb{E}	Expectation operator
\mathcal{LN}	Lognormal distribution
\mathcal{N}	Normal distribution
\mathbb{P}	Probability operator
\mathbb{R}	Real numbers
\mathcal{W}	Weibull distribution

Bibliography

- [1] **BSB* Holztragwerk - Technik*. «BSB», die Formel für tragfähige Verbindungen. URL: www.blumer-bsb.ch (visited on 2019-03-13).
- [2] 384:2016+A1:2018, E. *Structural Timber - Determination of Characteristic Values of Mechanical Properties and Density*. Brussels, Belgium: European Committee for Standardization CEN, 2018.
- [3] Aicher, S., Dill-Langer, G., and Ranta-Maunus, A. “Duration of Load Effect in Tension Perpendicular to the Grain of Glulam in Different Climates”. *Holz als Roh- und Werkstoff* 56 (1998), pp. 295–305.
- [4] Aicher, S. and Dill-Langer, G. “DOL Effect in Tension Perpendicular to the Grain of Glulam Depending on Service Classes and Volume; Paper 30-9-1”. *Proceedings of the CIB-W18 Meeting 30*. International Council for Building Research and Documentation. Vancouver, Canada, 1997-08.
- [5] Aicher, S., Dill-Langer, G., and Klöck, W. “Evaluation of Different Size Effect Models for Tension Perpendicular to Grain Design; Paper 35-6-1”. *Proceedings of the CIB-W18 Meeting 35*. International Council for Research and Innovation in Building and Construction. Kyoto, Japan, 2002.
- [6] Au, S.-K. and Beck, J.L. “Estimation of Small Failure Probabilities in High Dimensions by Subset Simulation”. *Probabilistic Engineering Mechanics* 16.4 (2001-10-01), pp. 263–277. ISSN: 0266-8920. DOI: 10.1016/S0266-8920(01)00019-4.
- [7] Baravalle, M. “Risk and Reliability Based Calibration of Structural Design Codes”. Doctoral Thesis. Trondheim, Norway: NTNU, 2017.
- [8] Blaß, H.J., Bienhaus, A., and Krämer, V. “Effective Bending Capacity of Dowel-Type Fasteners”. *Proceedings Pro022: International RILEM Symposium on Joints in Timber Structures*. Stuttgart, Germany, 2001, pp. 71–80.
- [9] Blaß, H.J., Ehlbeck, J., Kreuzinger, H., and Steck, G. *Erläuterungen zu DIN 1052:2004-08: Entwurf, Berechnung und Bemessung von Holzbauwerken*. Bruderverlag, 2004. 217 pp. ISBN: 3-87104-152-1.

- [10] Blaß, H.J. and Enders-Comberg, M. *Fachwerkträger für den industriellen Holzbau*. KIT Scientific Publishing, 2012. 176 pp. ISBN: 978-3-86644-854-4.
- [11] Blaß, H.J. and Sandhaas, C. *Timber Engineering - Principles for Design*. Karlsruhe, Germany: KIT Scientific Publishing, 2017. 646 pp. ISBN: 978-3-7315-0673-7. DOI: 10.5445/KSP/1000069616.
- [12] Blaß, H.J. and Schmid, M. “Tensile Strength Perpendicular to Grain of Glued Laminated Timber; Paper 32-6-4”. *Proceedings of the CIB-W18 Meeting 32*. International Council for Research and Innovation in Building and Construction. Working Commission W18 - Timber Structures. Graz, Austria, 1999-08.
- [13] *Bohrschraube TOPROC SAF*. URL: www.pro-fix.ch (visited on 2019-03-13).
- [14] Brandner, R. and Schickhofer, G. “Glued Laminated Timber in Bending: New Aspects Concerning Modelling”. *Wood Science and Technology* 42.5 (2008-06), pp. 401–425. ISSN: 0043-7719, 1432-5225. DOI: 10.1007/s00226-008-0189-2.
- [15] Brandner, R., Freytag, B., and Schickhofer, G. “Determination of Shear Modulus by Means of Standardized Four-Point Bending Tests; Paper 41-21-1”. *Proceedings of the CIB-W18 Meeting 41*. International Council for Research and Innovation in Building and Construction. St. Andrews, Canada, 2008.
- [16] Brandner, R., Gehri, E., Bogensperger, T., and Schickhofer, G. “Determination of Modulus of Shear and Elasticity of Glued Laminated Timber and Related Examinations; Paper 40-12-2”. *Proceedings of the CIB-W18 Meeting 40*. International Council for Research and Innovation in Building and Construction - Working Commission W18. Bled, Slovenia, 2007-08.
- [17] Brandner, R. and Schickhofer, G. “System Effects of Structural Elements - Determined for Bending and Tension”. 9th World Conference on Timber Engineering. Portland, Oregon, USA, 2006-01.
- [18] Brühl, F., Kuhlmann, U., and Jorissen, A. “Consideration of Plasticity within the Design of Timber Structures Due to Connection Ductility”. *Engineering Structures* 33 (2011-09-03), pp. 3007–3017. ISSN: 0141-0296.
- [19] Cabrero, J. and Yurrita, M. “Performance Assessment of Existing Models to Predict Brittle Failure Modes of Steel-to-Timber Connections Loaded Parallel-to-Grain with Dowel-Type Fasteners”. *Engineering Structures* 171 (2018-09), pp. 895–910. ISSN: 01410296. DOI: 10.1016/j.engstruct.2018.03.037.

- [20] Cabrero, J.M., Honfi, D., Jockwer, R., and Yurrita, M. “A Probabilistic Study of Brittle Failure in Dowel-Type Timber Connections with Steel Plates Loaded Parallel to the Grain”. *Wood Material Science & Engineering* 14.5 (2019-09-03), pp. 298–311. ISSN: 1748-0272, 1748-0280. DOI: 10.1080/17480272.2019.1645206.
- [21] Chatzi, E., Abbiati, G., and Agathos, K. *Method of Finite Elements II*. Lecture notes. Chair of Structural Mechanics and Monitoring, ETH Zurich, Switzerland, 2018.
- [22] Culmann, C. *Die graphische Statik*. Zürich: Meyer & Zeller, 1866. DOI: 10.3931/e-rara-20052.
- [23] Damkilde, L., Hoffmeyer, P., and Pedersen, T.N. “Compression Strength Perpendicular to Grain of Structural Timber and Glulam; Paper 31-6-4”. *Proceedings of the CIB-W18 Meeting 31*. International Council for Research and Innovation in Building and Construction. Working Commission W18 - Timber Structures. Savonlinna, Finland, 1998-08.
- [24] Dietsch, P. and Kreuzinger, H. “Guideline on the Assessment of Timber Structures: Summary”. *Engineering Structures* 33.11 (2011-11), pp. 2983–2986. ISSN: 01410296. DOI: 10.1016/j.engstruct.2011.02.027.
- [25] Dietsch, P. and Winter, S. “Structural Failure in Large-Span Timber Structures: A Comprehensive Analysis of 230 Cases”. *Structural Safety* 71 (2018-03), pp. 41–46. ISSN: 01674730. DOI: 10.1016/j.strusafe.2017.11.004.
- [26] Dubas, P., Gehri, E., and Steurer, A. *Einführung in die Norm SIA 164 (1981) Holzbau - Autographie zum Fortbildungskurs für Bauingenieure*. Zürich: Lehrstuhl für Baustatik und Stahlbau ETH Zürich, 1981.
- [27] Ehrhart, T. “European Beech Glued Laminated Timber”. Doctoral Thesis. ETH Zurich, 2019. 200 pp. DOI: 10.3929/ethz-b-000402805.
- [28] Ellingwood, B.R. “Status of Reliability-Based Design in North America: Impact for Engineered Wood Construction”. *Reliability-Based Design of Engineered Wood Structures*. Ed. by J. Bodig. Vol. 215. NATO ASI E: Applied Sciences. Dordrecht / Boston / London, 1992, pp. 3–19.
- [29] EN 14080:2013. *Timber Structures - Glued Laminated Timber and Glued Solid Timber - Requirements*. Brussels, Belgium: European Committee for Standardization CEN, 2013.
- [30] EN 1990:2002. *Basis of Structural Design*. Brussels, Belgium: European Committee for Standardization CEN, 2002.

- [31] EN 1995-1-1:2004. *Eurocode 5: Design of Timber Structures - Part 1-1: General - Common Rules and Rules for Buildings*. Brussels, Belgium: European Committee for Standardization CEN, 2004.
- [32] Erchinger, C.-D. “Zum Verhalten von mehrschnittigen Stahl-Holz-Stabdübelverbindungen im Brandfall”. Doctoral Thesis. ETH Zurich, 2009. ISBN: 9783728132543. DOI: 10.3929/ethz-a-005774542.
- [33] Eschmann, L. “Neue Prüfmethode zur Bestimmung der Lochleibungseigenschaften von Holz”. MA thesis. Zurich, Switzerland: ETH Zurich, 2021-01. 81 pp.
- [34] Faber, M. and Narasimhan, H. “COST Action TU0601–Robustness of Structures: A Summary”. *M. Faber, Robustness of Structures - Final Report of COST Action TU0601* (2011).
- [35] Fahrni, R. “Reliability-Based Code Calibration for Timber in Fire”. Doctoral Thesis. ETH Zurich, 2021. DOI: 10.3929/ethz-b-000475057.
- [36] *Feuerwiderstandsbemessung Bauteile und Verbindungen*. Lignum-Dokumentation Brandschutz 3.1. Zurich: Lignum, Holzwirtschaft Schweiz, 2011. 95 pp.
- [37] Fink, G. “Influence of Varying Material Properties on the Load-Bearing Capacity of Glued Laminated Timber”. Doctoral Thesis. ETH Zurich, 2014. DOI: 10.3929/ethz-a-010108864.
- [38] Fink, G., Jockwer, R., and Kohler, J. “Reliability Based Design of Timber Structures – System Focussed Application”. *Proceedings of the World Conference on Timber Engineering (WCTE 2016)*. World Conference on Timber Engineering. Vienna University of Technology, 2016, pp. 3702–3709.
- [39] Foschi, R. “Reliability of Structures with Timber and Wood-Based Products”. *Timber Engineering*. Wiley, 2003-03, pp. 177–199.
- [40] Foschi, R.O. and Barrett, J.D. “Consideration of Size Effects in Longitudinal Shear Strength for Uncracked Beams; Paper 13-6-2”. *Proceedings of the CIB-W18 Meeting 13*. International Council for Building Research and Documentation. Otaniemi, Finland, 1980-06.
- [41] Foschi, R.O., Folz, B., and Yao, F. “Reliability-Based Design of Wood Structures: Background to CSA-086.1-M89”. *Canadian Journal of Civil Engineering* 20.3 (1993), pp. 349–357.

- [42] Franke, S. and Franke, B. “Steel Dowel Connections in Beech Hardwood; Paper 52-07-4”. *Proceedings of the INTER Meeting 52*. International Network on Timber Engineering Research. Tacoma, USA: Timber Scientific Publishing KIT Holzbau und Baukonstruktionen Karlsruhe, 2019, p. 14.
- [43] Frese, M. “Computergestützte Verfahren zur pragmatischen Beurteilung der Tragwiderstände von Brettschichtholz: Zusammenfassung exemplarischer Simulationsstudien”. Habilitation Thesis. Karlsruhe, Germany: Karlsruher Institut für Technologie (KIT), 2016. 188 pp. DOI: 10.5445/KSP/1000052710.
- [44] Frese, M. and Blaß, H.J. “Reliability of Large Glulam Members Part 1: Data for the Assessment of Partial Safety Factors for the Bending Strength; Paper 49-17-1”. *Proceedings of the INTER Meeting 49*. International Network on Timber Engineering Research. Graz, Austria, 2016.
- [45] Frese, M., Egner, S., and Blaß, H.J. “Reliability of Large Glulam Members Part 2: Data for the Assessment of Partial Safety Factors for the Tensile Strength; Paper 50-17-1”. *Proceedings of the INTER Meeting 50*. International Network on Timber Engineering Research. Kyoto, Japan, 2017.
- [46] Fuhrmann, C. “Stabdübelverbindungen - Grundlagen, Revision der Bemessungsregeln und Nachweise, Beispiele”. Holzbautag Biel. Biel, Switzerland, 2011.
- [47] Gavin, H. *Geometric Stiffness Effects in 2D and 3D Frames*. Lecture notes. Duke University, 2012.
- [48] Gehri, E. “Betrachtungen zum Tragverhalten von Bolzenverbindungen im Holzbau”. *Schweizer Ingenieur und Architekt* (1980), pp. 1336–1344.
- [49] Gehri, E. “Zur Berechnung und Bemessung von Fachwerkträgern mit Knotenplatten in eingeschlitzten Hölzern”. *Schweizer Ingenieur und Architekt* 101 (1983), pp. 145–152. DOI: 10.5169/seals-75063.
- [50] Gehri, E. “Light Trusses with Screwed Joints”. *PRO 22: International RILEM Symposium on Joints in Timber Structures*. Stuttgart, Germany: RILEM Publications, 2001, pp. 173–182. ISBN: 978-2-912143-28-0.
- [51] Gehri, E., Steurer, A., and Fontana, M. *Fachwerkträger aus Buche und Fichte mit Stahlknotenplatten in eingeschlitzten Hölzern*. Baustatik und Stahlbau 82-1. ETH Zürich, 1982.
- [52] Gehri, E., Vogel, H., Menig, W., Häring, C., Bannholzer, H., and Blumer, H. *Entwurf und Bemessung von Schnittholz-Konstruktionen mit neuzeitlichen Verbindungen*. Fortbil-

- dukurs XI der SAH. Zürich: Schweizerische Arbeitsgemeinschaft für Holzforschung, 1979-11-08.
- [53] Guise, D. *Abstracts & Chronology of American Truss Bridge Patents, 1817-1900*. 2009.
- [54] Gustafsson, P.-J. *Lecture Notes on Some Probabilistic Strength Calculation Models*. TVSM-7161. Lund, Sweden: Division of Structural Mechanics, Lund University, 2014.
- [55] Hankinson, R.L. "Investigation of Crushing Strength of Spruce at Varying Angles of Grain". *Air service information circular* 3.259 (1921-07-15), pp. 3–15.
- [56] Hansson, M. and Ellegaard, P. "System Reliability of Timber Trusses Based on Non-Linear Structural Modelling". *Materials and Structures* 39.6 (2006-06-20), pp. 593–600. ISSN: 1359-5997, 1871-6873. DOI: 10.1617/s11527-006-9098-8.
- [57] Hansson, M. and Thelandersson, S. "Assesment of Probabilistic System Effects on the Reliability of Timber Trusses". *Materials and Structures* 35.9 (2002-11), pp. 573–578. ISSN: 1359-5997, 1871-6873. DOI: 10.1007/BF02483126.
- [58] Hansson, M. and Thelandersson, S. "Capacity of Timber Roof Trusses Considering Statistical System Effects". *Holz als Roh- und Werkstoff* 61.3 (2003-06), pp. 161–166. ISSN: 0018-3768, 1436-736X. DOI: 10.1007/s00107-003-0373-x.
- [59] *Häring*. URL: www.haring.ch (visited on 2019-03-12).
- [60] Hartmann, H. "Bemessung von Nagelplatten nach EC 5". *Bauingenieur* 90 (2015), pp. 185–192.
- [61] Herzog, T., Natterer, J., Schweitzer, R., Volz, M., and Winter, W. *Timber Construction Manual*. München: Birkhäuser, 2004. ISBN: 978-3-0346-1463-4.
- [62] Hochreiner, G., Riedl, C., Schweigler, M., Bader, T.K., and Eberhardsteiner, J. "Matrix Failure of Multi-Dowel Type Connections - Engineering Modelling and Parameter Study". World Conference on Timber Engineering. Vienna, Austria, 2016-08.
- [63] *Holzbautabellen HBT1 Handbuch für die Bemessung*. Zurich: Lignum, Holzwirtschaft Schweiz, 2012. 127 pp. ISBN: 978-3-906703-29-9.
- [64] *Holzbautabellen HBT2 Produktkompandium*. Zurich: Lignum, Holzwirtschaft Schweiz, 2017-03.

- [65] Huber, J.A.J., Ekevad, M., Girhammar, U.A., and Berg, S. “Structural Robustness and Timber Buildings – a Review”. *Wood Material Science & Engineering* (2018-03-13), pp. 1–22. ISSN: 1748-0272, 1748-0280. DOI: 10.1080/17480272.2018.1446052.
- [66] *Interview zu Holz-Hallen in der Schweiz*. In collab. with P. Makiol and L. Rügsegger. 2018-07.
- [67] Isaksson, T. “Length and Moment Configuration Factors; Paper 31-6-1”. *Proceedings of the CIB-W18 Meeting 31*. International Council for Research and Innovation in Building and Construction. Working Commission W18 - Timber Structures. Savolinna, Finland, 1998-08.
- [68] JCSS. *Probabilistic Model Code: Part 1 - Basis of Design*. Joint Committee of Structural Safety (JCSS), 2001-03. ISBN: 978-3-909386-79-6.
- [69] JCSS. *Probabilistic Model Code: Part 2 - Load Models*. Joint Committee of Structural Safety (JCSS), 2001-02.
- [70] JCSS. *Probabilistic Model Code: Part 3 - Resistance Models; 3.* Static Properties of Structural Steel (Rolled Sections)*. Joint Committee of Structural Safety (JCSS), 2001.
- [71] JCSS. *Probabilistic Model Code: Part 3 - Resistance Models; 3.5 Properties of Timber*. Joint Committee of Structural Safety (JCSS), 2006-05.
- [72] Jockwer, R., Caprio, D., and Jorissen, A. “Evaluation of Parameters Influencing the Load-Deformation Behaviour of Connections with Laterally Loaded Dowel-Type Fasteners”. *Wood Material Science & Engineering* 0.0 (2021-07-30), pp. 1–14. ISSN: 1748-0272. DOI: 10.1080/17480272.2021.1955297.
- [73] Jockwer, R. and Jorissen, A. “Load-Deformation Behaviour and Stiffness of Lateral Connections with Multiple Dowel Type Fasteners”. *Proceedings of the INTER Meeting 51*. International Network on Timber Engineering Research. Tallinn, Estonia: Timber Scientific Publishing KIT Holzbau und Baukonstruktionen Karlsruhe, 2018-08, p. 17.
- [74] Johansen, K. “Theory of Timber Connections”. *IABSE publications* 9 (1949), pp. 251–262.
- [75] Jorissen, A.J.M. “Double Shear Timber Connections with Dowel Type Fasteners”. Doctoral Thesis. Delft, The Netherlands: Delft University, 1998.
- [76] Jorissen, A. and Fragiacomio, M. “General Notes on Ductility in Timber Structures”. *Engineering Structures* 33.11 (2011-11), pp. 2987–2997. ISSN: 01410296. DOI: 10.1016/j.engstruct.2011.07.024.

- [77] “Kapitel 08 - Fachwerktraeger”. *BauBuche Buchen-Furnierschichtholz*. Pollmeier Massivholz GmbH & Co.KG, 2019-03.
- [78] Kirkegaard, P.H., Sørensen, J.D., Čizmar, D., and Rajčić, V. “System Reliability of Timber Structures with Ductile Behaviour”. *Engineering Structures* 33.11 (2011-11), pp. 3093–3098. ISSN: 01410296. DOI: 10.1016/j.engstruct.2011.03.011.
- [79] Klöck, W. “Statistical Analysis of the Shear Strength of Glued Laminated Timber Based on Full-Size Flexure Tests”. *Otto-Graf-Journal* 16 (2005), pp. 225–244.
- [80] Kobel, P. “Dowel-Type Connections in Beech LVL”. Doctoral Thesis. ETH Zurich, 2019. DOI: 10.3929/ethz-b-000407651.
- [81] Köhler, J. “A Probabilistic Framework for the Reliability Assessment of Connections with Dowel Type Fasteners; Paper 38-7-2”. *Proceedings of the CIB-W18 Meeting 38*. International Council for Research and Innovation in Building and Construction. Karlsruhe, Germany, 2005.
- [82] Köhler, J. “Reliability of Timber Structures”. Doctoral Thesis. ETH Zurich, 2006. DOI: 10.3929/ethz-a-005164254.
- [83] Köhler, J., Sørensen, J.D., and Faber, M.H. “Probabilistic Modeling of Timber Structures”. *Structural Safety*. Probabilistic Concepts in the Design of Timber Structures 29.4 (2007-10-01), pp. 255–267. ISSN: 0167-4730. DOI: 10.1016/j.strusafe.2006.07.007.
- [84] Kolb, J. *Systems in Timber Engineering*. Birkhäuser, 2008-04-23. ISBN: 978-3-7643-8690-0.
- [85] Kuhlmann, U. and Brühl, F. *Robustheit durch duktile Anschlüsse im Holzbau*. Bauforschung T 3312. Stuttgart: Fraunhofer-IRB-Verl, 2015. 119 pp. ISBN: 978-3-8167-9434-9.
- [86] Lam, F. “Length Effect on the Tensile Strength of Truss Chord Members”. *Canadian Journal of Civil Engineering* 27.3 (2000-06-01), pp. 481–489. DOI: 10.1139/199-084.
- [87] Langedijk, A. “Houtverbindingen met hoge sterkte staal”. BA thesis. Delft, The Netherlands: Technical University Delft, 2007. 49 pp.
- [88] Leijten, A., Köhler, J., and Jorissen, A. “Review of Probability Data for Timber Connections with Dowel-Type Fasteners; Paper 37-7-12”. *Proceedings of the CIB-W18 Meeting 37*. International Council for Research and Innovation in Building and Construction. Working Commission W18 - Timber Structures. Edinburgh, Scotland, 2004, p. 12.

- [89] Leyder, C., Klippel, M., Bartlomé, O., Heeren, N., Kissling, S., Goto, Y., and Frangi, A. “Investigations on the Sustainable Resource Use of Swiss Timber”. *Sustainability* 13.3 (3 2021-01), p. 1237. DOI: 10.3390/su13031237.
- [90] Li, H.-S., Ma, Y.-Z., and Cao, Z. “Subset Simulation for Assessing Structural Reliability of Multiple Limit State Functions”. *Proceedings of the 1st International Conference on Uncertainty Quantification in Computational Sciences and Engineering (UNCECOMP 2015)*. 1st International Conference on Uncertainty Quantification in Computational Sciences and Engineering. Crete Island, Greece: Institute of Structural Analysis and Antiseismic Research School of Civil Engineering National Technical University of Athens (NTUA) Greece, 2015, pp. 209–217. ISBN: 978-960-99994-9-6. DOI: 10.7712/120215.4265.756.
- [91] Manser, N. “Sensitivity Studies of Dowelled Timber Connections”. MA thesis. Zurich, Switzerland: ETH Zurich, 2021-07. 105 pp.
- [92] Marelli, S., Schöbi, R., and Sudret, B. *UQLab User Manual – Structural Reliability (Rare Event Estimation)*. UQLab-V1.4-107. Chair of Risk, Safety & Uncertainty Quantification, ETH Zurich, Switzerland, 2021.
- [93] *Mehrschnittige Stahl-Holz-Verbindungen einfacher und wirtschaftlicher fertigen mit dem System WS*. URL: www.sfs.com (visited on 2019-03-13).
- [94] Mischler, A. “Bedeutung der Duktilität für das Tragverhalten von Stahl-Holz-Bolzenverbindungen”. Doctoral Thesis. ETH Zurich, 1998. DOI: 10.3929/ethz-a-001917849.
- [95] Mistler, H.L. “Querzug-Bemessung von BSH-Trägern nach EC 5 - Ein Vergleich mit Forschungsergebnissen”. *Holz als Roh- und Werkstoff* 56 (1998), pp. 51–59.
- [96] Mistler, H.-L. “Design of Glulam Beams According to EN 1995 with Regard to Perpendicular-to-Grain Tensile Strength: Comparison with Research Results”. *European Journal of Wood and Wood Products* 74.2 (2016-03-01), pp. 169–175. ISSN: 1436-736X. DOI: 10.1007/s00107-015-0979-9.
- [97] Möhler, K. “Spannungen und Durchbiegungen parallelgurtiger Fachwerkträger aus Holz”. *Bauen mit Holz* 4 (1966), pp. 155–161.
- [98] Mtenga, P.V., Cramer, S.M., Peyrot, A.H., and Wolfe, R.W. “System Factors for Light-Frame Wood Truss Assemblies”. *Journal of Structural Engineering* 121.2 (1995-02), pp. 290–300. ISSN: 0733-9445, 1943-541X. DOI: 10.1061/(ASCE)0733-9445(1995)121:2(290).

- [99] Natterer, J., Herzog, T., and Volz, M. *Holzbau Atlas Zwei*. Studienausgabe. Arbeitsgemeinschaft Holz e. V., Düsseldorf und Institut für internationale Architektur-Dokumentation, München, 1996.
- [100] Neuhaus, H. *Ingenieurholzbau*. 4th ed. Wiesbaden, Germany: Springer Fachmedien Wiesbaden GmbH, 2017. ISBN: 978-3-658-14177-6 978-3-658-14178-3. DOI: 10.1007/978-3-658-14178-3.
- [101] Palma, P. “Fire Behaviour of Timber Connections”. Doctoral Thesis. ETH Zurich, 2016. DOI: 10.3929/ethz-a-010836621.
- [102] Pedersen, M.B.U., Damkilde, L., and Hoffmeyer, P. *Dowel Type Timber Connections Strength Modelling*. R-039. Lyngby, Denmark: Technical University of Denmark (DTU), 2001.
- [103] *Pilatus Aircraft Ltd*. URL: www.pilatus-aircraft.com (visited on 2019-12-03).
- [104] Ramage, M., Burrige, H., Wicher, M., Fereday, G., Reynolds, T., Shah, D., Wu, G., Yu, L., Fleming, P., Densley Tingley, D., Allwood, J., Dupree, P., Linden, P., and Scherman, O. “The Wood from the Trees: The Use of Timber in Construction”. *Renewable and Sustainable Energy Reviews* 68 (2017-02-28), pp. 333–359. DOI: 10.1016/j.rser.2016.09.107.
- [105] Rammer, D.R. “Shear Strength of Glued-Laminated Timber Beams and Panels”. *Proceedings of the National Conference on Wood Transportation Structures*. National Conference on Wood Transportation Structures. Madison, WI.: U.S. Department of Agriculture, Forest Service, Forest Products Laboratory., 1996-10, pp. 192–200.
- [106] Ranta-Maunus, A. “Duration of Load Effects in Tension Perpendicular to Grain in Curved Glulam; Paper 31-6-2”. *Proceedings of the CIB-W18 Meeting 31*. International Council for Research and Innovation in Building and Construction. Working Commission W18 - Timber Structures. Savonlinna, Finland, 1998-08.
- [107] Richard, R.M. and Abbott, B.J. “Versatile Elastic-Plastic Stress-Strain Formula”. *Journal of the Engineering Mechanics Division* 101.4 (1975-08), pp. 511–515. ISSN: 0044-7951, 2690-2427. DOI: 10.1061/JMCEA3.0002047.
- [108] Sandhaas, C. “Mechanical Behaviour of Timber Joints with Slotted-in Steel Plates.” Doctoral Thesis. Delft, The Netherlands: Technical University Delft, 2012. 313 pp.
- [109] Sanpaolesi, L. “The Background Document for Snow Loads”. *IABSE reports* 74 (1996). DOI: 10.5169/SEALS-56071.

- [110] Scheer, C. and Golze, B. "Berechnung von Fachwerkkonstruktionen unter Berücksichtigung des durchlaufenden Ober- und Untergurts". *Bauen mit Holz* 7 (1981).
- [111] Schickhofer, G. "Determination of Shear Strength Values for GLT Using Visual and Machine Graded Spruce Laminations; Paper 34-12-6". *Proceedings of the CIB-W18 Meeting 34*. International Council for Research and Innovation in Building and Construction. Venice, Italy, 2001-08.
- [112] Schilling, S. and Frangi, A. "Modellierung von Holzfachwerken mit Stabdübelverbindungen und eingeschlitzten Stahlblechen für Zuverlässigkeitsanalysen". 8. Doktorandenkolloquium „Holzbau Forschung + Praxis“ 2020. Stuttgart, Germany, 2020-03-05. DOI: 10.3929/ethz-b-000404166.
- [113] Schilling, S., Palma, P., Steiger, R., and Frangi, A. "Probabilistic Description of the Mechanical Properties of Glued Laminated Timber Made from Softwood; Paper 54-12-4". *Proceedings of the INTER Meeting 54*. International Network on Timber Engineering Research. online: KIT Scientific Publishing, 2021-08. DOI: 10.3929/ethz-b-000505371.
- [114] Scholz, F.W. "Maximum Likelihood Estimation". *Encyclopedia of Statistical Sciences*. American Cancer Society, 2006. ISBN: 978-0-471-66719-3. DOI: 10.1002/0471667196.ess1571.pub2.
- [115] Schweigler, M., Bader, T.K., and Hochreiner, G. "Engineering Modeling of Semi-Rigid Joints with Dowel-Type Fasteners for Nonlinear Analysis of Timber Structures". *Engineering Structures* 171 (2018-09), pp. 123–139. ISSN: 01410296. DOI: 10.1016/j.engstruct.2018.05.063.
- [116] Schweigler, M., Vedovelli, M., Lemaitre, R., Bocquet, J.-F., Sandhaas, C., and Bader, T.K. "Beam-on-Foundation Modeling as an Alternative Design Method for Timber Joints with Dowel-Type Fasteners – Part 3: Second Order Theory Effects for Considering the Rope Effect; Paper 54-7-8". *Proceedings of the INTER Meeting 54*. International Network on Timber Engineering Research. online: Timber Scientific Publishing KIT Holzbau und Baukonstruktionen Karlsruhe, 2021, p. 16.
- [117] SIA 260:2013. *Grundlagen der Projektierung von Tragwerken*. SN 505 260. Zurich, Switzerland: Schweizerischer Ingenieur- und Architektenverein SIA, 2013.
- [118] SIA 261:2020. *Einwirkungen auf Tragwerke*. SN 505 261. Zurich, Switzerland: Schweizerischer Ingenieur- und Architektenverein SIA, 2020.
- [119] SIA 263:2013. *Stahlbau*. SN 505 263. Zurich, Switzerland: Schweizerischer Ingenieur- und Architektenverein SIA, 2013.

- [120] SIA 265:2012. *Holzbau*. SN 505 265. Zurich, Switzerland: Schweizerischer Ingenieur- und Architektenverein SIA, 2012.
- [121] SIA 265:2021. *Holzbau*. SN 505 265. Zurich, Switzerland: Schweizerischer Ingenieur- und Architektenverein SIA, 2021.
- [122] SIA 265/1:2018. *Holzbau - Ergänzende Festlegungen*. SN 505 265/1. Zurich, Switzerland: Schweizerischer Ingenieur- und Architektenverein SIA, 2018.
- [123] Starossek, U. and Haberland, M. “Robustness of Structures”. *International Journal of Lifecycle Performance Engineering* 1.1 (2012), pp. 3–21. ISSN: 2043-8648, 2043-8656. DOI: 10.1504/IJLCPE.2012.051279.
- [124] Steiger, R. and Gehri, E. “Interaction of Shear Stresses and Stresses Perpendicular to the Grain; Paper 44-6-2”. *Proceedings of the CIB-W18 Meeting 44*. International Council for Research and Innovation in Building and Construction. Alghero, Italy, 2011, p. 16.
- [125] Sudret, B. and Marelli, S. *Lecture Notes on Structural Reliability and Risk Analysis*. ETH Zurich, 2018.
- [126] Sudret, B. and Marelli, S. *Lecture Notes on Uncertainty Quantification in Engineering*. ETH Zurich, 2018.
- [127] Theiler, M. “Stabilität von Axial auf Druck beanspruchten Bauteilen aus Vollholz und Brettschichtholz”. Doctoral Thesis. ETH Zurich, 2014. DOI: 10.3929/ethz-a-010273734.
- [128] Tölke, F. “Bedenkliche Trugschlüsse in der Bemessung gespreizter Druckstäbe”. *Der Bauingenieur* 34 (1929), pp. 600–604.
- [129] Van Groesen, J. and Kranenburg, M. “Houtverbindingen met hoge sterkte staal”. BA thesis. Delft, The Netherlands: Technical University Delft, 2007. 101 pp.
- [130] Weibull, W. *A Statistical Theory of the Strength of Materials*. 151. Stockholm, Sweden: Royal Swedish Institute for Engineering Research, Technical University, 1939.
- [131] Zhu, X. and Sudret, B. “Use of Generalized Lambda Distributions to Emulate Stochastic Simulators”. 3rd International Conference on Uncertainty Quantification in Computational Sciences and Engineering (UNCECOMP 2019). Crete Island, Greece, 2019, 38 p. DOI: 10.3929/ETHZ-B-000352754.
- [132] Zimmermann, H. “Systembasierte Bemessung von Holzfachwerken”. MA thesis. Zurich, Switzerland: ETH Zurich, 2020-01. 151 pp.

- [133] Zok, F.W. “On Weakest Link Theory and Weibull Statistics”. *Journal of the American Ceramic Society* 100.4 (2017), pp. 1265–1268. ISSN: 1551-2916. DOI: 10.1111/jace.14665.